NASA CR-132605-2

NASA CONTRACTOR
REPORT

Prediction and Verification of Creep Behavior in Metallic Materials and Components for the Space Shuttle Thermal Protection System

VOLUME II

Phase II Subsize Panel Cyclic Creep Predictions

JUNE 1975

Prepared By **B. A. Cramer** *and* **J. W. Davis**

MCDONNELL DOUGLAS ASTRONAUTICS COMPANY • EAST

MCDONNELL DOUGLAS CORPORATION

NATIONAL AERONAUTICS AND SPACE ADMINISTRATION • WASHINGTON, D.C. • JUNE 1975

ABSTRACT

A method of analysis developed for predicting permanent cyclic creep deflections in stiffened panel structures has been developed. The resulting computer program (TPSC, for Thermal Protection System Creep) applies either the time hardening or strain hardening theories of creep accumulation. Iterative techniques are used to determine structural rotations, creep strains, and stresses as a function of time. Deflections are determined by numerical integration of structural rotations along the panel length. The analytical approach was developed for purposes of analyzing thin gage entry vehicle metallic thermal protection system panels subjected to cyclic bending loads at high temperatures, however, it is applicable to any panel subjected to bending loads.

Predicted panel creep deflections are compared with results from cyclic tests of subsize corrugation and rib stiffened panels fabricated from L605, Rene '41, Ti-6Al-4V, and TDNiCr thin gage sheet. Empirical equations used in the analysis were developed for each material based on correlation with tensile cyclic creep data. Both the subsize panels and tensile specimens used in development of the empirical equations were fabricated from the same sheet material.

FORWARD

This report was prepared by McDonnell Douglas Astronautics Company - East under Contract NAS 1-11774 for the National Aeronautics and Space Administration, Langley Research Center, Hampton, Virginia. It was administered under the direction of the Materials Division, Materials Research Branch, with Mr. D. R. Rummler acting as the technical representative of the contracting officer. The McDonnell Douglas program manager was Mr. J. W. Davis. Mr. B. A. Cramer was responsible for structural considerations involved in testing, panel fabrication, analytical approaches, and data analysis. The experimental portion was performed by Mr. M. B. Munsell. Mr. M. B. Gedera assisted in programming the TPSC program.

This report covers the period from July 1973 to November 1974.

SUMMARY

Phase II was directed toward developing and verifying capability for prediction of creep deflection in metallic heat shields subjected to cyclic entry environments.

A computer program, Thermal Protection System Creep (TPSC) was developed for predicting panel creep deflections. This program offers an approach to creep deflection predictions through application of iterative techniques and numerical integration. In the analysis, panel length is divided into segments over which bending moments are assumed constant and panel depth is divided into increments over which stresses and strains are assumed constant. Using a linear strain assumption, beam rotations are iteratively determined, based on either the time hardening or strain hardening theories of creep accumulation. Material cyclic creep response properties are defined by empirical equations developed from cyclic creep tests of tensile creep specimens in Phase I (Reference 1). Program output includes definition of both elastic and creep deflected shapes, residual stresses, and creep strains as a function of cycle.

The TPSC computer program provides needed capability for prediction of permanent deflections, due to creep, in entry vehicle metallic thermal protection system panels. Application is also envisioned for other structures where creep deflections may be important such as in missiles and nuclear reactors. The TPSC program is written in Fortran IV and is operational on the CDC 6600. User's Manual (Reference 2) is available for the TPSC program.

Seventeen subsize panel specimens, 6.35 cm by 30.5 cm, were tested to provide creep deflection data for verification of prediction capability. Corrugation cross section specimens were fabricated for test using thin gage (~.025 cm) L605, Rene' 41, Ti-6Al-4V, and TDNiCr sheet material. Rib cross section specimens were also

fabricated for test using thicker gage (∿.060 cm) L605 and Ti-6Al-4V sheet material. These materials were procured for use both in Phase I and II. Each test consisted of cycling the panel for up to 100 entry thermal and bending load profiles representative of Shuttle entry missions. Testing was conducted in a vacuum furnace, using a load mechanism specifically designed to apply panel loads that would be independent of panel deflection. Permanent deflections, due to creep, were measured as a function of cycle.

Comparisons of subsize panel creep deflection predictions with test results are provided along with typical residual stress and creep strain distributions. The approach for creep deflection analysis, incorporated in the TPSC computer program, yielded predicted panel cyclic creep deflections between half and twice the test deflections. Factors affecting both prediction capability and test deflections were evaluated.

The International system of units (SI) are used in this report. U.S. Customary Units are also generally provided. Applicable conversion factors are presented in Appendix A.

TABLE OF CONTENTS

TABLE OF CONTENTS (Continued)

LIST OF FIGURES

LIST OF FIGURES - (Continued)

LIST OF FIGURES - (Continued)

LIST OF FIGURES - (Continued)

LIST OF TABLES

LIST OF TABLES - (Continued)

1.0 INTRODUCTION

One of the design requirements of reentry vehicle metallic thermal protection systems (TPS) is that deflections, occurring during ascent and entry mission phases, due to differential pressure and thermal loading, do not exceed design limits. These deflection limitations were established to minimize localized aerodynamic heating and to minimize the need for panel refurbishment (Reference 3). Because deflections include permanent deformation due to creep, methods for predicting these deformations are needed.

During Phase I of this program, the influence of cyclic entry conditions on creep response was investigated for four material alloys: Ti-6Al-4V, Rene' 41, L605, and TDNiCr. Analysis of tensile creep test data during this phase resulted in empirical equations, for each material, which describe cyclic creep response characteristics as a function of stress, temperature, and time. These equations were used in conjunction with the time and strain hardening theories of creep accumulation to investigate creep prediction capability for cyclic trajectory stress and temperature profiles.

The goal in Phase II was to develop analytical capability for determining creep deflections in TPS panels and verify this capability through testing of subsize panel specimens. Subsize panel test results, comparisons with predictions, and the Thermal Protection System Creep Computer Program developed in Phase II are presented in this report.

The TPSC program will be used in Phase III in the prediction of available full size panel test data.

2.0 TPS DESIGN CRITERIA

2.1 TPS DESCRIPTION

Several arrangements of metallic TPS components have been investigated in the course of previous spacecraft studies. The baseline design used in the McDonnell Douglas Phase B Shuttle Study Program is shown in Figure 2-1. Following is a discussion of this design, which incorporates features required for the TPS system.

Radiative metallic panels form the outer moldline. These panels are backed by fibrous insulation blankets. Differential air pressure loads on the panels are transmitted by beam bending to hat shaped transverse support beams located at approximately a 50 cm (20 inches) spacing. Retaining straps are attached to the transverse support beams with bolts to transmit outward acting pressure loads from the panel to the beams. Panels are simply supported by the transverse support beams and retaining straps. The retaining strap is flat to allow the face sheet of the forward panel to be continuous over the transverse joint between panels. This continuity across the joint serves as both a water and a hot gas seal. An additional function of the continuous face sheet is to provide in-plane panel reaction points by the bolts which attach the retaining strap to the transverse support beam. Longitudinal joints between panels provide normal-to-panel shear continuity between adjacent panels, preventing joint gapping by forcing adjacent panels to deflect simultaneously under applied loads.

The transverse support beams transmit loads to support struts which carry the loads to primary load carrying structure. Drag links, spanning diagonally between transverse support beams and primary structure, provide support structure system stability and carry longitudinal loads. Generally, the support struts and transverse support beams are of the same material as the panels.

Provisions for thermal expansion are a major consideration in the design of the

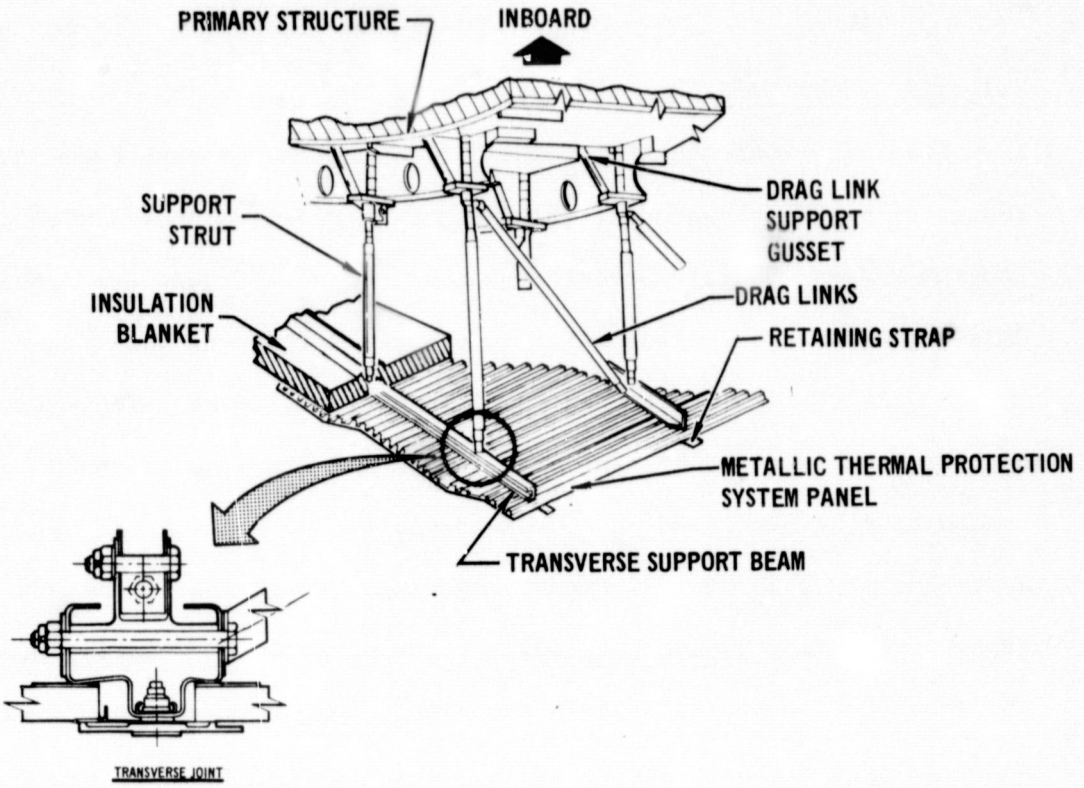

FIGURE 2–1 TYPICAL METALLIC THERMAL PROTECTION SYSTEM STRUCTURE

TPS. Allowing components to deform thermally with minimum restraint minimizes thermally induced stresses. Longitudinal growth of panel is absorbed on the forward end of each panel. The aft end is attached firmly to the transverse support beam. Transverse panel growth capability is provided in the longitudinal joints. Panels are "keyed" to the transverse support beams at one bolt location, and expand in both directions. Relative thermal expansions between the panel retaining strap and transverse support beam is accomplished by slotted holes in the support beam. One bolt hole for each retaining strap in the support beam is not slotted to stabilize the strap against movement.

2.2 ENVIRONMENT

This program was associated with the use of metallic materials for the Space Shuttle TPS. Therefore, the test conditions were representative of Shuttle design criteria and environments (Reference 3). In these studies, entry trajectories for metallic TPS were shaped to minimize peak surface temperatures so that the metals would not overheat. This resulted in high total heat input and a relatively long time at peak surface temperature. The Shuttle orbiter design ascent trajectory for a metallic TPS is shown in Figure 2-2. Limit pressures resulting from this trajectory are multiplied by a 1.4 factor of safety to obtain design ultimate pressures shown in Figure 2-3. In addition to the aerodynamic pressure, a minimum vent pressure of +9.7 kPa ultimate was used over the entire vehicle for TPS design. These pressures occur while the panel temperature is less than 366 K.

The design entry trajectory is shown in Figure 2-4. Resulting ultimate differential pressures and bottom centerline temperatures are shown in Figures 2-5 and 2-6. Design limit temperatures for this trajectory over the Orbiter surface are shown in Figure 2-7.

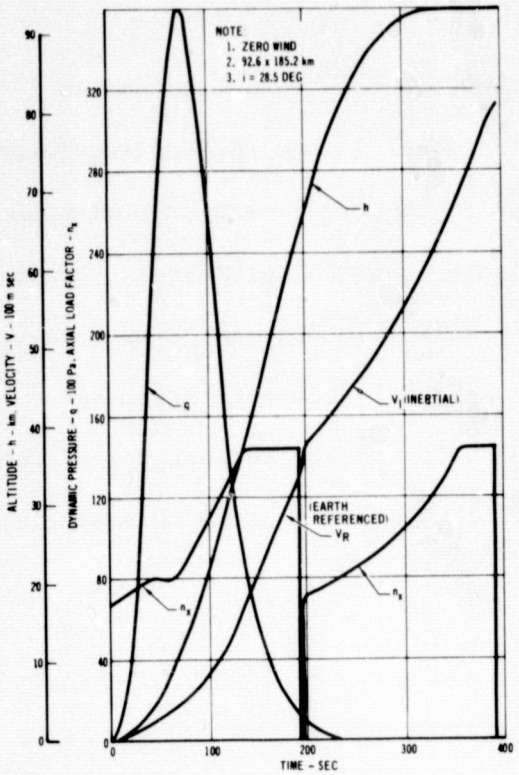

FIGURE 2–2 DESIGN ASCENT TRAJECTORY

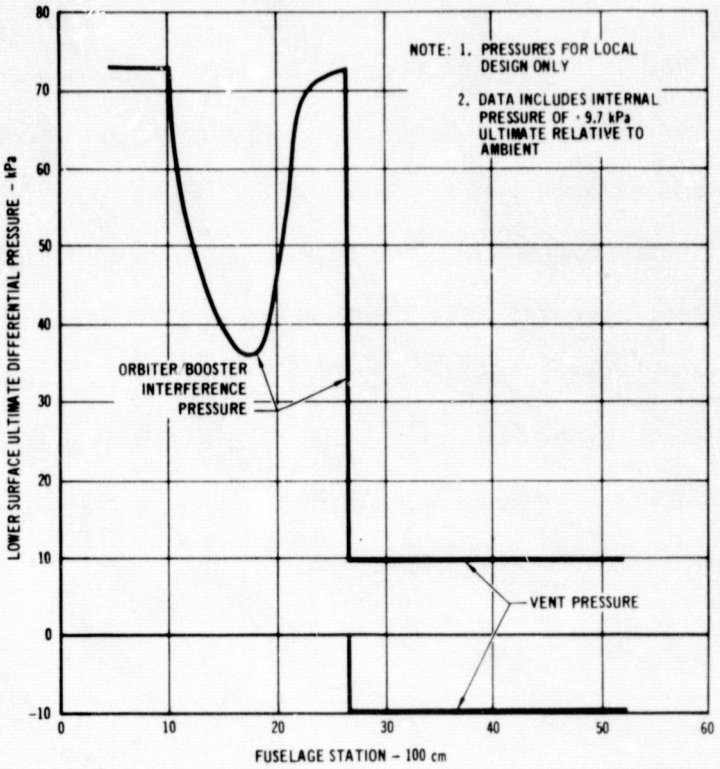

FIGURE 2–3 ENVELOPE OF ASCENT PRESSURES ON FUSELAGE LOWER SURFACE

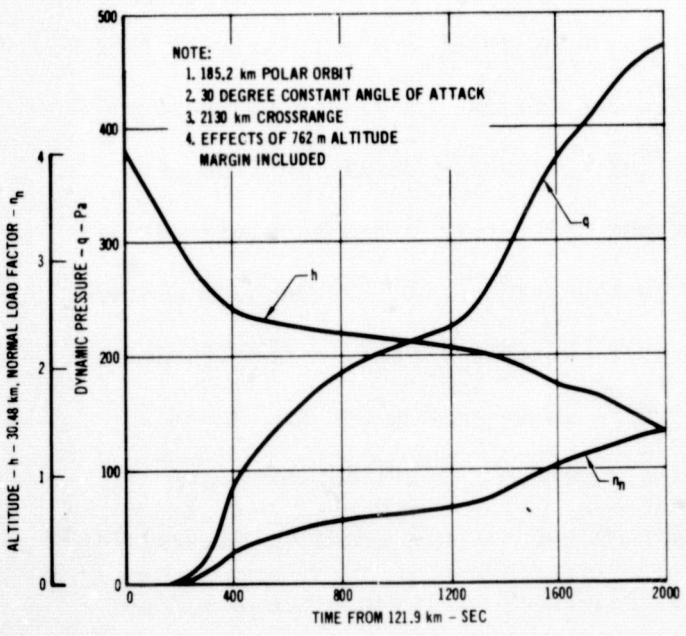

FIGURE 2–4 DESIGN ENTRY TRAJECTORY

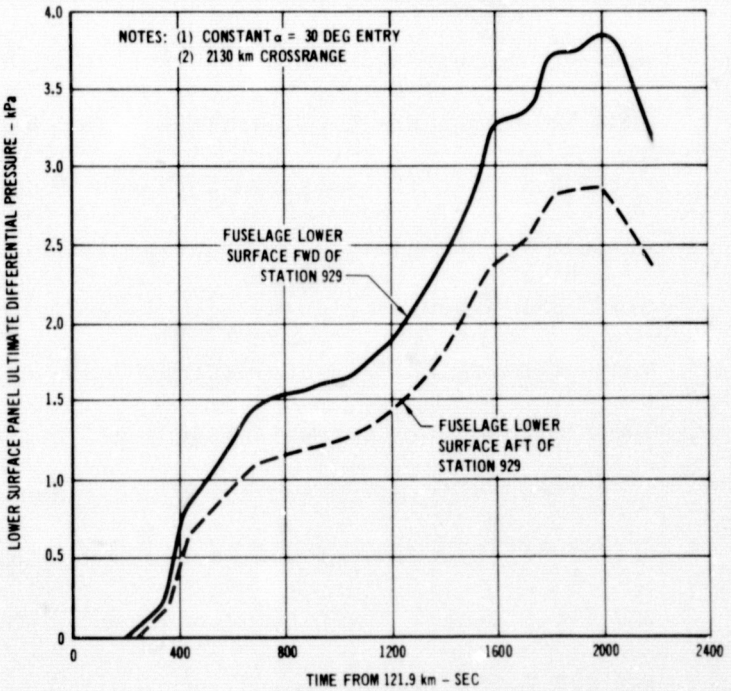

FIGURE 2–5 LOWER SURFACE ENTRY PRESSURE

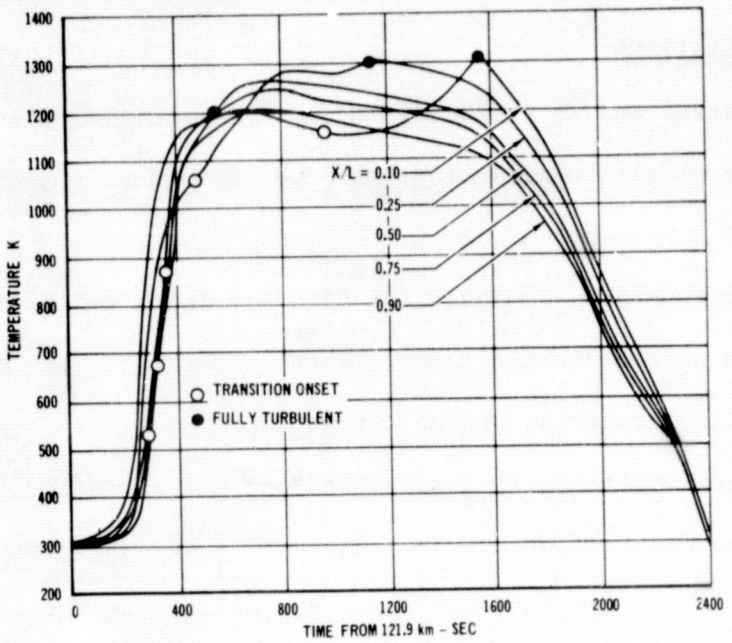

FIGURE 2–6 ORBITER BOTTOM CENTERLINE ENTRY TEMPERATURES

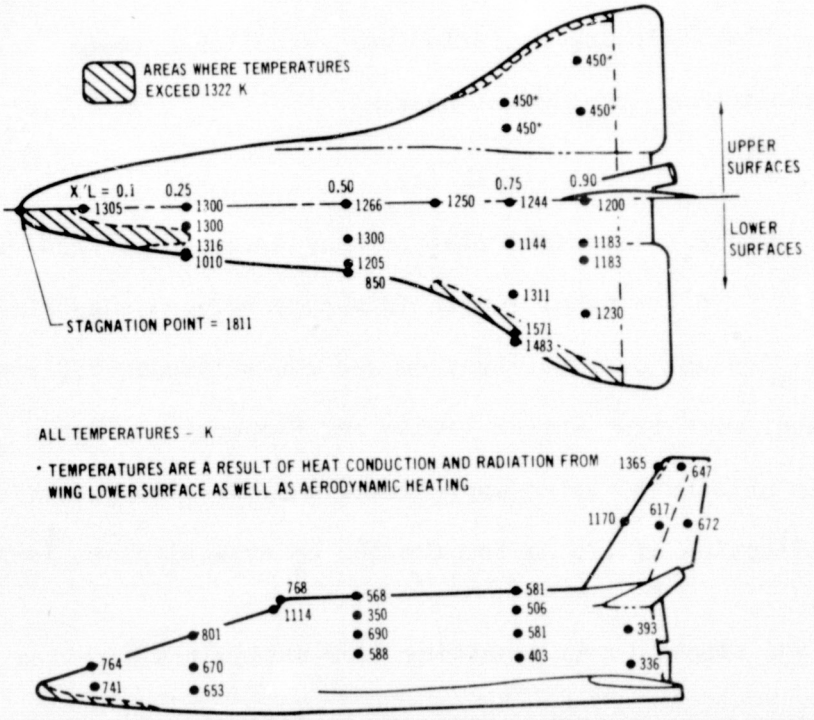

FIGURE 2–7 MAXIMUM ENTRY TEMPERATURE FOR A SPACE SHUTTLE WITH A METALLIC TPS

2.3 DESIGN CONSIDERATIONS

Primary considerations in the design of metallic thermal protection system panels are that the panels be minimum weight and have reuse capability for up to 100 missions.

The panels are generally designed for high air loads at low temperatures occuring during the ascent mission phase. These panels are then checked for combined loads and temperatures occurring during entry. The TPS panels are sized for strength to prevent detrimental yielding at limit loads and for no failure at ultimate load. Because of the reuse requirement over a variety of missions, critical ascent and entry conditions will, in general, not occur during the same mission.

In addition to strength requirements, TPS panels must be designed so that out of plane deflections, due to combined elastic, thermal, and accumulated creep, are not excessive. The following criterion was established (Reference 3) for TPS deflection, based on minimizing local panel heating.

$$\delta = .25 + .01L \text{ (cm)} \qquad (2\text{-}1)$$

where δ = maximum elastic plus creep deflection at panel midspan

L = panel length (distance between supports)

For typical 2.5 cm. deep corrugation and rib stiffened TPS panels, this criterion is consistent with test stress levels and temperature levels designed to yield 100 cycle creep strains of up to approximately 0.5%. The criterion provides for a maximum deflection of .75 cm.for the 50. cm typical panel length defined in Figure 2-1.

Loads and temperatures resulting from design trajectories are normally used to size TPS panels for strength. However, in designing for creep deflections, nominal loads and temperatures are usually used. The differences in loads and temperatures

for the design and nominal trajectories is (1) nominal pressures = design limit pressure/1.13 and (2) nominal temperatures = design temperatures -25°K (10°K per 304.8 m altitude dispersion from nominal trajectory).

Although selection of optimum systems is based largely on weight, other factors such as cost, fabricability, inspectability, and confidence in design are also considered.

3.0 MATERIAL SELECTION AND PROCUREMENT

3.1 BACKGROUND TO MATERIAL SELECTION

Materials used for subsize panel fabrication in this Phase II of the program were from the same sheet as used for tensile creep specimen fabrication in Phase I. This was done to eliminate property variations from sheet to sheet as a variable in deflection verification analysis under this program phase.

During the Space Shuttle Phase B studies a review was made of the most promising titanium, nickel, cobalt, and dispersion strengthened alloys to determine which alloy should be used on shuttle. Factors considered included availability in thin sheet, fabricability, and strength.

Based on these studies and the goals of this program, Ti-6Al-4V, in the annealed condition, was selected as the titanium alloy for evaluation, Rene'41 was selected as the nickel base alloy, L605 was selected as the cobalt base alloy, and TDNiCr was selected as the dispersion strengthened alloy. A more complete review of these background studies and material comparisons are presented in Reference (1).

3.2 PROCUREMENT OF MATERIALS

The baseline material gage selected for testing was thinnest sheet available of approximately .025 cm thickness (.025 for L605, .031 for titanium, .025 for TDNiCr, and .027 for Rene' 41). Thicker gage sheet (.064 for L605, .056 for titanium, .051 for TDNiCr, and .054 for Rene' 41) was also obtained for each of the four alloys for use in comparison testing of gage effects and for application in subsize panel fabrication.

To ensure that the material was representative of current technology, Rene '41, L605, and Ti-6Al-4V sheet were procured to existing AMS or Military specifications. TDNiCr was obtained from NASA. This material was produced for NASA's Lewis Research

Center by Fansteel Inc., under NASA Contract NAS-3-13490. In addition, for each alloy, all material of the same gage was procured from one heat of material. This eliminated the possibility of chemistry and/or property variation in different heats of material from influencing the creep tests.

Summarized in Table 3-1 are the supplier certifications and purchase specifications of materials procured.

TABLE 3-1

SUPPLIER CERTIFICATION

ALLOY DESIGNATION	APPLICABLE SPECIFICATION	NOMINAL GAUGE (cm)	HEAT NO.	SUPPLIER	CHEMISTRY - % BY WEIGHT																			R. T. MECH. PROPERTIES				
					C	O	H	N	Al	Co	Cr	Fe	Mn	Mo	Ni	Ti	V	W	B	S	P	C_b	ThO_2	F_{tu} MPa	F_{ty} MPa	E.LONG. %5.1cm	TEST DIR.	COND.
L605	AMS-5537	0.024	1860-2-1396	CABOT CORP	0.09	-	-	-	-	BAL	20.20	2.45	1.70	-	10.60	-	-	14.55	-	0.005	0.011	0.13	-	897.7	421.3	48%	T	A
L605	AMS-5537	0.064	1860-2-1399	CABOT CORP	0.09	-	-	-	-	BAL	19.95	2.30	1.25	-	10.55	-	-	14.50	-	0.005	0.005	0.09	-	927.3	427.8	45%	T	A
RENE'41	AMS-5545	0.027	2490-0-8207	TELEDYNE-RODNEY	0.09	-	-	-	1.52	10.40	18.30	3.05	0.04	9.65	BAL	3.07	-	-	0.005	0.006	-	0.13	-	1144.5	710.2	32%	T	A
RENE'41	AMS-5545	0.051	2490-7-8279	TELEDYNE-RODNEY	0.08	-	-	-	1.50	11.48	19.05	0.24	0.01	9.87	BAL	3.15	-	-	0.005	0.003	-	0.07	-	-	-	-	-	A
Ti-6AL-4V	MIL-T-9046F TYPE 3 COMP C	0.031	N-0358	TIMET	0.026	0.100	0.009	0.011	6.0	-	-	0.06	-	-	-	BAL	4.0	-	-	-	-	-	-	1006.6 1013.5	910.1 923.9	10 10	T L	A
Ti-6AL-4V	MIL-T-9046F TYPE 3 COMP C	0.051	N-0263	TIMET	0.022	0.140	0.010	0.009	6.0	-	-	0.07	-	-	-	BAL	4.0	-	-	-	-	-	-	1006.6 1013.5	930.8 930.8	10 10	T L	A
TD-Ni-Cr	NONE	0.024	TC-3875	NASA	0.016	-	-	-	-	-	19.80	-	-	-	BAL	-	-	-	-	0.0057	-	-	1.94	766.2	547.1	16	T	A
TD-Ni-Cr	NONE	0.51	TC-3876	NASA	0.022	-	-	-	-	-	19.92	-	-	-	BAL	-	-	-	-	0.0051	-	-	1.96	887.4	592.5	20	T	A

A - ANNEALED
T - TRANSVERSE
L - LONGITUDINAL

4.0 SUBSIZE PANEL DESIGN

Two subsize panel configurations were selected for testing in this phase of the program. These were the single face corrugation and rib stiffened designs shown in Figure 4-1. Considerations for establishing panel configurations were based on previous MDAC experience in the design of metallic TPS in connection with Shuttle studies and various in-house studies. In addition, ease of fabrication and applicability to Space Shuttle TPS designs were considered. The section geometry designs were closely coordinated with the test mechanism design to assure compatibility. The end plates, shown in the figure, were included to serve as support pads during testing.

4.1 BACKGROUND TO CONFIGURATION SELECTION

Trade studies comparing these concepts along with others, such as the single skin beaded panel and the honeycomb sandwich panel, were performed during the Space Shuttle Phase B studies at MDAC-East. Based on these studies, the single face corrugation design was selected as the baseline panel configuration. The rib stiffened concept was not selected because of concern over potential rib instabilities under bending loads, even though it offered a potential weight advantage and was easier to inspect than the single face corrugation concept. Subsequent to the Phase B studies, inhouse IRAD studies (Reference 10) demonstrated that the rib stiffened concept is capable of carrying the predicted bending loads and, as a result, was selected for inclusion in this program.

Because beaded skins could be required in full size TPS panels, they were considered for possible application in the subsize panel designs. However, because beaded skins were judged to have a negligible effect on panel creep deflections and add unnecessary complexity to the creep deflection verification, they were not

FIGURE 4-1 RIB AND CORRUGATION SUBSIZE PANEL CONFIGURATIONS FOR PHASE II TESTING

included in the final subsize panel configurations. In addition, beads would have created added fabrication and possible load application and deflection measurement complexity. The requirement for beaded skins in full size metallic TPS panels was originally defined during the testing of TDNiCr panels as part of the Dispersion-Strengthened Metals Structural Program (Reference 9) conducted at MDAC-W. Panels designed with a flat face sheet and tested at elevated temperatures exhibited permanent buckles. Subsequent panels incorporating shallow beads between stiffeners showed no detectable permanent set after cyclic testing. Preliminary testing performed on a Haynes 188 panel during the Space Shuttle Supplementary Structural Test Program at MDAC-East (Reference 4) also demonstrated this requirement. Buckling of flat skin TPS panels is due to excessively high compression stresses developed in the TPS panel skin, in the direction of panel width, due to thermal gradients along the length. However, analysis has demonstrated that these thermal loads are not sufficient to produce buckling in narrow subsize panels.

4.2 SUBSIZE PANEL GEOMETRY CONSTRAINTS

Subsize panel overall dimensions were based on furnace and load mechanism constraints (see Section 5.3) as well as available fabrication tooling. The panel length of 30.5 cm (12.0 inches) was the maximum length which could be tested in conjunction with the furnace test zone capabilities. Load mechanism geometry in conjunction with furnace dimensions constrained panel width to be less than 6.6 cm (2.6 inches) and panel depth to be less than 1.65 cm (.65 inches). Therefore, panel dimensions of 6.35 cm by approximately 1.3 cm were selected, to allow adequate clearance in the test mechanism. Panel load and deflection requirements were checked to assure compatibility with furnace test mechanism capability, as will be discussed in Section 5.2.

4.3 CORRUGATION PANEL DESIGN

Corrugated panels are generally critical for positive bending loads (skin in compression) because allowable bending loads in the positive and negative directions are approximately equal while design loads are higher in the positive direction. Typical pitch lengths used for optimum thin gage metallic TPS corrugated panels have been approximately 3.0 cm (~1.2 inches). Pitch lengths less than 3.0 cm are desirable in order to minimize possible response to acoustic loadings associated with Shuttle trajectories. Optimum panel depths vary, depending upon design loads and material strength properties, but are usually in the range of 1.0 to 2.5 cm (0.4 to 1.0 inch).

Existing tooling was used for forming the subsize test panel corrugations. Therefore, the corrugation panel specimen cross sections were the same for each of the four materials. This tooling, originally optimized for a titanium TPS panel, provided a pitch of 1.9 cm (0.75 inch) and a depth of 1.27 cm (0.50 inch). The panel dimensions, while not optimum, fall within the range of typical TPS panel dimensions. Corrugated stiffened panels were fabricated for each of the four alloys (L605, Rene' 41, Ti-6Al-4V, and TDNiCr) in this program to the dimensions shown in Figure 4-2.

4.4 RIB STIFFENED PANEL DESIGN

Optimization studies of rib stiffened TPS panel concepts (Reference 11) indicate that minimum gage skins provide minimum weight panels. However, thicker gage ribs are required in order to provide adequate negative bending (ribs in compression) strength. Previous experience at MDAC-East in analysis and testing of Ti-6Al-4V rib stiffened panels with .025 cm (.010 inch) skin and .050 cm (.020 inch) rib gages has revealed that ultimate allowable strengths in negative bending are about 50% of those in positive bending. Therefore, for the rib stiffened TPS concept,

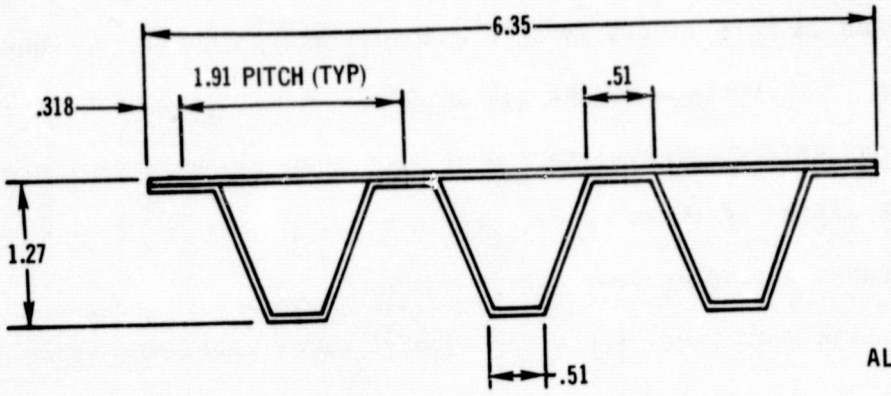

ALL DIMENSIONS IN CM

MATERIAL	NOMINAL THICKNESS (CM)	HEAT NUMBER
L605	.024	1860–2–1399
RENE'41	.027	2490–0–8207
Ti–6Al–4V	.031	N–0358
TDNiCr	.024	TC–3875

FIGURE 4–2 SINGLE FACE CORRUGATION SUBSIZE PANEL DESIGN

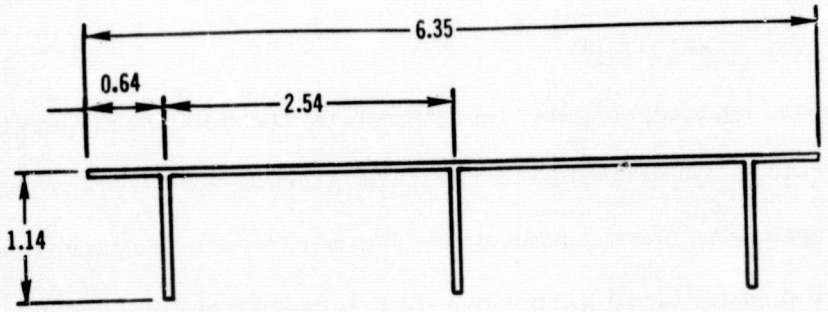

ALL DIMENSIONS IN CM

MATERIAL	NOMINAL THICKNESS (CM)	HEAT NUMBER
L605	.064	1860–2–1396
Ti–6Al–4V	.051	N–0358

FIGURE 4–3 RIB STIFFENED SUBSIZE PANEL DESIGN

negative bending is more likely to be a critical design condition than with corrugation stiffened TPS. Optimum weight rib stiffened panel designs have utilized skin b/t (rib spacing/skin thickness) ratios of less than 150 to minimize acoustic response. Rib depths of these panels have generally been in the 1.0 to 2.5 cm (.4 to 1.0 inch) range depending upon design loads.

Cross section geometry, of the rib subsize panel specimens shown in Figure 4-3, utilizes a rib spacing of 1.0 inch, which is consistent with typical TPS panels and with the panel width allowed for testing. Although a thinner gage skin would be used for an optimum design, it was decided to fabricate subsize panels with the skin the same thickness as the rib to simplify manufacturing and analysis of the panels. Panel depth of .45 inch was established in conjunction with test mechanism loading requirements. Because of potential welding problems with Rene' 41 and brazing difficulties with TDNiCr, to manufacture rib stiffened panels from these alloys might require a development effort beyond the scope of this program. Therefore, the decision was made to fabricate the rib stiffened panels only from Ti-6Al-4V and L605.

4.5 SUBSIZE PANEL FABRICATION

Subsize panel specimens were fabricated in the McDonnell Douglas Advanced Material Fabrication Facility using the thin gage sheet material procured for this program. All specimens were formed with the material's longitudinal material rolling direction coinciding with the panel longitudinal direction.

Corrugation stiffened panels were fabricated from each of the materials without difficulty, using continuous spot welding techniques to join the skin to the corrugation and the end plate to the corrugation. Corrugations were formed, using available tooling, to the dimensions shown in Figure 4-2.

The rib stiffened panel ribs and skins were joined by electron beam welding

using the "burn through" technique. Curvature or bowing (midspan deflection of approximately 0.1 cm toward the rib side of the panels) along the length of the rib stiffened panels was evident after fabrication. This was attributed to material shrinkage in the weld zone. The titanium panels were subsequently flattened and stress relieved at 1300°F. Oxide removal by pickling followed the flattening process, resulting in the removal of approximately .001 inch of material. This yielded somewhat thinner gages than previously reported for specimens tested under steady state conditions in Phase I (Reference 1). No attempt was made to flatten the L605 rib panels because the temperatures required produce a microstructure different from that used in the Phase I cyclic tensile tests. Therefore, to keep material in the panel structure consistent with material used in the original cyclic tests, the decision was made to not straighten the L605 panels. As will be discussed in Section 6.1, however, L605 rib stiffened panels were tested both in positive bending (skin in compression) and in negative bending (skin in tension) to provide a comparison of creep deflections for determining any detrimental effects or initial curvature on creep deflection results.

4.6 ROOM TEMPERATURE ELASTIC DEFLECTION TEST

To provide increased confidence in the elastic distribution of stresses existing in the thin gage corrugation subsize panels, a room temperature bending test was performed on an L605 panel to check test deflections with predicted elastic deflections.

The panel loading arrangement and resulting midspan deflection vs load data are shown in Figure 4-4. Also shown is the predicted load-deflection curve based on the following calculation (Reference 12) for panel midspan deflection at the peak applied load.

FIGURE 4-4 ROOM TEMPERATURE DEFLECTION TESTING OF L605 CORRUGATION SUBSIZE PANEL

$$Y_{\frac{L}{2}} = 2\left(\frac{P}{2}\right)\frac{a\left(\frac{L}{2}\right)}{6\,EI\,L}\left(2\,Lb - b^2 - \left(\frac{L}{2}\right)^2\right) = .0706 \text{ cm } (.0278 \text{ in.})$$

where L = panel length between supports = 27.94 cm (11.0 in.)

a = distance from support to applied load = 11.43 cm (4.5 in.)

b = L - a = 16.51 cm (6.5 in.)

P = total maximum applied load = 40.8 Kg (90 lbs.)

E = elastic modulus = 236. G Pa (34.2×10^6 psi)

I = moment of inertia = .1041 cm^4 ($.0025\ in.^4$)

Deflections were measured at each of the three corrugation locations. This test was performed before the end plates had been welded to the corrugations (Figure 4-1). Therefore, a small amount of curvature existed across the panel width resulting in initial deflections at low load in the outer two corrugations. Based on this test, however, it was noted that there was good agreement between predicted elastic deflections and test results. The 40.8 Kg load yields a predicted tensile stress of 198.6 KPa (28,800 psi) which is approximately 50% of the room temperature material yield strength.

5.0 SUBSIZE PANEL CREEP TESTING

Thirteen corrugation stiffened subsize panels and four rib stiffened subsize panels listed in Table 5-1 were subjected to cyclic bending loads during Phase II. These tests were conducted in vacuum using a specially designed loading mechanism to obtain creep deflection data for comparison with predictions. Presented in this section are test profiles, deflection requirements, and discussion of the test equipment used.

TABLE 5-1 SUBSIZE PANEL TEST SUMMARY

MATERIAL	PANEL CONFIGURATION	PANELS TESTED	TOTAL CYCLES
L605	RIB	2	150
	CORRUGATION	4	300
RENE '41	CORRUGATION	3	200
Ti-6Al-4V	RIB	2	150
	CORRUGATION	4	200
TDNiCr	CORRUGATION	2	150
	TOTAL	17	1250

5.1 TEST PROFILES

Two types of profiles were used in subsize panel testing. These profiles were (1) constant stress and temperature for twenty minutes with a constant, low atmospheric pressure as shown in Figure 5-1(a), and (2) mission profile load, temperature, and atmospheric pressure profiles as shown in Figure 5-1(b). These were the same profiles used in Phase I tensile creep testing except that an additional five minutes was allowed for cool down for a total cycle time of sixty minutes.

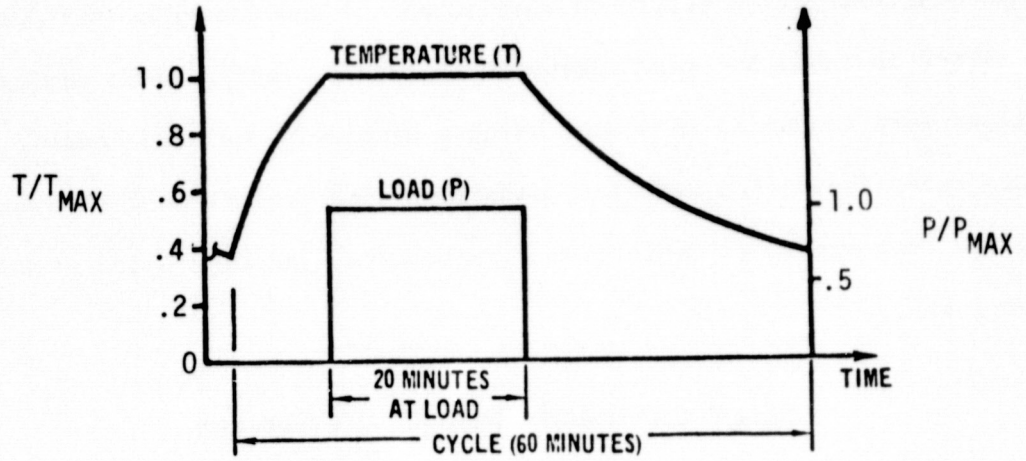

(a) Constant Temperature and Load Profiles

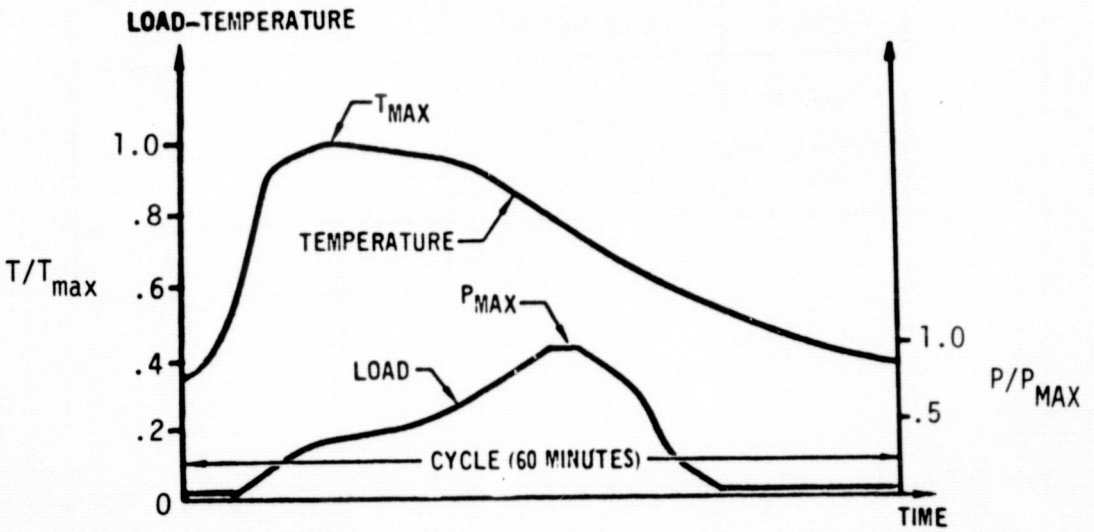

(b) Mission Temperature and Load Profiles

FIGURE 5–1 SUBSIZE PANEL TEST PROFILES

The mission load profile presented in Figure 2-5 was based on the Shuttle Orbiter lower surface entry pressure profile aft of station 929 (inches) and the mission temperature profile, presented in Figure 2-6, was based on the orbiter bottom centerline entry temperature at X/L = .50. These profiles were used as typical for testing all four materials. Load and temperature were ratioed up or down to meet specific testing requirements for each material.

5.2 TEST DEFLECTION REQUIREMENTS

The purpose of subsize panel testing during this Phase was to provide deflection data for verification of prediction capability. In line with this purpose, the primary requirement of panel testing was that, for each material, creep strains attained were in the range of data obtained in Phase I tensile creep tests. This was necessary because empirical equations developed in Phase I for cyclic creep response were used in analysis during Phase II. In conjunction with this it was also desirable to obtain realistic permissible deflections as defined by the criterion, $\zeta = .25 + .01L$ presented in Section 2.3. The following approach was used to establish test load levels for the mission profiles. For the 30.5 cm (27.9 cm between supports) subsize panels, the allowable creep plus elastic deflection per this criterion is .53 cm. Therefore, a reasonable range of creep deflection desirable to attain was from approximately .25 to .50 cm. Load levels required to yield desired test deflections were obtained based on the assumption that creep deflections obtained in testing would be approximately 50% of those obtained using a linear creep stress-strain assumption. This assumption tends to account for the redistribution of beam stresses due nonlinear creep strain-stress properties. The assumption is expressed in the following equation:

$$\frac{\Delta_c}{\varepsilon_c} = .5 \frac{\Delta_E}{\varepsilon_E} \qquad (5\text{-}1)$$

where: Δ_E = BEAM midspan elastic deflection

ε_E = Maximum midspan elastic strain (extreme fiber)

Δ_c = Beam midspan creep deflection

ε_c = Maximum midspan creep strain (extreme fiber)

Applying equation 2-1 and assuming an elastic deflection based on a uniform pressure loading the following equation was derived for creep strain at the beam midspan.

$$\varepsilon_c = \frac{2\Delta_c}{\Delta_E} \quad \varepsilon_E = \frac{2\Delta_c}{\left[\frac{5}{384}\right]\frac{WL^4}{EI}} \quad \left[\frac{WL^2}{8\ EI}\overline{Y}\right] = 19.2\ \frac{\Delta_c \overline{Y}}{L^2} \tag{5-2}$$

where: W = Beam pressure load

L = Panel length

E = Elastic modulus

I = Panel moment of inertia

$\overline{Y}$ = Maximum distance from neutral axis to extreme fiber

Calculated creep strains from equation 5-2 were entered in plots of creep strain vs stress obtained from phase I tensile creep tests for the same mission profiles and temperature. The corresponding stress level (σ) was then applied to calculate the required beam bending moment (M):

$$M = \sigma \frac{I}{\overline{Y}} \tag{5-3}$$

It is of interest to note that if this calculation was carried out for a full sized 51 cm (20 inch) TPS panel, the creep strain required to attain the same creep deflection is lower because the strain is inversely proportional to the square of beam length.

Therefore, use of the deflection criterion (Equation 2-1) with subsize panels results in requirements for greater creep strains than would be attained in a full size panel under the same criterion. As long as the cyclic creep test data and corresponding empirical equation developed in Phase I was applicable over the creep range required (as in the case of L605), the criterion was used. That is, subsize panel creep deflections of up to approximately .5 cm were acceptable. However, in the case of Rene' 41 panels, where the Phase I cyclic tensile specimen creep data was generally less, lower deflections were used in order to stay within the limits of empirical equation prediction capability.

5.3 TEST EQUIPMENT

5.3.1 ASTROFURNACE

Subsize panel creep tests were conducted in the MDC 17.8 cm diameter Astro Industries graphite tube furnace, modified by the MDC Materials Laboratory for this type of testing. The furnace and associated controlling equipment are shown in Figure 5-2. The furnace consists of a ceramic tube sealed at both ends with water-cooled steel plates, and heated by radiation from the resistance-heated graphite element in the Astrofurnace. The furnace test zone diameter is 11.4 cm (4.5 inches). This furnace allows simultaneously varying temperature, pressure, and load. All test conditions are automatically programmed and controlled. Pressure is controlled by a pressure transducer in the Alphatron gage which sends an electrical signal to the pressure controller, which, in turn, compares this signal with one previously programmed on the Data-Trak. The transducer triggers a servovalve which opens or closes as required to control the airflow. The airflow rate through the test section at 10-torr pressure is 1640 cm^3/min. (100 $in.^3$/min.) for the large furnace.

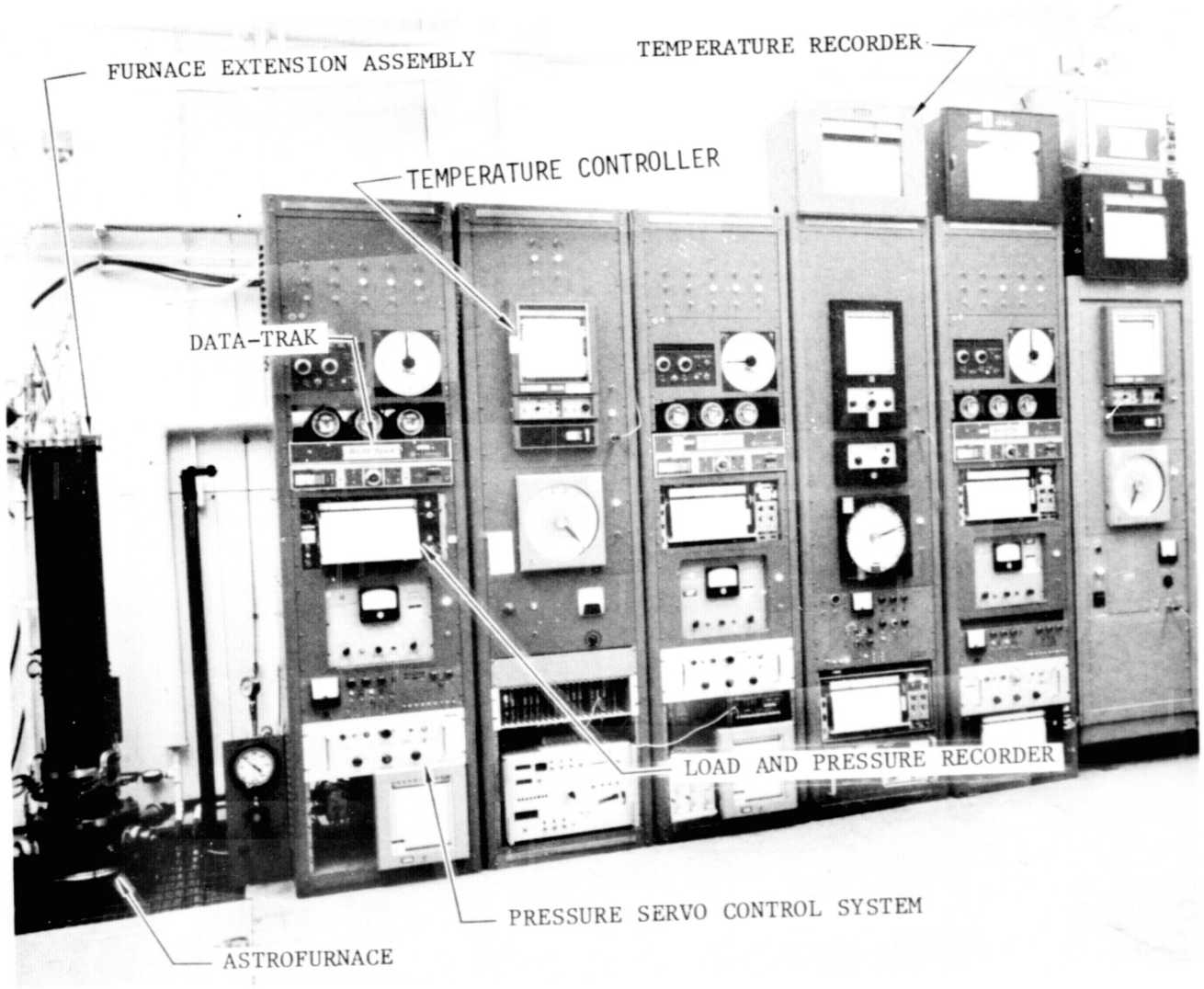

FIGURE 5-2 ASTRO FURNACE FOR PANEL SPECIMEN CREEP TESTING

Loads are applied with the use of a 20 rpm reversible motor. A strain link between the motor and load rod (outside the furnace) compares the applied load with that programmed on the Data Trak and controls the motor accordingly.

Temperature is controlled by a platinum thermocouple in the furnace which is connected to a recorder and the Data-Trak. The furnace has a uniform temperature zone up to 1700 K (2600°F) that is 30.5 cm (12 inches) long.

Data acquisition during the cyclic creep testing was obtained from a specially designed digital data acquisition system. This system contained 50 channels which were scanned every 50 seconds. The accuracy of this system is $\pm$ 0.15%. The system recorded the data on tape, and also contained an 8-character digital printer which was used to check the taped data. During testing the digital acquisition system recorded outputs from the strain indicator and a thermocouple positioned on this indicator.

A Scientific Control Corporation Digital Computer (SCC-670-2) was programmed to calculate mean loads and standard deviations from the cassette tape data. A portion of a typical load data printout, for a constant load profile (Figure 5-1a), obtained from the digital acquisition system is as follows:

CYCLE	MEAN	SIGMA
1	188.392	0.148
2	189.515	0.158
3	189.939	0.134
4	189.833	0.115
5	189.818	0.148
6	189.449	0.187
7	189.596	0.152
8	189.707	0.123
9	189.632	0.170
10	189.535	0.093
11	189.476	0.097
12	189.435	0.165
13	189.438	0.113
14	189.321	0.104
15	189.126	0.106
TOTAL:	189.481	0.134

Mean load for each cycle is calculated from readouts at 50-second intervals during the twenty minute period at maximum load. The "sigma" shown is the standard deviation of these readings about the mean. In tests using the mission profiles (Figure 5-1(b)), average load-time profiles were obtained by data averaging loads at common times in each cycle at 30 second intervals over the duration of the test. Load reproducibility was within 1%, based on replicate L605 panel test data.

Within the hot zone of the furnace were two platinum-platinum-10% rhodium thermocouples. One of these thermocouples was used to measure the temperature within the hot zone, while the other controlled the furnace. Both of these thermocouples were connected to a thermocouple reference junction compensator, which maintained a constant reference to within $\pm$0.14°K. From this compensator the output of the measuring thermocouple was fed to a Honeywell strip chart recorder (Model #15, 30.48 cm. scale). Prior to testing the temperature recording system which included thermocouples, reference junction, and Honeywell strip recorder was calibrated and found to be accurate to within 1.7°K.

The output from the control thermocouple was fed from the reference junction to a Leeds and Northrup recorder/controller. This controller compared the electrical signal from the controlling thermocouple to one that was previously programmed into the Data Trak and adjusted the power input to the furnace to compensate for the differences in signal. The temperature control was found to be accurate to within $\pm$ 1% of the desired temperature.

Calibrations were conducted to determine the magnitude of temperature variations on the subsize panels. Calibrations were accomplished using platinum/platinum-10% rhodium thermocouples spotwelded to the panel. Testing was performed under a constant pressure of 1.33 Pa and temperature measurements were made after the furnace stabilized. Temperatures measured are presented in Figure 5-3 for each of the four materials. Plots of the panel length-wise temperature variations are provided in Figure 5-4.

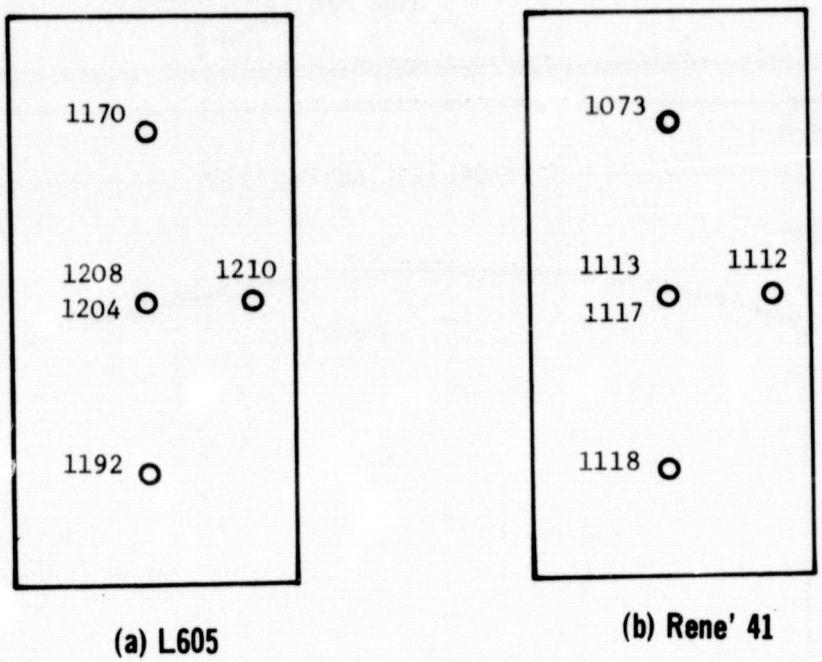

(a) L605

(b) Rene' 41

TEMPERATURES IN °K

(c) Ti-6Al-4V

(d) TDNiCr

FIGURE 5–3 SUBSIZE PANEL TEMPERATURE MEASUREMENTS

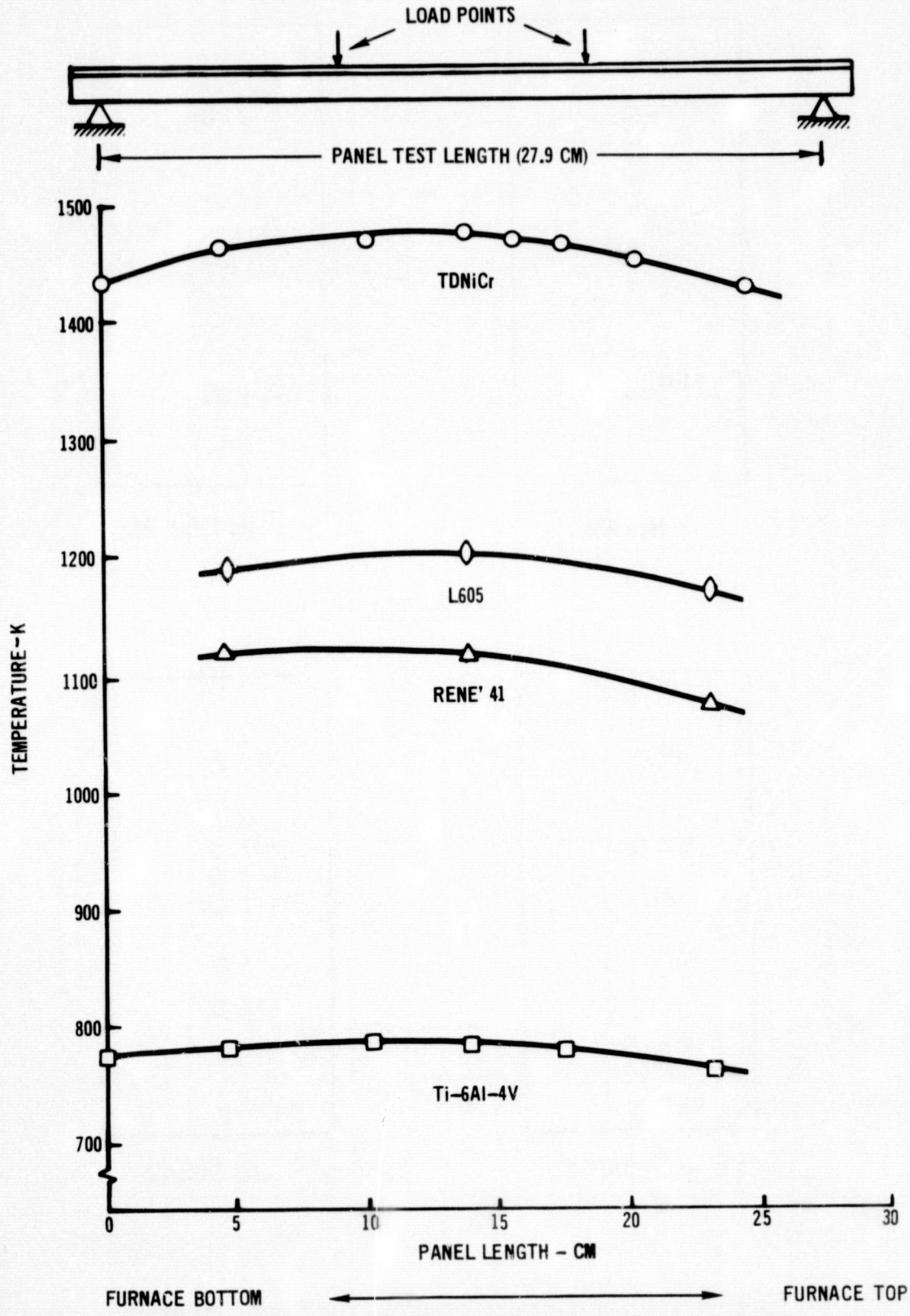

FIGURE 5–4 LONGITUDINAL TEMPERATURE DISTRIBUTIONS ON SUBSIZE PANEL SPECIMENS

Pressure within the test chamber was controlled by a regulated leak rate operated by a servo-valve coupled to an Alphatron Vacuum gage (Model 530). The Alphatron gage sent an electrical signal to a Gran-Phillips automatic controller (series 213). The controller compared the signal from the Alphatron with that programmed on the Data Trak. The controller actuated the servo valve as required to control the air pressure. Some manual control of a bleed valve was necessary in testing of panels to mission pressure profile (pressure variation from 1.33 Pa to one atmosphere). In these profiles the controller maintained a programmed change in pressure from 1.33 to 66.5 Pa. At that point the operator changed scales and the controller continued the program from 66.5 to 2666 Pa. Beyond this point the vacuum pump was shut off and the pressure was allowed to stabilize at atmospheric pressure.

5.3.2 LOAD MECHANISM

Creep deflection testing was accomplished using the mechanism shown in Figure 5-5(a) and (b) to convert axial load, applied by the furnace hydraulic load actuator, to a bending load on the subsize panel. This mechanism was specifically designed to minimize the dependence of applied panel moment on panel deflection. This independence of panel moment and panel deflection was required to maintain applied load accuracies since panel creep deflections continuously changed during testing and were therefore unknown between times at which deflection measurements were recorded.

The mechanism consists of loading straps which attach to the furnace loading rod and serve to transfer applied axial load into the mechanism. Loads are transfered through shear pins to the bending plates and loading pins where they are reacted by axial load in the connecting links and bending loads on the subsize panel as shown in Figure 5-6. Retaining clips are used to secure connections between

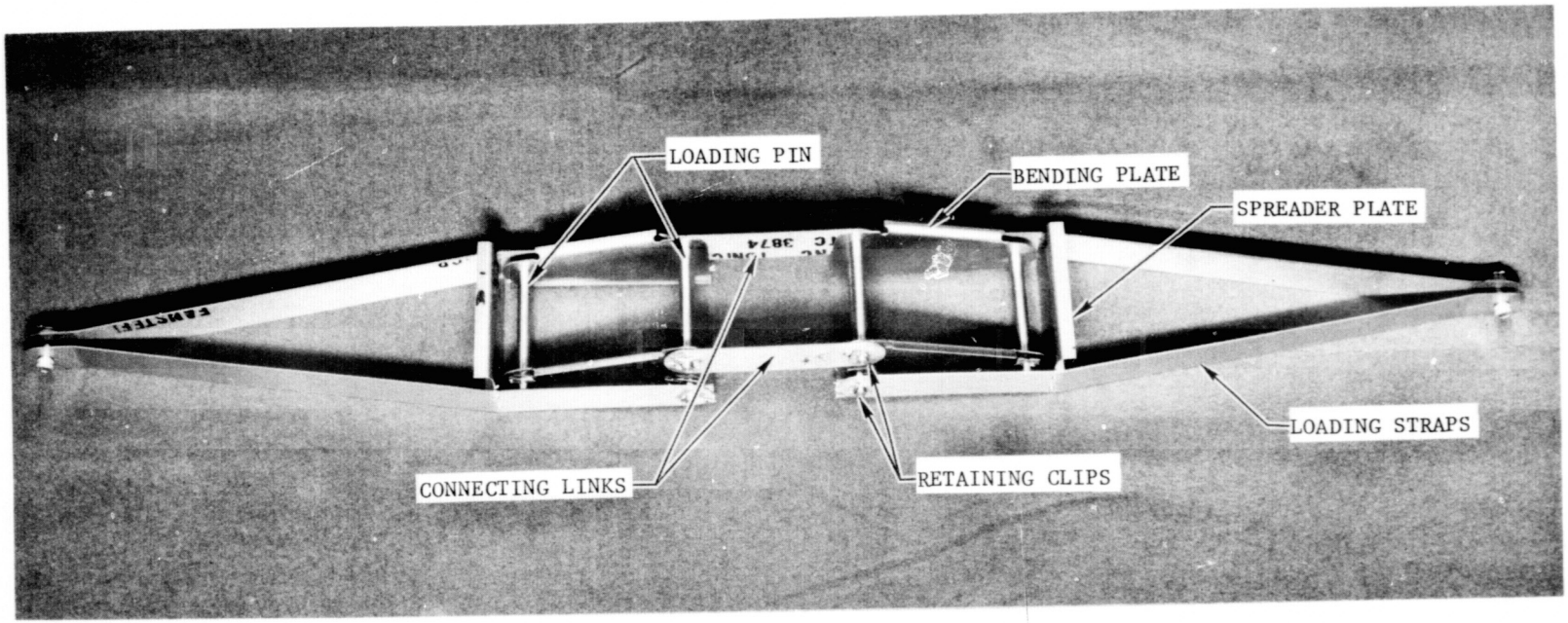

FIGURE 5-5(a) LOAD MECHANISM FOR SUBSIZE PANEL TESTING

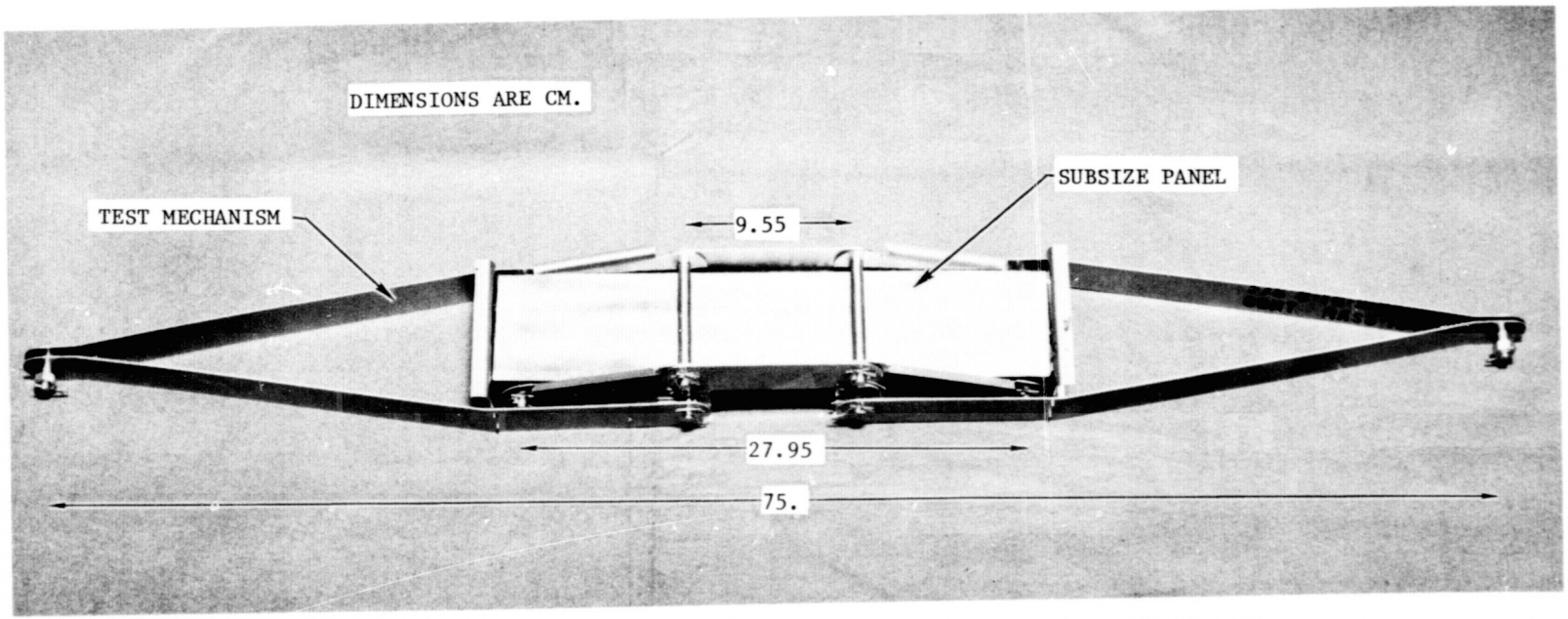

FIGURE 5-5(b) LOAD MECHANISM WITH SUBSIZE PANEL INSTALLED

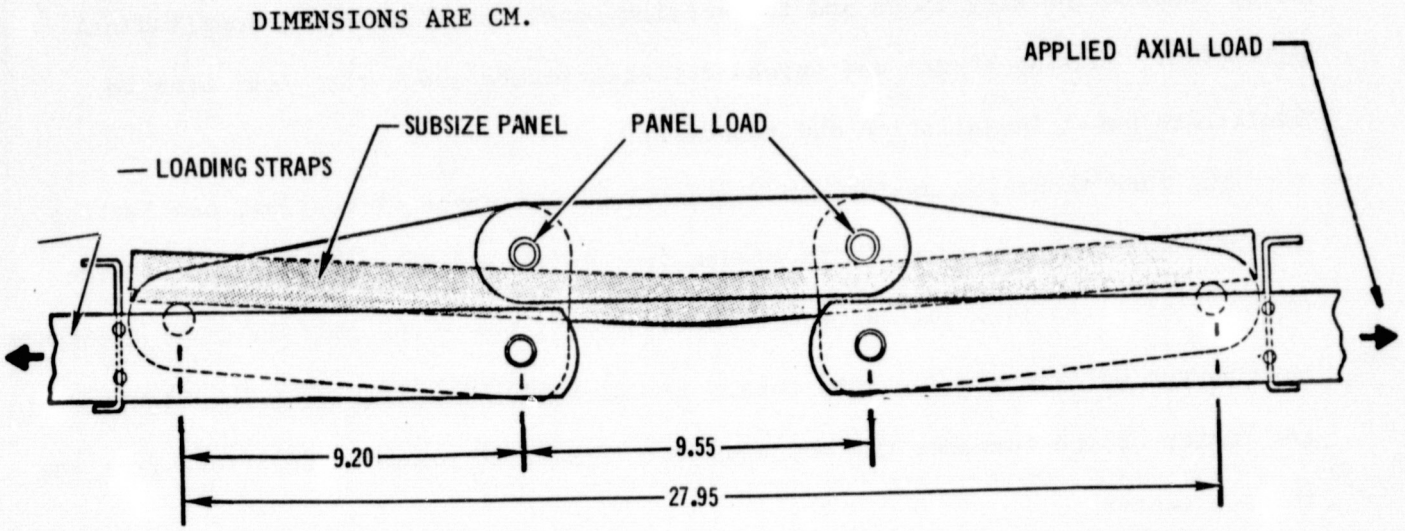

FIGURE 5–6(a) MECHANISM CONVERTS AXIAL LOAD TO PANEL BENDING LOAD

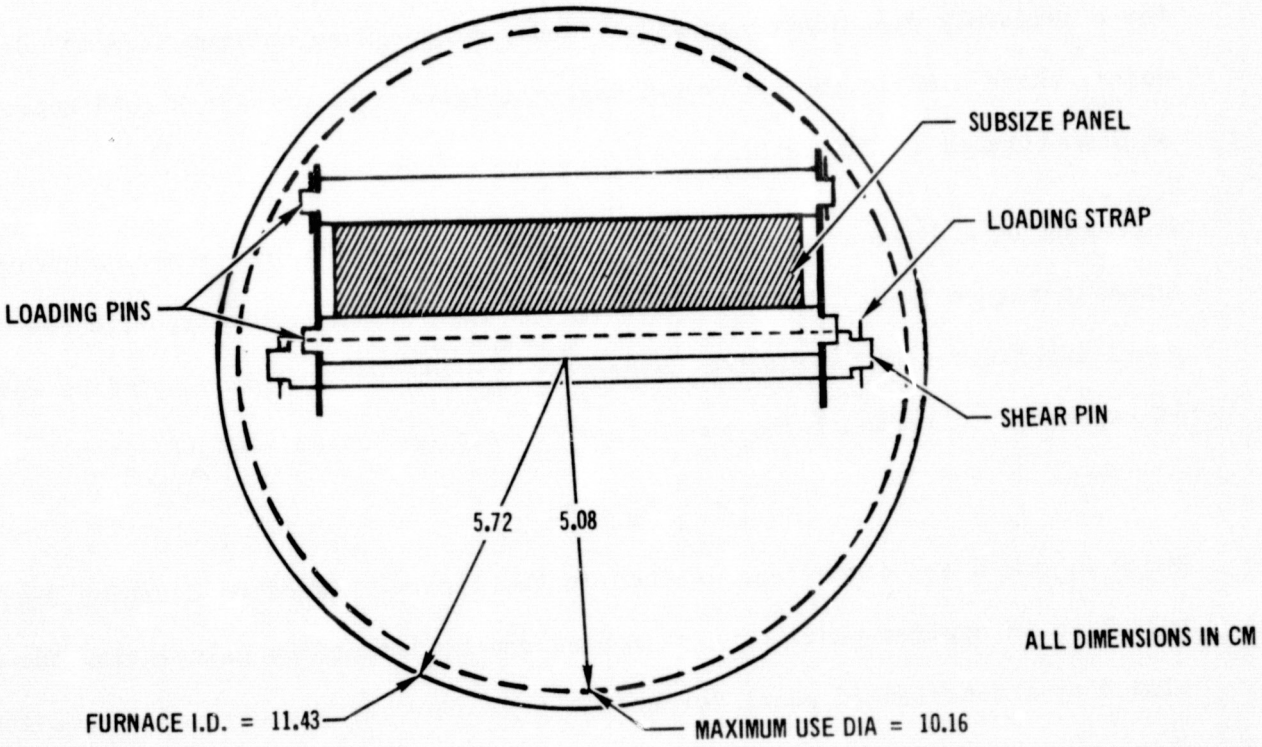

FIGURE 5–6(b) POSITION OF MECHANISM AND PANEL IN TEST FURNACE

the pins and the straps and plates. Spreader plates are provided to react loading strap compression kick loads and to restrict panel movement in the longitudinal direction. Loading straps and spreader plates rotate about the shear pins to facilitate panel installation and removal.

The load mechanism design (in conjunction with panel dimensions, see Section 3.0) was constrained, as shown in Figure 5-6, by the furnace muffler tube inside diameter of 11.43 (4.5 inches) and the requirement for a .64 cm (.25 inch) clearance between the mechanism and muffle tube. The mechanism loading straps are located at the center of the furnace, thereby causing the subsize panel to be offset from the furnace center.

Loading pin locations for applying load to the subsize panel specimens were established to provide a bending moment distribution which would approximate that for a uniformly distributed pressure load. Although an optimum location does not exist, those used in the mechanism design (Figure 5-6) provide a good approximation, as demonstrated in Figure 5-7.

Following is a discussion of the geometry considerations in the mechanism operation. Shown in figure 5-8(a) and (b) are diagrams of mechanism geometry with the subsize panel undeflected and deflected respectively. The applied panel bending moment (M) is expressed in terms of the panel load (P) and mechanism load (F) as

$$M = \frac{P}{2} L_1 = Fd \qquad (5\text{-}4)$$

where L_1 and d are dimensions defined in the figure. Based on Equation 5-4, the variation in applied panel bending moment can be defined by calculating the dimension d as a function of panel deflection (δ). For the purposes of discussion in this section, δ is defined as the deflection under the applied load.

As the panel deflects, the pin locations A and c rotate to A′ and C′ through an angle θ about pin B, as shown in Figure 5-8(b). This yields the following

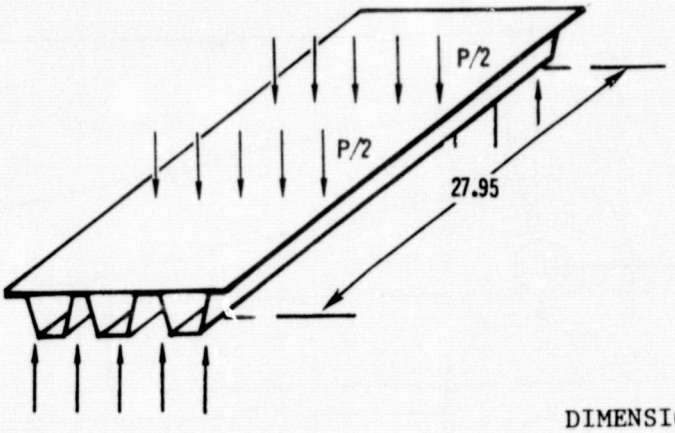

DIMENSIONS ARE CM.

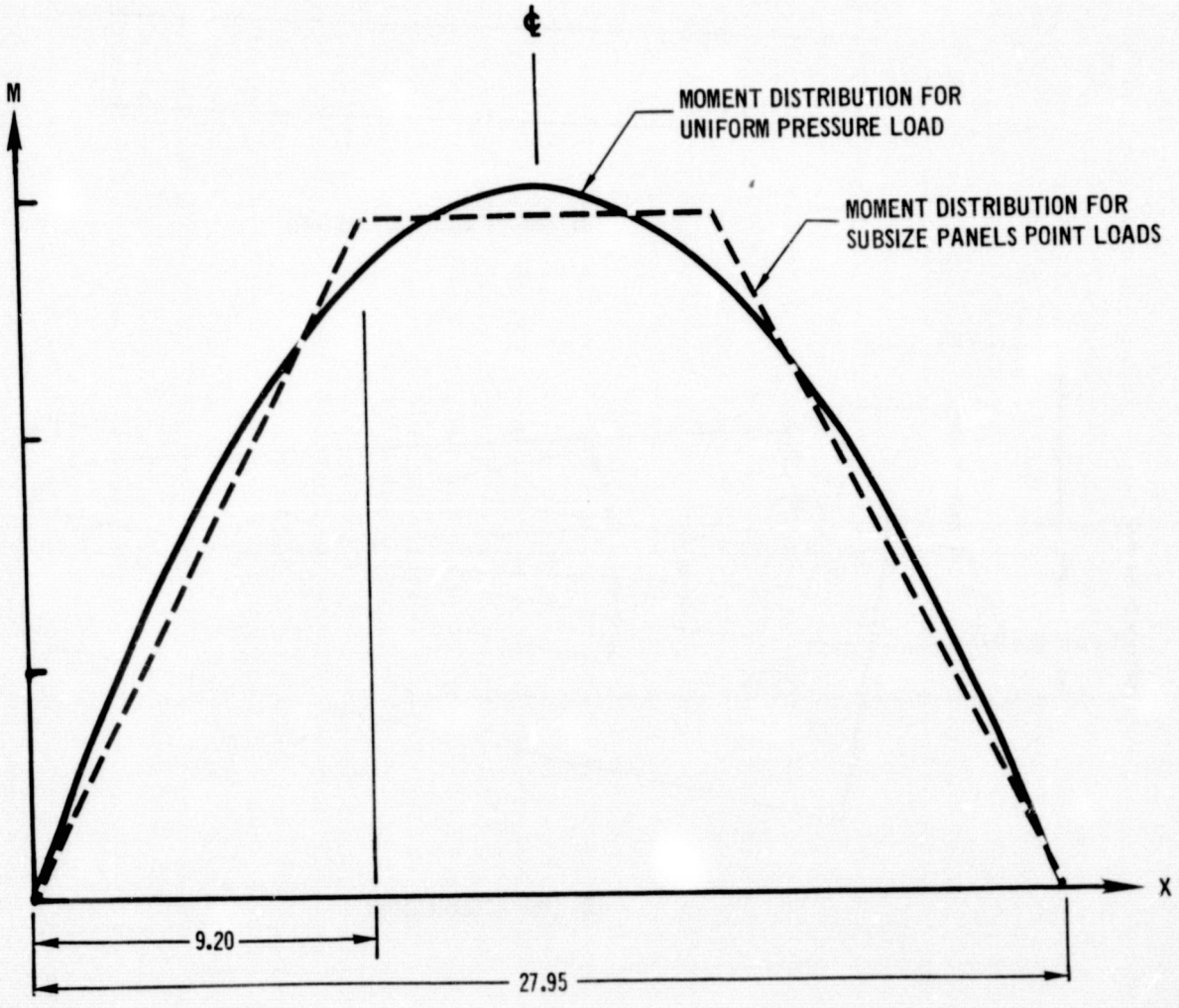

FIGURE 5–7 SUBSIZE PANEL LOAD AND BENDING MOMENT DISTRIBUTIONS

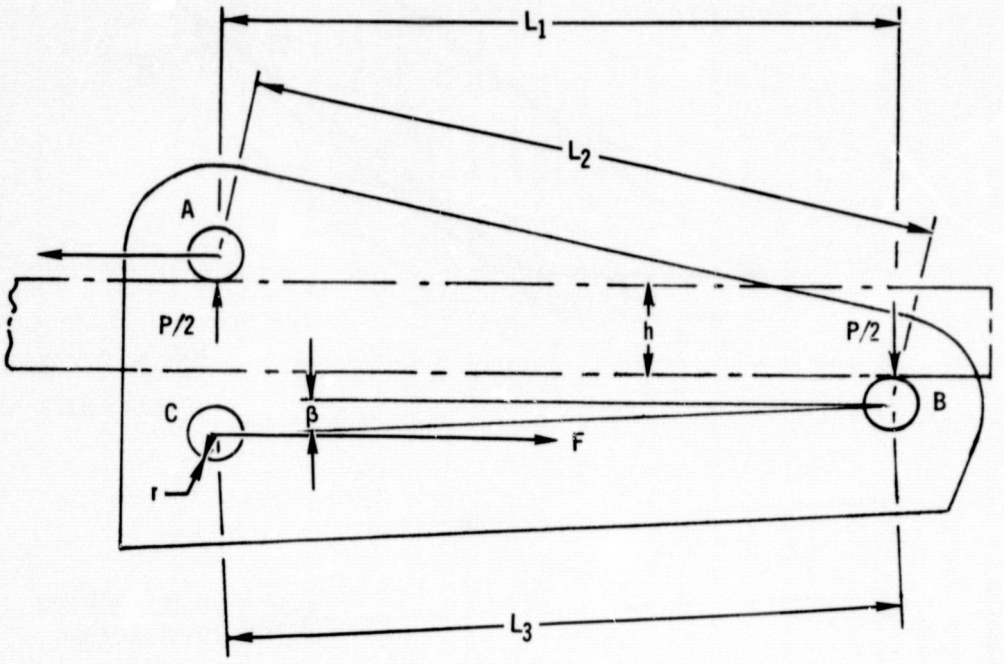

(a) Zero Panel Deflection

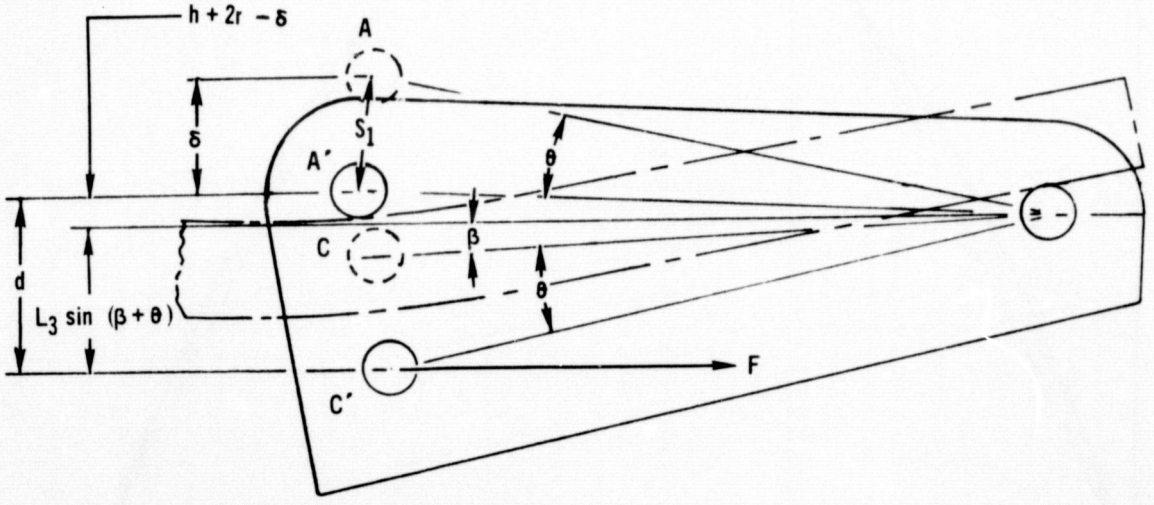

(b) Deflected Panel

FIGURE 5–8 TEST LOAD MECHANISM CONFIGURATION

expression for the dimension d:

$$d = L_3 \sin(\beta + \theta) + h + 2r - \delta$$

$$= L_3 [\sin\beta \cos\theta + \cos\beta + \sin\theta] + h + 2r - \delta \qquad (5\text{-}5)$$

where h, β, r, and L_3 are fixed mechanism dimensions.

Expressions for sin θ and cos θ are:

$$\sin\theta \cong \theta = \frac{S_1}{L_2}$$

$$\cos\theta = \sqrt{1-\sin^2\theta}$$

The dimension S_1, shown in Figure 5-8(b), is calculated as:

$$S_1 = \sqrt{\delta^2 + \left[L_1 - \sqrt{L_2^2 - (h + 2r)^2} \right]^2}$$

where

$$L_1 = \sqrt{L_2^2 - (h + 2r - \delta)^2}$$

Calculations of the ratio of panel bending moment to applied mechanism load (M/F) is listed in table 5-2 as a function of panel deflection (δ) for the mechanism configuration.for a panel depth of 1.19 cm (.47 inches). The results show a variation in bending moment of less than 1% for deflections of up to 1.27 cm (.50 inches).

TABLE 5-2 CALCULATIONS OF PANEL BENDING LOAD AS FUNCTION OF DEFLECTION

Mechanism Dimensions

β = 2.847°

r = .381 cm (.15 inch)

L_2 = 9.401 cm (3.701 inch)

L_3 = 9.205 cm (3.624 inch)

Panel Deflection		d		% Variation
cm	in	cm	in	
0	0	2.413	.9500	0
.25	.1	2.412	.9496	.0380
.51	.2	2.409	.9486	.1456
.76	.3	2.405	.9470	.3153
1.02	.4	2.400	.9448	.5414
1.27	.5	2.393	.9422	.8175

5.3.3 PANEL DEFLECTION MEASUREMENTS

The cumulative creep strain of each specimen was measured after 1, 5, 15, 25, 50, 75, and 100 cycles (variations from this plan were made in some cases and are shown with the specific test data). To make the creep strain measurements, specimens were removed from the furnace. This was accomplished by separating the furnace extension assembly from the top of the furnace (Figure 5-2) and raising the assembly until the panel could be removed from the loading mechanism.

To facilitate measurements a box was fabricated as shown in Figure 5-9(a). This box consisted of a top and bottom plate with panel support points located at 27.94 cm (11.0 inches) spacing to coincide with panel load support points. The panel was supported in this box as shown in the figure for making deflection measurements. Deflections were determined at hole locations in the top plate by using a dial gage to determine distances from the top surface of the plate to the panel skin. Readings were subtracted from reference readings made prior to testing to determine panel deflections. This approach simplified the measurements, provided consistent locations for deflection data, and allowed measurement of either positive or negative deflections.

Deflections were recorded at several locations on the panel, selected to allow adequate definition of the deflected shape. The sketch in Figure 5-9(b) indicates the location of measurement points relative to the panel cross section and points of load application. Measurement locations across the panel width were selected to coincide very closely with the stiffeners for both the rib stiffened and corrugation stiffened subsize panels. For the rib stiffened panels, deflections at each panel station were computed as the average of measurements at three points, the center and outer locations. For the corrugation stiffened panels, deflections at each station were computed as the average of measurements at four points, all but the center location.

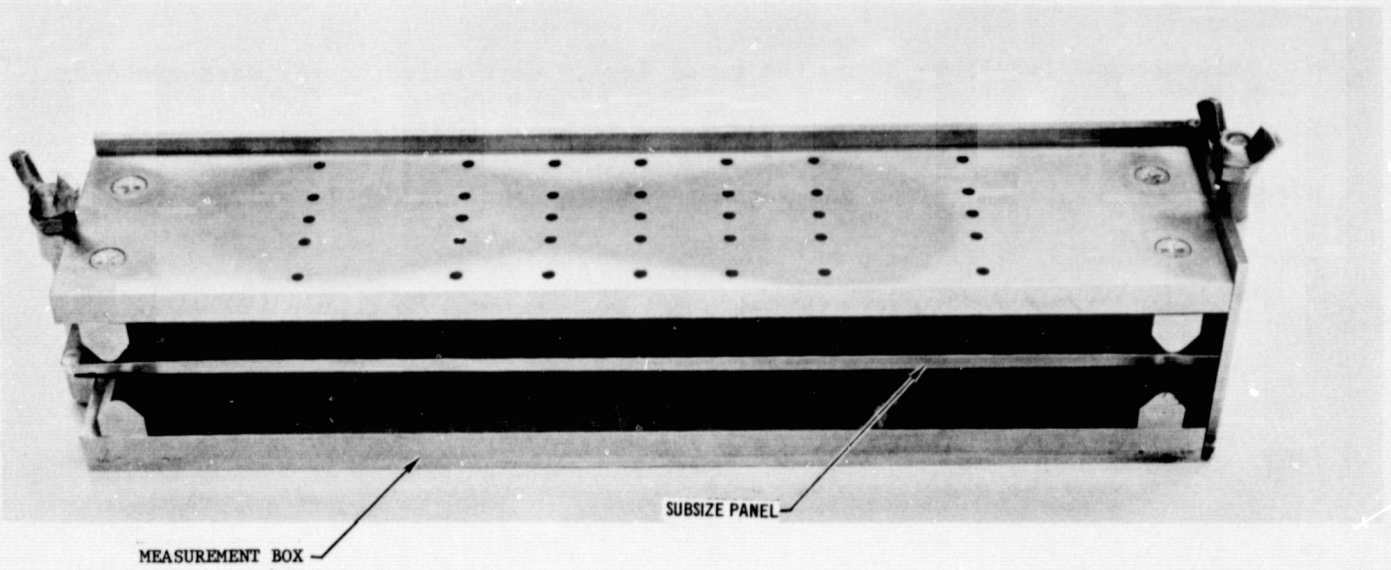

(a) Box Designed for Measurements

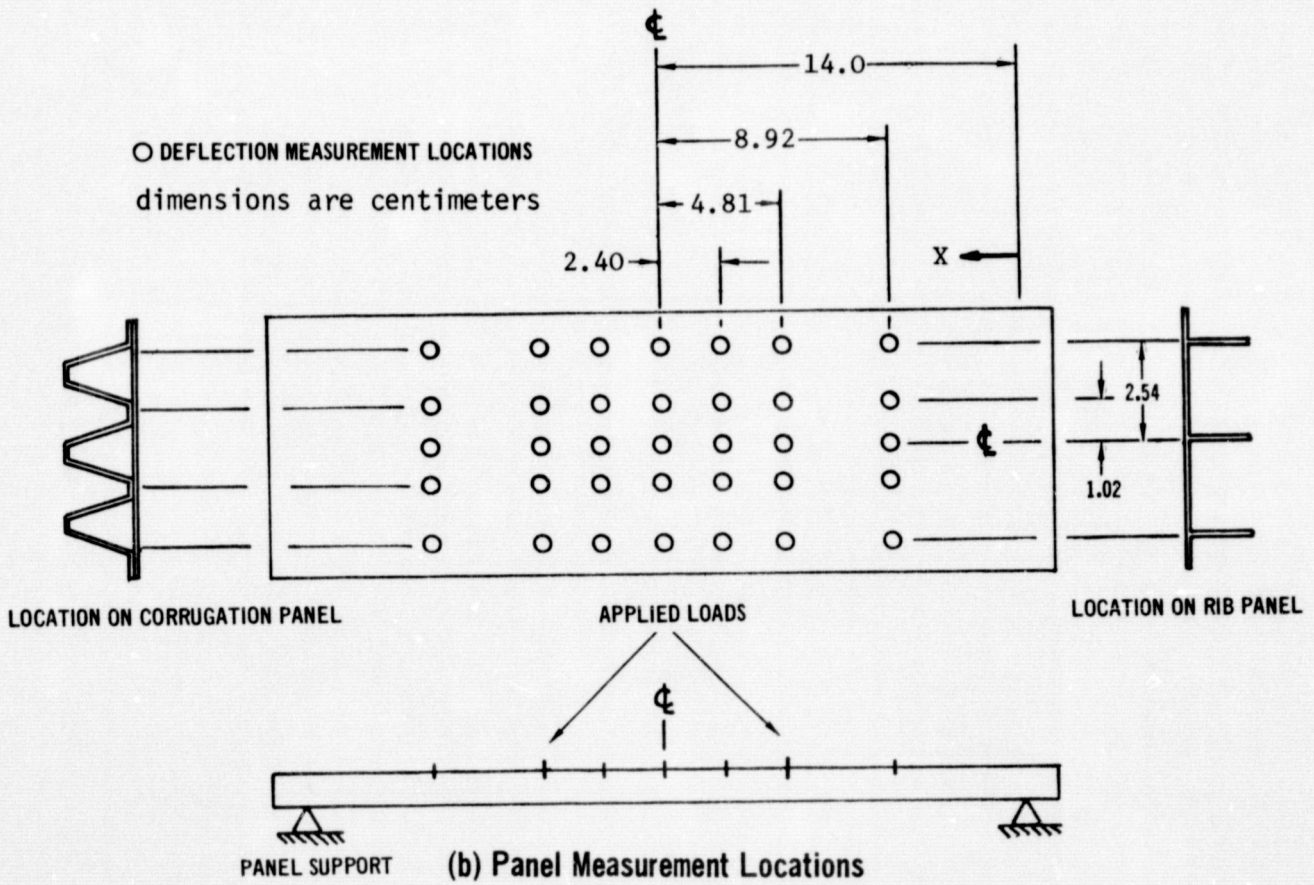

(b) Panel Measurement Locations

FIGURE 5–9 APPROACH FOR CREEP DEFLECTION MEASUREMENTS

Measurement locations along the panel length were selected for adequate definition of the deflected shape. This was accomplished by providing measurements at the point of load application and panel center line as well as one location between these points and between the panel support and loading point.

6.0 TEST RESULTS AND DISCUSSION

Discussed in this section are test results for the six L605, three Rene' 41, six titanium, and two TDNiCr subsize panels tested in Phase II. Deflection data, trajectory data, and photographs for each panel test are presented in Appendix B.

Cyclic panel tests were conducted on the corrugation and rib-stiffened specimens using the two types of mission profiles shown in Figure 5-1. These are: 1) constant temperature, load and atmospheric pressure (1.3 Pa) profiles where time at load and peak temperature is 20 minutes; and 2) actual temperature, load, and atmospheric pressure profiles. These same type profiles were used in Phase I tensile specimen cyclic testing, with the exception of cool-down time which was increased by five minutes to allow additional panel cooling time. Total time per cycle for each set of profiles was 60 minutes. Temperature and load levels for each test were selected to yield desired creep deflections as discussed in Section 5.1. A set of measured atmospheric pressure data are listed in Table 6-1. These data are considered typical for all mission profile tests.

Dimensions of each panel were recorded at several locations along the panel length and across the width. The dimensions provided are based on averages accounting for minor variations in geometry, such as corrugation spot weld spacing.

Temperatures, loads, and panel bending moments are presented for each test. Two point panel loads were applied, as shown in Figure 5-7, using the mechanism discussed in Section 5.3.2.

Beam load and bending moment data are calculated from mechanism axial load data using the mechanism geometry considerations as discussed in Section 5. Mechanism axial load is the average of recorded values taken at 50 second intervals in each trajectory. Temperatures presented in the appendices are based on measurements taken at the midspan panel skin. Temperatures are typical for each test with a system accuracy of $\pm 3°F$. Variations in temperature along the panel length

TABLE 6-1 MEASURED ATMOSPHERIC PRESSURE PROFILE - TYPICAL FOR PANEL PROFILE TESTS

CYCLE TIME (SEC.)	ATMOSPHERIC PRESSURE		CYCLE TIME (SEC)	ATMOSPHERIC PRESSURE	
	TORR.	Pa.		TORR.	Pa.
100	.024	3.20	1900	.950	127.
200	.021	2.80	2000	2.00	267.
300	.022	2.93	2100	5.00	667.
400	.023	3.07	2200	10.0	1333.
500	.029	3.87	2300	120.	15996.
600	.036	4.80	2400	320.	42600.
700	.046	6.13	2500	550.	73300.
800	.056	7.46	2600	705.	93980.
900	.064	8.53	2700	740.	98640.
1000	.070	9.33	2800	760.	101300.
1100	.075	10.0	2900	760.	101300.
1200	.085	11.3	3000	760.	101300.
1300	.093	12.4	3100	760.	101300.
1400	.135	18.0	3200	15.	2000.
1500	.250	33.3	3300	.400	53.3
1600	.400	53.3	3400	.053	7.06
1700	.560	74.6	3500	.033	4.40
1800	.740	98.6	3600	.028	3.73
			3700	.024	3.20

were measured during system calibration. These data are discussed in Section 5.3.1. Variations in temperature across the panel width (∿4°F) and through the panel depth (∿8°F) were very small relative to variations along the length.

Deflection data are tabulated for each panel as a function of cycle at seven stations along the length. Deflections at each beam station are averages of measurements taken at four locations (three for rib panels) across the panel width as discussed in Section 5.3.3. Section 7 contains plots of deflection versus cycle and deflections along the length.

A photograph of each panel is provided showing top view after testing. None of the panels tested exhibited cracking or spot weld failure. Skin waviness was noted after testing in some of the panels, particularly in the titanium single skin corrugation panels. Formation of oxides was noted for all panels tested. These observations will be discussed, for each alloy, in the following sections.

The series of panel tests for each material are designated by the material name and a number, starting with the number 21 (e.g., L605-21). This designation was established to avoid any test number confusion with Phase I tensile creep tests.

6.1 L605 SUBSIZE PANEL TEST RESULTS

Four single skin corrugation and two rib-stiffened subsize L605 panels were tested as outlined in Table 6-2. Test temperatures were selected to be the same as those used in testing tensile creep specimens in Phase I of the program. In conjunction with the temperature levels, loads were applied to yield approximately .5 cm deflection in 100 cycles. A uniform green oxide coating was observed on all the L605 panel specimens tested. These coatings ranged from light to dark green depending on the test temperature and atmospheric pressure. No skin waviness could be detected in the L605 panel specimens.

TABLE 6-2 L605 SUBSIZE PANEL TEST SUMMARY

TEST	PANEL SPECIMEN		TRAJECTORY					CYCLES	FINAL MIDSPAN CREEP DEFLECTION	
	DESIGNATION	CONFIGURATION	PROFILES	PEAK LOAD (P)		PEAK TEMPERATURE				
				LBS.	Kg.	°F	K		IN.	CM.
L605-21	L1	Corrugation	Mission (Fig. 5-1b)	74.3	33.7	1700.	1200.	100	.2259	.5738
L605-22	L2	Corrugation	Constant (Fig. 5-1a)	19.8	8.98	1800.	1255.	50	.9775	.1969
L605-23	L3	Corrugation	Constant (Fig. 5-1a)	65.7/ 79.6	29.8/ 36.1	1435.	1053.	100	.1551	.3940
L605-24	L4	Corrugation	Mission (Fig. 5-1b)	74.4	33.7	1700.	1200.	50	.1408	.3576
L605-25	L6	Rib	Mission (Fig. 5-1b)	52.8	24.0	1700.	1200.	50	.1273	.3233
L605-26	L7	Rib	Mission (Fig. 5-1b)	52.9	24.0	1700.	1200.	50	-.1162	.2951

TABLE 6-3 RENE'41 SUBSIZE PANEL TEST SUMMARY

TEST	PANEL SPECIMEN		TRAJECTORY					CYCLES	FINAL MIDSPAN CREEP DEFLECTION	
	DESIGNATION	CONFIGURATION	PROFILES	PEAK LOAD (P)		PEAK TEMPERATURE				
				LBS.	Kg.	°F	K		IN.	CM.
Rene'-21	R1	Corrugation	Mission (Fig. 5-1b)	84.2	37.4	1645.	1169.	100	.1249	.3172
Rene'-22	R2	Corrugation	Constant (Fig. 5-1a)	99.7	45.2	1540.	1111.	50	.0689	.1750
Rene'-23	R3	Corrugation	Constant (Fig. 5-1a)	127.7	56.6	1540.	1111.	50	.1729	.4392

All panels were tested in positive bending (skin in compression) except for panel test L605-26. For this test, load was applied such that the skin was in tension. Load, temperature and pressure profiles applied were the same as for test L605-25. This test was performed because the L605 rib panels exhibited initial curvature due to weld shrinkage. Because of initial resudual stresses in these specimens, it was considered desirable to compare creep deflections for beams tested in both positive and negative bending.

6.2 RENE' 41 SUBSIZE PANEL TEST RESULTS

Three single skin corrugation subsize Rene' 41 panels were tested as outlined in Table 6-3.

All panels were tested in positive bending (skin in compression). Test temperatures were selected to be the same as those used in tests of tensile creep specimens in Phase I of the program. Because the 50 cycle creep strains obtained in Phase I at 1111 K (1540°F) were only up to approximately .2%, a lower panel deflection of approximately .25 cm (.1 inch) was used to select test load level. Uniform oxide coatings were evident on the specimens and slight waviness of the panel skins occurred.

6.3 Ti-6Al-4V SUBSIZE PANEL TEST RESULTS

Four single skin corrugation and two rib-stiffened subsize Ti-6Al-4V panels were tested as outlined in Table 6-4. All panels were tested in positive bending (skin in compression).

The first titanium panel tested (corregation stiffened panel T1, Reference Table 6-4) was loaded to a calculated skin stress of approximately 10,000 psi which was 38% of the calculated skin crippling allowable stress. Wrinkles in the skin were noted after twenty-five test cycles and increased

TABLE 6–4 TI–6AL–4V SUBSIZE PANEL TEST SUMMARY

TEST	PANEL SPECIMEN		TRAJECTORY					CYCLES	FINAL MIDSPAN CREEP DEFLECTION	
	DESIGNATION	CONFIGURATION	PROFILES	PEAK LOAD (P)		PEAK TEMPERATURE				
				LBS.	Kg.	°F	K		IN.	CM.
Titanium-21	T1	Corrugation	Constant (Fig. 5-1a)	94.7	43.0	950.	783.	50	.2283	.5799
Titanium-22	T2	Corrugation	Constant (Fig. 5-1a)	68.6	31.1	950.	783	100	.1856	.4714
Titanium-23	T3	Corrugation	Profile (Fig. 5-1b)	127.2	57.7	950.	783.	100	.1162	.2951
Titanium-24	T4	Corrugation	Profile (Fig. 5-1b)	126.9	57.6	950.	783.	50	.0922	.2342
Titanium-25	T7	Rib	Profile (Fig. 5-1b)	66.8	30.3	950.	783.	50	.0803	.2040
Titanium-26	T8	Rib	Constant (Fig. 5-1a)	114.1	51.8	825.	714.	50	.1005	.2553

TABLE 6–5 TDNiCR SUBSIZE PANEL TEST SUMMARY

TEST	PANEL SPECIMEN		TRAJECTORY					CYCLES	FINAL MIDSPAN CREEP DEFLECTION	
	DESIGNATION	CONFIGURATION	PROFILES	PEAK LOAD (P)		PEAK TEMPERATURE				
				LBS.	Kg.	°F	K		IN.	CM.
TDNiCr-21	TD1	Corrugation	Constant (Fig. 5-1a)	22.7	10.3	2200.	1478.	50	.0154	.0391
TDNiCr-22	TD2	Corruation	Mission (Fig. 5-1b)	26.3	11.9	2200.	1478.	100	.0225	.0572

after fifty test cycles. Therefore, this test was suspended at the completion of fifty cycles. Because of this skin buckling, loads in subsequent tests of titanium panels were reduced and only a very slight skin waviness could be detected in titanium tests 22, 23, and 24, as evidenced in the panel photographs in Appendix B. No apparent reason for the occurance of the titanium panel skin waviness was found. However, investigation of the Phase I tensile creep data reveals the creep strain-stress relationship to be more linear than that obtained for L605. Therefore, the preliminary approach for establishing test loads required was modified from that discussed in Section 5.2 to a more linear relationship between creep deflection and elastic deflections.

Oxide coatings were obtained on all of the titanium panels tested. These oxides ranged in color from purple-gold to a silvery blue as will be noted for the individual specimens (Appendix B).

6.4 TDNiCr SUBSIZE PANEL TEST RESULTS

Two single skin corrugation TDNiCr subsize panels were tested as outlined in Table 6-5. Both panels were tested in positive bending (skin in compression).

A peak temperature of 1478 K (2200°F) was used in testing to agree with tensile creep tests conducted during Phase I. Because very low creep strains were attained in Phase I testing, small creep deflections were expected in panel testing. Loads used in testing were, therefore, based on elastic stresses below that which would result in failure, as determined during Phase I, rather than on deflection considerations.

7.0 TEST DATA ANALYSIS

The prime requirement under this phase of the contract was to develop needed capability for prediction of permanent deflections, due to creep, in metallic thermal protection system panels. Toward this goal, the thermal protection system creep (TPSC) computer program was developed. Initiated at MDAC-East in 1971, the program was modified, during this phase to increase its capability. The TPSC program uses iterative techniques and numerical integration to predict creep strains, residual stresses, and permanent deflection, due to creep, in stiffened panel structures. Input includes geometry and definition of loading and temperature profiles. Panel temperature distributions can be defined both along the panel length and through the depth by either polynomial equation coefficients or tabular input. Temperatures are calculated internally at each panel segment based on these distributions and the input temperature time profile data. Also, input are equation coefficients to define material creep response. Appropriate creep strain response data to be used are based on temperatures calculated at each location in the panel. Program output includes a record of geometry input and calculated geometrical data (elastic moment of inertia), trajectory load and temperature data, and creep equation definition as well as the calculated deflections, creep strains, and residual stresses.

The TPSC program was developed specifically for analysis of thermal protection system panels. Therefore, structural definition of leading candidates, corrugation stiffened, rib stiffened, and zee stiffened concepts, is incorporated into the TPSC program. Modeling of the specific panel structural concept for analysis is accomplished automatically based on overall section input definition. An option is provided for including a beaded skin into any of the cross sections since beads are frequently required in thermal protection system panel designs.

Panel bending moments are based on uniform pressure load input or point load input. In addition, the bending moments can be calculated as a function of panel edge stiffness and the ratio of panel stiffness in the longitudinal and transverse directions. This option is based on combining solutions for an isotropic plate with two sides simply supported and two sides elastically supported (Reference 13) and the solution for an orthotropic plate with four sides simply supported (Reference 14). This option provides a first order approach to account for Poisson's effects in orthotropic plate structures. This option will be utilized in analysis of full size panel data during Phase III.

Presented in this section are comparisons of creep deflection predictions with subsize panel test data, based on application of the TPSC program. Review of results includes presentation of related cyclic tensile creep test data obtained in Phase I of this contract. Typical creep strain distributions and residual stress distributions calculated are also presented although comparative test data were not obtained.

7.1 TENSILE CREEP DATA BACKGROUND FROM PHASE I

During Phase I of this program, the influence of entry conditions on creep response was investigated, through cyclic tensile creep testing, for the four subsize panel materials. Based on these background data, several factors were determined that affect specimen creep, and will therefore, affect the subsize panel creep deflection prediction capability of the TPSC computer program. These factors, summarized here, are (a) empirical equation applicability, (b) effect of time at load, (c) hardening theory applicability, (d) applicability of idealizing trajectories, (e) atmospheric pressure, (f) recovery phenomena, and (g) material thickness.

(a) Analysis of cyclic tensile test data for each material resulted in empirical equations which describe cyclic creep response characteristics as a function of stress, temperature, and time. These equations are presented in Table 7-1. Each equation represents a fit of cyclic data based on regression analysis. For each material considerable effort was directed toward determining appropriate equation forms, including stress, time, and temperature interaction terms, to provide a "best fit" over the entire range of data resulting in the different equation forms shown. Typical comparisons of the tensile cyclic data and empirical equation predictions for each material are shown in Figures 7-1 through 7-4.

(b) The empirical equations presented in Table 7-1 were derived from cyclic tensile test data generated at the temperature and stress profiles shown in Figure 7-5. These tests were conducted for 100 cycles of twenty minutes per cycle and, therefore, the total time of applicability of each of the equations is 33.3 hours. This total time of equation applicability will be important in the analysis of subsize mission profile test data where the longer time of the idealized stress and temperature profiles (32 minutes) will result in a reduction of the number of cycles ($\sim$60) over which the equation is applicable. Tests were also conducted for each material using the profile shown in Figure 7-5 with a ten-minute per cycle time at load and peak temperature. These tests were designed to establish applicability of the empirical equations to trajectories other than that for which they were derived. Results of these comparisons for each of the 10 minute per cycle and 20 minute per cycle materials are shown in Figure 7-6 for equal total time at load. Close agreement between these test data was obtained. The variation noted for the titanium data is the greatest of the four materials. However, even this variation was well within the range of expected data scatter. Therefore the derived empirical

TABLE 7-1 CYCLIC CREEP EQUATIONS DEVELOPED FOR PHASE I TENSILE CREEP DATA

MATERIAL	EQUATION (t = time, hours; σ = stress, MPa; T = Temperature, K/1000)	APPLICABLE TEMPERATURE MAXIMUM
L605	(7-1) $\ln \varepsilon = -2.89413 - .01743t + .54892 \ln t + 1.31015 \ln\sigma - 6.66548 (1/T) + .19131 \sigma \ln T + .00021 (T\sigma t)$.	1255 K (1800°F)
TITANIUM	(7-2) $\ln \varepsilon = -28.94077 + 26.24850 T + 2.52 \times 10^{-6} \sigma^2 + 1.40406 \ln\sigma + .46894 \ln t$	839 K (1050°F)
RENE'41	(7-3) $\ln\varepsilon = -39.55860 + 29.13646T + .71922 \ln t + .92125 (\ln\sigma - 1.931) -.000016\sigma^2 + .08183 (\ln\sigma - 1.931)^3 - .000125 t\sigma T + .0000105t^3$	1155 K (1620°F)
TDNiCr	(7-4) $\ln \varepsilon = -3.48443 - 10.37282 (\frac{1}{T}) + .28314 \ln t + 2.00118 \ln\sigma$	1478 K (2200°F)

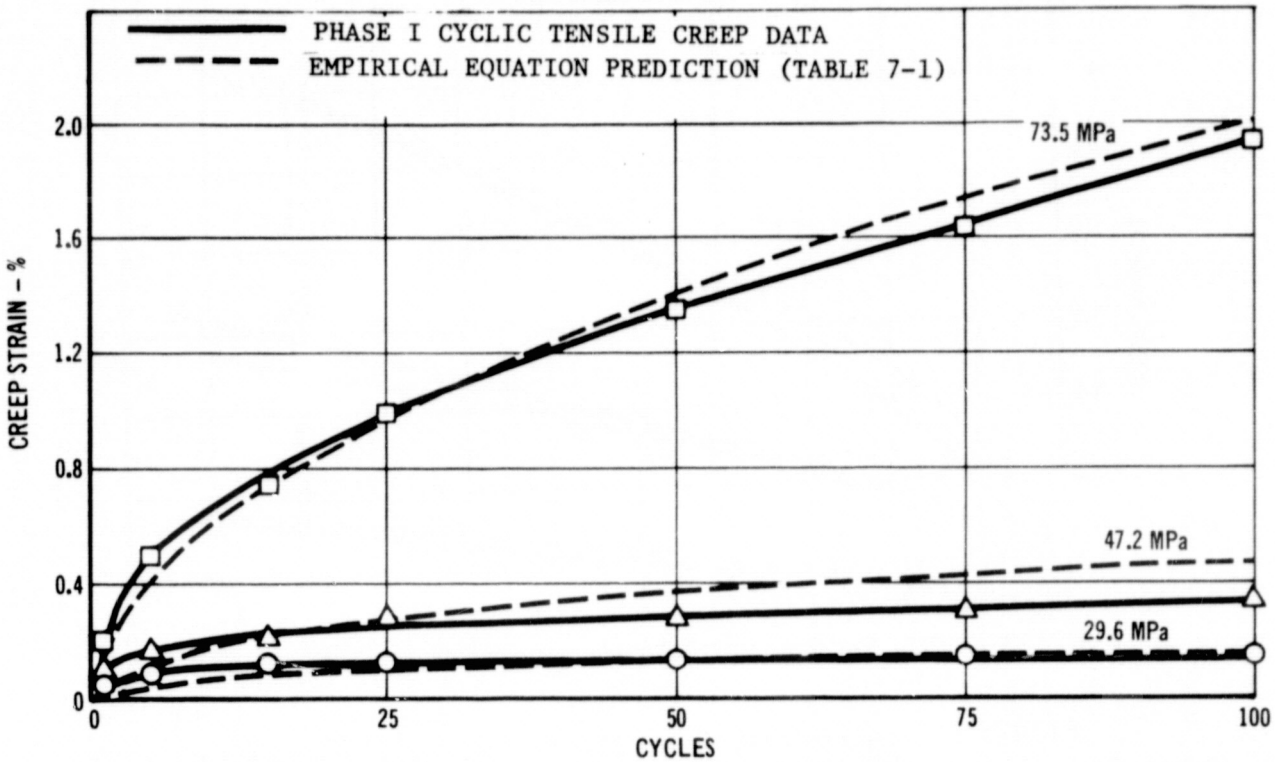

FIGURE 7–1 COMPARISON OF L605 PREDICTED AND CYCLIC TEST CREEP STRAINS AT 1144 K

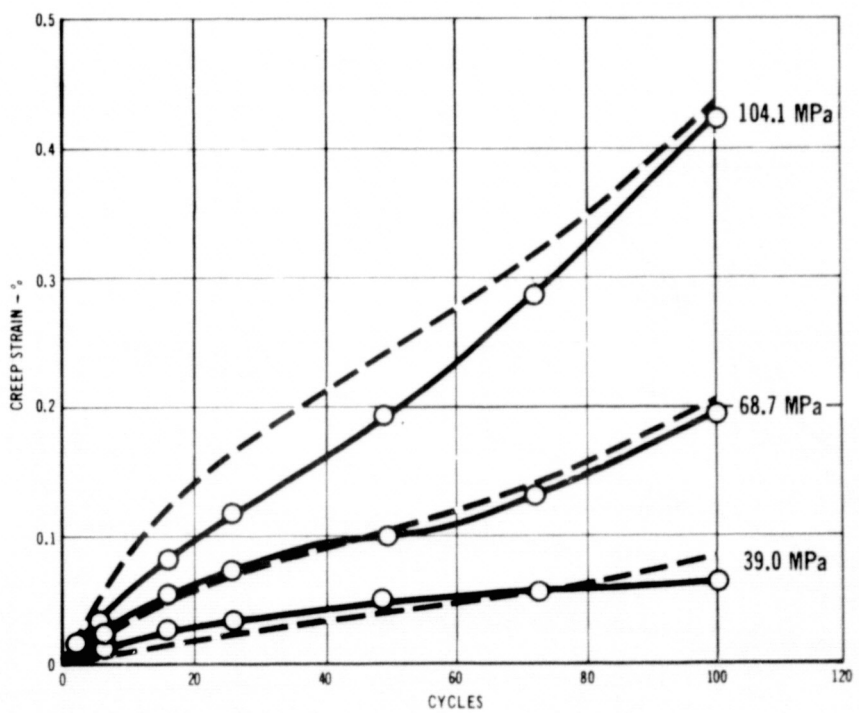

FIGURE 7–2 COMPARISON OF RENE 41 PREDICTED AND CYCLIC TEST CREEP STRAINS AT 1111 K

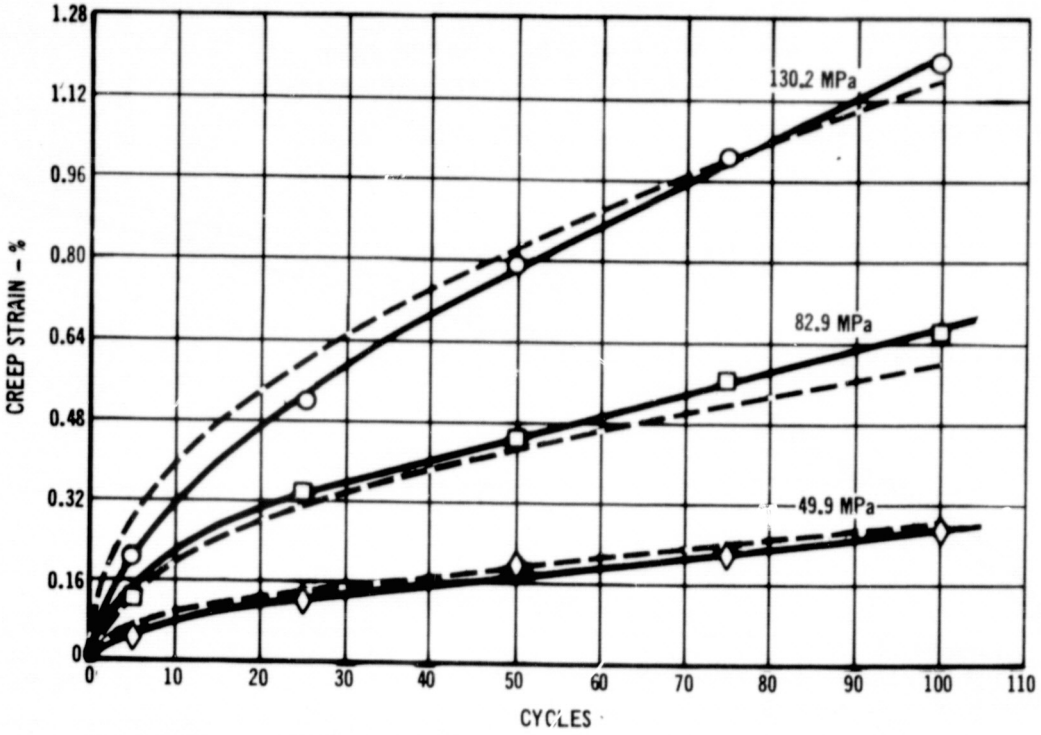

FIGURE 7–3 COMPARISON OF Ti-6Al-4V PREDICTED AND CYCLIC TEST CREEP STRAINS AT 783 K

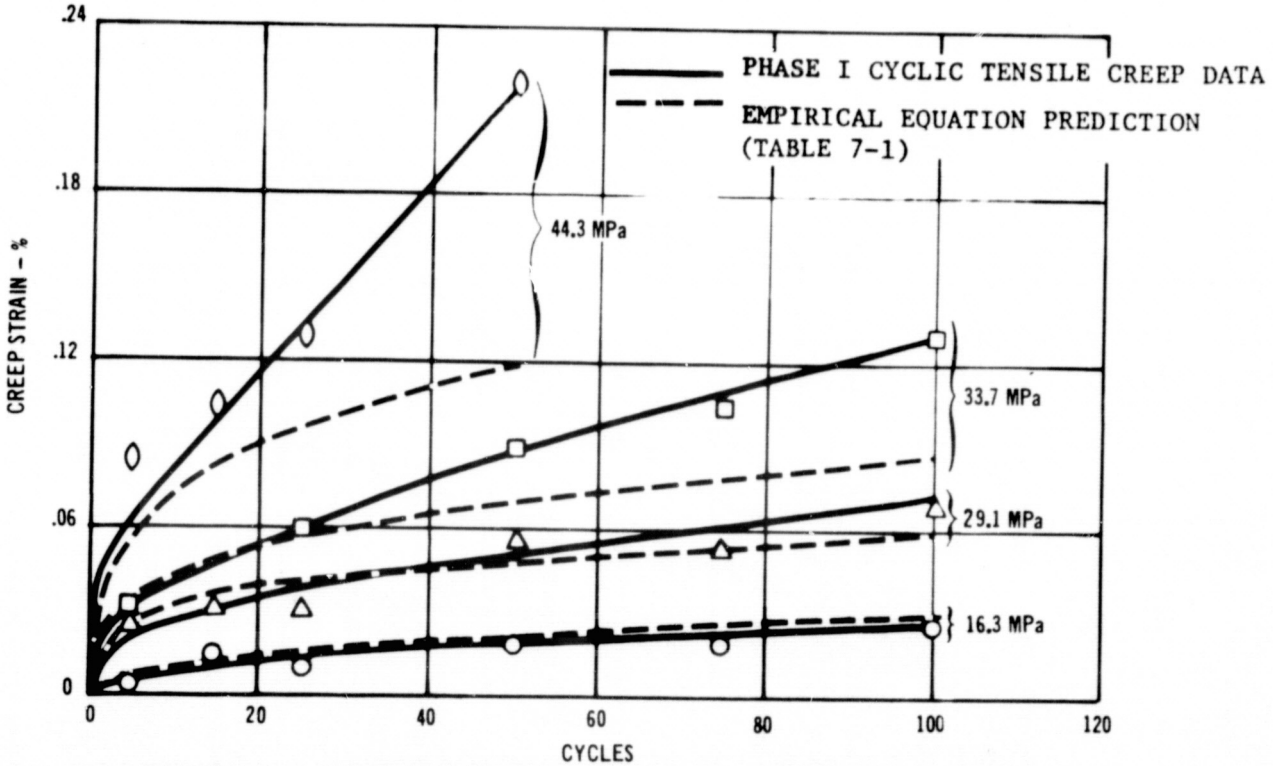

FIGURE 7–4 COMPARISON OF TDNiCr PREDICTED AND CYCLIC TEST CREEP STRAINS AT 1478 K

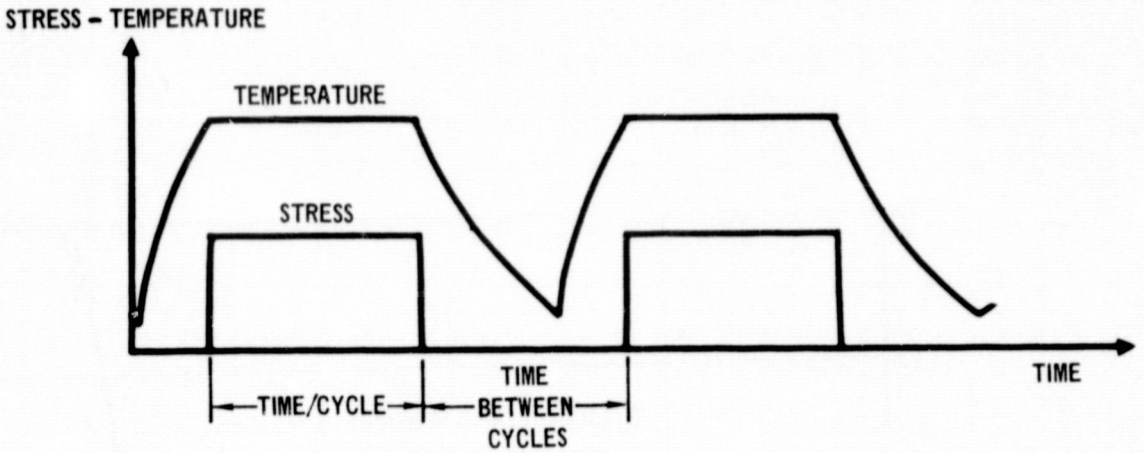

FIGURE 7–5 STRESS AND TEMPERATURE PROFILES FOR PHASE I TENSILE CYCLIC CREEP TESTS

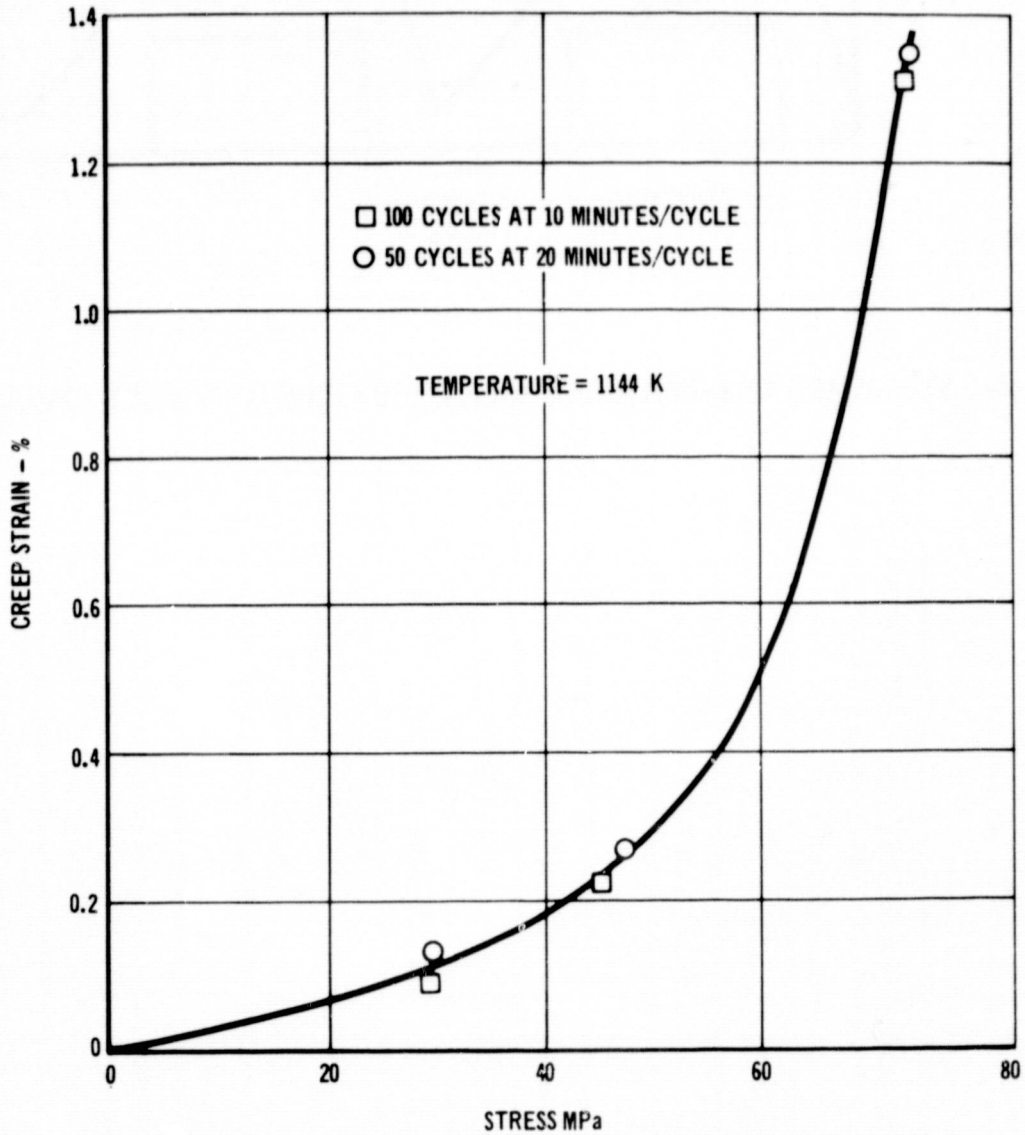

FIGURE 7–6(a) L605 CYCLIC CREEP STRAINS AS FUNCTION OF TOTAL TIME AT LOAD

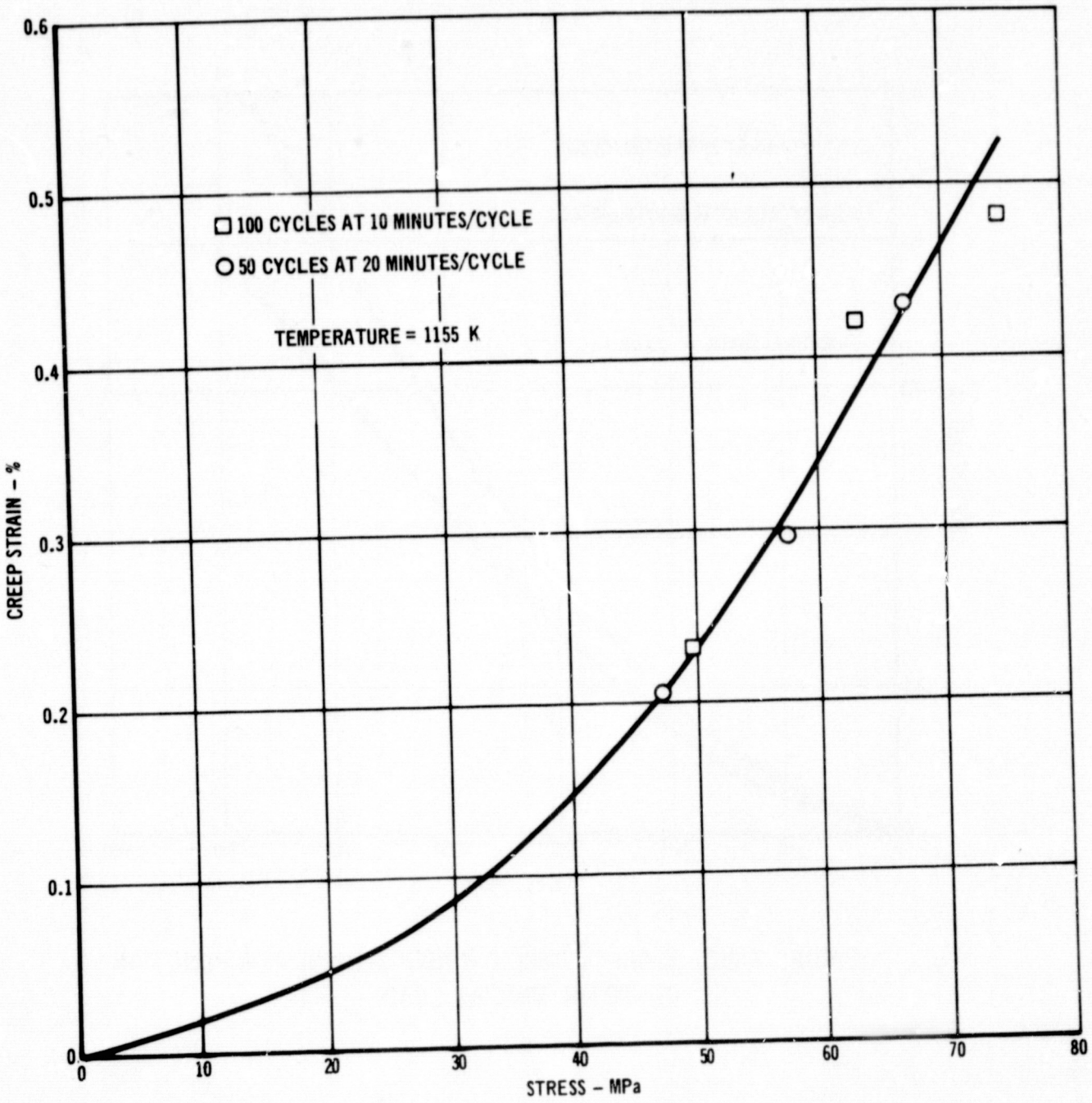

FIGURE 7–6(b) RENE '41 CYCLIC CREEP STRAINS AS A FUNCTION OF TOTAL TIME AT LOAD

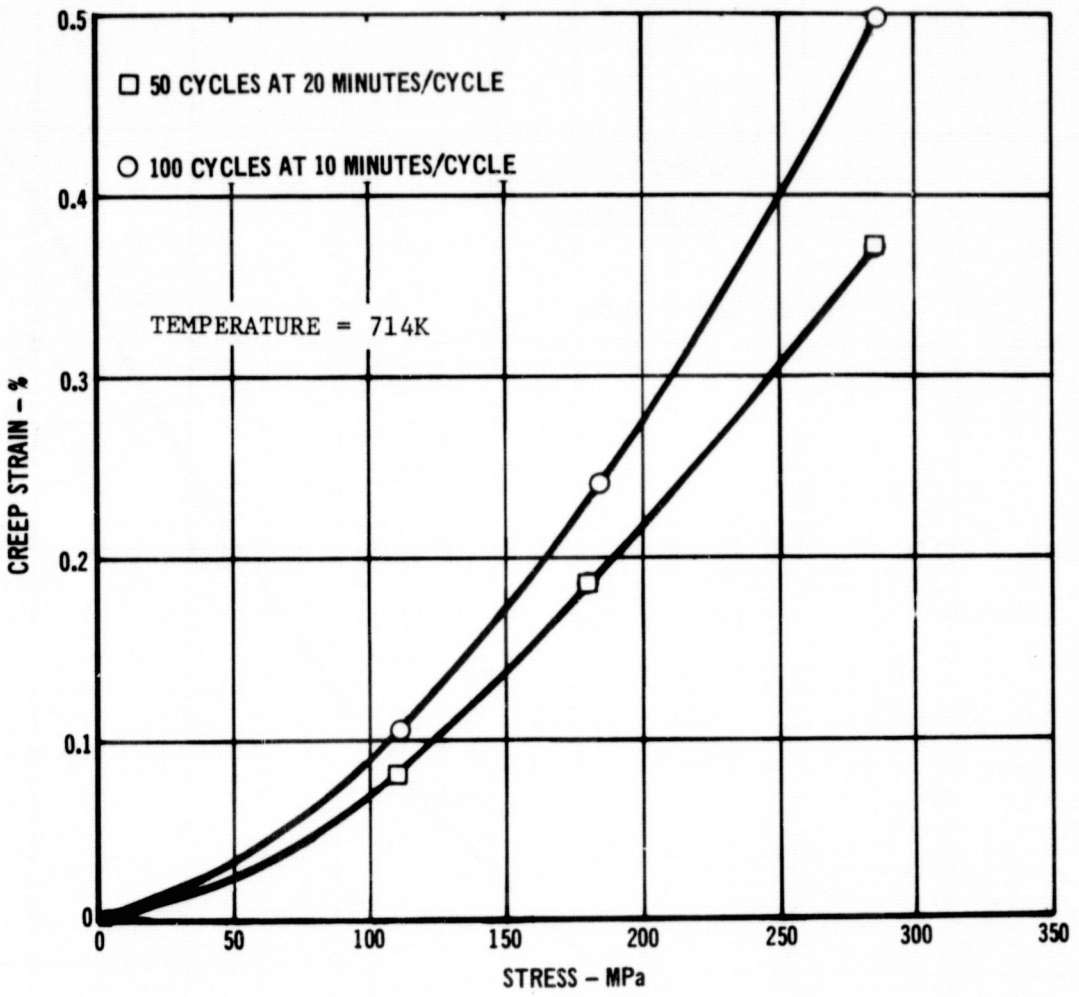

FIGURE 7–6(C) Ti-6Al-4V CYCLIC CREEP STRAINS AS A FUNCTION OF TOTAL TIME AT LOAD

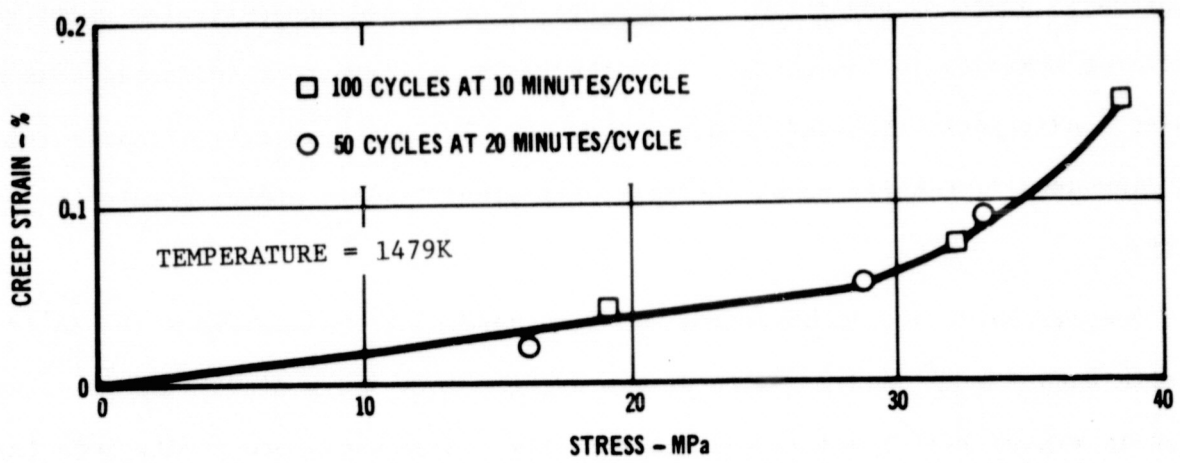

FIGURE 7–6 (d) TDNiCr CYCLIC CREEP STRAINS AS A FUNCTION OF TOTAL TIME AT LOAD

equations are considered to be applicable in analysis of idealized mission profiles where smaller time steps are used.

(c) Tensile tests were also conducted where stress was varied as a function of cycle, using the profiles shown in Figure 7-5 and where stress and temperature were varied within each cycle, using Mission profiles as shown in Figure 7-7. These test data were used to evaluate the applicability of the time and strain hardening theories of creep accumulation. Comparison of predicted creep strains using these hardening theories in conjunction with the empirical equations indicated that neither theory consistently provided good predictions. The applicability of hardening theories used in subsize panel analysis will significantly effect prediction capability.

Comparison of strain hardening and time hardening predictions with cyclic tensile data for an L605 two step stress profile test and a mission profile test are shown in Figure 7-8(a) and 7-8(b) respectively. Also shown are predictions based on use of both strain and time hardening theories depending on whether the creep strain rate is decreasing or increasing, respectively. This approach was proposed, based on the results of L605 tensile tests where stress was stepped as a function of cycle because results showed that the strain hardening theory provided the best predictions for tests where stress was continually decreased as a function of cycle and the time hardening theory provided the best predictions for tests where stress was continually increased as a function of cycle. Although this provided good predictions for the L605 complex trajectory tests, it did not improve prediction for the other three materials.

Similar comparisons of predicted tensile creep strains with Rene' 41 test data are shown in Figure 7-9. Generally for Rene' 41, the predictions based on the time hardening theory of creep accumulation were considered best. Predictions based on

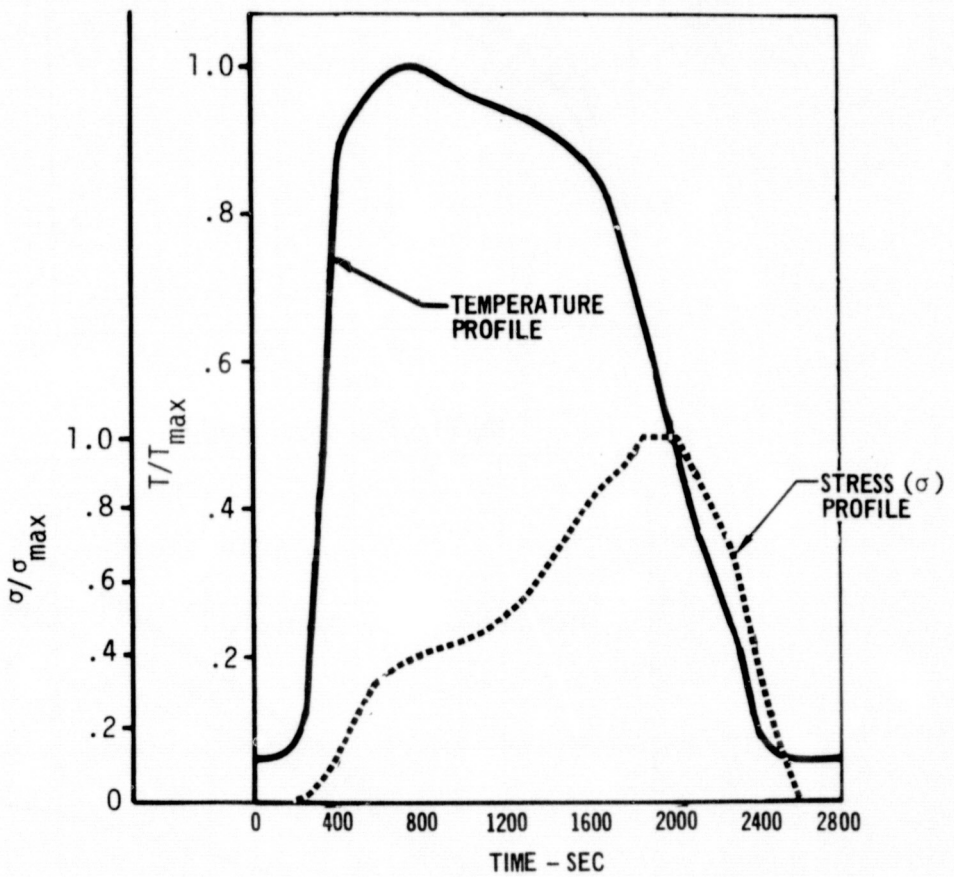

FIGURE 7–7 SIMULATED MISSION ENTRY PROFILE

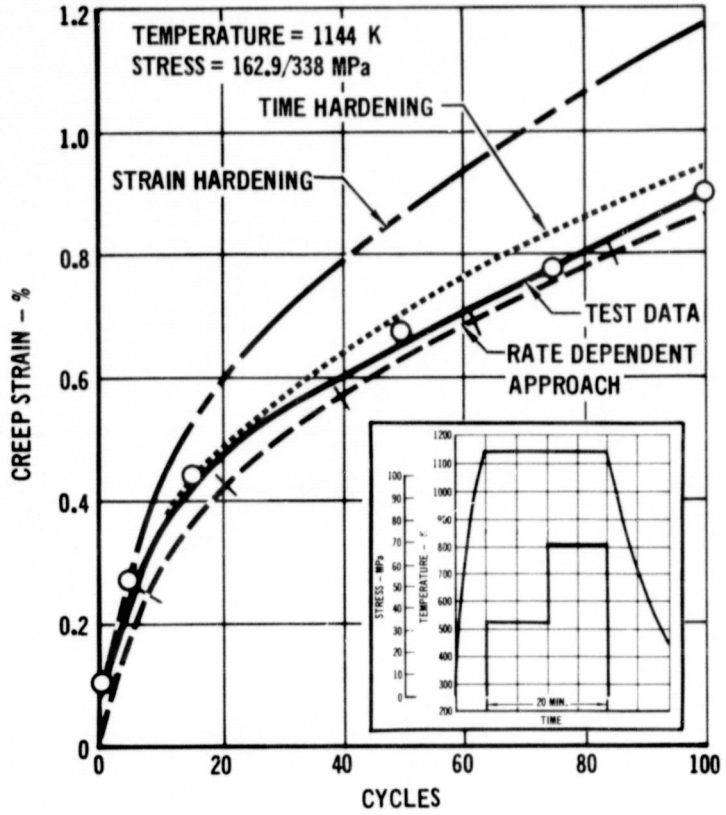

(a) Two Step Stress Profile

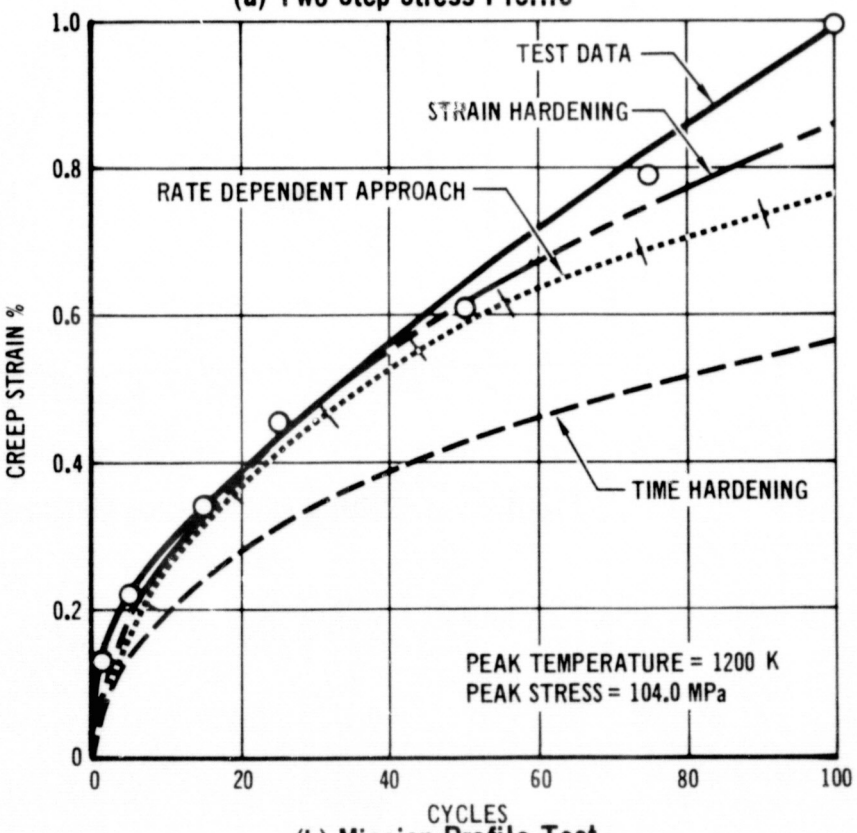

(b) Mission Profile Test

FIGURE 7–8 PHASE I PREDICTIONS FOR L605 CYCLIC TENSILE CREEP TESTS

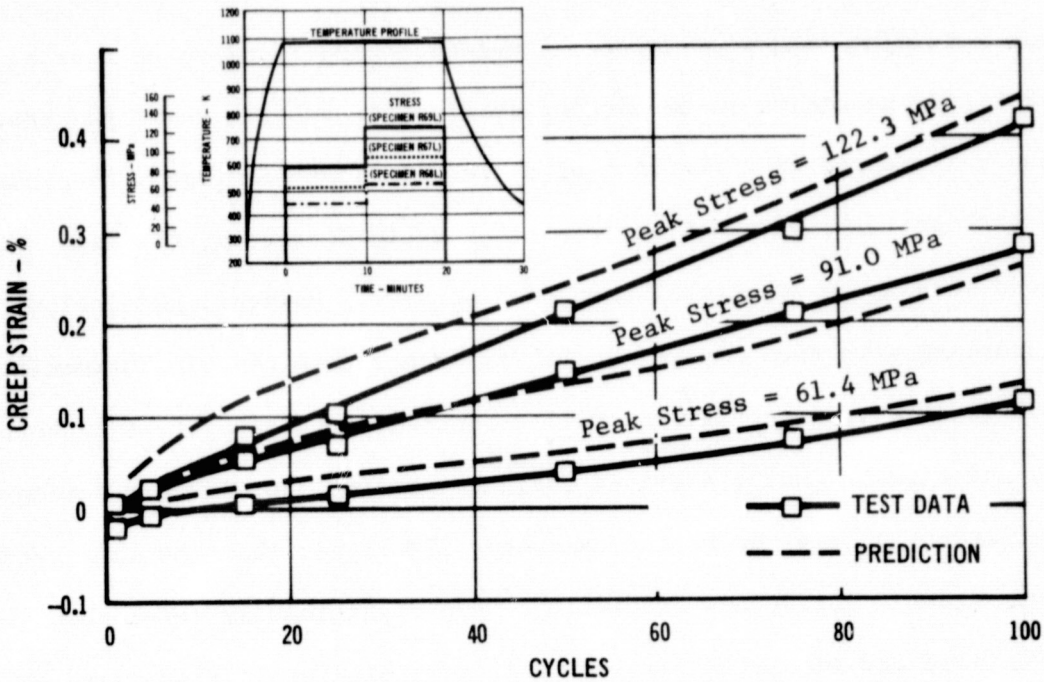

(a) Two Step Stress Profile

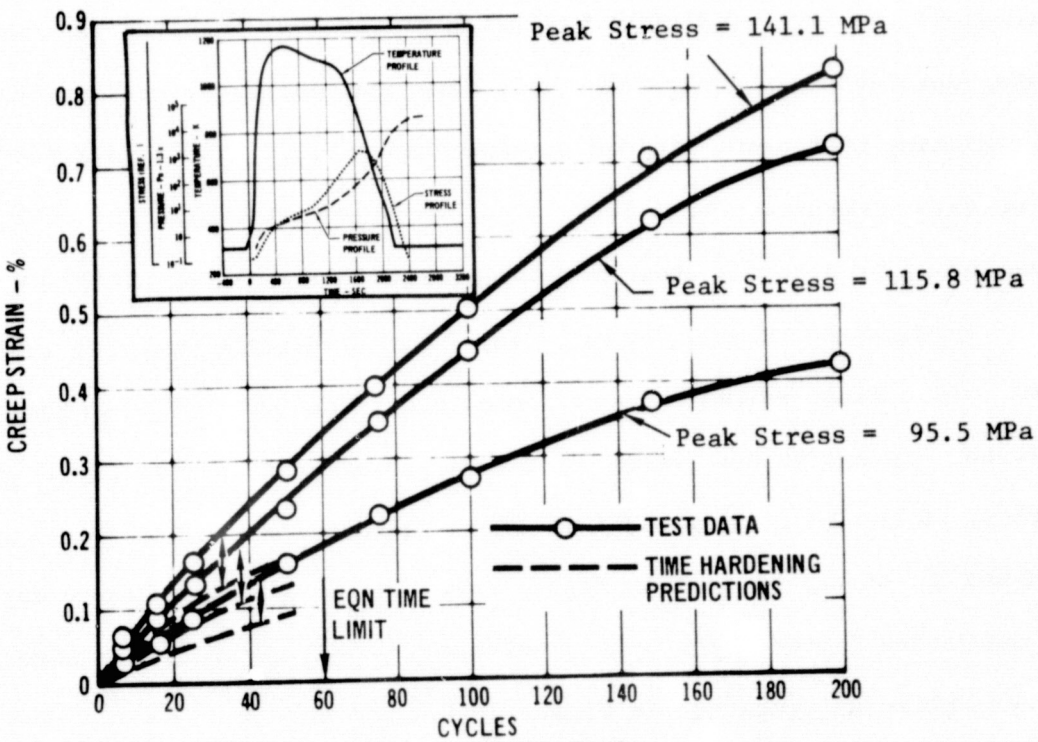

(b) Mission Profile Test

FIGURE 7–9(a) PHASE I PREDICTIONS FOR RENE '41 CYCLIC TENSILE CREEP TESTS

the strain hardening theory of creep accumulation were found to be approximately the same as for time hardening in predicting strains for testing where the stress was continuously increased as a function of cycle. Both predictions were close to test values. For specimens where stress was continually decreased, the time hardening predictions were up to 30% higher than test strains. However, predictions based on strain hardening were even higher, up to 75% higher than the time hardening predictions. For the two step stress profile test shown in Figure 7-9(a) both strain hardening and time hardening provided adequate predictions with predictions based on strain hardening being up to approximately 20% higher than the time hardening predictions shown. All strain predictions were significantly lower than test results in the idealized and simulated mission tests as indicated in Figure 7-9(b).

For titanium cyclic tensile creep tests the strain hardening theory was found to yield the best predictions although predictions resulted in lower creep strain than obtained in testing. The rate dependent approach, used successfully in predicting L605 data, yielded strains comparable to the time hardening predictions for these titanium data. These predictions were approximately 20% below the strain hardening predictions shown for the mission profile test in Figure 7-10.

Predictions of creep strains for TDNiCr trajectory profile tensile tests using the cyclic creep equation, were found to be from 30% to 70% of test strains at 100 cycles. Investigation showed that this was at least partly due to prediction capability of the equation at 1478 K, where the complex trajectory tests had been conducted, as can be seen in Figure 7-4. The strain hardening theory of creep accumulation provided the best predictions with time hardening theory yielding even lower values as presented in Figure 7-11.

(d) In the analysis of test data, mission stress and temperature profiles must be idealized into constant stress and temperature steps. During Phase I, tests were conducted to investigate possible variations in test data which could result and

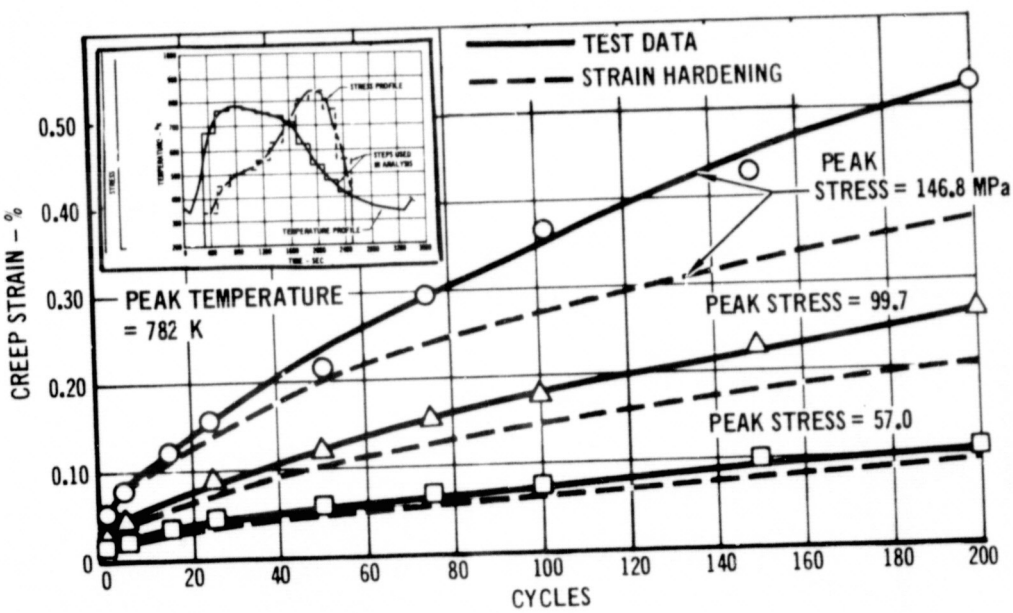

FIGURE 7–10 PHASE I PREDICTIONS FOR Ti–6Al–4V CYCLIC TENSILE CREEP MISSION PROFILE TEST

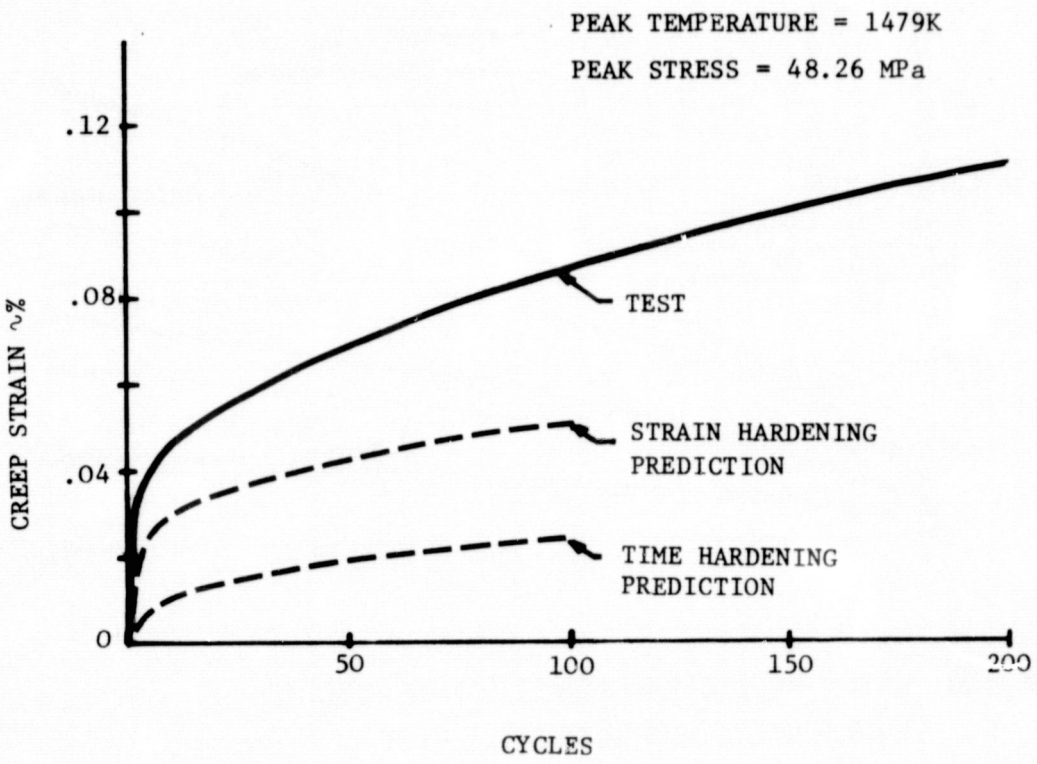

FIGURE 7-11 PHASE I PREDICTIONS FOR TDNiCr CYCLIC TENSILE CREEP MISSION PROFILE TEST

thus affect the predictions. Shown in Figure 7-12 is a comparison of typical test data for L605 mission profile and idealized profile tests. The reasonable degree of agreement attained indicates that adequate cyclic creep response analyses can be performed using only a few constant load and temperature steps in the trajectory idealization.

(e) For each of the four alloys, cyclic tensile tests were conducted in Phase I to obtain data for the assessment of possible effects of atmospheric pressure on creep response. To provide these data, replicate tests were conducted, using idealized mission stress and temperature profiles. However, atmospheric pressure was held constant at 1.33 Pa, in one of the tests while the pressure profile shown in Figure 7-7 was applied in the other test. Comparisons of results for each of the alloys are shown in Figures 7-13(a) through 7-13(d). In each case variations in creep strain results were relatively small and were considered within the range of scatter for replicate tests. Therefore, no effect was attributed to atmospheric pressure in Phase I.

(f) Another variable considered in Phase I tensile creep testing was the possible effect of recovery phenomena. To investigate this, tests were conducted where the stress profile was maintained for a longer period of time while temperature was being decreased rapidly, as shown in Figure 7-14(a), similar to the temperature-stress relationship occurring in mission profile tests (Figure 7-7). These comparative tests were conducted on L605 and Rene' 41 tensile specimens. Test results, shown in Figure 7-14(b), indicated that no variation in creep strains could be determined for the L605 specimens, as indicated by the strain-time data plots. However, for Rene' 41 creep strain results were consistently higher for each of three specimens tested. These results, plotted as a function of the stress levels, at 100 cycles are shown in Figure 7-14(c). This variation in creep strains for Rene' 41

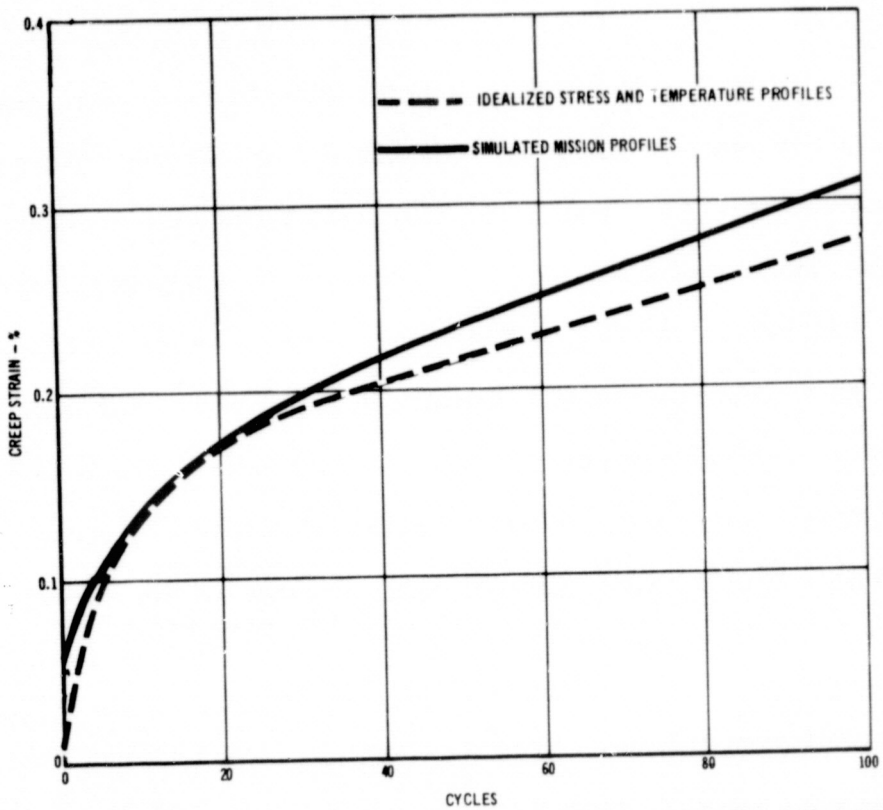

FIGURE 7–12 COMPARISON OF L605 CYCLIC TENSILE CREEP STRAINS FOR SIMULATED MISSION AND IDEALIZED TRAJECTORIES

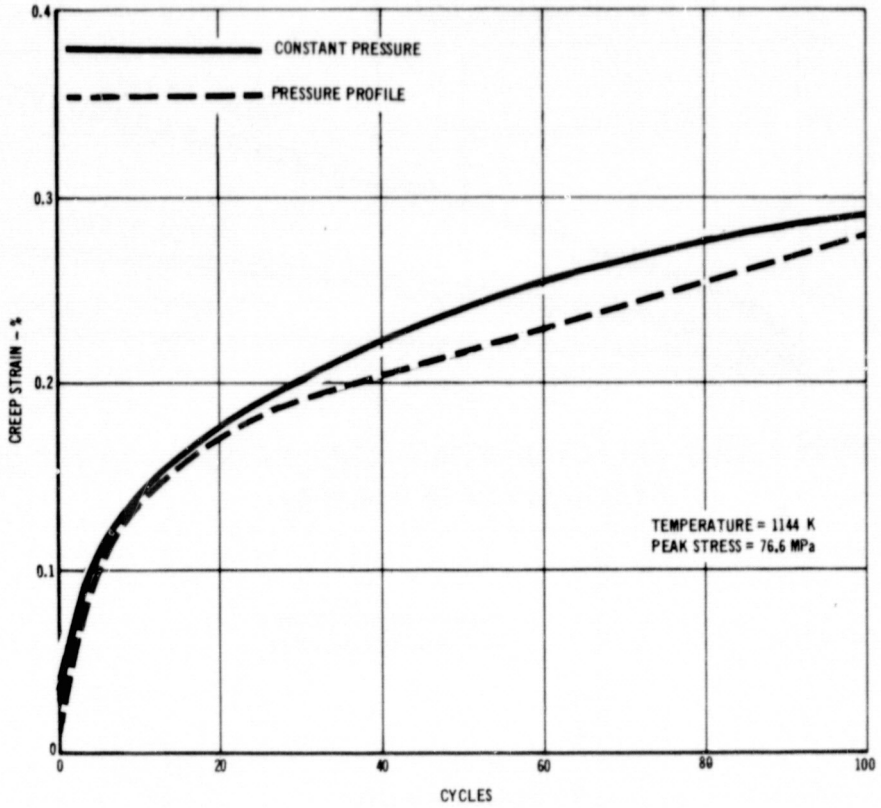

FIGURE 7–13(a) EFFECT OF ATMOSPHERIC PRESSURE ON THE CYCLIC CREEP OF L605

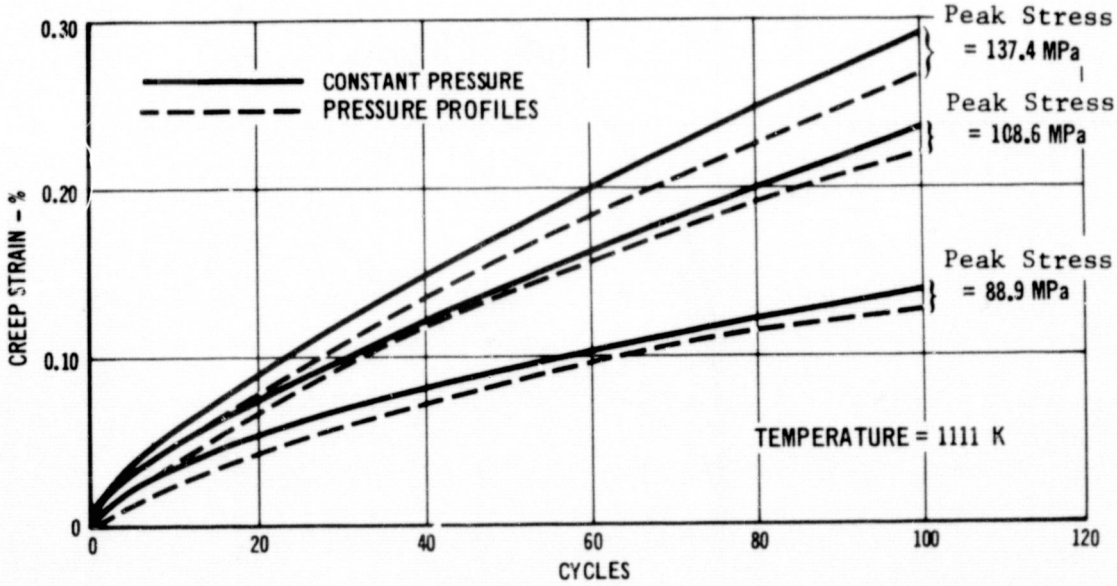

FIGURE 7–13(b) EFFECT OF ATMOSPHERIC PRESSURE ON THE CYCLIC CREEP OF RENE '41

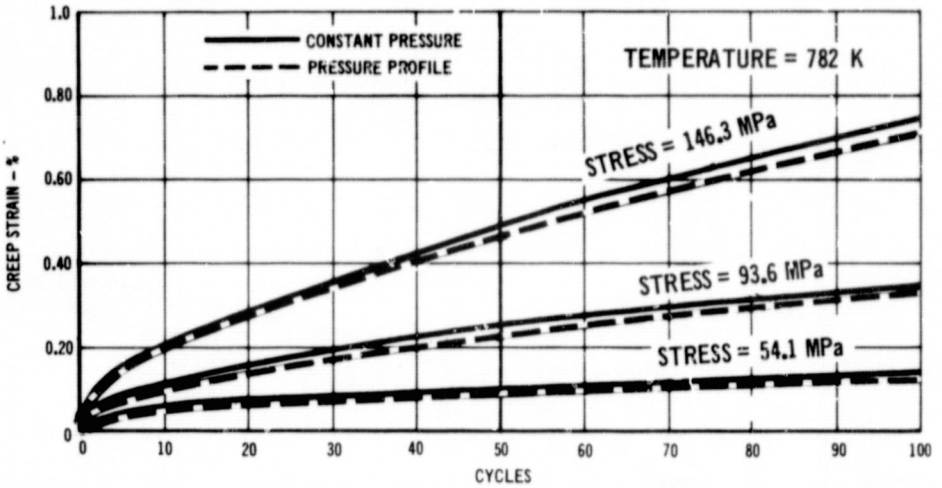

FIGURE 7–13(c) EFFECT OF ATMOSPHERIC PRESSURE ON THE CYCLIC CYCLIC CREEP OF Ti-6Al-4V

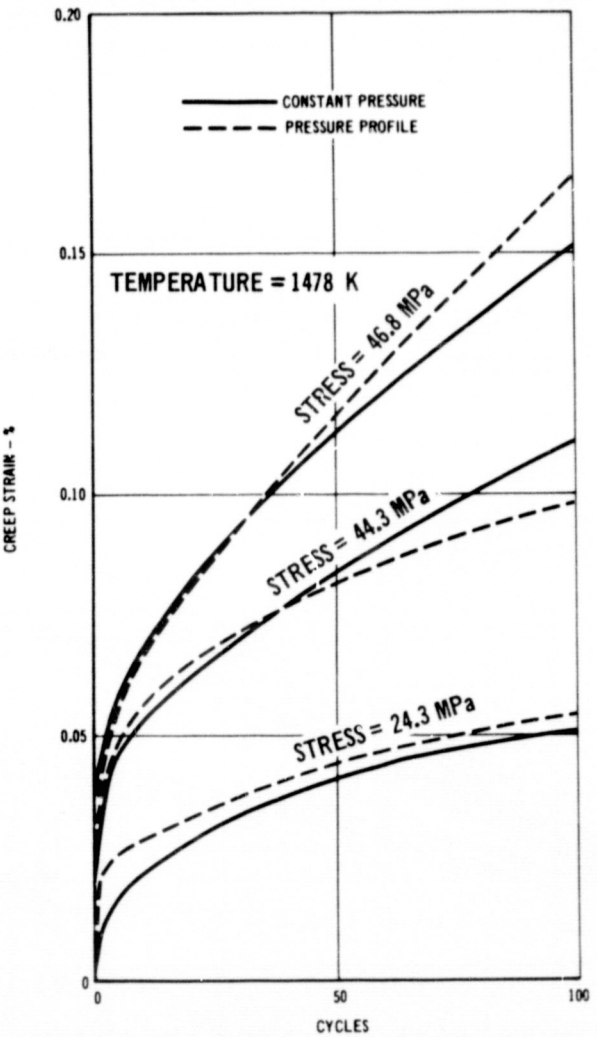

FIGURE 7–13(d) EFFECT OF ATMOSPHERIC PRESSURE ON THE CYCLIC CREEP OF TDNiCr

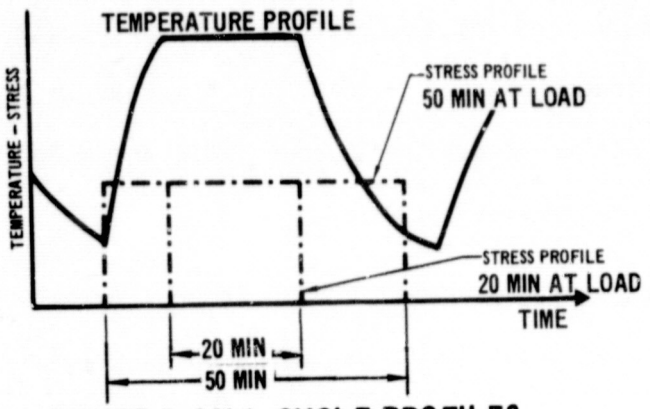

FIGURE 7–14(a) CYCLE PROFILES

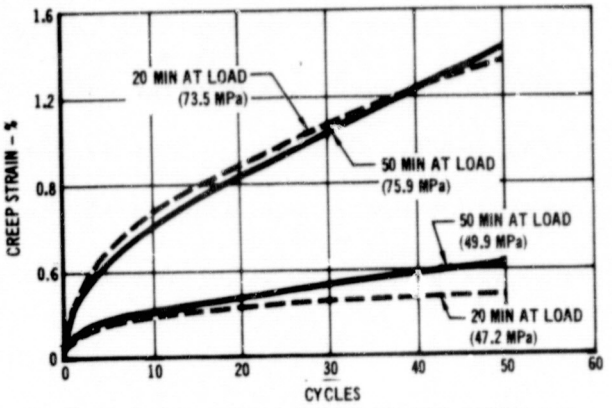

FIGURE 7–14(b) EFFECT OF TIME AT LOAD ON L605 AT 1144 K

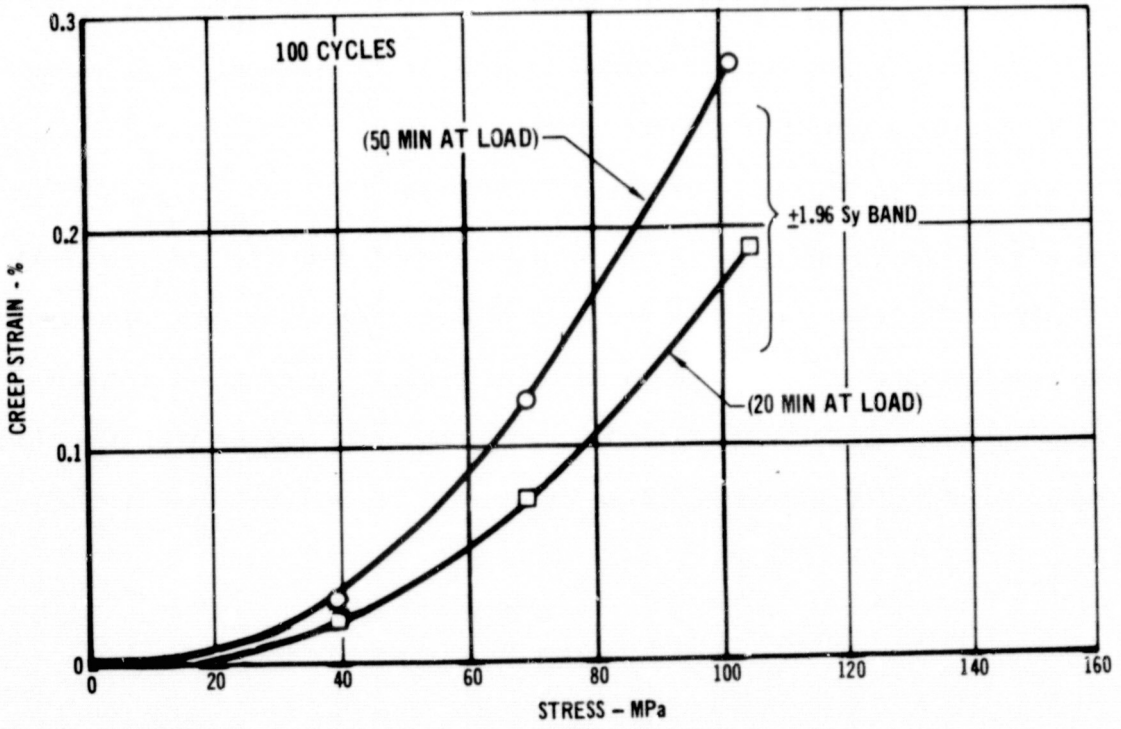

FIGURE 7–14(c) EFFECT OF TIME AT LOAD ON RENE '41 AT 1111 K

was demonstrated to be greater than that expected based on data scatter as determined in the development of empirical equations. From these results it is difficult to draw conclusions as to the differences between the mission profile test results and predictions based on empirical equations developed for the twenty minute per cycle stress level. However, it has been demonstrated that an effect, due possibly to a material recovery phenomena, may exist to different degrees in the different materials, which may affect the subsize panel deflection predictions.

(g) The empirical cyclic creep strain equations developed in Phase I were based on tests conducted on the thin gage sheet specimens ($\sim$.025 cm) for each material. Therefore predictive capability using the equation is applicable for the single skin corrugation subsize panels, fabricated from the same sheet. However, for rib stiffened panels fabricated for L605 and titanium, thicker gages were used ($\sim$.064 cm). Steady state creep tests were conducted on each of these sheet thicknesses during Phase I to evaluate possible effects of gage on creep. Comparisons of these test results are shown in Figure 7-15(a) and 7-15(b) for L605 and titanium respectively.

An effect of gage on creep response (thin gages creep faster) was noted in the L605 steady state literature data base and L605 supplemental test data shown. This effect, is attributed to a change in material processing at about t = .064 cm.

Although the thicker gage titanium specimens crept faster than the thin gage specimens, no definite effect could be determined since test data were within expected scatter.

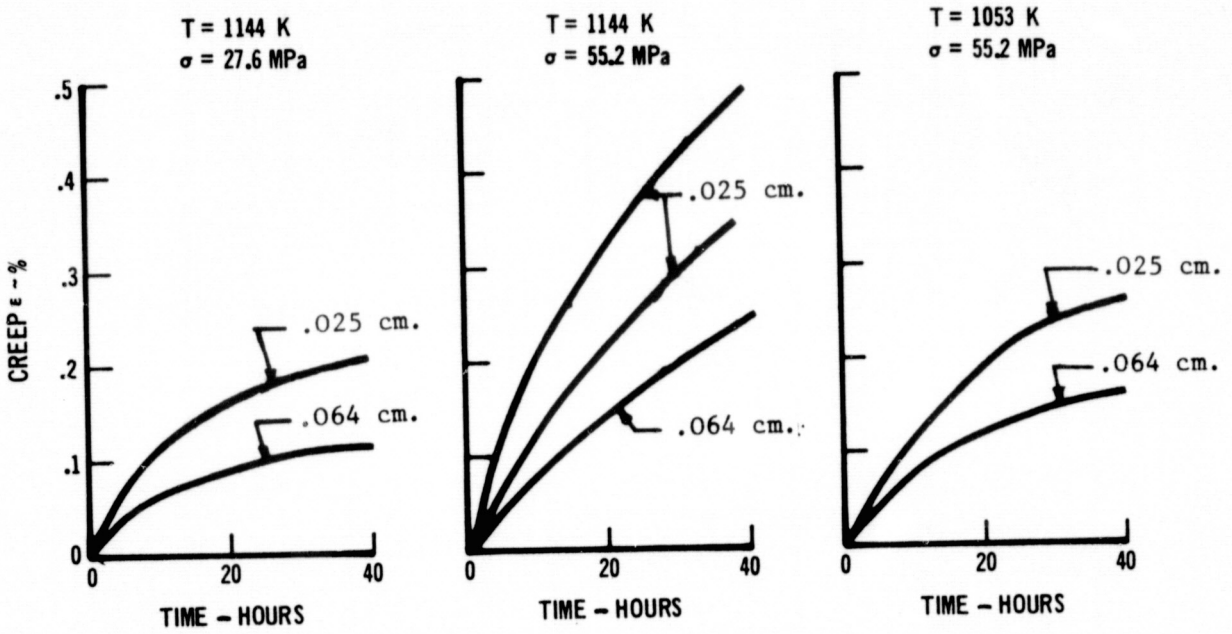

FIGURE 7–15 (a) PHASE I STEADY STATE TENSILE CREEP DATA SHOWING EFFECT OF GAGE ON L605 CREEP

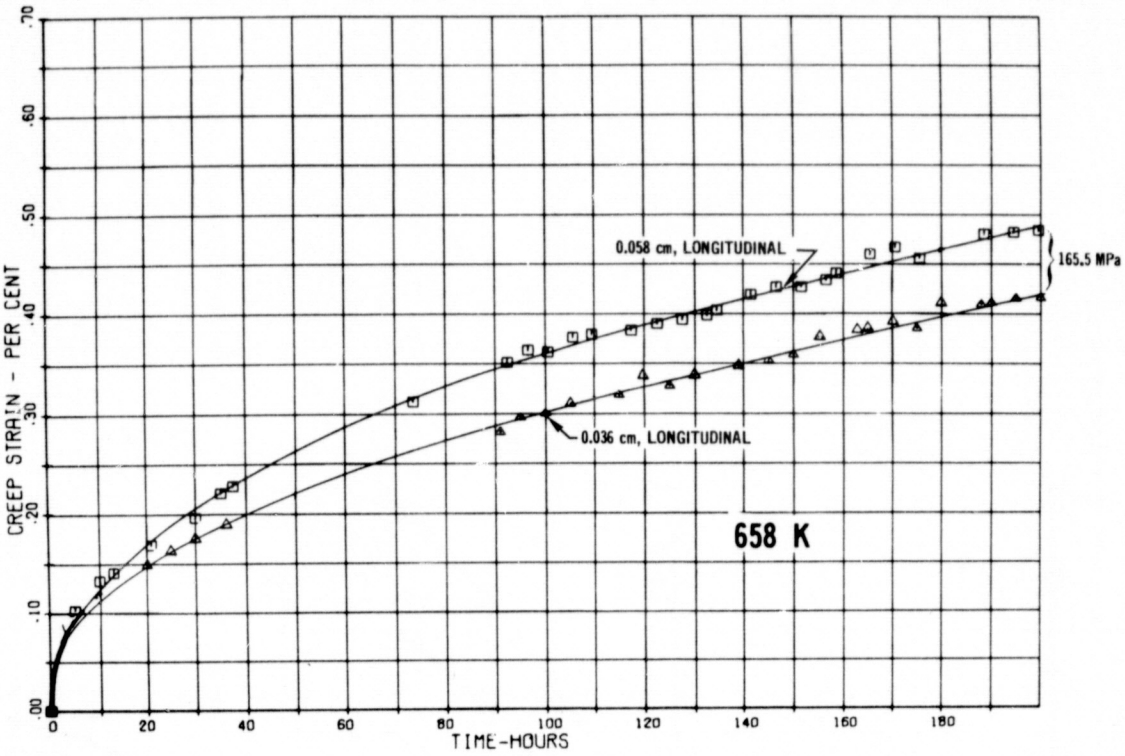

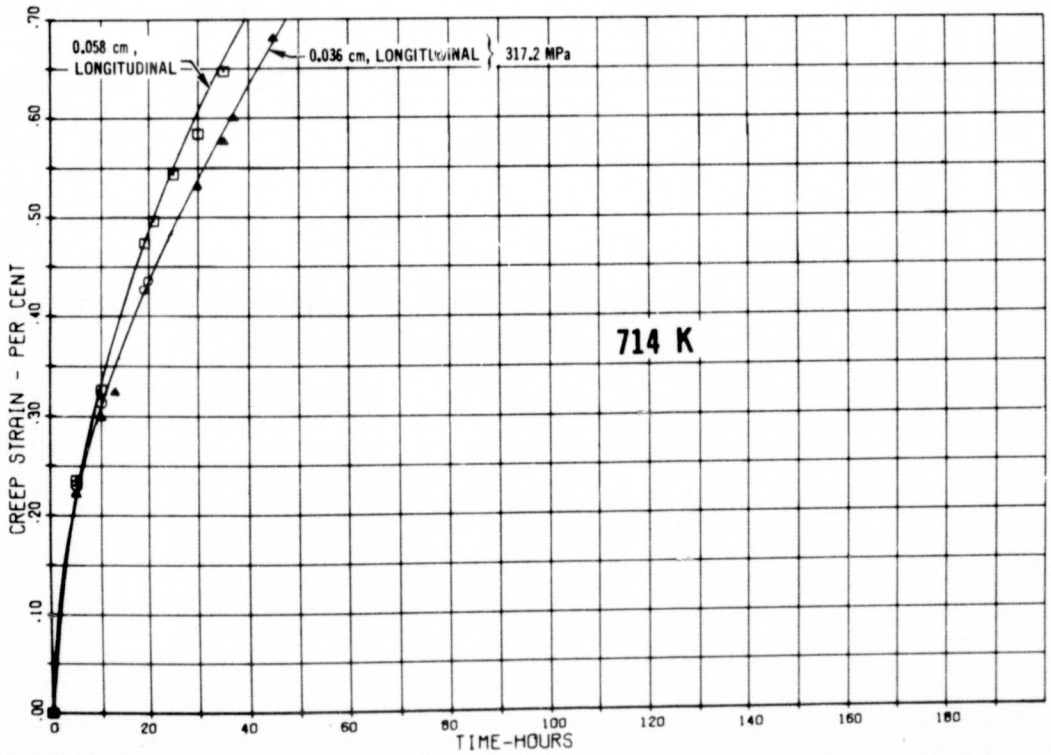

FIGURE 7–15 (b) PHASE I STEADY STATE TENSILE CREEP DATA SHOWING EFFECT OF GAGE ON Ti CREEP

7.2 TPSC COMPUTER PROGRAM - METHOD OF ANALYSIS

One of the primary outputs during this phase is the Thermal Protection System Creep (TPSC) computer program for prediction of creep deflection predictions. This computer program uses iterative techniques and numerical integration to predict creep strains, residual stresses, and permanent deflection, due to creep, in stiffened panel structures subjected to bending loads.

The program was developed specifically for analysis of thermal protection system panels. Therefore, structural definition of leading candidates, corrugation stiffened, rib stiffened, and zee stiffened concepts, is incorporated into the TPSC program. Modeling of the specific panel structural concept for analysis is accomplished automatically, based on overall section input definition. An option is provided for including a beaded skin into any of the cross sections since beads are frequently required in thermal protection system panel designs.

Bending moments along the panel length are computed based on uniform pressure load input or two point load input. In addition, the moments can be calculated as a function of panel edge support stiffness and the ratio of panel stiffness in the longitudinal and transverse directions. This option is based on combining solutions for an isotropic plate with two sides simply supported and two sides elastically supported as offered by Timoshenko[2] and the solution for an orthotropic plate with four sides simply supported as offered by Lekhnitskii[3]. This option provides a first order approach to account for Poisson's effects in orthotropic plate structures. The effect of biaxial stress distributions on creep response is not included in the analysis.

Using the assumption of a linear total elastic plus creep strain distribution through the depth, the neutral axis and incremental rotation are systematically varied at each increment along the length and analysis time step to determine the unique stress distribution which satisfies force balance and moment balance

requirements. At each point in the panel the creep component of total strain is iteratively determined based on either the time hardening or strain hardening theory of creep accumulation applied in conjunction with input analytical expressions defining material tensile creep response as a function of stress, temperature and time. Residual stresses are calculated at each time step by subtracting the elastic stress distribution from the total calculated stress distributions. These residual stresses are used at initiation of analysis for the next time step. Analysis proceeds through all the time steps at each designated station along the panel length, accumulating and storing structural rotations, creep strains, and residual stresses. At the completion of analysis, rotations are numerically integrated to determine creep deflections.

A flexible user oriented input format is used. Input includes geometry and definition of loading and temperature profiles. Panel temperature can be varied both along the panel length and through the depth by either polynominal equation coefficients or tabular input. Temperatures at each panel location are based on these distributions and the input temperature time profile data. Also input are equation coefficients to define material creep response. Appropriate creep strain response data are based on temperatures at each location in the panel.

Program output includes a record of geometry input and calculated geometrical data (moment of inertia), trajectory load and temperature data, and creep equation definition. Calculated deflections, creep strains, and residual stresses are output at desired times specified by the program user.

The following basic assumptions are made in the analysis:

(a) Only bending stresses are considered. Deflections due to shear are considered negligible.

(b) Strain distributions through the panel depth are linear.

(c) Creep response equations, defined by the user, are assumed to be applicable for both tensile and compressive stresses.

(d) Load and temperature distributions and calculated deflections are assumed symmetrical with respect to the panel centerline.

A brief description of appraoches used for important program calculations applicable to subsize panel analysis are presented in this section. The program users manual (Reference 2) contains a more detailed description. The general analysis flow is shown in Figure 7-16 for reference purposes.

7.2.1 GEOMETRY DEFINITION

The panel length is divided into increments (ΔX) over which bending moments are assumed constant and the panel depth is divided into increments (ΔY) over which stresses and strains are assumed constant. This approach for modeling the corrugation stiffened and rib stiffened subsize TPS panels is shown in Figure 7-17. The assumption of thin gages allows skin and horizontal stiffener sections to be defined as area increments. Vertical portion of the stiffeners are divided into ΔY elements based on the defined total number of elements to be used in analysis. Centroids and areas of the cross section increments are used in all subsequent calculations.

7.2.2 LOAD DEFINITION

Panel bending loads are calculated based on input loads for each time step in the mission profile. The option for applying point loads (P) to the panel, as shown in Figure 5-7, was specifically included in the TPSC program to allow analysis of the subsize panels tested during this phase. The bending moment distribution under this loading condition is also shown in Figure 5-7. Applied loading is assumed symmetrical about the panel centerline.

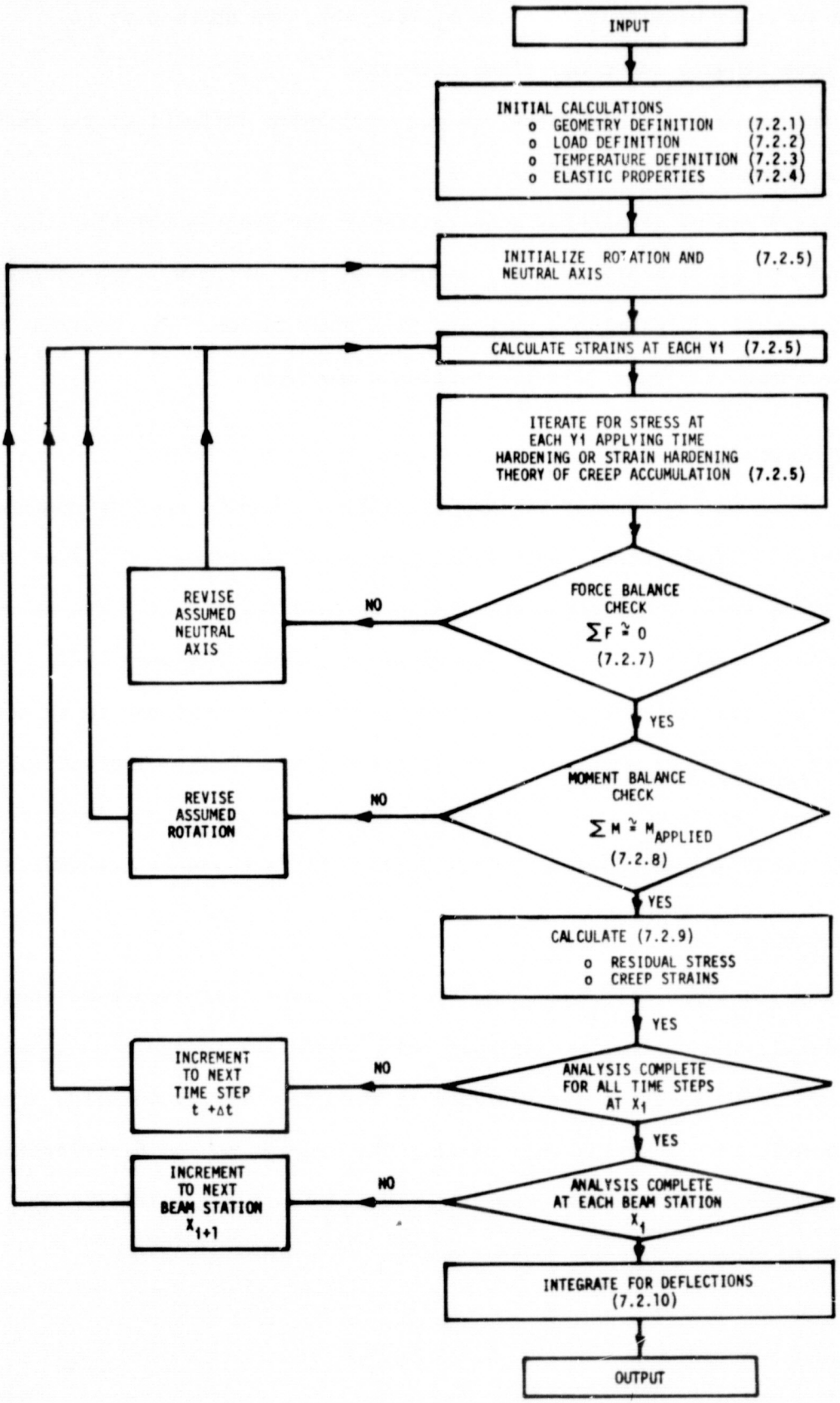

FIGURE 7–16 TPSC PROGRAM ANALYSIS FLOW

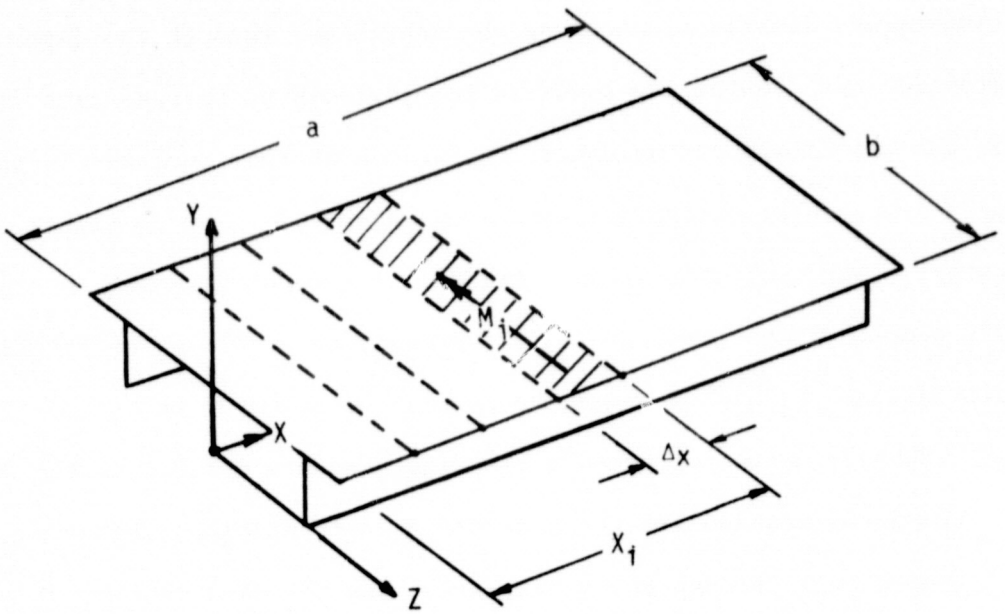

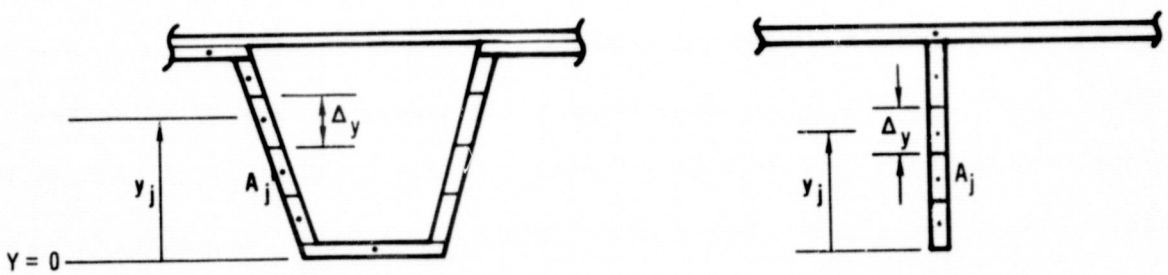

FIGURE 7–17 GEOMETRY DEFINITION OF SUBSIZE PANELS FOR ANALYSIS

7.2.3 TEMPERATURE DEFINITION

Creep response, as a function of temperature, is accounted for in the TPSC program through the input of panel midspan skin temperatures and normalized panel temperature distributions along the length and through the depth. This capability provides the flexibility required for analysis of thermal protection system panels. It was not considered necessary to include thermal stresses in the analysis since only temperature variations across the panel width or nonlinear distributions through the depth will yield longitudinal thermal stresses in a simply supported TPS panel. These gradients will typically be small and of relatively short duration during the high temperature portion of the mission.

Subsize panel temperature distributions are defined in the analysis by input of the panel midspan skin temperature at each mission time step, the distribution of temperature through the panel depth, and the distribution of temperature along the length. Normalized temperature distributions, referenced to the midspan skin temperature, are input, as indicated in Figure 7-18(a). The distributions (T_x and T_y) are assumed to be the same for each time step. The temperature is calculated, at each point in the panel, as the product of T (function of time, T_x ((function of length), and T_y (function of depth)). A table lookup routine is included in the program to calculate T_x and T_y as functions of X and Y respectively, based on tabular input. T_x and T_y are determined using linear interpolation between input points as shown in Figure 7-18(b). Elastic modulus data, as a function of temperature, are also calculated using a table lookup routine, as indicated in Figure 7-18(c). The option for definition of distributions through the panel depth was not used in the analysis of the subsize panels.

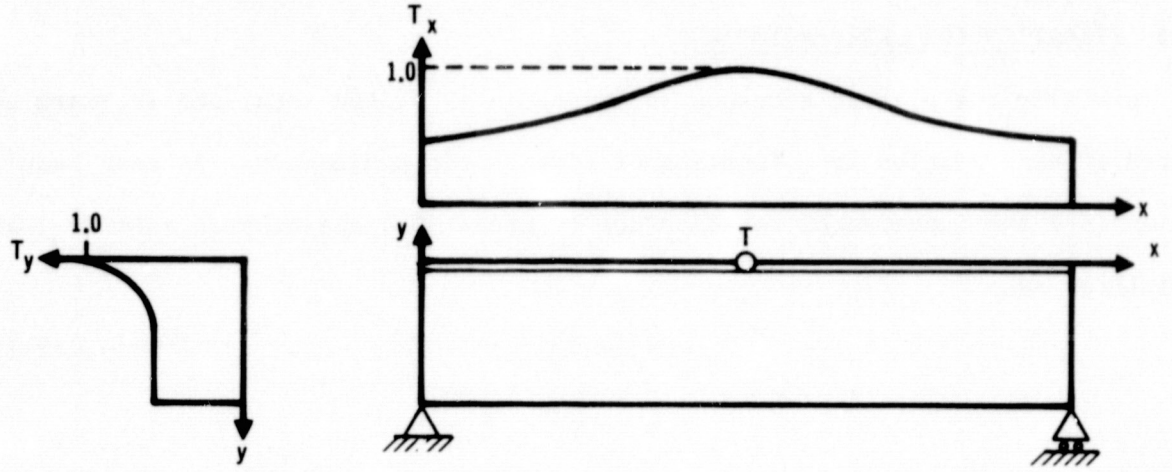

$$T_{xy} = T(T_x)(T_y)$$

(a) Temperature Defined as Function of Panel Length and Depth

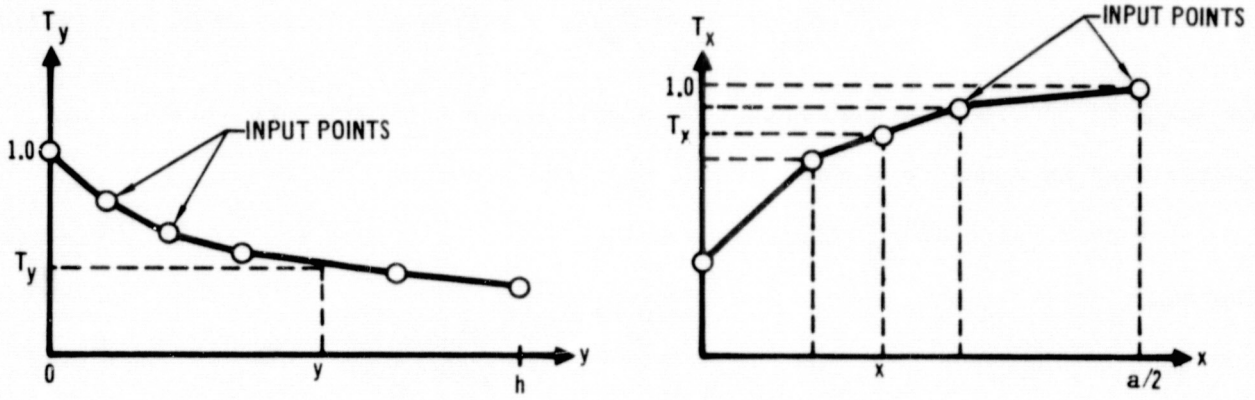

(b) Linear Interpolation for Temperatures

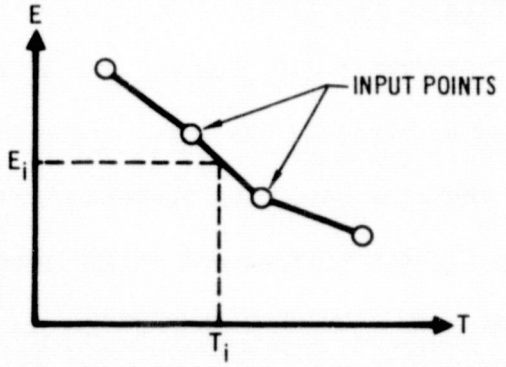

(c) Linear Interpolation for Elastic Modulus

FIGURE 7–18 PANEL TEMPERATURE CALCULATIONS

7.2.4 ITERATION FOR CREEP ROTATIONS

Initially the elastic stresses (σ_j), strain (ε_j), and rotations (θ_j) are calculated at each station as a function of time in the trajectory. At each beam station (X_i) the incremental rotation due to creep (θ_c) and neutral axis ($\bar{y}_e$) are initialized as

$$\theta_c = \theta_e \qquad (7\text{-}1)$$

$$\bar{y} = \bar{y}_e$$

Based on these values, the initial total strain assumed at each y_j element is calculated, using the linear total strain (ε_{T_j}) assumption

$$\varepsilon_{T_j} = (\theta_c + \theta_e)(\bar{y} - y_j)/\Delta X \qquad (7\text{-}2)$$

As analysis proceeds through each time step, the neutral axis and rotation are initialized as equal to those calculated in the previous time step.

For each value of ε_{T_j} there is a unique value of stress (σ_j) which satisfies the equation

$$\varepsilon_{T_j} = \varepsilon_{c_j} + \frac{\sigma_j + \sigma_{RESIDUAL_j}}{E} \qquad (7\text{-}3)$$

where $\sigma_{RESIDUAL_j}$ is the residual stress based on results from calculations in the previous time step and E is the material elastic modulus at the element temperature. The incremental creep strain (ε_{c_j}) is a function of stress (σ_j), temperature, time, and incremental time step Δt based on the input creep strain equation applied in conjunction with either the time hardening or strain hardening theories of creep accumulation as shown in Figures 7-19(a) and 7-19(b) respectfully. Stresses are iteratively determined at each time step (designated by the subscript k) based on the particular empirical creep strain equation used. The time hardening theory of creep accumulation is based on the assumption that the creep rate is dependent upon the total time under load. Therefore a vertical shift from one temperature-stress

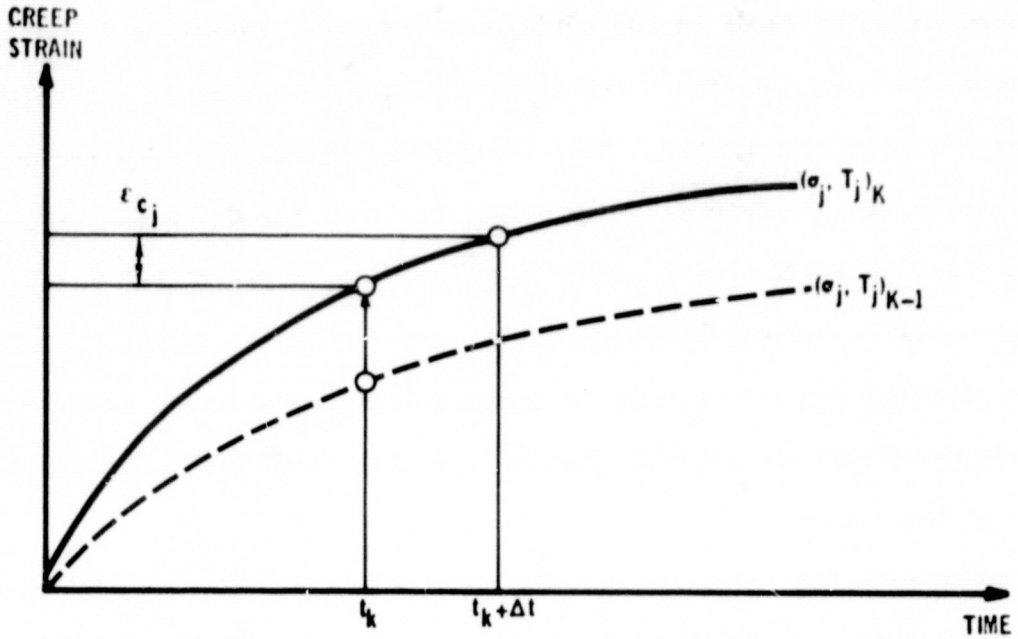

(a) Time Hardening

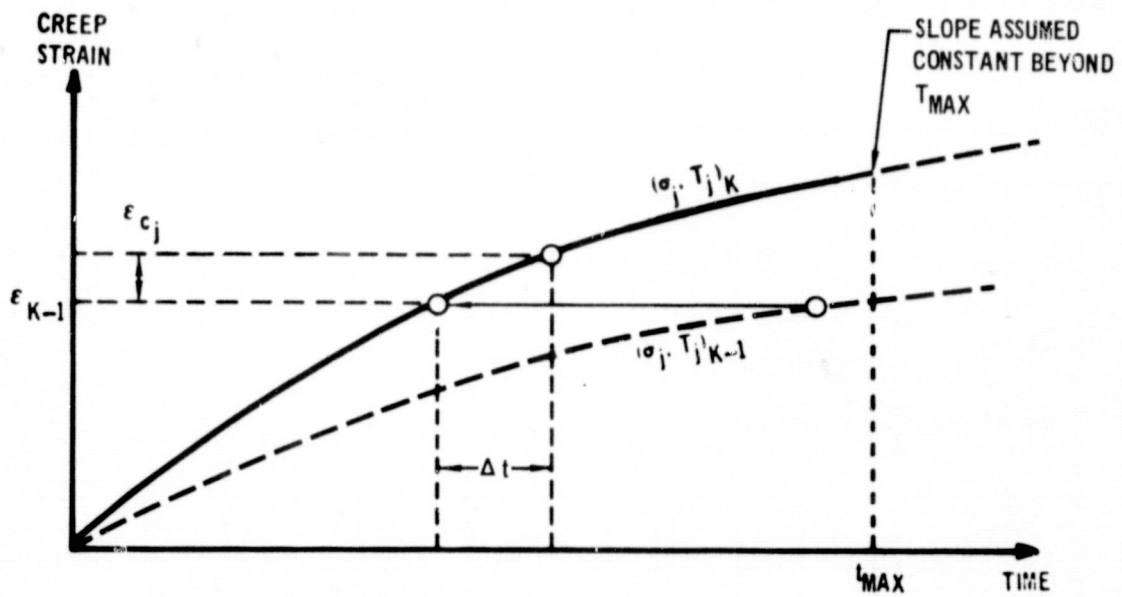

(b) Strain Hardening

FIGURE 7–19 HARDENING THEORIES FOR CREEP ACCUMULATION

creep curve to the next is used for time hardening. The strain hardening theory of creep accumulation is based on the assumption that the creep rate is dependent upon total accumulated creep strain. Therefore a horizontal shift is used between the temperature-stress creep curves. Additional calculations are required when applying strain hardening to determine the effective time, for which the given value of strain applies, at a new stress and/or temperature. To facilitate analysis of mission profiles, a maximum time cutoff (t_{max}) is input to prevent application of the creep equation beyond its range of applicability. For times beyond this time cutoff, the creep rate is assumed constant for each stress and temperature as indicated in the figure.

In determining the values of σ_j, at each time step, which satisfy equation (7-3), assumed stresses (designated by the subscript ℓ) are systematically varied. The initially assumed value of stress is that obtained from analysis in the previous time step (elastic stress for the first time step). The assumption for the second value of stress is dependent on the first value of stress and the relationship between ε_{T_j} and the calculated strains. Subsequent stresses are calculated, as indicated in Figure 7-20 by applying the equation

$$\sigma_\ell = \sigma_{\ell-1} + (\varepsilon_{T_j} - \varepsilon_{\ell-1})\ \text{SLOPE} \qquad (7\text{-}4)$$

where $\text{SLOPE} = (\sigma_{\ell-1} - \sigma_{\ell-2})/(\varepsilon_{\ell-1} - \varepsilon_{\ell-2})$

The process is contined until the σ_j is determined such that

$$\frac{\varepsilon_{T_j}}{\varepsilon_j} - 1.0 < 0.001.$$

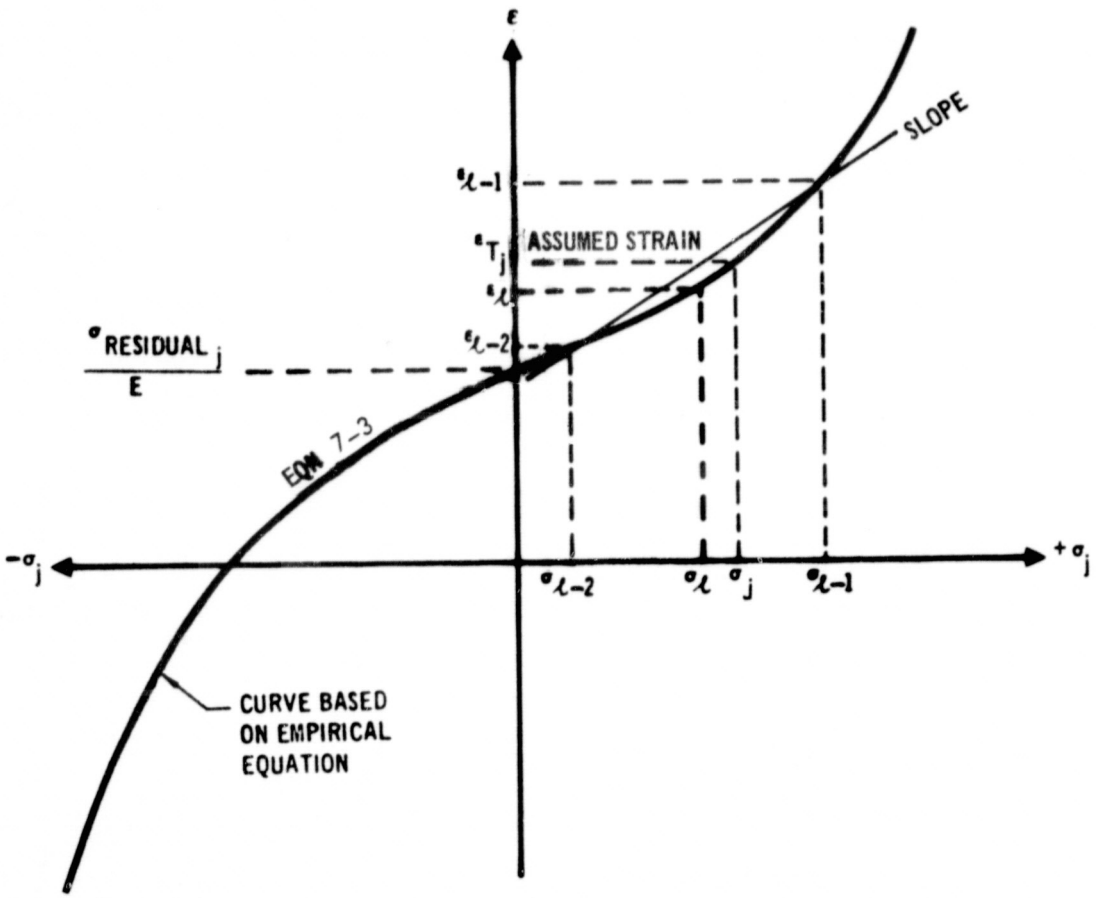

FIGURE 7–20 ITERATION APPROACH FOR STRESS CALCULATION

7.2.5 FORCE BALANCE REQUIREMENTS

Having solved for stresses at each of the j element locations, the check for a zero force balance on the cross section is calculated as

$$F_m = \sum_{j=1}^{N} \sigma_j A_j \qquad (7\text{-}5)$$

where N is the total number of elements through the section.

Based on the resulting sign (plus or minus) of F_m, the neutral axis location is changed by plus or minus ΔY. That is, for example, if the neutral axis is located toward the tension side of the panel, resulting in an overall net compression load (F_m = negative), then the neutral axis must be moved toward the compression side (+Y direction). Strains and stresses are then recalculated. This process is continued until the sign of F_m changes, at which time the neutral axis location is calculated by linear interpolation using the equation

$$\bar{y} = \bar{y}_m - \frac{|F_m|(\bar{y}_m - \bar{y}_{m-1})}{|F_m| + |F_{m-1}|} \qquad (7\text{-}6)$$

This process, indicated in Figure 7-21, shows that the neutral axis location is not constrained to coincide with the y_j increments.

7.2.6 MOMENT BALANCE REQUIREMENTS

After force balance is attained on the cross section, the check for moment balance at the station is calculated as

$$M_1 = \sum_{j=1}^{N} |\sigma_j A_j (\bar{y} - \bar{y}_j)| \qquad (7\text{-}7)$$

The calculated moment is based on the initially assumed value of rotation ($\theta_1 = \theta_c + \theta_e$) and will not, in general be equal to the applied moment.

C-2

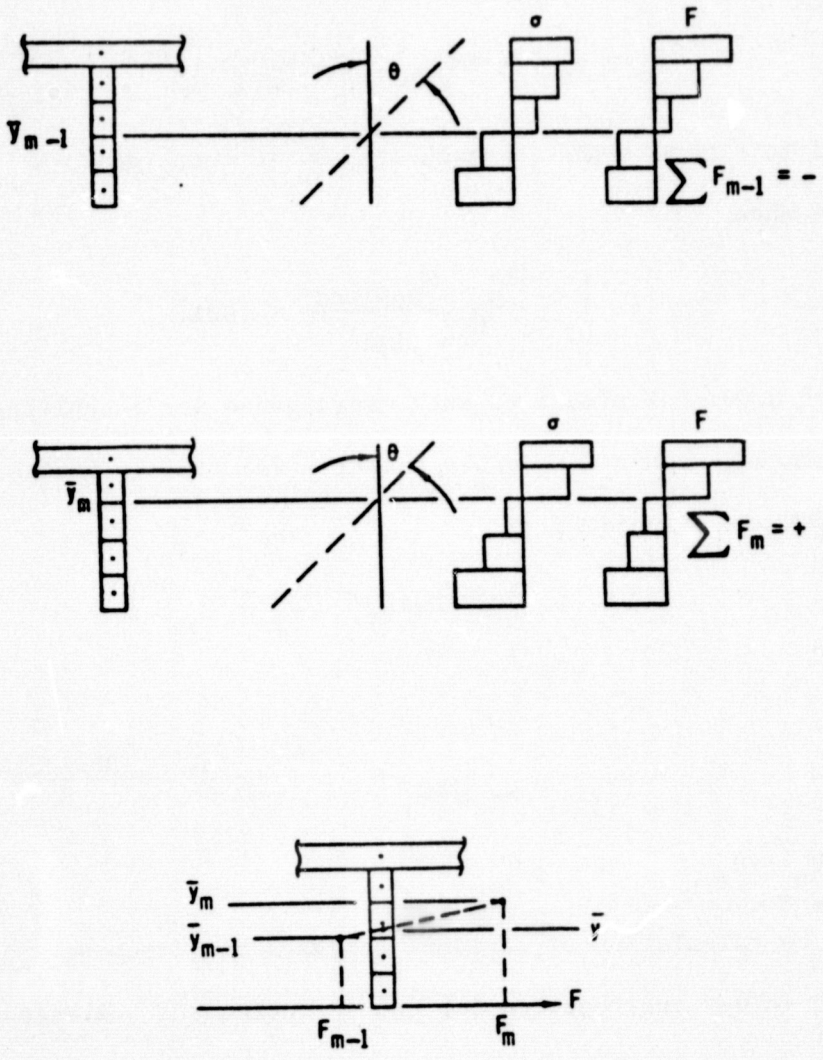

FIGURE 7–21 FORCE BALANCE ITERATION APPROACH

Therefore, a second estimate of θ is calculated as

$$\theta_2 = \theta_1 \left(\frac{M_{applied}}{M_1}\right) \tag{7-8}$$

Subsequent iterations for moment balance are based on the calculation

$$\theta_n = \theta_{n-1} + (M_{applied} - M_{n-1}) \frac{(\theta_{n-1} - \theta_{n-2})}{(M_{n-1} - M_{n-2})} \tag{7-9}$$

as depicted in Figure 7-22. At each step M_n is compared to $M_{applied}$. Balance is established when

$$\frac{|M_n - M_{applied}|}{M_{applied}} < .001.$$

The value of 0.001 for moment balance convergence was established to provide good solution accuracy within reasonable computer run times. Residual stresses and creep strains are calculated as

$$\sigma_{RESIDUAL_j} = \sigma_{e_j} - \sigma_j \tag{7-10}$$

and

$$\varepsilon_{c_j} = \varepsilon_{T_j} - \varepsilon_{ELASTIC_j} = \theta_c \frac{(y - y_j)}{\Delta X} - \frac{\sigma_{RESIDUAL}}{E} \tag{7-11}$$

where $\theta_c = \theta_n - \theta_e$

In addition to calculation of residual stresses and creep strains for output purposes, these values are retained for use in subsequent analysis. Creep strains are required for use in strain hardening analysis and residual stresses are added to elastic stresses for initiation of the next analysis time step.

7.2.7 INTEGRATION FOR DEFLECTIONS

Structural creep rotations (θ_c) and elastic rotations (θ_e) are calculated as a function of time and stored for use in deflection calculations. These deflections are calculated at each station by applying the following equations where I is the

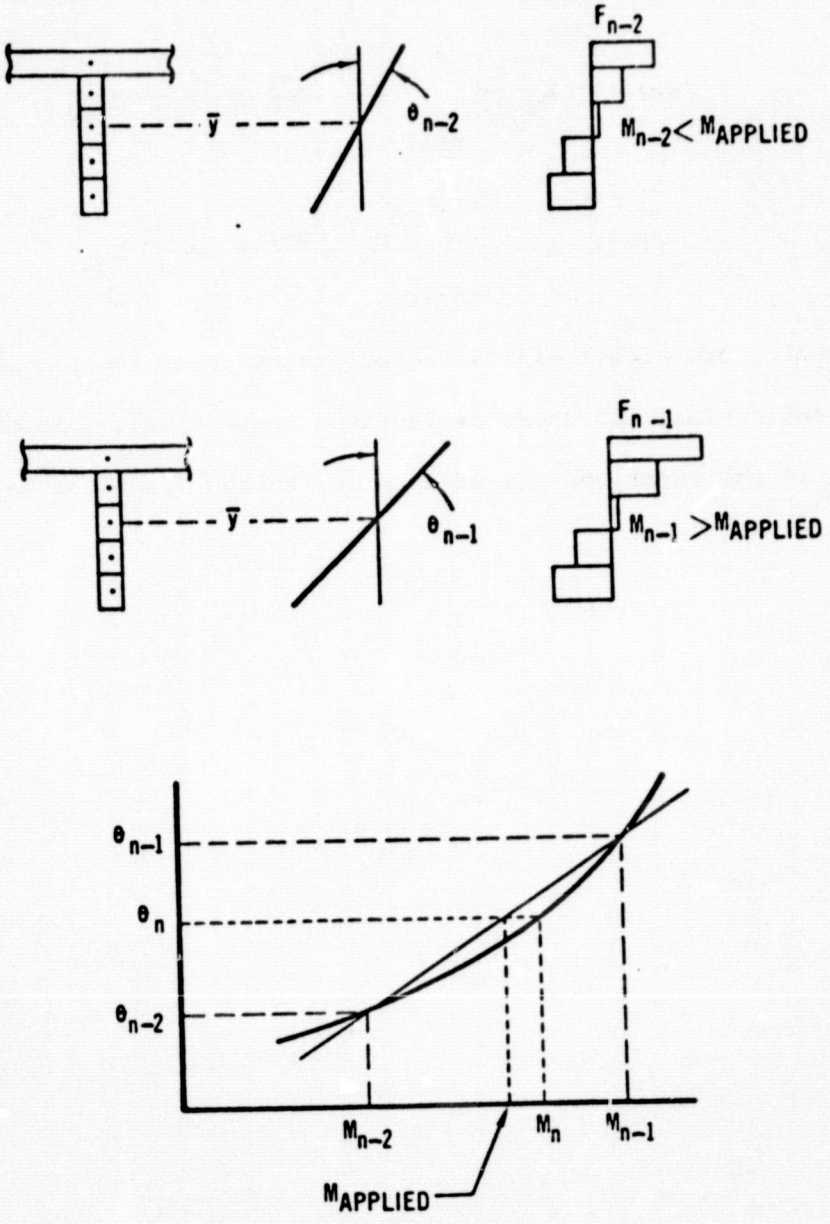

FIGURE 7–22 MOMENT BALANCE ITERATION APPROACH

total number of beam stations in half the beam length and n is a dummy variable used to designate beam stations.

$$\left(\begin{matrix} i=1 \\ I-2 \end{matrix} \text{ to}\right) \delta_{X_i} = \sum_{n=1}^{i} \frac{\theta_n + \theta_{n+1}}{2} X_n + \frac{\theta_{i+1}}{2} X_i + X_i \sum_{n=i+2}^{I} \theta_n \qquad (7\text{-}12)$$

$$(i=I-1),\ \delta_{X_i} = \sum_{n=1}^{i} \frac{\theta_n + \theta_{n+1}}{2} X_n + \frac{\theta_I}{2} X_{I-1} \qquad (7\text{-}13)$$

$$(i=I),\ \delta_{X_i} = \sum_{n=1}^{i} \frac{\theta_n + \theta_{n+1}}{2} X_n + \frac{\theta_I}{2} X_{I-1} \qquad (7\text{-}14)$$

Values of θ are either elastic rotations or creep rotations for calculation of elastic deflections and creep deflections respectively. Shown in Figure 7-23 is a sketch of the rotations and midspan deflection (equation 7-14) for a beam with I = 3.

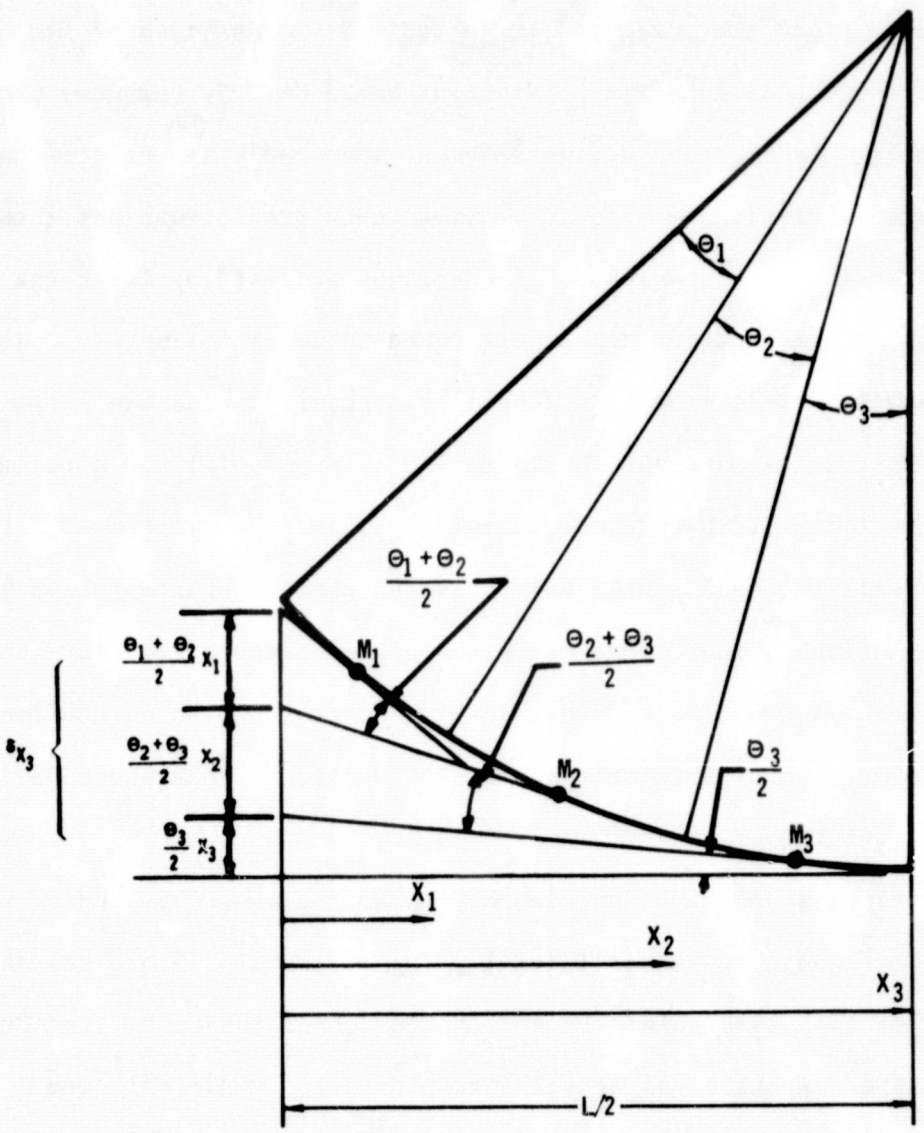

FIGURE 7–23 NUMERICAL INTEGRATION APPROACH FOR CALCULATION OF DEFLECTIONS

7.3 L605 SUBSIZE PANEL DEFLECTION ANALYSIS

Results of the six L605 subsize panel tests were summarized in Section 6, and deflection data obtained are presented in Appendix B. Comparison is made in this section between these test data and predictions based on TPSC computer program analysis. Predicted panel creep deflections obtained applying the time hardening theory of creep accumulation were found to yield good predictions and these predictions are shown in the comparisons. Predictions obtained applying the strain hardening theory of creep accumulation were found to be approximately twice those using time hardening. This result is generally consistent with the Phase I tensile specimen analysis results as shown in Figure 7-8(a) and 7-8(b) for a two-step stress profile and a mission profile cyclic test respectively.

Analysis of all the L605 panels was conducted using a constant temperature along the panel length. Predictions using the actual temperature distributions as shown in Figure 5-4 would be somewhat lower than those based on the constant temperature. Comparison of predictions for a $\pm 1\%$ uniform temperature variation is shown for panel test L605-22.

Predicted deflections, as a function of cycle, for the L605 subsize panels tended to be lower than test values initially (approximately 15 cycles) and then increase to higher than test values by the conclusion of the test. This same trend can be noted in the comparison of tensile creep data and empirical equation predictions as shown in Figure 7-1. Therefore this effect in the subsize panel predictions is attributed to the empirical equation prediction capability.

L605 single skin corrugation stiffened panels L1 and L4 were tested to replicate mission profiles in tests L605-21 and L605-24 respectively. For analysis purposes the beam load profile (P) and temperature load profile (T), shown in Figure 7-24, were idealized into the four steps shown. These load and temperature steps were applied in sequence in the analysis using the L605 empirical L605 cyclic creep

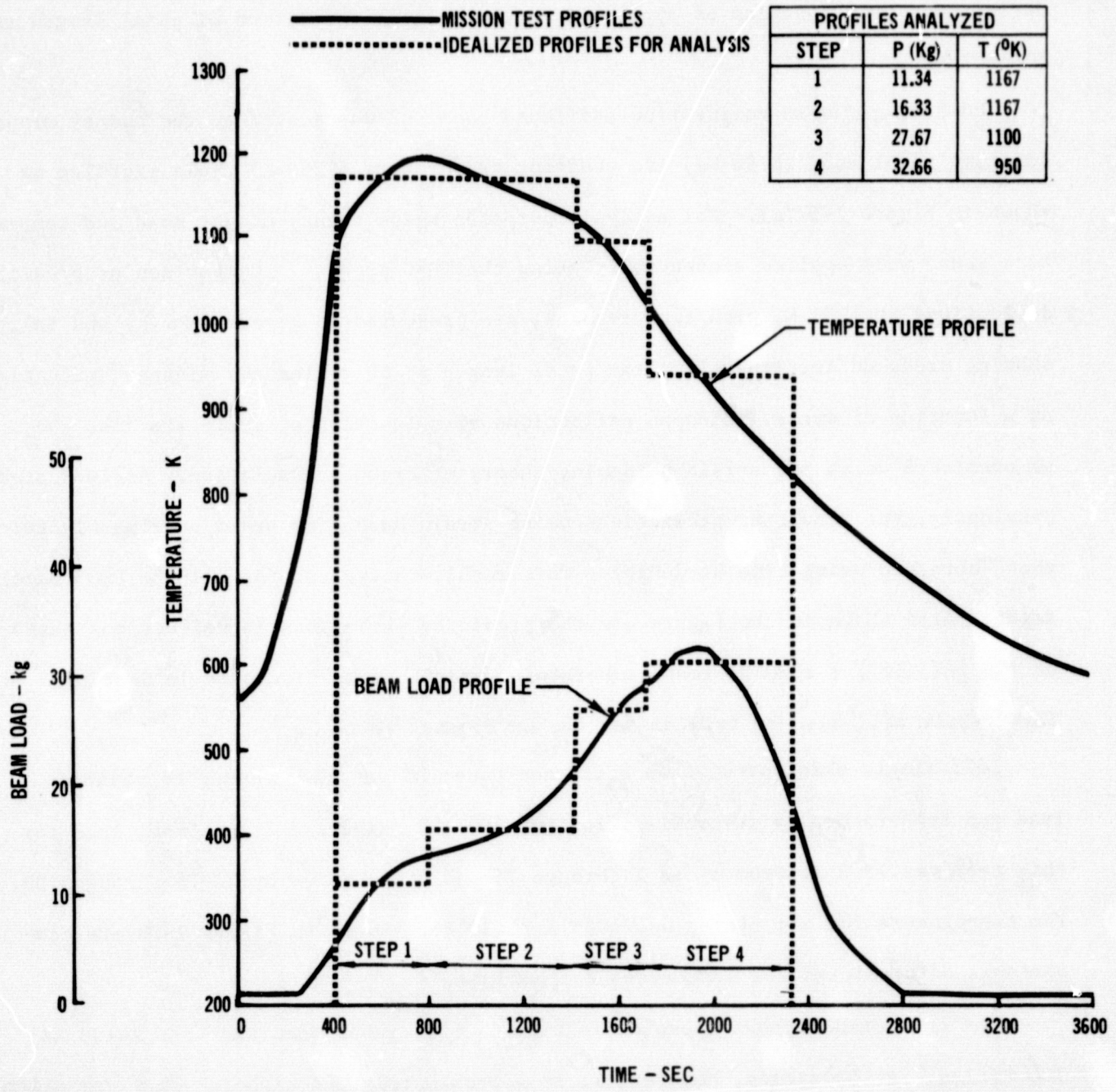

FIGURE 7-24 PROFILE IDEALIZATION FOR ANALYSIS OF SUBSIZE PANEL TEST L605–21 AND L605–24

equation (Table 7-1) in conjunction with the time hardening theory of creep accumulation. Shown in Figure 7-25 are comparisons of midspan predicted and test creep deflections as a function of cycle and deflections as a function of panel length at 50 cycles.

L605 single skin corrugation stiffened panel L2 was tested to the twenty minute constant panel load (8.98 Kg) and constant temperature (1255 K) cycle profiles as shown in Figure 7-26 (a). For analysis purposes these twenty-minute load and temperature steps were applied sequentially using the TPSC program. Comparison of predicted deflections at 1255 K, with test results, are presented in Figure 7-26 (b) and (c), showing creep deflections along the panel length at 50 cycles and midspan deflections as a function of cycle. Midspan deflections as a function of cycle are also shown as predicted using the strain hardening theory of creep accumulation. As indicated previously, the resulting predictions using strain hardening are approximately twice those obtained using time hardening. This result is typical for all the L605 panel tests. Also shown in the figure are the predicted variations in deflections based on the $\pm$1% (18°F @ 1800°F) test temperature variations as discussed in Section 5.3.1. This result will also be typical for the L605 panel tests.

L605 single skin corrugation stiffened panel L3 was also tested to constant load and temperature cycle profiles in test L605-23 (Figure 7-27). Panel load for this test was 29.8 Kg from cycle 1 through 75 and 36.1 Kg for cycle 76 through 100. The temperature for all cycles was 1053 K (1435°F). Shown in Figure 7-28 are comparisons of predicted and test creep deflections.

The predicted midspan creep deflection is 55% higher than the test value at 100 cycles. At 50 cycles, however, it is approximately 30% higher. This variation between predicted and test results is the greatest of any of the L605 corrugation panels tested.

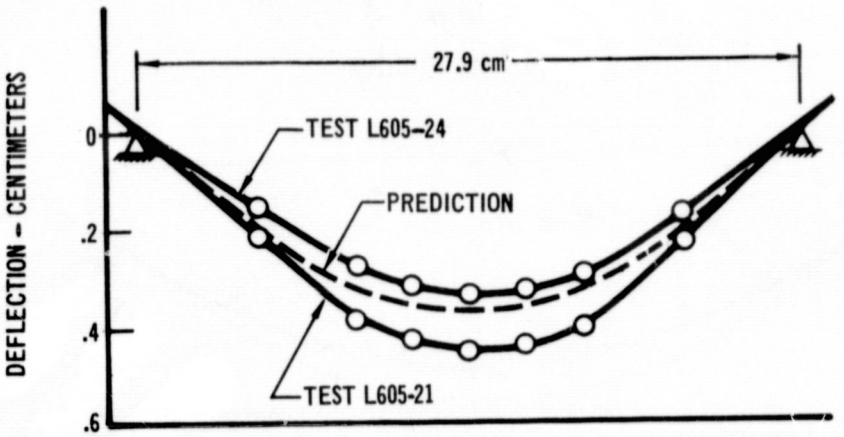

(a) Creep Deflection vs Beam Length at 50 Cycles

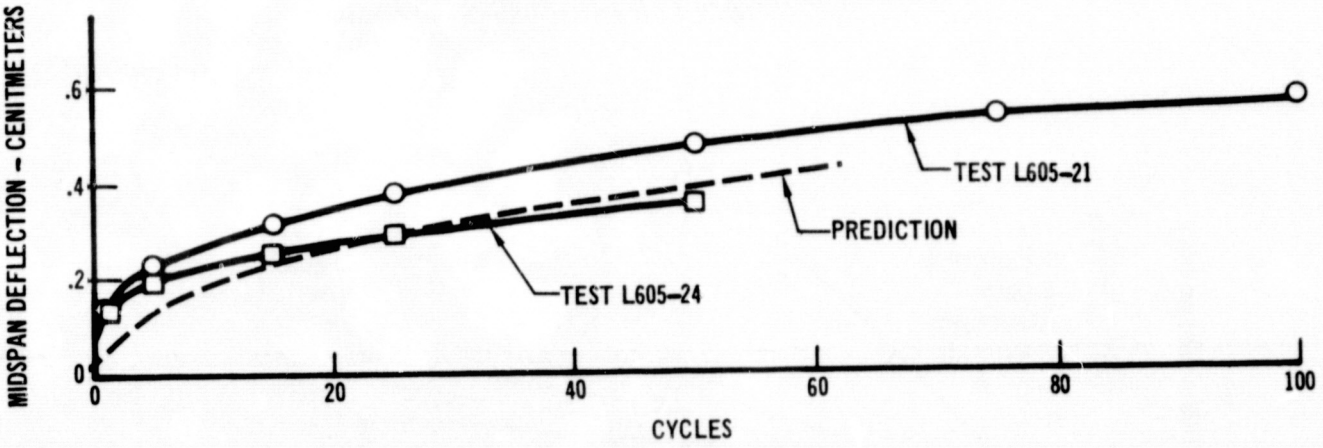

(b) Panel Midspan Creep Deflection

FIGURE 7– 25 COMPARISON OF PREDICTED CREEP DEFLECTIONS WITH RESULTS OF CORRUGATION PANEL TESTS L605–21 AND L605–24

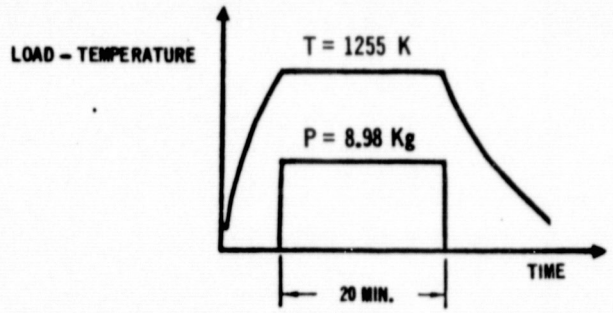

(a) Test Profiles

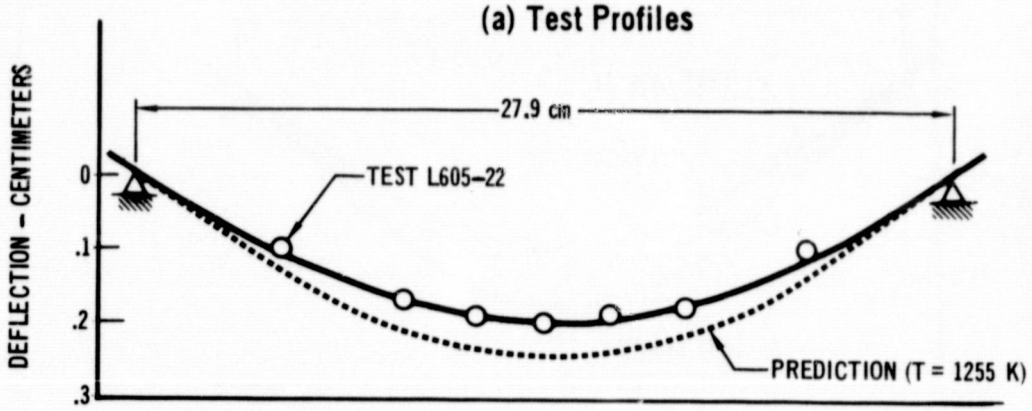

(b) Creep Deflection vs Beam Length at 50 Cycles

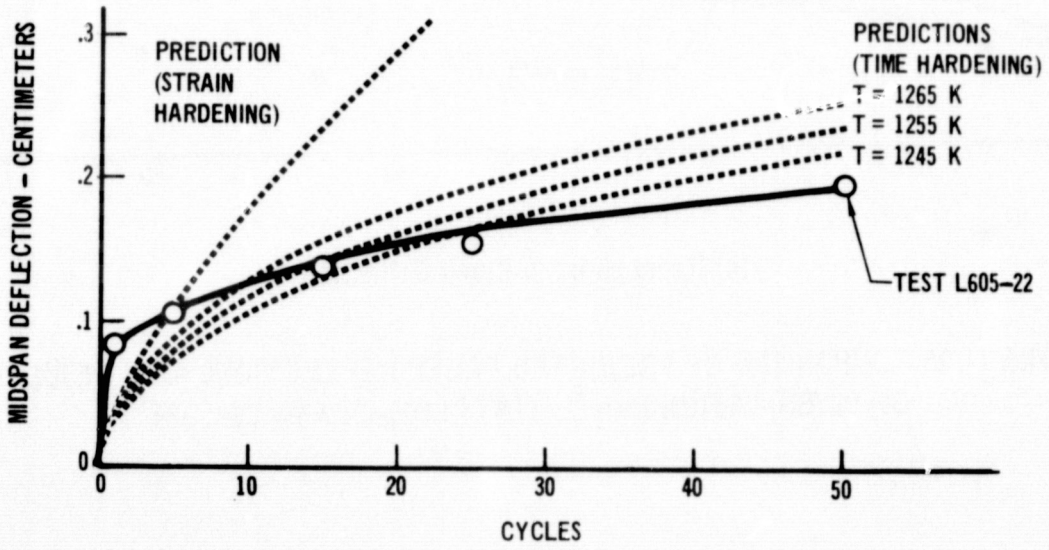

(c) Panel Midspan Creep Deflection

FIGURE 7- 26 COMPARISON OF PREDICTED CREEP DEFLECTION WITH RESULTS OF CORRUGATION PANEL TEST L605–22

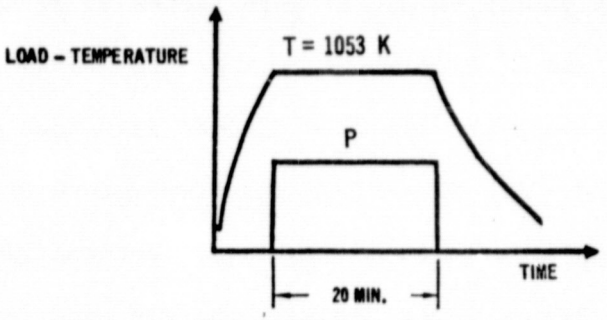

(a) Test Profiles

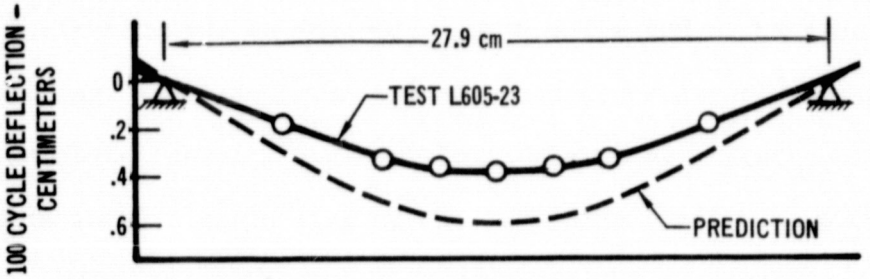

(b) Creep Deflection vs Beam Length at 100 Cycles

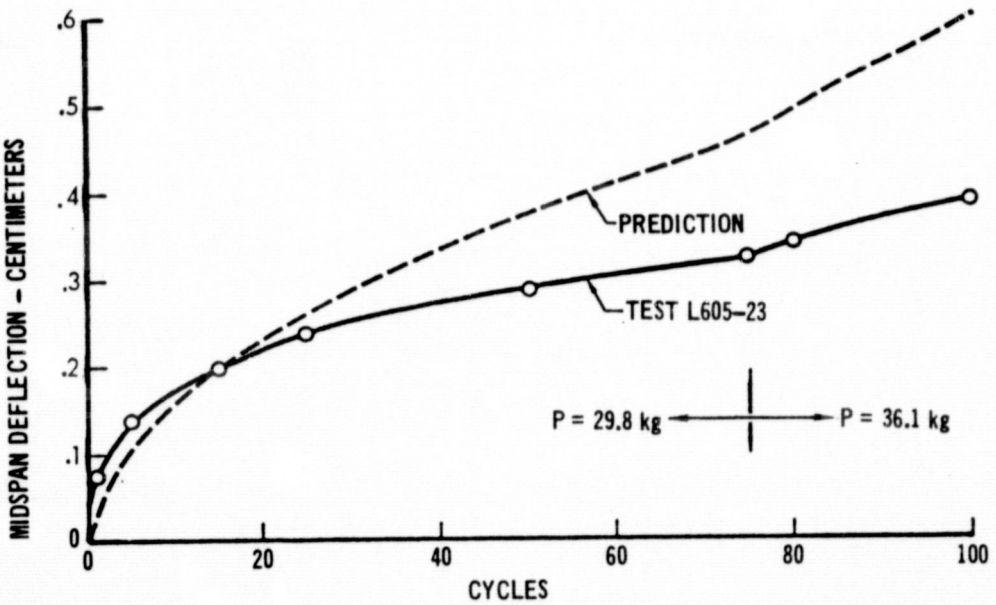

(c) Panel Midspan Creep Deflection

FIGURE 7- 27 COMPARISON OF PREDICTED CREEP DEFLECTIONS WITH RESULTS OF CORRUGATION PANEL TEST L605–23

L605 rib stiffened panels L6 and L7 were tested to 50 replicate mission profiles in tests L605-25 and L605-26 respectively. For analysis purposes the beam load profile and temperature profile were divided into four steps in the same manner as for tests L605-21 and -24. These load and temperature steps are presented in Figure 7-28. Comparison of predicted midspan deflections with test values for these two panels is shown in Figure 7-29. Because the rib panel gage was .064 cm while the equation used in analysis is based on .025 cm gage specimen tests, the material gage effect identified in Phase I was accounted for in the analysis. Therefore, the predicted deflection shown is based on the L605 empirical creep equation, modified to reflect this gage effect. This was accomplished by using the average ratio of .064 cm gage creep strains to .025 cm gage creep strains at 26 hours (50 cycles) from the Phase I tensile test data (Figure 7-15). This average ratio of .62 changed the constant in the empirical equation (Table 7-1) from -.3645 to -.8425 for use in the analysis.

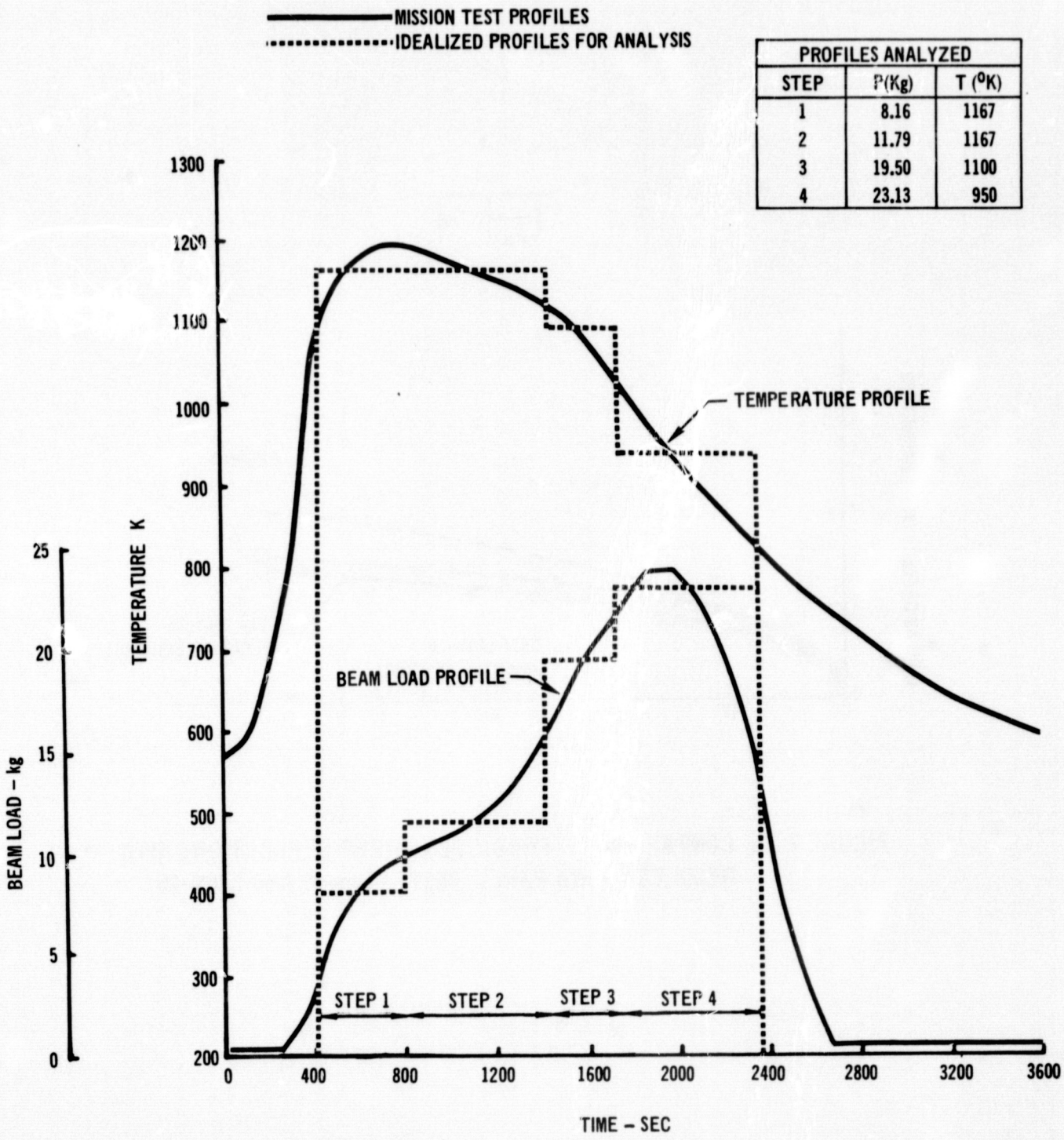

FIGURE 7- 28 PROFILE IDEALIZATION FOR ANALYSIS OF SUBSIZE PANEL TEST L605–25 AND L605–26

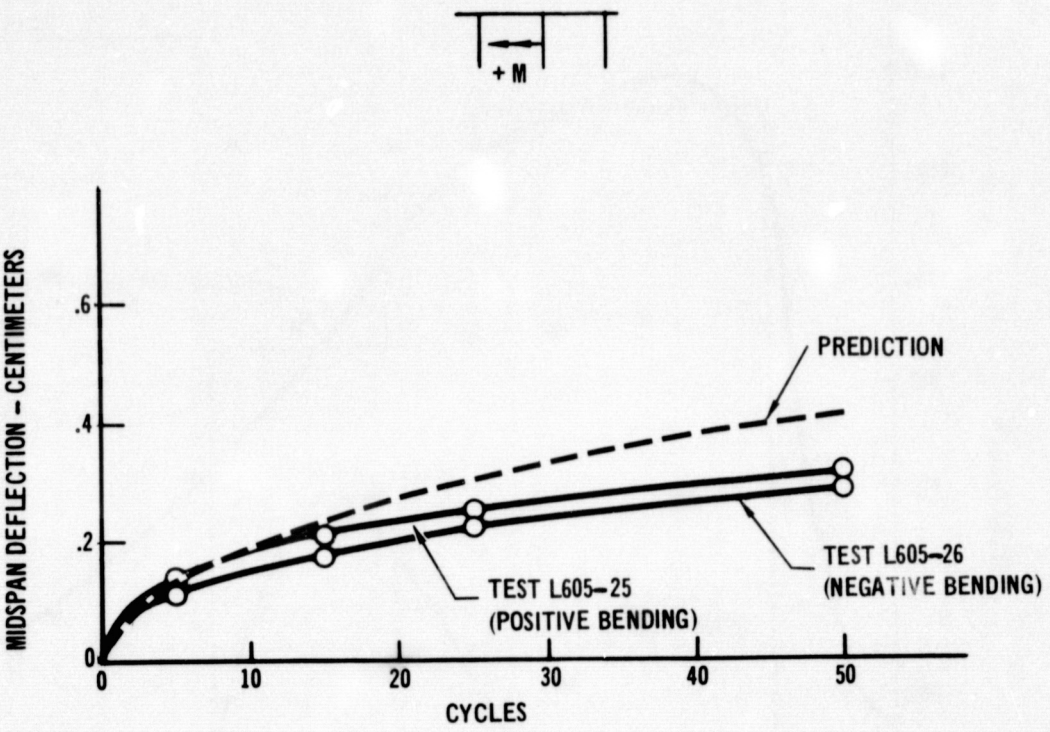

FIGURE 7–29 COMPARISON OF PREDICTED CREEP DEFLECTIONS WITH RESULTS OF RIB PANEL TESTS L605–25 AND L605–26

7.4 RENE' 41 SUBSIZE PANEL DEFLECTION ANALYSIS

Comparison is made in this section between the Rene' 41 subsize panel deflection test data and predictions based on TPSC computer program analysis. Results of the three Rene' 41 corrugation stiffened subsize panel tests were summarized in Section 6, and deflection data presented in Appendix B.

Predicted deflections for the Rene' 41 panels were not as close to test values as had been demonstrated in the case of L605. However, results were generally consistent with Rene' 41 cyclic tensile creep test data obtained in Phase I. As in the case of Phase I analysis results (Figure 7-9), the time hardening theory of creep accumulation provided the best deflection predictions, although these predictions were lower than test data for the mission profile and higher than test data for the constant load and temperature profiles.

Single skin corrugation stiffened subsize panel R1 was tested to mission temperature and load profiles in test Rene-21. For analysis purposes these profiles were idealized into four steps, as shown in Figure 7-30, for application in conjunction with the Rene' 41 empirical cyclic creep equation (Table 7-1). Presented in Figure 7-31 are comparisons of predicted and test midspan creep deflections as a function of cycle and deflections as a function of panel length at 50 cycles. Predictions are plotted to 60 cycles in Figure 7-31(b). This represents approximately the time limit of applicability of the Rene' 41 empirical equation. Beyond this time predictions increase rapidly due to the t^3 term in the equation.

Both the time hardening and strain hardening theories of creep accumulation yield comparable deflection predictions with the time hardening theory 27% below the test value and strain hardening theory 35% above the test value at 50 cycles. In the analysis for this panel the temperature was assumed constant along the panel length. The effect of temperature distribution and temperature levels on panel deflection predictions will be considered in the analysis of subsize panel test Rene-22.

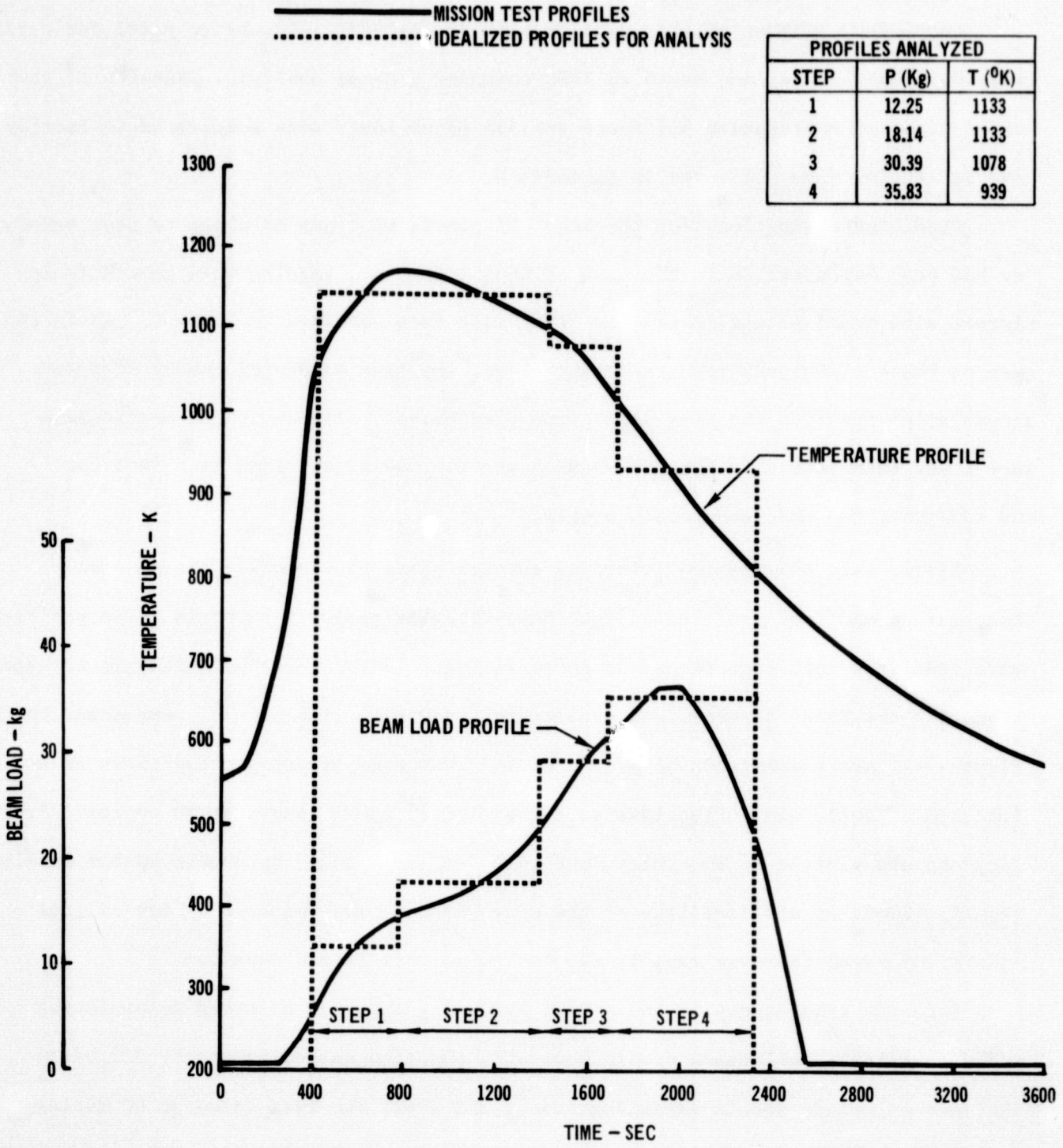

FIGURE 7–30 PROFILE IDEALIZATION FOR ANALYSIS OF SUBSIZE PANEL TEST RENE' – 21

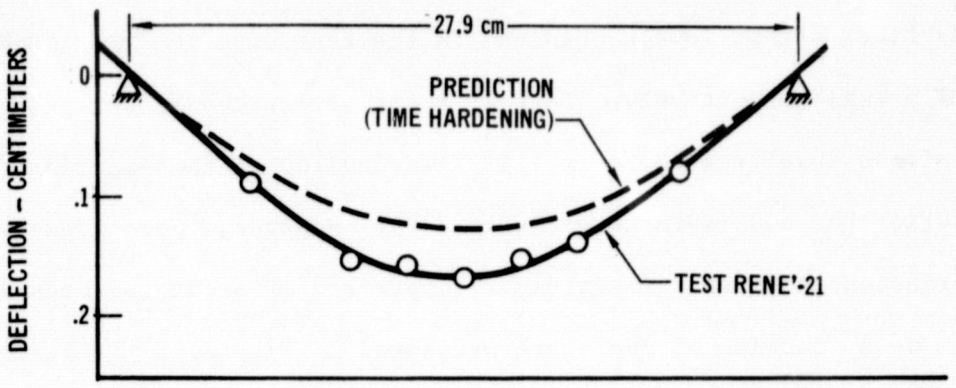

(a) Creep Deflection vs Beam Length at 50 Cycles

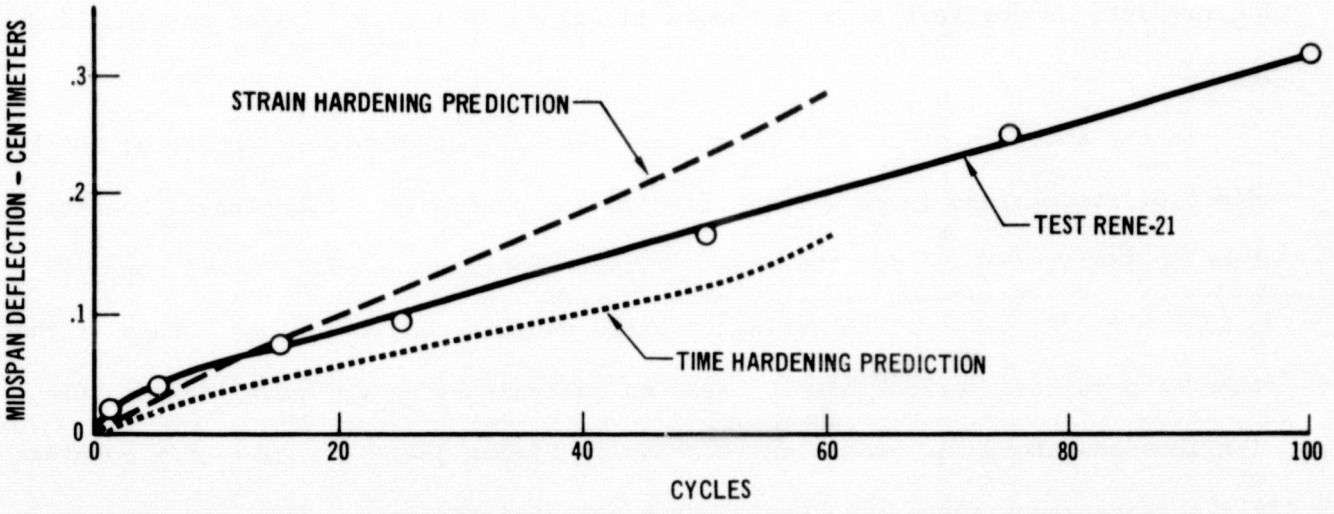

(b) Panel Midspan Creep Deflection

FIGURE 7-31 COMPARISON OF PREDICTED CREEP DEFLECTIONS WITH RESULTS OF CORRUGATION STIFFENED PANEL TEST RENE-21

Rene' 41 single skin corrugation stiffened panels R2 and R3 were tested to constant panel load and temperature profiles in tests Rene-22 and Rene-23 respectively. Applied loads were 45.2 Kg (99.7 lbs) and 56.6 Kg (127.7 lbs) respectively for the two panels over the twenty-minute cycle time as shown in Figures 7-32(a) and 7-33(a). Temperature in both tests was 1111 K (1540°F). Panel outer fiber stress levels obtained in the test were 165 MPa (23.7 ksi) and 224 MPa (32.5 Ksi) respectively. Both of these stress levels were above the 104.1 MPa stress level tested to at 1111 K in developing the empirical creep equation during Phase I (Reference Figure 7-2). However, these loads were applied to attain reasonable creep deflections. Comparison of predicted midspan creep deflections as a function of cycle are presented in Figures 7-32(b) and 7-33(b). Predictions based on the strain hardening theory of creep accumulation were again higher than those based on time hardening, as shown for test Rene-22 in Figure 7-32(b). The predictions for test Rene-23, shown in Figure 7-33(b) are based on time hardening.

In the analysis of subsize panel test Rene-22, studies were conducted on the effect of temperature level and distribution on predicted deflections. Results are shown in Figure 7-32(b) for the peak midspan temperature of 1111 K and for $\pm$ 1% ($\pm$ 15°F $\sim$ $\pm$ 8°K) temperature variation based on furnace limitations. Each of these lines of predicted deflections is based on analysis using the panel temperature distributions along the panel length shown in Figure 5-4. The case of a constant 1111 K temperature along the panel length was also analyzed. This resulted in a midspan 50 cycle creep deflection of .485 cm. (.191 inch) as compared to the .424 cm (.167 inch) deflection when the panel temperature distribution was applied (Figure 7-32). This study demonstrates the sensitivity of Rene' 41 panel creep deflections to temperature used in the predictions.

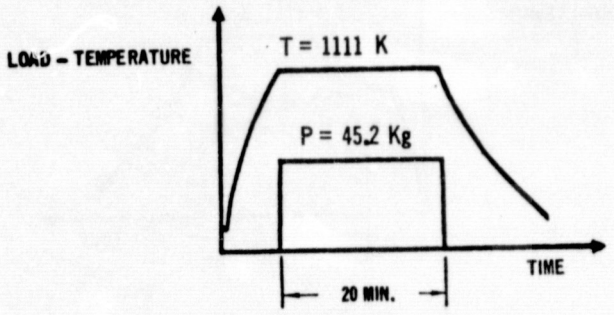

(a) Test Profiles

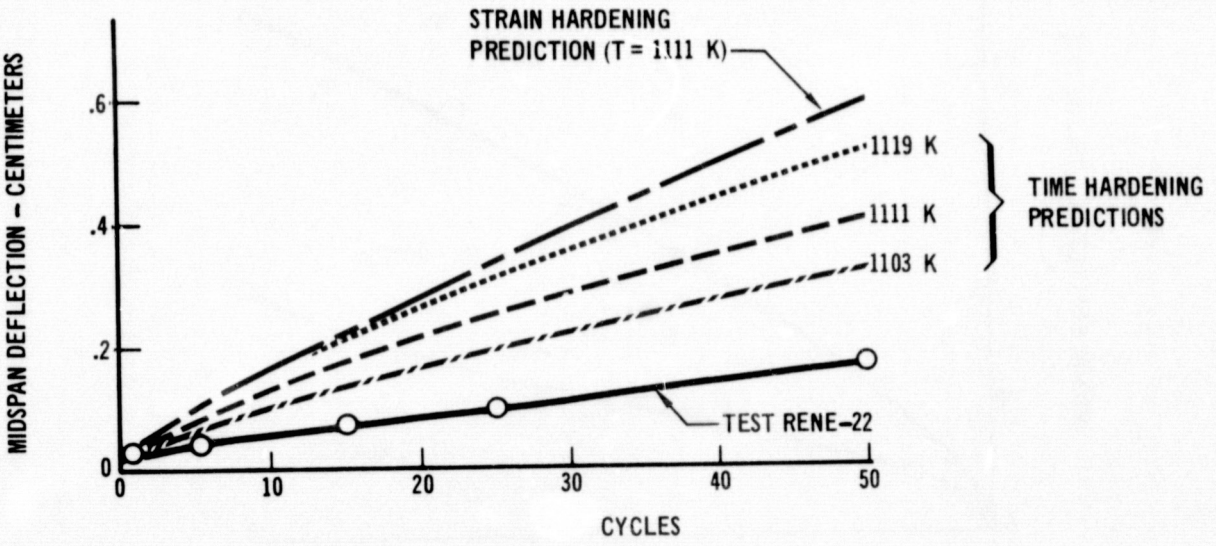

(b) Panel Midspan Creep Reflection

FIGURE 7–32 COMPARISON OF PREDICTED CREEP DEFLECTIONS WITH RESULTS OF CORRUGATION STIFFENED PANEL TEST RENE-22.

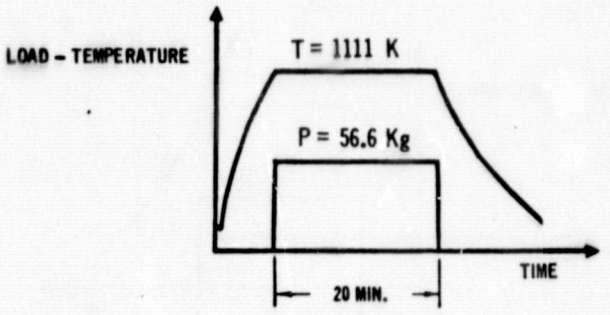

(a) Test Profiles

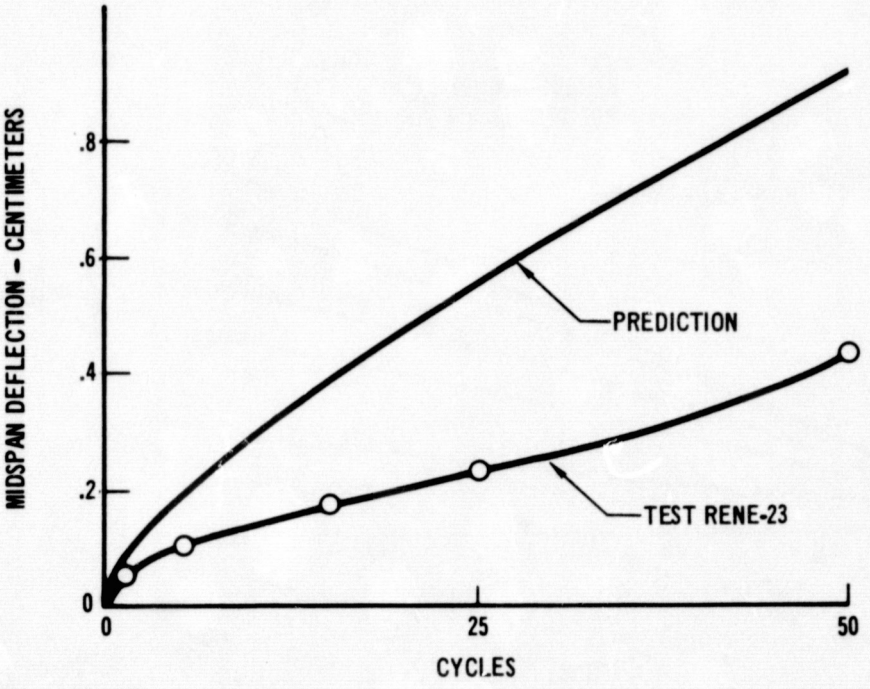

(b) Panel Midspan Creep Deflection

FIGURE 7–33 COMPARISON OF PREDICTED DEFLECTIONS WITH RESULTS OF CORRUGATION STIFFENED PANEL TEST RENE–23

7.5 TITANIUM SUBSIZE PANEL DEFLECTION ANALYSIS

Four 6Al-4V titanium corrugation stiffened panels and two rib-stiffened panels were tested in this Phase. Data obtained in these tests were summarized previously in Section 6.0 and are presented in Appendix B.

Analysis for these panels, using the time hardening theory of creep accumulation in conjunction with the titanium empirical creep strain equation (Table 7-1), resulted in reasonably good agreement between predicted and test deflections. These predictions were very good for tests Titanium-22 and Titanium-25, approximately 60% lower than test values for replicate tests Titanium-23 and -24, and approximately double the test values for test Titanium-26. Predictions based on the strain hardening theory of creep accumulation were significantly higher than those based on time hardening. This is generally consistent with Phase I tensile creep results where strain hardening resulted in higher creep strain predictions, although even the strain hardening predictions were below test values for the mission profile test as shown in Figure 7-10.

The shape of the predicted deflection curves as a function of time (or cycle) are in good agreement with the test data. This is consistent with the prediction capability of the empirical equation as indicated in Figure 7-3.

Titanium single skin corrugation stiffened panels T1 and T2 were tested to constant panel load and temperature profiles in tests Titanium-21 and Titanium-22 respectively. Applied loads were 43.0 Kg (94.7 lbs) and 31.1 Kg (68.6 lbs). The temperature was 783 K (950°F) for both tests over the twenty minute cycle time. Because of the skin buckling which occurred in test Titanium-21, (Ref. Section 6.3) no creep deflection analysis was conducted. Comparison of predicted creep deflections with data obtained in test Titanium 22 are, however, shown in Figure 7-34, based on time hardening. Also presented are the effects of applying $\pm$1% ($\pm$10°F $\sim$ 6 K) temperature variation in the analysis, again demonstrating the sensitivity of creep deflections to temperature. In the analysis of this panel temperatures shown

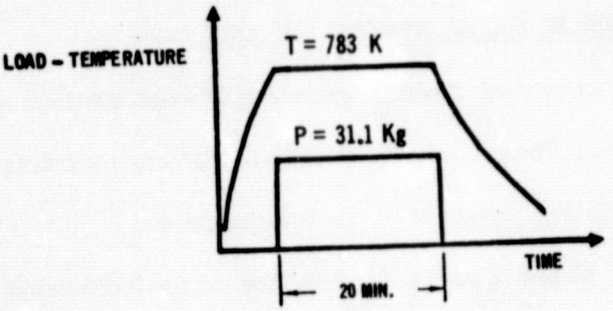

(a) Test Profiles

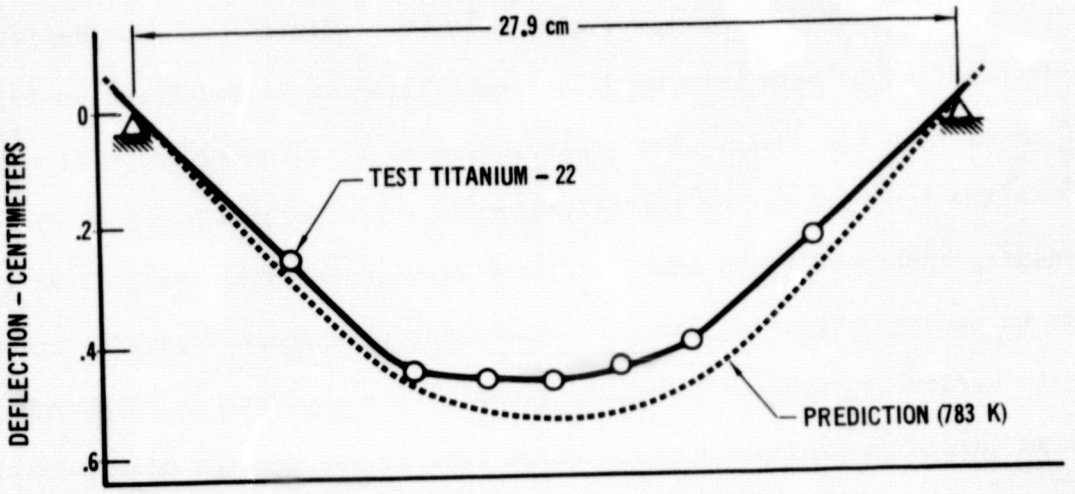

(b) Creep Deflection vs Beam Length at 100 Cycles

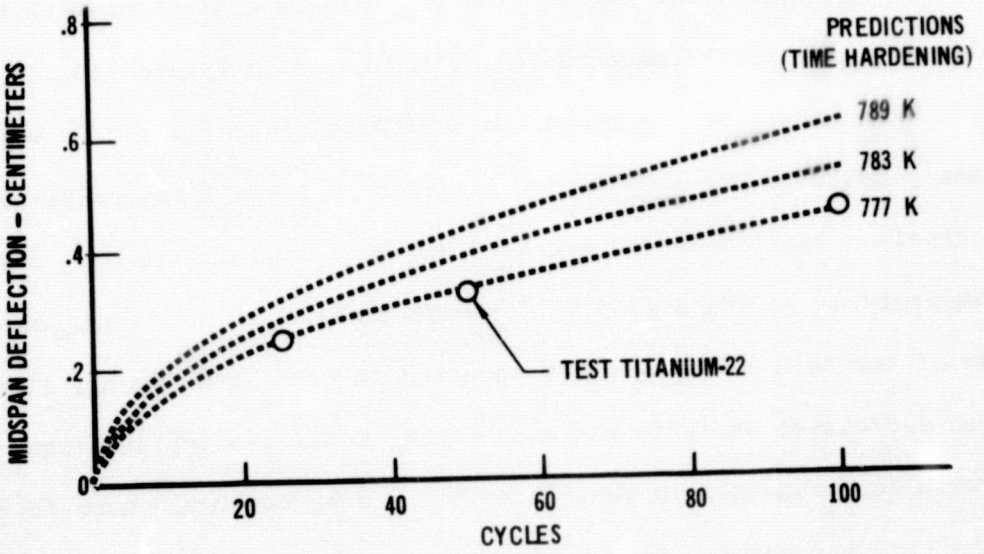

(c) Midspan Panel Deflections

FIGURE 7–34 COMPARISON OF PREDICTED CREEP DEFLECTIONS WITH RESULTS OF CORRUGATION STIFFENED PANEL TEST TITANIUM – 22.

were assumed constant along the panel length. No further analysis was conducted because of the good agreement, although use of the actual panel temperature distribution shown in Figure 5-4 would result in an improvement in the prediction.

Titanium corrugation stiffened panels T3 and T4 were tested to repliace mission profiles in tests Titanium-23 and Titanium-24 respectively. For analysis purposes the load and temperature profile were divided into four steps as done in analysis of previous mission profile tests. These load and temperature steps analyzed are shown in Figure 7-35. Comparison of predicted midspan deflections with test values for these two panels is presented in Figure 7-36. An additional study was conducted for this panel using a five-step idealization of the load and temperature profiles between the times of 200 and 2400 seconds. Analysis results using this independent idealization, however, resulted in only a 5% increase in predicted deflections. The low predicted deflections relative to the test values is consistent with Phase I tensile creep results as shown in Figure 7-10.

Titanium rib stiffened subsize panel T7 was also tested to mission load and temperature profiles, in test Titanium-25. These profiles and the idealization used in analysis are shown in Figure 7-37. Good agreement was obtained between test deflections and predictions based on time hardening. These deflections are presented in Figure 7-38. The actual panel temperature distribution shown in Figure 5-4 was used in this analysis.

Titanium rib-stiffened subsize panel T8 was tested to the constant load (51.8 Kg) and temperature (714 K) profiles shown in Figure 7-39(a). Comparison of predicted and test deflections for this panel are presented in Figure 7-39 (b) and (c). Predicted deflections as a function of cycle are shown for both time hardening and strain hardening theories of creep accumulation.

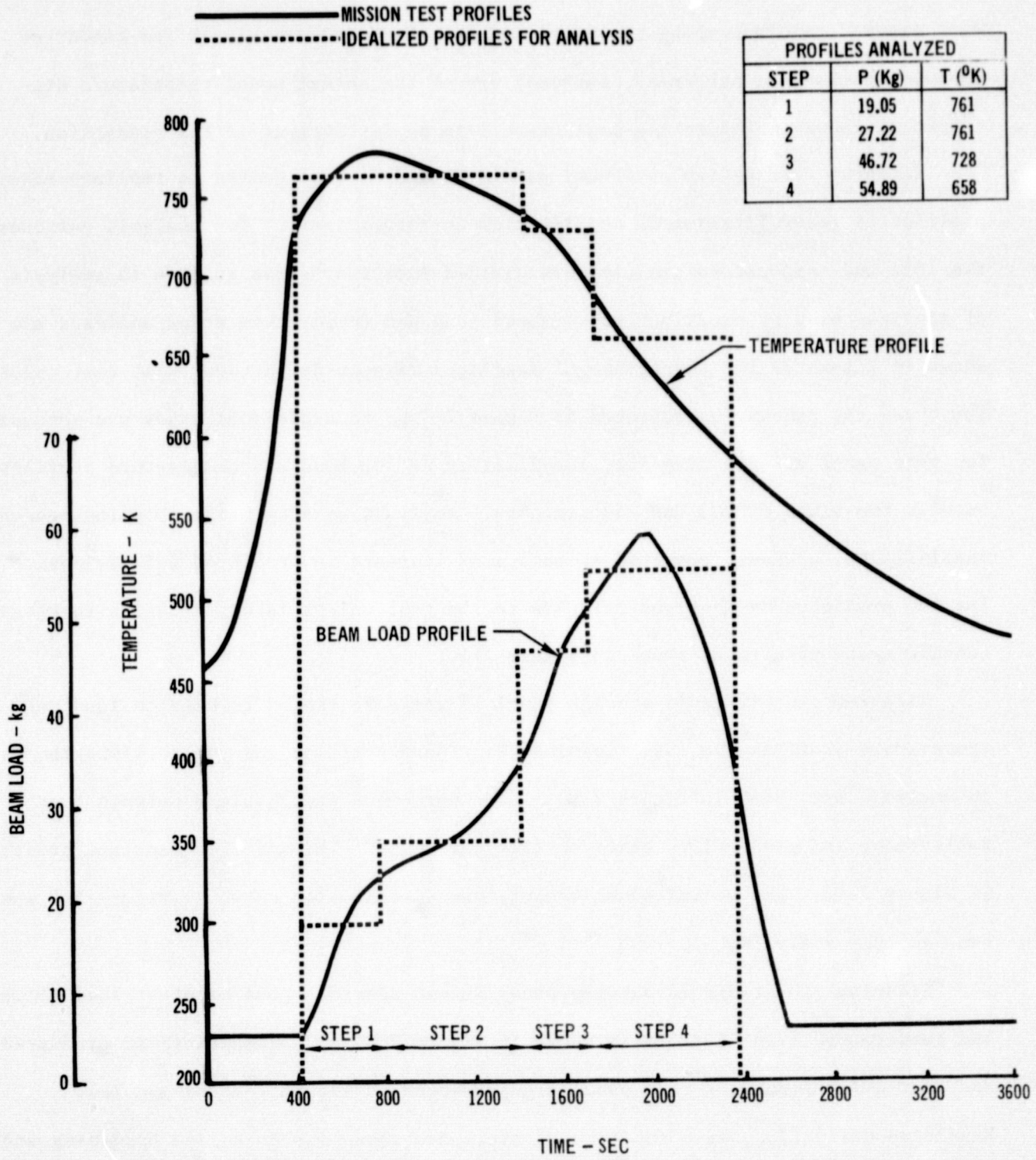

FIGURE 7–35 PROFILE IDEALIZATION FOR ANALYSIS OF SUBSIZE PANEL TEST TITANIUM–23 AND TITANIUM–24

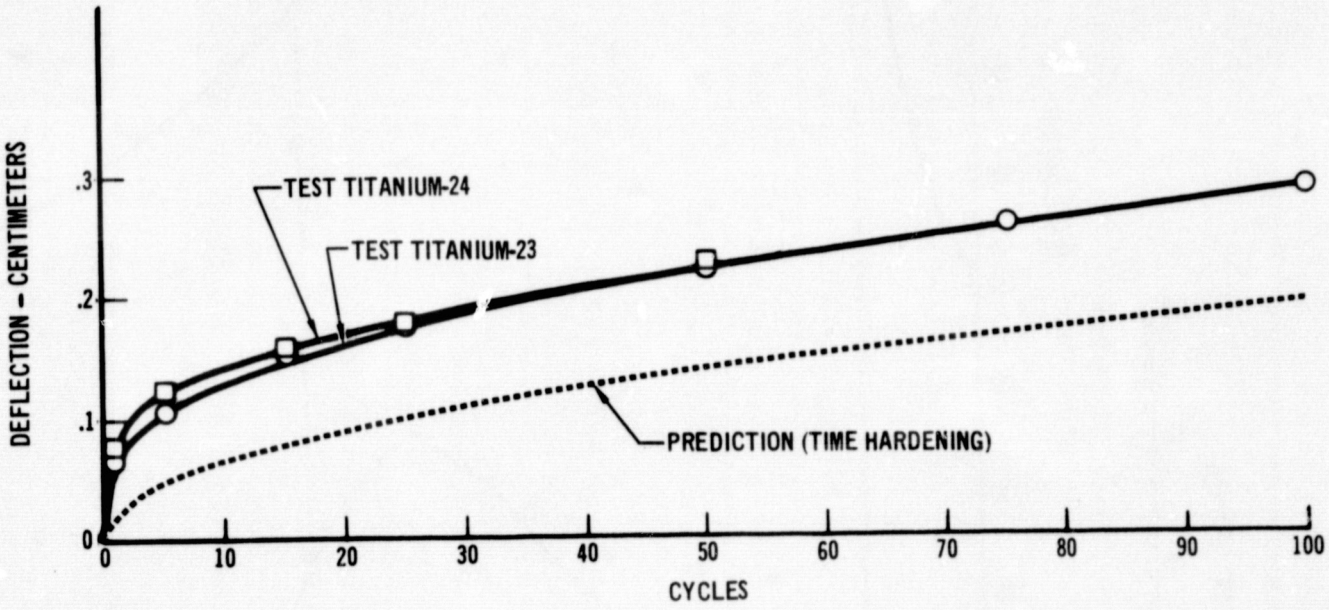

FIGURE 7-36 COMPARISON OF PREDICTED CREEP DEFLECTION WITH RESULTS OF CORRUGATION STIFFENED PANEL TEST TITANIUM-23 AND -24

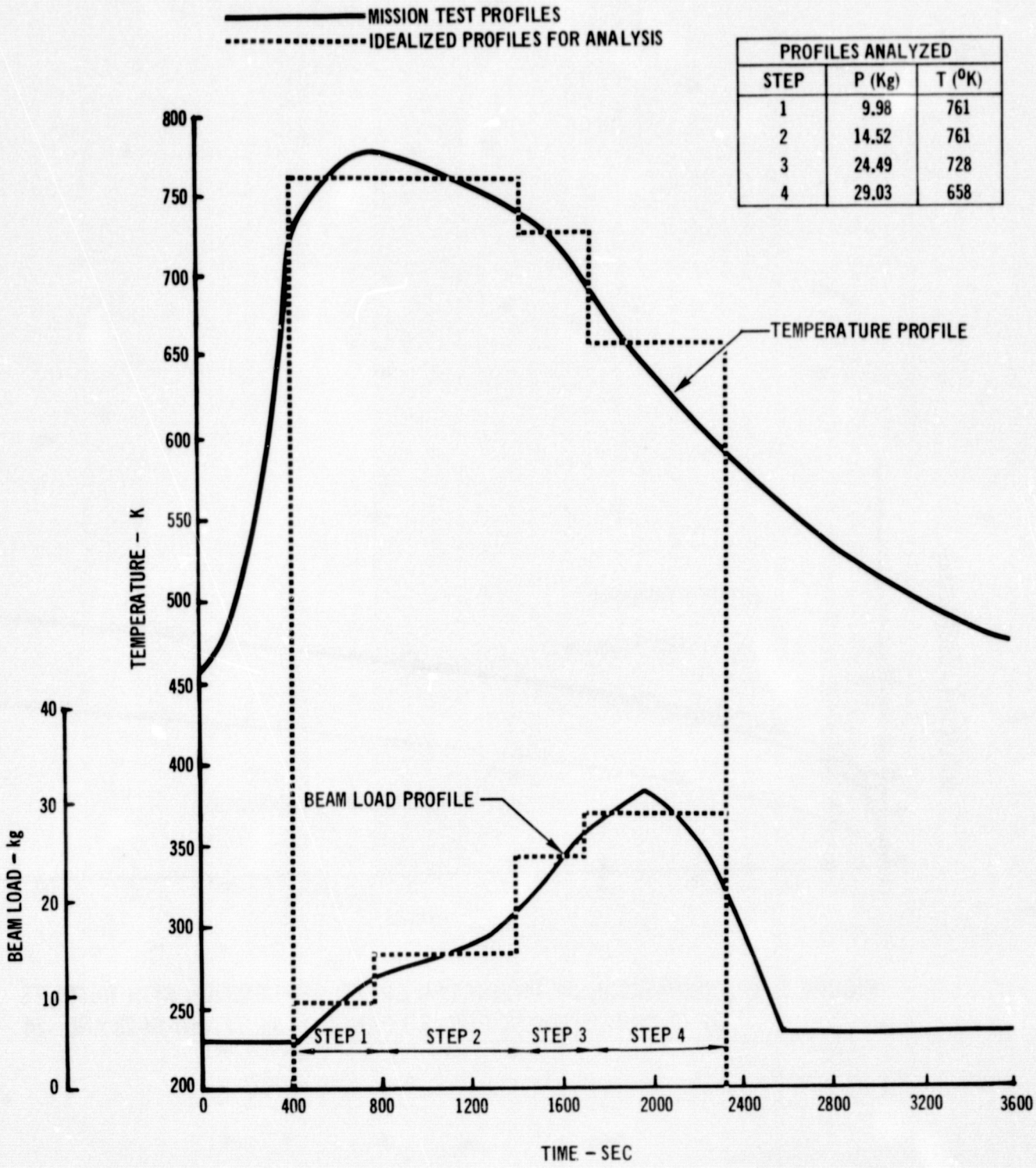

FIGURE 7–37 PROFILE IDEALIZATION FOR ANALYSIS OF SUBSIZE PANEL TEST TITANIUM – 25

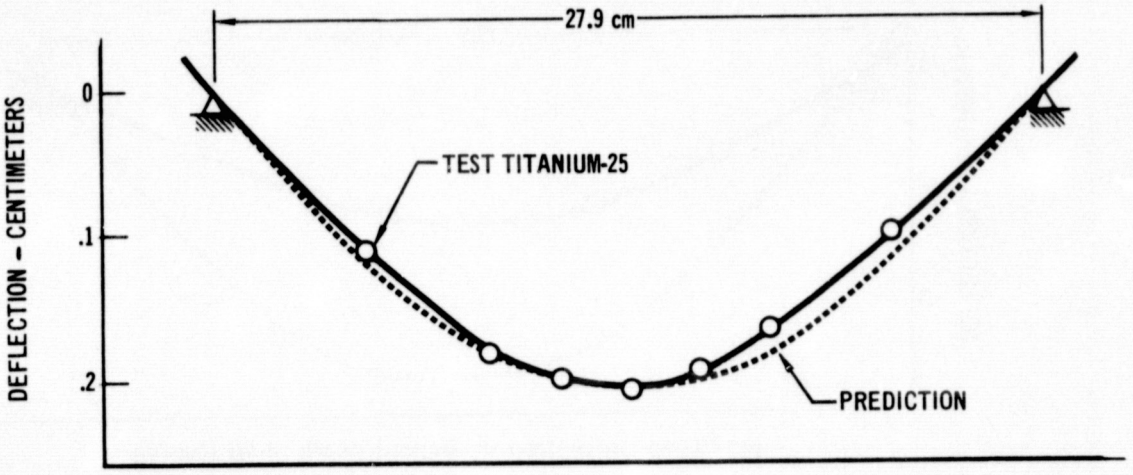

(a) Creep Deflection vs Beam Length at 50 Cycles

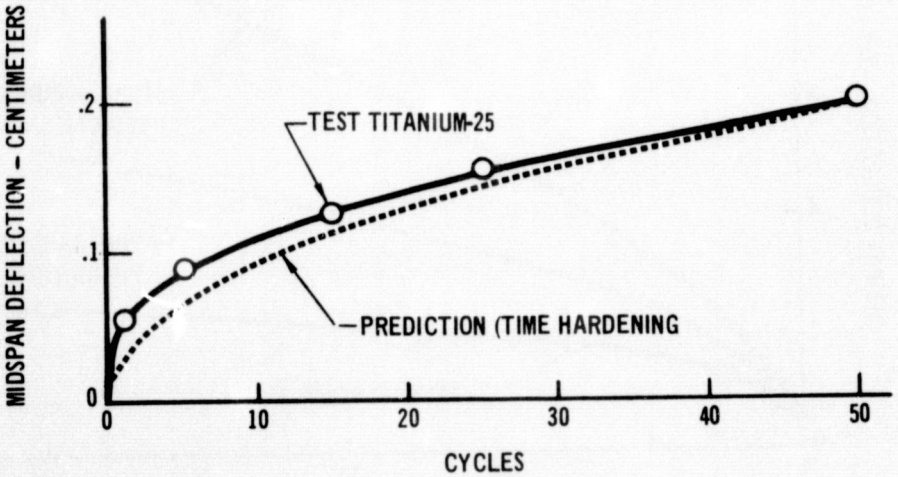

(b) Midspan Panel Deflections

FIGURE 7- 38 COMPARISON OF PREDICTED CREEP DEFLECTIONS WITH RESULTS OF RIB STIFFENED PANEL TEST TITANIUM-25

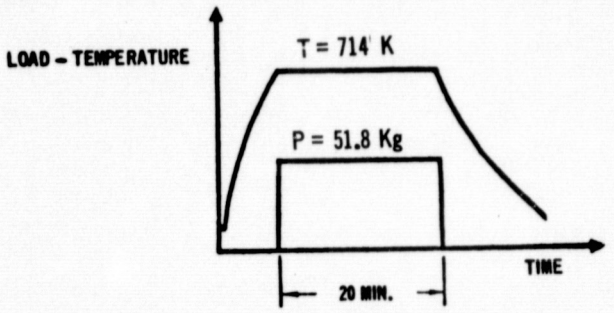

(a) Test Profiles

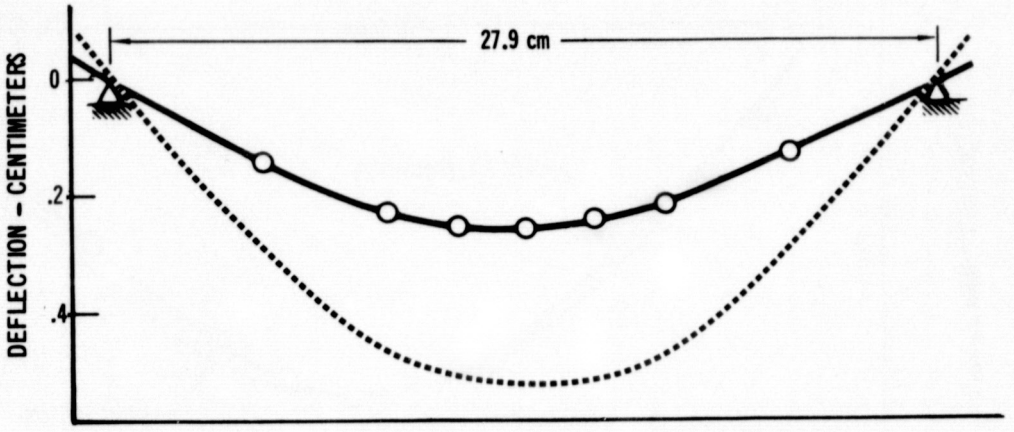

(b) Creep Deflection vs Beam Length at 50 Cycles

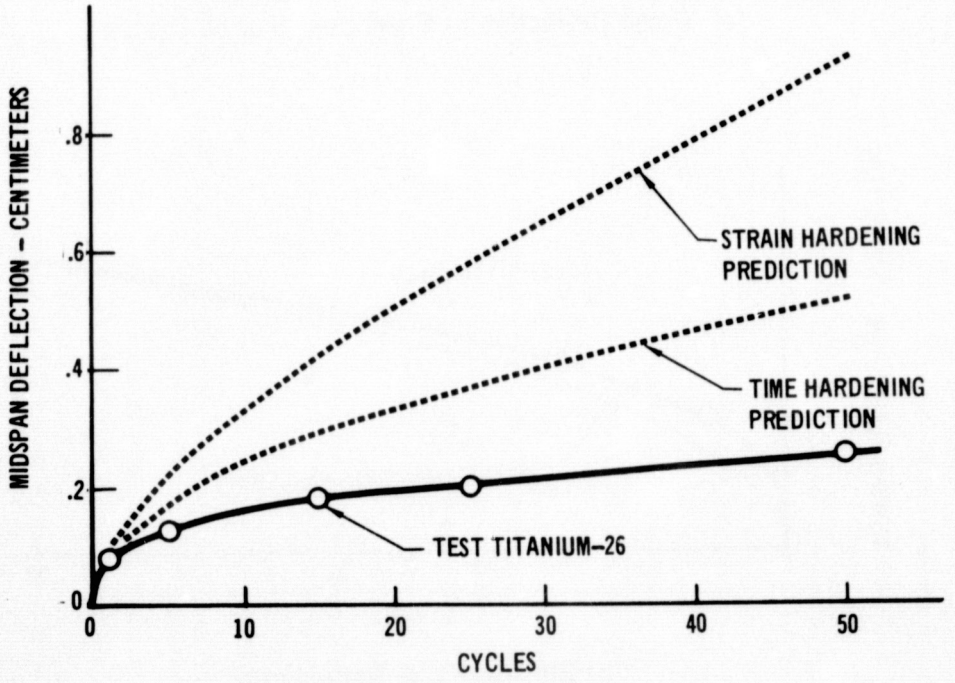

(c) Midspan Panel Deflections

FIGURE 7– 39 COMPARISON OF PREDICTED CREEP DEFLECTIONS WITH RESULTS OF RIB STIFFENED PANEL TEST TITANIUM-26

7.6 TDNiCr SUBSIZE PANEL DEFLECTION ANALYSIS

Two corrugation stiffened subsize panels were tested. TDNiCr panel TD1 was tested to 50 constant load and temperature profiles and panel TD2 was tested to 100 mission load and temperature profiles. These profiles are presented in Figures 7-40(a) and 7-41. Also shown in Figure 7-41 is the four-step idealization used in analysis for subsize panel TD1. Deflection data for these panel tests are presented in Appendix B.

During Phase I it was noted that because TDNiCr exhibited very low creep strains before failure occurred, creep deflections should not be a designing criteria for thermal protection system panels fabricated of this material. Therefore, additional emphasis was placed on obtaining stress-temperature data where failures occurred. Test load levels for the subsize panels were therefore selected to be less than those at which panel failures would occur and very little panel creep deflection was expected. Comparison of test and predicted deflections for the two panels are shown in Figures 7-40(b) and 7-42. Also shown with the prediction for test TDNiCr-21 is the effect of a $\pm$ 1% (22°F $\sim$ 12°K) temperature variation. Predicted deflections using the strain hardening theory of creep accumulation were found to be approximately twice those based on time hardening. The time hardening prediction obtained for mission profile test TDNiCr-22 is approximately 50% of test values as shown in Figure 7-42. This result is consistent with results of Phase I tensile creep tests, for the same profiles, shown in Figure 7-11. Predicted deflections for test TDNiCr-21 are higher than test values. No rationale has been determined for this apparent inconsistency between the two tests.

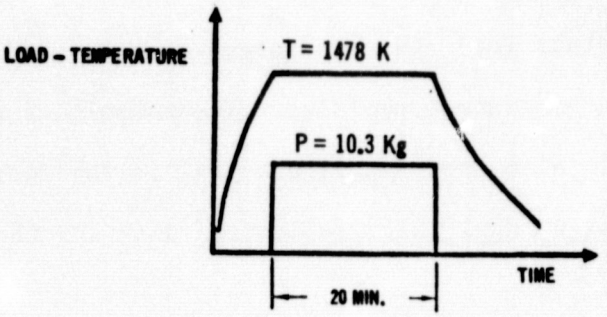

(a) Test Profiles

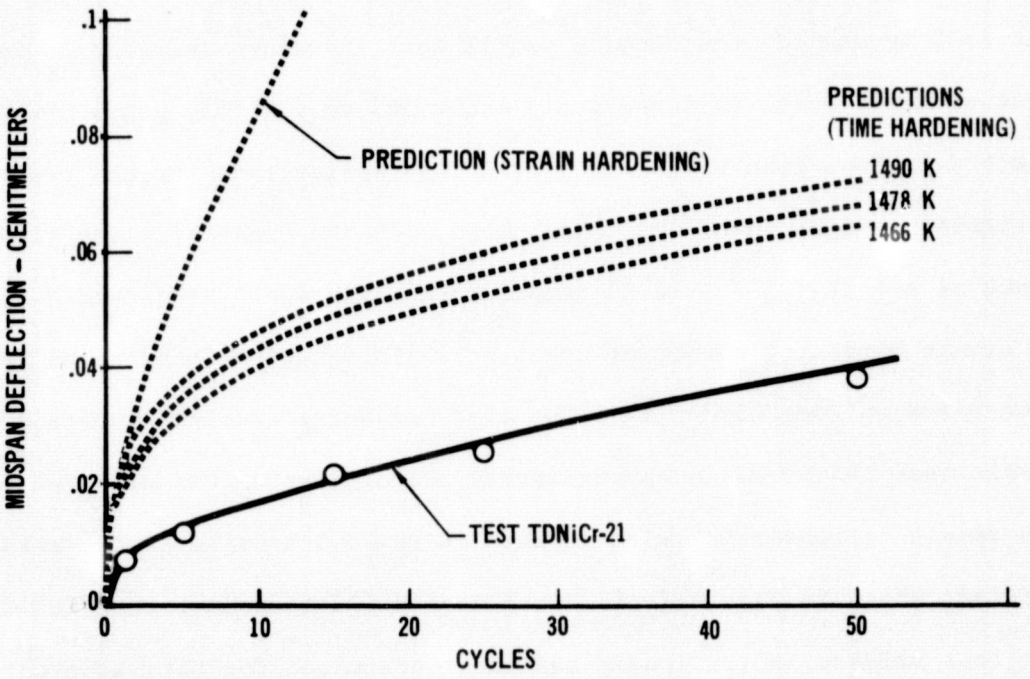

(b) Midspan Panel Deflection

FIGURE 7–40 COMPARISON OF PREDICTED CREEP DEFLECTIONS WITH RESULTS OF CORRUGATION STIFFENED PANEL TEST TDNiCr–21

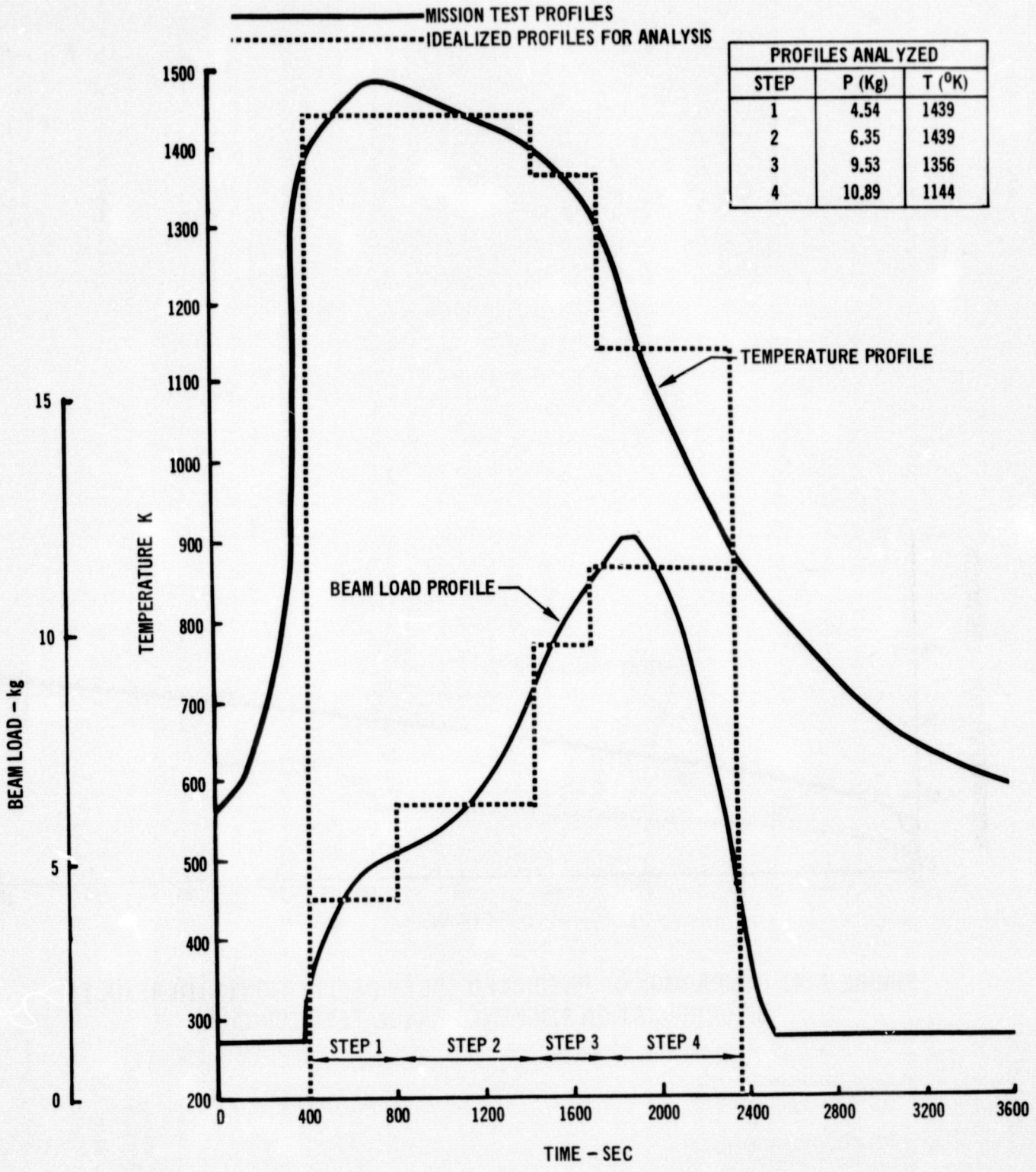

FIGURE 7–41 PROFILE IDEALIZATION FOR ANALYSIS OF SUBSIZE PANEL TEST TDNiCr–22.

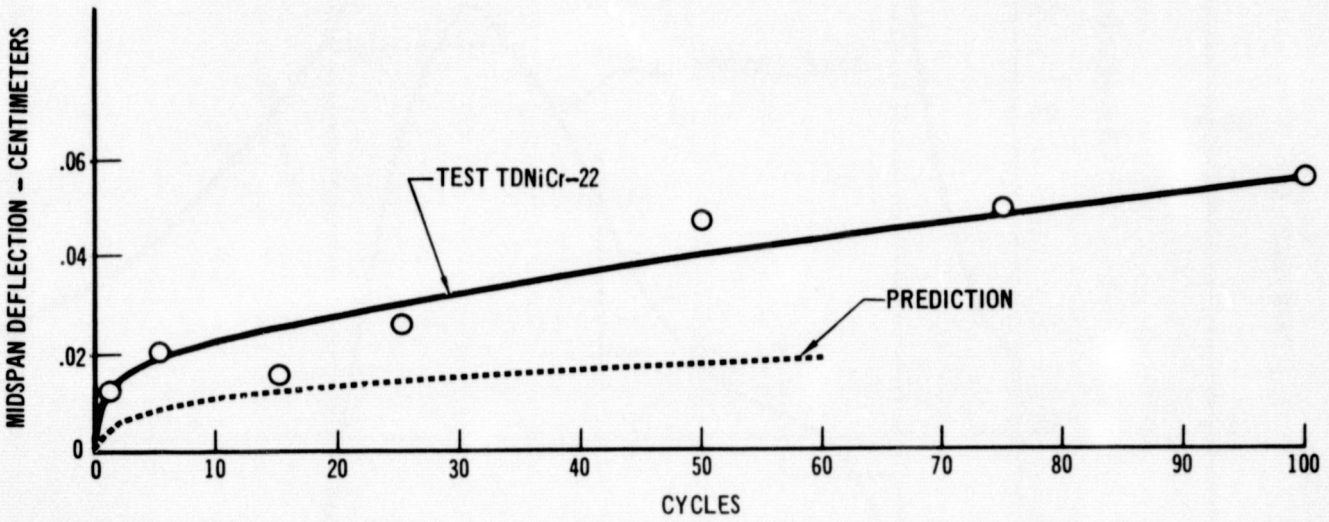

FIGURE 7–42 COMPARISON OF PREDICTED CREEP DEFLECTIONS WITH RESULTS OF CORRUGATION STIFFENED PANEL TEST TDNiCr-22

7.7 RESIDUAL STRESS AND CREEP STRAIN DISTRIBUTIONS

TPSC computer program output includes calculated creep strain and residual stress distributions through the panel depth at the X stations along the panel length and as a function of cycles. These calculations were discussed previously in Section 7.2. Although no data are available from the subsize panel tests to substantiate these calculations, typical predictions are presented in this section for a corrugation and rib-stiffened panel. Shown in Figure 7-43 and 7-44 are the distributions at panel midspan for panels in tests L605-21 and L605-22 respectively.

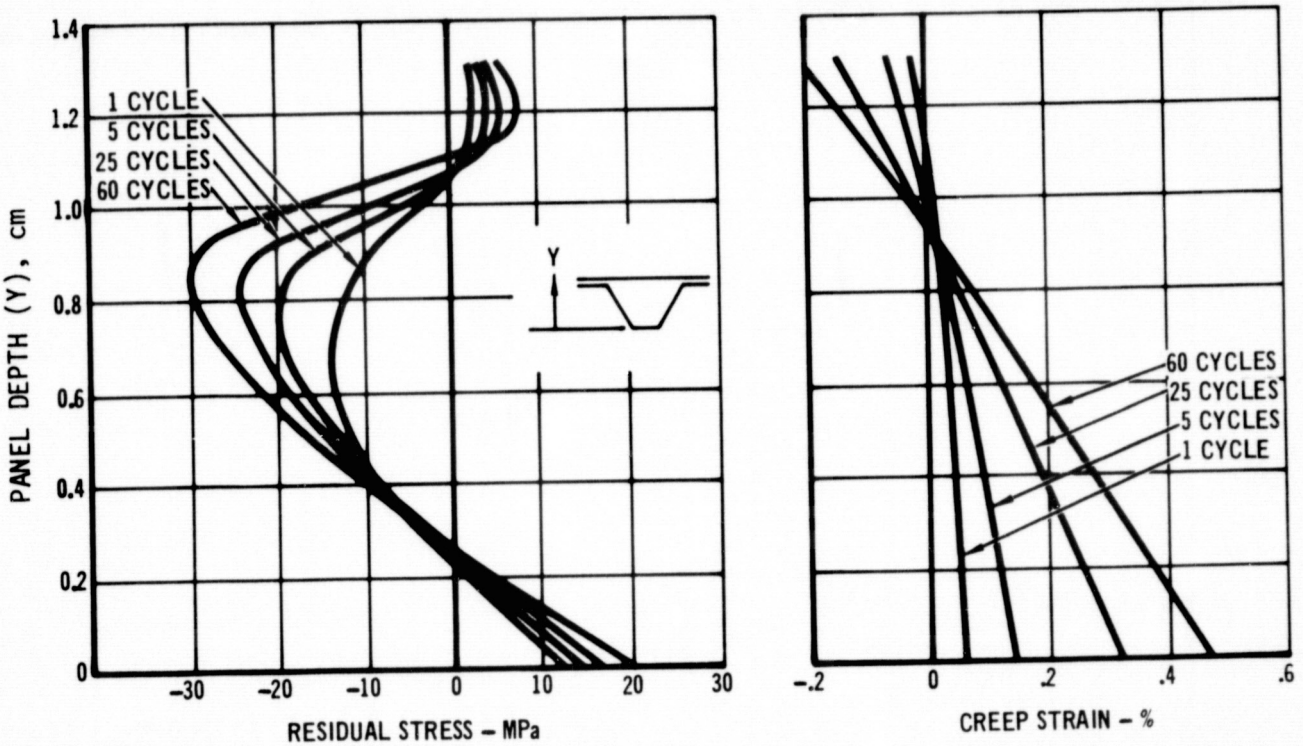

FIGURE 7–43 CALCULATED MIDSPAN RESIDUAL STRESS AND CREEP STRAIN DISTRIBUTIONS IN CORRUGATION STIFFENED SUBSIZE PANEL L1 (TEST L605–21)

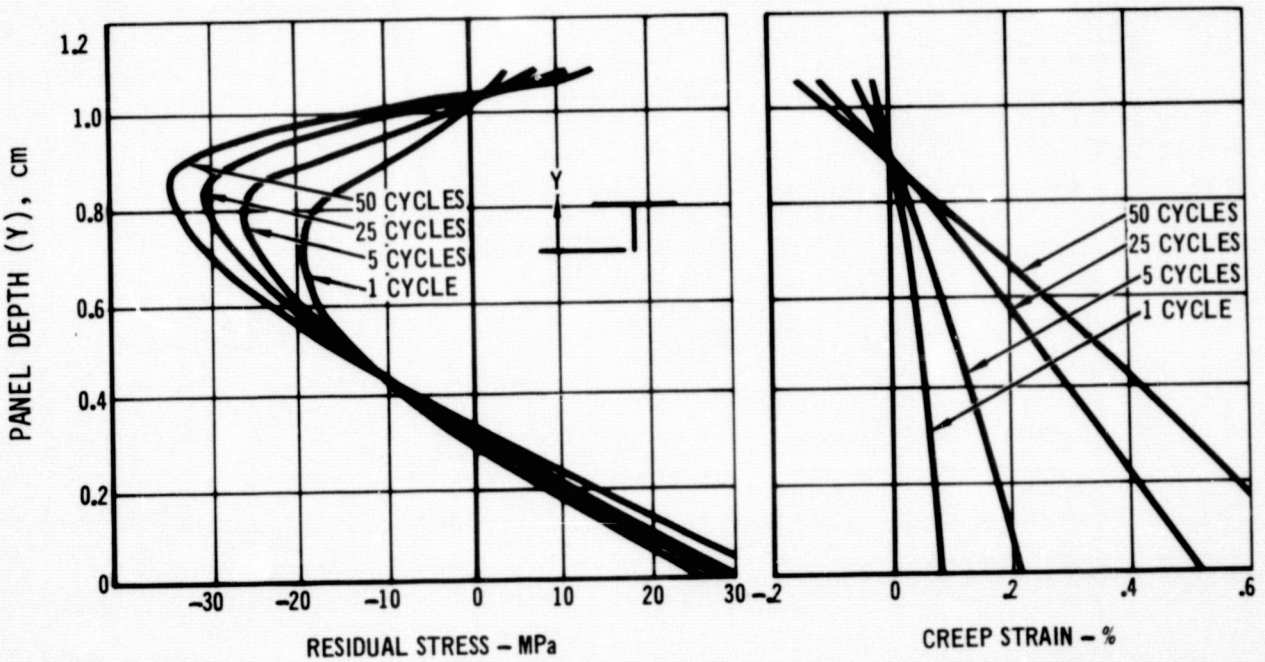

FIGURE 7- 44 CALCULATED MIDSPAN RESIDUAL STRESS AND CREEP STRAIN DISTRIBUTIONS IN RIB STIFFENED SUBSIZE PANEL L6 (TEST L605–25)

8.0 EVALUATION OF ANALYTICAL CAPABILITY

It is difficult to determine to what extent each analytical assumption and test parameter influences the predictive capability of the TPSC program. Additionally, during tensile testing (Reference 1) several factors were identified which can affect panel creep deflections. These include the applicability of empirical equations, based on regression analysis of tensile creep data, and the applicability of strain hardening or time hardening theories of creep accumulation. Atmospheric pressure and material recovery phenomena, not accounted for by either the empirical equations or hardening approaches, may also be important. Resulting predictions of cyclic creep deflection have been shown to be sensitive to both stress level and temperature. Such factors as overshoot in temperature for only one cycle or a few cycles could significantly increase the total test deflections.

Review of subsize panel test results and associated predictions (presented in Section 7.3 through 7.6) reveal two trends. First, for tests to similar cyclic profiles, the thinner gage corrugation stiffened panels exhibited larger deflections, relative to predictions, than the thicker gage rib stiffened panels. Secondly, panels tested applying mission temperature and load profiles exhibited larger deflections, relative to predictions, than similar panels tested applying constant temperature and load cycle profiles. The shape of the predicted deflection-time curves relative to subsize panel test results, in most cases, was found to be similar to the relation between the shape of the predicted tensile strain-time curves (based on the empirical equations derived) and the Phase I tensile creep data. This is indicative that panel deflection predictions can only be as good as the empirical equations (representing the material creep response) upon which the predictions are based.

Trends showing that rib stiffened specimens tended to creep less, relative to predictions, than corrugation stiffened specimens were investigated by changing rib specimen modeling techniques to allow an element at the very tip of the rib. This, however, did not significantly change the predictions.

No relation could be found between stress levels, as a percentage of yield strength or crippling strength, and the prediction capability. A summary of panel stress levels as percentages of the skin crippling stress and as a percentage of material yield strength are provided in Table 8-1. However, it is reasonable to expect that test deflections for thinner gage panels might be higher than predicted because less section area is effective in carrying the bending load. Therefore, higher stresses, causing greater creep strain, may occur.

temperature and load steps was demonstrated to have only a small effect on predicted deflections as long as time steps of very low creep are not included. It is recognized that including these low temperature and/or load steps when applying the time hardening theory of creep accumulation can effect predictions.

TABLE 8-1 PANEL TEST STRESS SUMMARY

TEST	PANEL CONCEPT	SECTION GEOMETRY (cm)	TEST TRAJECTORY	SKIN STRESS (COMPRESSION)		% OF SKIN CRIPPLING STRESS		MAX. FIBER STRESS (TENSION)		% OF YIELD STRESS	
				HIGH TEMP. COND.	LOW TEMP. COND.	HIGH TEMP. COND.	LOW TEMP. COND.	HIGH TEMP. COND.	LOW TEMP. COND.	HIGH TEMP. COND.	LOW TEMP. COND.
L605-21 L605-24	Corrugation	Depth = 1.321 Gage = .025 $\bar{Y}$ = .904	Mission Profile	(T = 1200 K) 25.2 MPa	(T = 950 K) 60.3 MPa	32	52	54.8 MPa	131.0 MPa	34	67
L605-22	Corrugation	Depth = 1.321 Gage = .025 $\bar{Y}$ = .904	Constant	(T = 1256 K) 16.1 MPa		24		35.2 MPa		27	
L605-23	Corrugation	Depth = 1.321 Gage = .025 $\bar{Y}$ = .904	Constant	(T = 1053 K) 53.4 MPa		51		115.8 MPa		60	
L605-25 L605-26	Rib	Depth = 1.105 Gage = .064 $\bar{Y}$ = .881	Mission Profile	(T = 1200 K) 17.2 MPa	(T = 950 K) 41.0 MPa	13	20	67.6 MPa	162.0 MPa	42	82
RENE-21	Corrugation	Depth = 1.270 Gage = .028 $\bar{Y}$ = .836	Mission Profile	(T = 1169 K) 32.8 MPa	(T = 940 K) 78.6 MPa	22	24	63.1 MPa	151.0 MPa	20	18
RENE-22	Corrugation	Depth = 1.270 Gage = .028 $\bar{Y}$ = .836	Constant	(T = 1111 K) 95.2 MPa		44		183.4 MPa		36	
RENE-23	Corrugation	Depth = 1.219 Gage = .028 $\bar{Y}$ = .836	Constant	(T = 1111 K) 118.6 MPa		54		228.2 MPa		46	
Ti-22	Corrugation	Depth = 1.321 Gage = .033 $\bar{Y}$ = .859	Constant	(T = 783 K) 52.0 MPa		27		96.5 MPa		21	
Ti-23 Ti-24	Corrugation	Depth = 1.270 Gage = .033 $\bar{Y}$ = .859	Mission Profile	(T = 783 K) 39.6 MPa	(T = 658 K) 94.5 MPa	21	40	73.8 MPa	175.1 MPa	16	31
Ti-25	Rib	Depth = 1.092 Gage = .056 $\bar{Y}$ = .884	Mission Profile	(T = 783 K) 23.1 MPa	(T = 658 K) 55.2 MPa	10	20	97.9 MPa	233.7 MPa	22	42
Ti-26	Rib	Depth = 1.092 Gage = .056 $\bar{Y}$ = .884	Constant	(T = 714 K) 97.2 MPa		36		413.7 MPa		80	
TDNiG-21	Corrugation	Depth = 1.219 Gage = .025 $\bar{Y}$ = .851	Constant	(T = 1478 K) 20.2 MPa		53		42.4 MPa		77	
TDNiG-22	Corrugation	Depth = 1.245 Gage = .025 $\bar{Y}$ = .848	Mission Profile	(T = 1478 K) 10.2 MPa	(T = 1144 K) 24.4 MPa	27	30	21.8 MPa	52.4 MPa	40	38

9.0 CONCLUDING REMARKS

A method of analysis for predicting permanent deflections, due to creep, in stiffened panel structures has been developed at MDAC-E during this phase of the program. The resulting computer program, Thermal Protection System Creep (TPSC) uses iterative techniques and numerical integration to determine creep strains, deflections, and residual stresses. The TPSC computer program provides needed capability for prediction of permanent deflections, due to creep. Although developed for analysis of creep deflections in thermal protection system panels, the approach is applicable to creep analysis in any beam or stiffened plate structure subjected to bending loads. The approach for creep deflection analysis incorporated in the TPSC computer program has been found to yield predicted panel cyclic creep deflections that are generally between half and twice the test deflections. Elastic deflections are predicted within expected numerical accuracy using only a few section elements and beam stations. Similarly, predicted creep deflection solutions converge rapidly.

The time hardening theory of creep accumulation was generally found to be better than strain hardening in predicting the cyclic test data. However, caution must be used in its application, since including portions of the load and temperature profiles where no creep is occurring will extend the time for calculation in subsequent cycles. Much more work needs to be done toward defining material creep accumulation processes since it appears that this could be the most significant limitation to the analysis in the TPSC program.

Empirical equations developed from cyclic tensile tests in Phase I were used in the analysis of subsize panel deflections in Phase II. However, no difference could be determined between the cyclic and steady state test data, in Phase I, for

equal total times. Therefore, the resulting equations for either of these data sets could be used to predict the panel creep deflections.

Many factors influence the creep deflections and predictions, including effects on thin gage sections and the degree to which material creep response can be characterized. During Phase I several factors were identified which can effect panel creep deflections. Primary factors include the applicability of empirical equations, based on regression analysis of tensile creep data, and the applicability of hardening theories of creep accumulation. Other factors investigated as also effecting deep deflections are atmospheric pressure and material recovery phenomena not accounted for by either the empirical equation or hardening approaches. Additionally, assumptions are made in the Phase II panel analysis which will influence predictions. Primary assumptions are that creep response in the thin gage materials are the same for both tension and compression stresses, that uniform $(\frac{Mc}{I})$ stress distribution exists in the thin gage specimens under bending loads, and that deflections due to shear are negligible. It appears, however, that if tensile creep data are available to provide adequate definition of a material's creep response characteristics, then creep deflection predictions can be made in thin gage panel structures subjected to complex cyclic thermal and bending loads.

10. REFERENCES

1. Davis, J. W., and Cramer, B. A., "Prediction and Verification of Creep Behavior in Metallic Materials and Components for the Space Shuttle Thermal Protection System Phase I - Cyclic Creep Prediction of Materials." NASA CR-132605-1.

2. Cramer, B. A., "Thermal Protection System Creep (TPSC) Computer Program Users Manual," To be Published.

3. Space Shuttle Program Phase B Studies NAS-8-26016

4. ANON, "Supplementary Structural Test Program (SSTP), Large TPS Panel Tests," MDC E0562, 30 March 1972.

5. Hughes, W. P., etc. al., "A Study of the Strain-Age Crack Sensitivity of Rene' 41", AFML-TR-66-324, 1966.

6. Private Communications with General Electric Company.

7. Harris, H. G., and Morman, K. N., "Creep of Metallic Thermal Protection Systems," NASA-TWX-2273, Presented at NASA Space Shuttle Technology Conference, NASA-Langley Research Center, March 2-4, 1971

8. Klingler, L. J., et. al., "Development of Dispersion Strengthened Nickel-Chromium Alloy (Ni-Cr-ThO_2) Sheet for Space Shuttle Vehicles", NASA-CR-120796, NASA Lewis Research Center.

9. Johnson, R. E., and Killpatrick, "Evaluation of Disperson Strengthened Nickel-Base Alloy Heat Shields for Space Shuttle Application" NASA CR-132360, NASA Langley Research Center.

10. Otto, O.R., "Integrated Structures 1972 Progress Report", MDC E0710.

11. "A Proposal to Deliver Panels for Structural Evaluation of Candidate Space Shuttle Thermal Protection Systems", MDC E0347, 12 April 1971, Submitted in Response to RFP L15-1689 to NASA Langley Research Center.

12. Roark, R. J., "Formulas for Stress and Strain", McGraw-Hill Book Company, 1954.

13. Timeshenko, S., and Woinowsky-Kreiger, S., Theory of Plates and Shells, McGraw-Hill Book Company, 1959, Pages 214-218.

14. Lekhnitskii, S. G., Anisotropic Plates, Translated from 2nd Russian edition by S. W. Tsai and T. Cheron, Gordon and Breach Science Publishers, 1968, Pages 329-333.

APPENDIX A

CONVERSION OF U. S. CUSTOMARY UNITS TO SI UNITS

CONVERSION OF U.S. CUSTOMARY UNITS TO SI UNITS

The International System of Units (designated SI) was adopted by the Eleventh General Conference on Weights and Measures in 1960. The units and conversion factors used in this report are taken from or based on NASA SP-7012, "The International System of Units, Physical Constants and Conversion Factors - Revised, 1969".

The following table expresses the definitions of miscellaneous units of measure as exact numerical multiples of coherent SI units, and provides multiplying factors for converting numbers and miscellaneous units to corresponding new numbers of SI units.

The first two digits of each numerical entry represent a power of 10. An asterisk follows each number that expresses an exact definition. For example, the entry "-02 2.54*" expresses the fact that 1 inch = 2.54×10^{-2} meter, exactly, by definition. Most of the definitions are extracted from National Bureau of Standards documents. Numbers not followed by an asterisk are only approximate representations of definitions, or are the results of physical measurements.

ALPHABETICAL LISTING

To convert from	to	multiply by
atmosphere (atm)	pascal (Pa)	+05 1.0133*
Fahrenheit (F)	kelvin (K)	$t_k = (5/9)(t_f + 459.67)$
foot (ft)	meter (m)	-01 3.048*
inch (in.)	meter (m)	-02 2.54*
mil	meter (m)	-05 2.54*
millimeter of mercury (mm Hg)	pascal (Pa)	+02 1.333
nautical mile, U.S. (n.mi.)	meter (m)	+03 1.852*
pound force (lb_f)	newton (N)	+00 4.448*
pound mass (lb_m)	kilogram (kg)	-01 4.536*
torr (0°C)	pascal (Pa)	+02 1.333

APPENDIX A - Continued

PHYSICAL QUANTITY LISTING

Area

To convert from	to	multiply by	
foot^2 (ft^2)	meter^2 (m^2)	-02	9.290*
inch^2 (in^2)	meter^2 (m^2)	-04	6.452*
inch^2 (in^2)	cemtimeter^2 (cm^2)	+00	6.452

Density

pound mass/foot^3 (pcf, lb$_m$/ft^3)	kilogram/meter^3 (kg/m^3)	+01	1.602
pound mass/inch^3 (lb$_m$/in^3)	kilogram/meter^3 (kg/m^3)	+04	2.768
pound mass/inch^3 (lb$_m$/in^3)	gram/centimeter^3 (g/cm^3)	+01	2.768

Force

kilogram force (kg$_f$)	newton (N)	+00	9.807*
pound force (lb$_f$)	newton (N)	+00	4.448*

Length

foot (ft)	meter (m)	-01	3.048*
inch (in.)	meter (m)	-02	2.54*
micron	meter (m)	-06	1.00*
mil	meter (m)	-05	2.54*
mile, U.S. nautical (n.mi.)	meter (m)	+03	1.852*

Mass

pound mass (lb$_m$)	kilogram (kg)	-01	4.536*

Pressure

atmosphere (atm)	pascal (Pa)	+05	1.013*
millimeter of mercury (mm Hg)	pascal (Pa)	+02	1.333
newton/meter	pascal (Pa)	00	1.00*
pound/foot^2 (psf, lb$_f$/ft^2)	pascal (Pa)	+01	4.788
pound/inch^2 (psi, lb$_f$/in^2)	pascal (Pa)	+03	6.895

Temperature

Fahrenheit (F)	Kelvin (K)	$t_k = (5/9)(t_f + 459.67)$

APPENDIX A - Continued

Volume

To convert from	to	multiply by	
foot^3 (ft^3)	meter^3 (m^3)	-02	2.832*
inch^3 (in^3)	meter^3 (m^3)	-05	1.639*
inch^3 (in^3)	centimeter^3 (cm^3, cc)	-01	1.639

PREFIXES

The names of multiples and submultiples of SI units may be formed by application of the prefixes:

Multiple	Prefix
10^{-6}	micro (μ)
10^{-3}	milli (m)
10^{-2}	centi (c)
10^{-1}	deci (d)
10^{3}	kilo (k)
10^{6}	mega (M)
10^{9}	giga (G)

APPENDIX B

SUBSIZE PANEL TEST DATA

Presented in this appendix are data for each of the subsize panels tested, including the load and temperature profiles, deflection data as a function of cycle and panel station, and observations on the color changes due to oxidation. Also included is a photograph of each panel after testing and the cross section dimensions.

These data supplement the data and analysis presented in the remainder of the report. Photographs of the panels showing side views after testing were not included because in general they do not provide any additional information over what can be attained from the deflection data. Plots of the deflected shape at the conclusion of each panel test are included in the analysis sections 7.3 through 7.6.

Subsize Panel Test L605-21

Corrugation stiffened Panel L1 was tested to 100 mission load, temperature (1200°K peak) and atmospheric pressure profiles. A 100 cycle midspan creep deflection of .5738 cm (.2259 inches) was attained. The panel cross section and photograph after testing are shown in Figure B-1. Deflection and trajectory data are shown in Tables B-1 and B-2, respectively.

Panel dimensions are centimeters

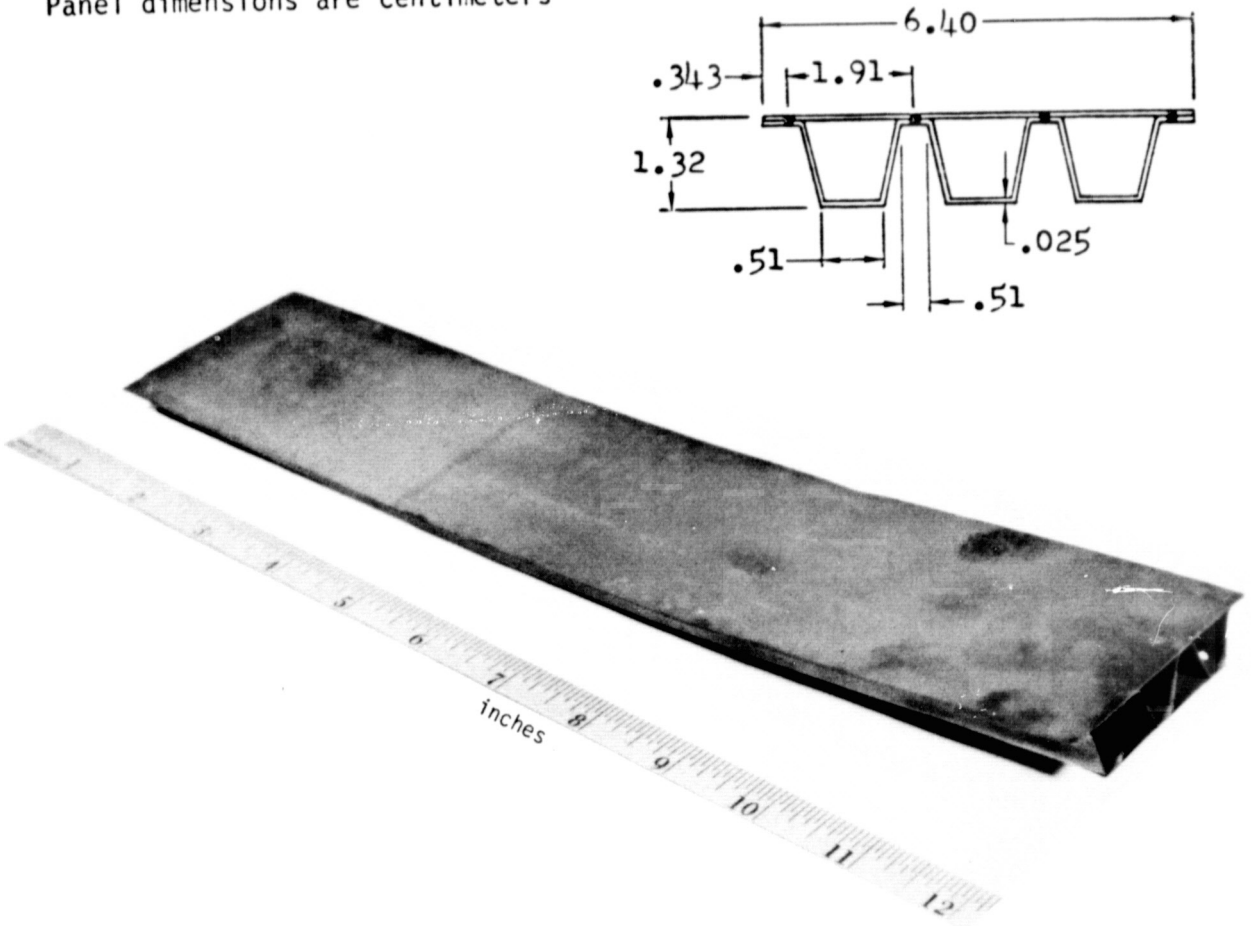

FIGURE B–1 SUBSIZE PANEL L1 CROSS SECTION AND PHOTOGRAPH AFTER TEST

MEASUREMENT LOCATION (REF. FIGURE 5-9)	CYCLES						
	1	5	15	25	50	75	100
X=5.08 CM. (2.00 IN.)	.0701 (.0276)	.1166 (.0459)	.1603 (.0631)	.1867 (.0735)	.2309 (.0909)	.2537 (.0999)	.2766 (.1089)
X=9.19 CM. (3.62 IN.)	.1194 (.0470)	.1979 (.0779)	.2700 (.1063)	.3259 (.1283)	.4079 (.1606)	.4498 (.1771)	.4884 (.1923)
X=11.6 CM. (4.56 IN.)	.1321 (.0520)	.2222 (.0875)	.3020 (.1189)	.3642 (.1434)	.4557 (.1794)	.5024 (.1978)	.5448 (.2145)
X=14.) CM. (5.50 IN.)	.1374 (.0841)	.2332 (.0918)	.3160 (.1244)	.3833 (.1509)	.4816 (.1896)	.5309 (.2090)	.5738 (.2259)
X=16.4 CM. (6.44 IN.)	.1346 (.0530)	.2273 (.0895)	.3119 (.1228)	.3729 (.1468)	.4676 (.1841)	.5144 (.2025)	.5575 (.2195)
X=18.7 CM. (7.38 IN.)	.1242 (.0489)	.2118 (.0834)	.2835 (.1116)	.3426 (.1349)	.4293 (.1690)	.4760 (.1874)	.5141 (.2024)
X=22.9 CM. (9.00 IN.)	.0734 (.0289)	.1252 (.0493)	.1666 (.0656)	.2002 (.0788)	.2474 (.0974)	.2715 (.1069)	.2946 (.1160)

TABLE B–1 DEFLECTION DATA FOR SUBSIZE PANEL TEST L605–21

CYCLE TIME (Seconds)	TYPICAL MEASURED TEMPERATURE		AVERAGE MEASURED BEAM LOAD (P)	
	°F	K	LBS	Kg
100	597.	587.	-	-
200	765.	680.	-	-
300	1040.	833.	-	-
400	1524.	1102.	12.45	5.65
500	1600.	1144.	20.59	9.34
600	1650.	1172.	26.02	11.80
700	1696.	1198.	29.28	13.28
800	1697.	1198.	31.10	14.11
900	1680.	1189.	31.91	14.47
1000	1655.	1175.	33.08	15.01
1100	1635.	1164.	35.61	16.15
1200	1613.	1151.	38.54	17.48
1300	1599.	1144.	42.80	19.41
1400	1574.	1130.	47.71	21.64
1500	1538.	1110.	55.41	25.13
1600	1494.	1085.	62.37	28.29
1700	1410.	1041.	65.97	29.92
1800	1335.	997.	71.42	32.40
1900	1267.	959.	74.28	33.69
2000	1210.	928.	73.29	33.24
2100	1150.	894.	66.98	30.38
2200	1095.	864.	58.69	26.62
2300	1045.	836.	47.65	21.61
2400	995.	808.	30.40	13.79
2500	937.	776.	15.94	7.23
2600	905.	758.	11.11	5.04
2700	860.	733.	-	-
2800	829.	716.	-	-
2900	790.	694.	-	-
3000	760.	678.	-	-
3100	727.	659.	-	-
3200	700.	644.	-	-
3300	672.	629.	-	-
3400	658.	621.	-	-
3500	628.	604.	-	-
3600	610.	594.	-	-
3700	597.	587.	-	-

TABLE B-2 TRAJECTORY DATA FOR SUBSIZE PANEL TEST L605-21

Subsize Panel Test L605-22

Corrugation stiffened Panel L2 was tested to 50 constant load (8.98 Kg) and temperature (1255 K) profiles per Table 6-1 and Figure 5-1(a). Cycle time at load and peak temperature was 20 minutes and atmospheric pressure was maintained constant at approximately 1.3 Pa. A 50 cycle midspan creep deflection of .1968 cm (.0775 inches) was attained. A slightly heavier green oxide coating was present on this panel than had been observed on panel test L605-21. This was attributed to the higher test temperature. The panel photograph after testing and deflection data are shown in Figure B-2 and Table B-3, respectively.

Panel dimensions are centimeters

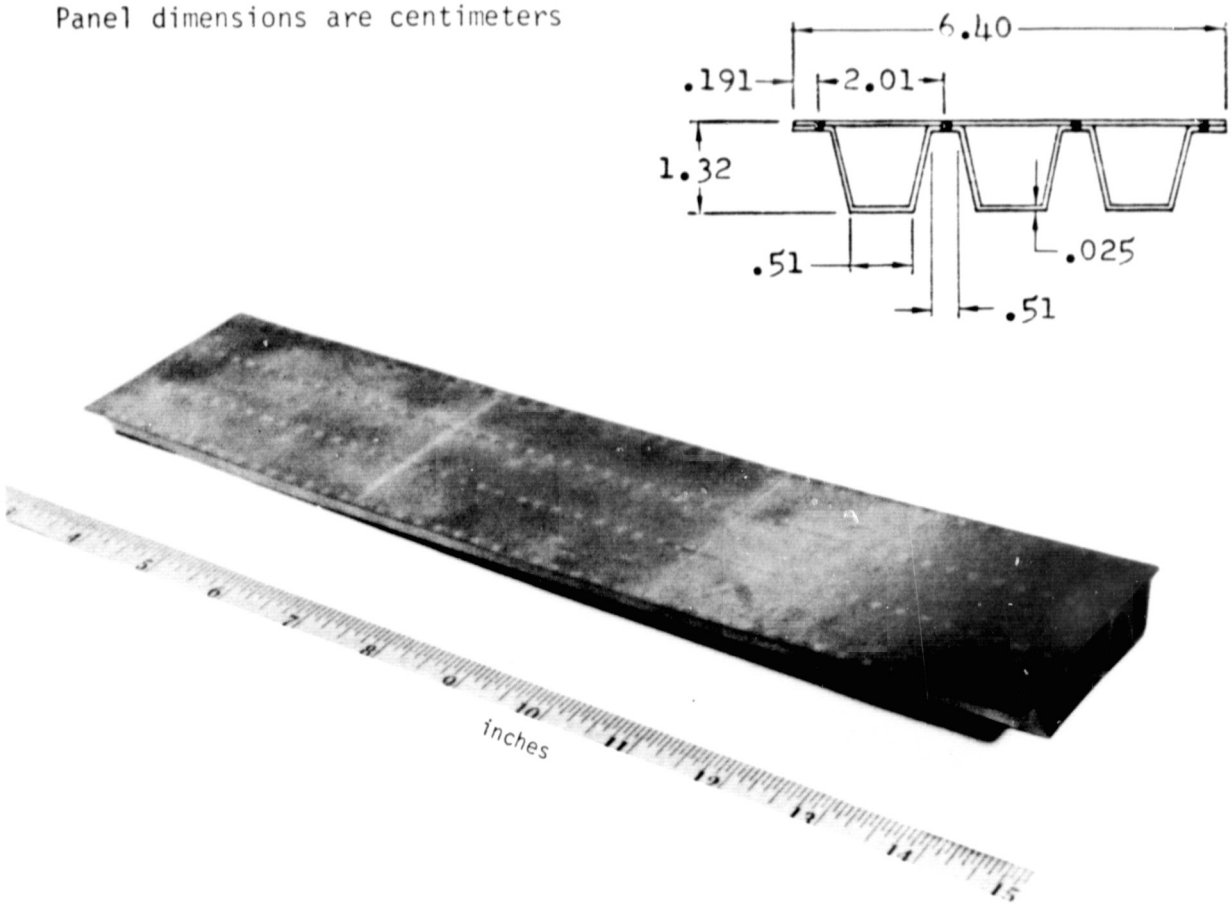

FIGURE B-2 SUBSIZE PANEL L2 CROSS SECTION AND PHOTOGRAPH AFTER TEST

MEASUREMENT LOCATION (REF. FIGURE 5-9)	CYCLES				
	1	5	15	25	50
X=5.08 CM. (2.00 IN.)	.0409 (.0161)	.0523 (.0206)	.0683 (.0269)	.0732 (.0288)	.0955 (.0376)
X=9.19 CM. (3.62 IN.)	.0752 (.0296)	.0975 (.0384)	.1245 (.0490)	.1374 (.0541)	.1740 (.0685)
X=11.6 CM. (4.56 IN.)	.0828 (.0326)	.1077 (.0424)	.1422 (.0560)	.1509 (.0594)	.1864 (.0734)
X=14.0 CM. (5.50 IN.)	.0838 (.0330)	.1077 (.0424)	.1400 (.0551)	.1560 (.0614)	.1969 (.0775)
X=16.4 CM. (6.44 IN.)	.0810 (.0319)	.1064 (.0419)	.1346 (.0530)	.1501 (.0591)	.1882 (.0741)
X=18.7 CM. (7.38 IN.)	.0749 (.0295)	.0953 (.0375)	.1217 (.0479)	.1356 (.0534)	.1692 (.0666)
X=22.9 CM. (9.00 IN.)	.0472 (.0186)	.0597 (.0235)	.0759 (.0299)	.0828 (.0326)	.1024 (.0403)

TABLE B-3 DEFLECTION DATA FOR SUBSIZE PANEL TEST L605-22

Subsize Panel Test L605-23

Corrugation stiffened Panel L3 was tested to 100 constant load (36.1 Kg) and temperature (1052 K) profiles as presented in Table 6-1 and Figure 5-1(a). Cycle time at load and peak temperature was 20 minutes and atmospheric pressure was maintained constant at approximately 1.3 Pa. The applied load was increased by approximately 20% during cycle 76-100. A 100 cycle midspan creep deflection of .3940 cm (.1551 inches) was attained. A uniform light green oxide coating existed on the panel after testing. This lighter coating than obtained in tests L605-21 and L605-22 was attributed to the constant low oxygen pressure. The panel photograph after testing and deflection data are shown in Figure B-3 and Table B-4, respectively.

Panel dimensions are centimeters

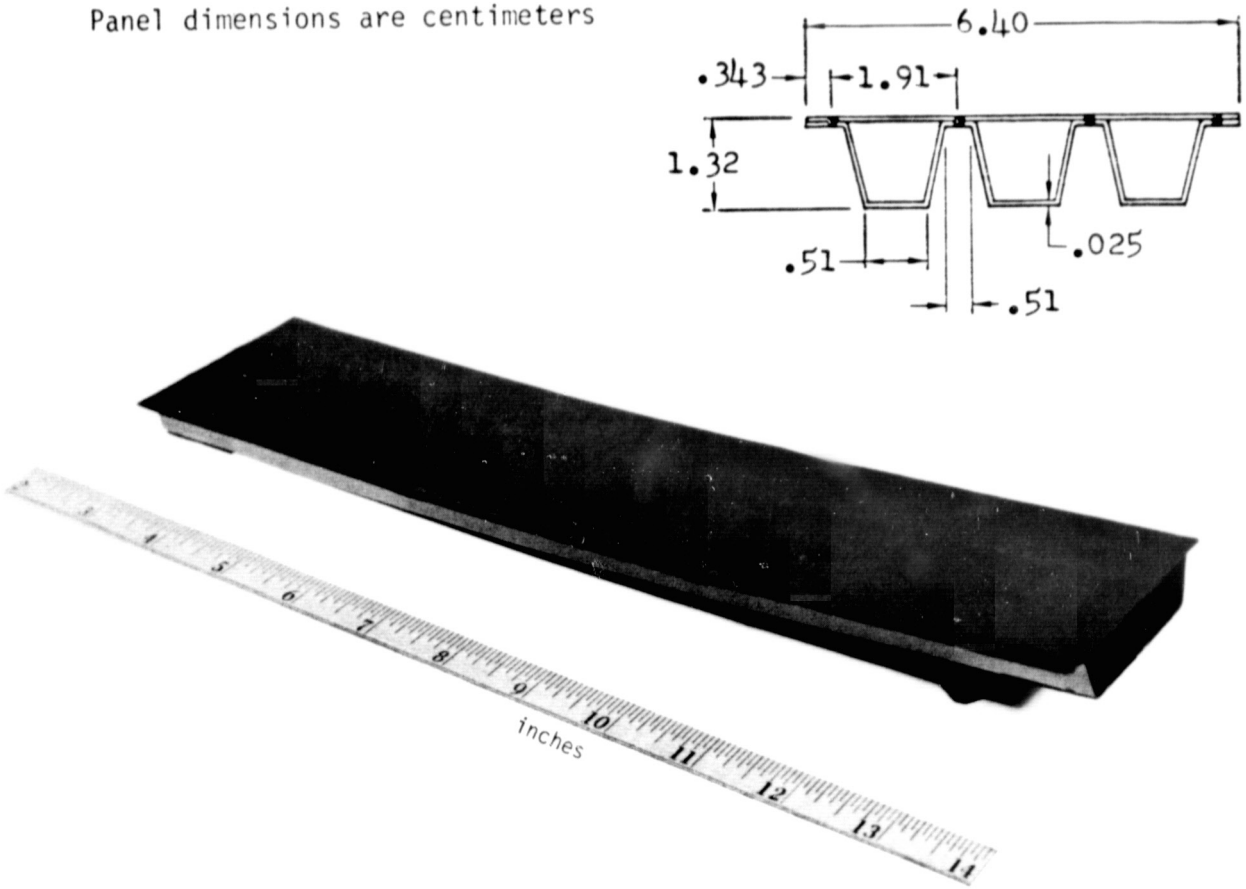

FIGURE B-3 SUBSIZE PANEL L3 CROSS SECTION AND PHOTOGRAPH AFTER TEST

MEASUREMENT LOCATION (REF. FIGURE 5-9)	CYCLES							
	1	5	15	25	50	75	80	100
X=5.08 CM. (2.00 IN.)	.0320 (.0126)	.0658 (.0259)	.0947 (.0373)	.1143 (.0450)	.1400 (.0551)	.1585 (.0624)	.1702 (.0670)	.1938 (.0763)
X=9.19 CM. (3.62 IN.)	.0605 (.0238)	.1153 (.0454)	.1671 (.0658)	.1989 (.0783)	.2428 (.0956)	.2756 (.1085)	.2929 (.1153)	.3343 (.1316)
X=11.6 CM. (4.56 IN.)	.0676 (.0266)	.1260 (.0496)	.1831 (.0721)	.2184 (.0860)	.2677 (.1054)	.3038 (.1196)	.3213 (.1265)	.3670 (.1445)
X=14.0 CM. (5.50 IN.)	.0757 (.0298)	.1445 (.0569)	.2032 (.0800)	.2408 (.0948)	.2911 (.1146)	.3279 (.1291)	.3465 (.1364)	.3940 (.1551)
X=16.4 CM. (6.44 IN.)	.0655 (.0258)	.1311 (.0516)	.1831 (.0721)	.2040 (.0803)	.2687 (.1058)	.3033 (.1194)	.3274 (.1289)	.3698 (.1456)
X=18.7 CM. (7.38 IN.)	.0638 (.0251)	.1214 (.0478)	.1748 (.0688)	.2070 (.0815)	.2517 (.0991)	.2840 (.1118)	.2995 (.1179)	.3426 (.1349)
X=22.9 CM. (9.00 IN.)	.0371 (.0146)	.0688 (.0271)	.0986 (.0388)	.1179 (.0464)	.1443 (.0568)	.1625 (.0640)	.1717 (.0676)	.1943 (.0765)

TABLE B-4 DEFLECTION DATA FOR SUBSIZE PANEL TEST L605-23

Subsize Panel Test L605-24

Corrugation stiffened Panel L4 was tested to 50 mission load, temperature (1200 K peak) and atmospheric pressure profiles. A 50 cycle midspan creep deflection of .3576 cm (.1408 inches) was attained.

The panel cross section and photograph after testing are shown in Figure B-4. Deflection and trajectory data are presented in Tables B-5 and B-6, respectively.

This test was intended to be a replicate of panel test L605-21.

Panel dimensions are centimeters

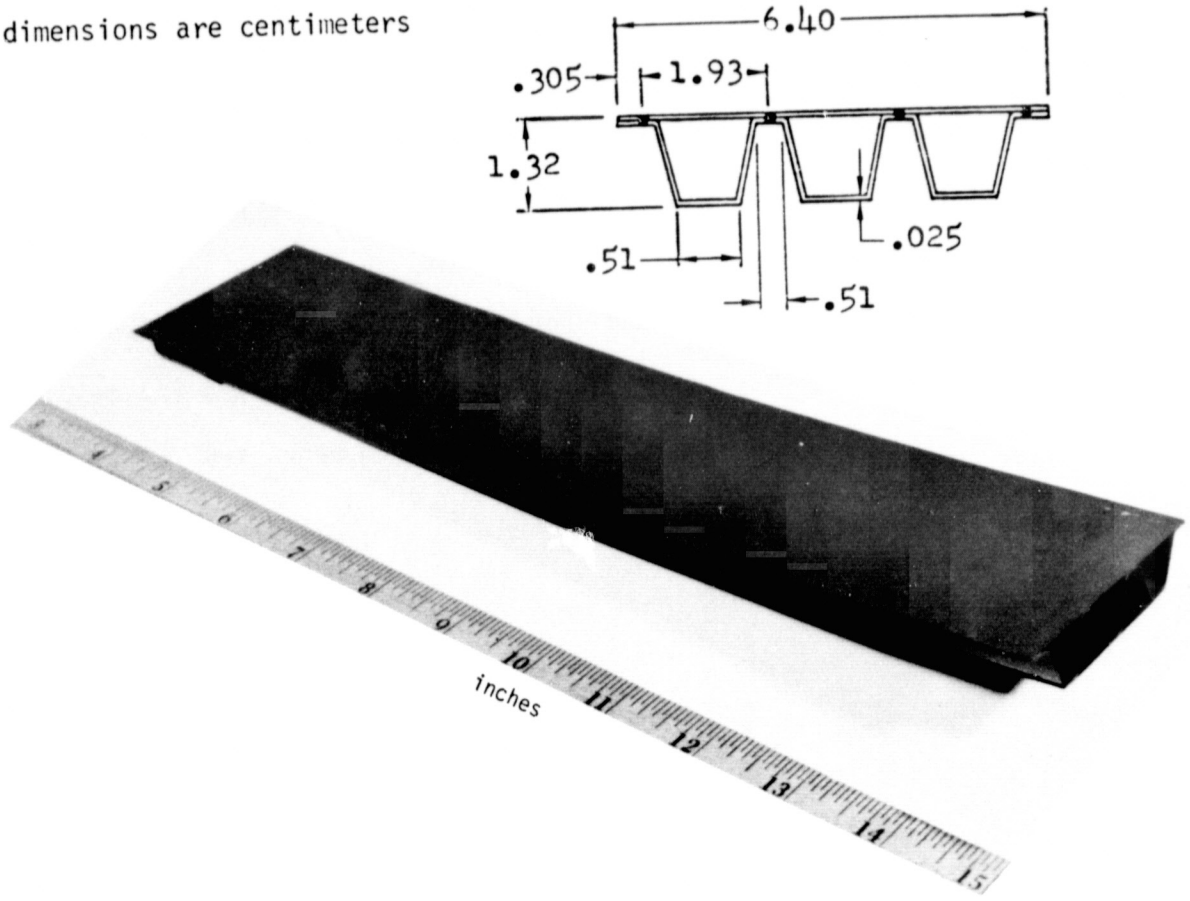

FIGURE B–4 SUBSIZE PANEL L4 CROSS SECTION AND PHOTOGRAPH AFTER TEST

MEASUREMENT LOCATION (REF. FIGURE 5-9)	CYCLES				
	1	5	15	25	50
X=5.08 CM. (2.00 IN.)	.0668 (.0263)	.0955 (.0376)	.1227 (.0483)	.1430 (.0563)	.1737 (.0684)
X=9.19 CM. (3.62 IN.)	.1140 (.0449)	.1692 (.0666)	.2154 (.0848)	.2477 (.0975)	.3025 (.1191)
X=11.6 CM. (4.56 IN.)	.1295 (.0510)	.1908 (.0751)	.2426 (.0955)	.2789 (.1098)	.3391 (.1335)
X=14.0 CM. (5.50 IN.)	.1361 (.0536)	.2014 (.0793)	.2550 (.1004)	.2934 (.1155)	.3576 (.1408)
X=16.4 CM. (6.44 IN.)	.1303 (.0513)	.1933 (.0761)	.2449 (.0964)	.2814 (.1108)	.3444 (.1356)
X=18.7 CM. (7.38 IN.)	.1245 (.0490)	.1829 (.0720)	.2299 (.0905)	.2639 (.1039)	.3175 (.1250)
X=22.9 CM. (9.00 IN.)	.0744 (.0293)	.1087 (.0428)	.1359 (.0535)	.1570 (.0618)	.1892 (.0745)

TABLE B–5 DEFLECTION DATA FOR SUBSIZE PANEL TEST L605–24

CYCLE TIME (Seconds)	TYPICAL MEASURED TEMPERATURE		AVERAGE MEASURED BEAM LOAD (P)	
	°F	K	LBS	Kg
100	597.	587.	-	-
200	765.	680.	-	-
300	1040.	833.	-	-
400	1524.	1102.	11.45	5.19
500	1600.	1144.	19.94	9.04
600	1650.	1172.	25.85	11.73
700	1696.	1198.	29.56	13.41
800	1697.	1198.	31.44	14.26
900	1680.	1189.	32.22	14.61
1000	1655.	1175.	33.20	15.06
1100	1635.	1164.	35.71	16.20
1200	1613.	1151.	38.55	17.49
1300	1599.	1144.	42.80	19.41
1400	1574.	1130.	47.65	21.61
1500	1538.	1110.	55.27	25.07
1600	1494.	1085.	62.55	28.37
1700	1410.	1041.	66.17	30.01
1800	1335.	997.	71.85	32.59
1900	1267.	959.	74.45	33.77
2000	1210.	928.	73.78	33.47
2100	1150.	894.	67.13	30.45
2200	1095.	864.	58.64	26.60
2300	1045.	836.	47.24	21.43
2400	995.	808.	29.34	13.31
2500	937.	776.	12.42	5.63
2600	905.	758.	-	-
2700	860.	733.	-	-
2800	829.	716.	-	-
2900	790.	694.	-	-
3000	760.	678.	-	-
3100	727.	659.	-	-
3200	700.	644.	-	-
3300	672.	629.	-	-
3400	658.	621.	-	-
3500	628.	604.	-	-
3600	610.	594.	-	-
3700	597.	587.	-	-

TABLE B–6 TRAJECTORY DATA FOR SUBSIZE PANEL TEST L605–24

Subsize Panel Test L605-25

Rib stiffened Panel L6 was tested to 50 mission load, temperature (1200 K peak) and atmospheric pressure profiles. The load was applied in the positive direction (skin in compression). A 50 cycle midspan creep deflection of .3233 cm (.1273 inches) was attained. A uniform darker green oxide, similar to that obtained in Test L605-22, was obtained. The panel cross section and photograph after testing are shown in Figure B-5. Deflection and trajectory data are presented in Tables B-7 and B-8, respectively.

Panel dimensions are centimeters

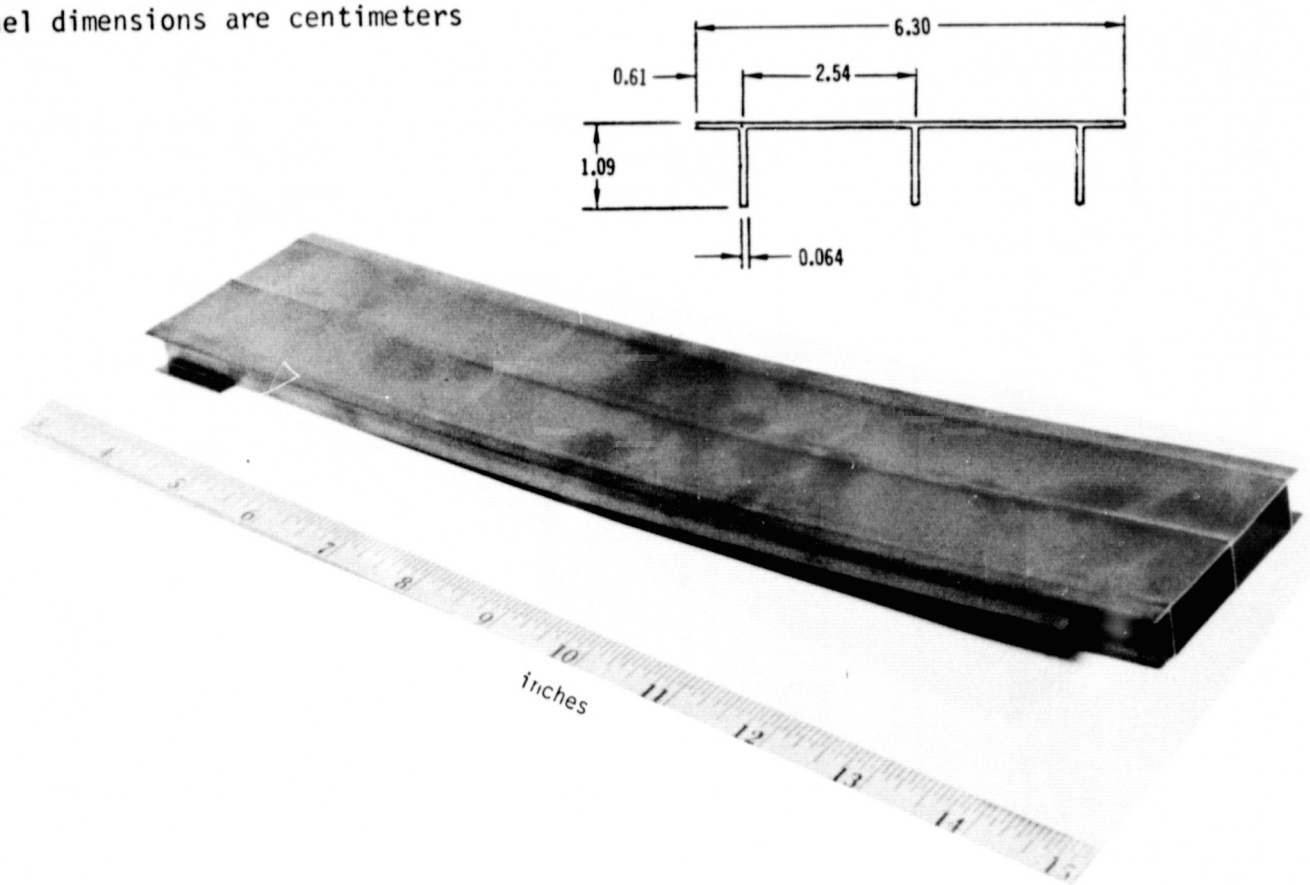

FIGURE B–5 SUBSIZE PANEL L6 CROSS SECTION AND PHOTOGRAPH AFTER TEST

MEASUREMENT LOCATION (REF. FIGURE 5-9)	CYCLES				
	1	5	15	25	50
X=5.08 CM. (2.00 IN.)	.0363 (.0143)	.0724 (.0285)	.1087 (.0428)	.1283 (.0505)	.1631 (.0642)
X=9.19 CM. (3.62 IN.)	.0592 (.0233)	.1181 (.0465)	.1811 (.0713)	.2154 (.0848)	.2725 (.1073)
X=11.6 CM. (4.56 IN.)	.0678 (.0267)	.1346 (.0530)	.2057 (.0810)	.2451 (.0965)	.3106 (.1223)
X=14.0 CM. (5.50 IN.)	.0711 (.0280)	.1392 (.0548)	.2151 (.0847)	.2560 (.1008)	.3233 (.1273)
X=16.4 CM. (6.44 IN.)	.0660 (.0260)	.1326 (.0522)	.2057 (.0810)	.2464 (.0970)	.3081 (.1213)
X=18.7 CM. (7.38 IN.)	.0589 (.0232)	.1176 (.0463)	.1816 (.0715)	.2167 (.0853)	.2710 (.1067)
X=22.9 CM. (9.00 IN.)	.0343 (.0135)	.0711 (.0280)	.1118 (.0440)	.1313 (.0517)	.1720 (.0677)

TABLE B–7 DEFLECTION DATA FOR SUBSIZE PANEL TEST L605–25

CYCLE TIME (Seconds)	TYPICAL MEASURED TEMPERATURE		AVERAGE MEASURED BEAM LOAD (P)	
	°F	K	LBS	Kg
100	597.	587.	-	-
200	765.	680.	-	-
300	1040.	833.	-	-
400	1524.	1102.	7.82	3.55
500	1600.	1144.	14.00	6.35
600	1650.	1172.	18.24	8.27
700	1696.	1198.	20.90	9.48
800	1697.	1198.	22.35	10.14
900	1680.	1189.	22.92	10.40
1000	1655.	1175.	23.55	10.68
1100	1635.	1164.	25.24	11.45
1200	1613.	1151.	27.08	12.28
1300	1599.	1144.	29.94	13.58
1400	1574.	1130.	33.26	15.09
1500	1538.	1110.	37.73	17.11
1600	1494.	1085.	43.84	19.89
1700	1410.	1041.	46.25	20.98
1800	1335.	997.	50.30	22.82
1900	1267.	959.	52.86	23.98
2000	1210.	928.	52.84	23.97
2100	1150.	894.	49.33	22.38
2200	1095.	864.	43.77	19.85
2300	1045.	836.	36.80	16.69
2400	995.	808.	25.64	11.63
2500	937.	776.	12.60	5.72
2600	905.	758.	5.91	2.68
2700	860.	733.	-	-
2800	829.	716.	-	-
2900	790.	694.	-	-
3000	760.	678.	-	-
3100	727.	659.	-	-
3200	700.	644.	-	-
3300	672.	629.	-	-
3400	658.	621.	-	-
3500	628.	604.	-	-
3600	610.	594.	-	-
3700	597.	587.	-	-

TABLE B-8 TRAJECTORY DATA FOR SUBSIZE PANEL TEST L605-25

Subsize Panel Test L605-26

Rib stiffened Panel L7 was tested to 50 of the same mission load, temperature (1200 K peak), and atmospheric pressure profiles as applied in test L605-25. The load, however, was applied in the negative direction (skin in tension). A 50 cycle mid span creep deflection of -.2951 cm (-.1162 inches) was attained. The panel cross section and photograph after testing are shown in Figure B-6. Deflection and trajectory data are presented in Tables B-9 and B-10, respectively.

This test was intended to be a replicate of test L605-25 except for the loading direction. If the residual stress state within these panels was zero then panel stress distributions would be the same in the two tests except that tension, and compression stresses would be reversed. Because the resulting deflections are within expected scatter, no conclusions could be drawn as to the effect of initial residual stresses due to weld shrinkage.

Panel dimensions are centimeters

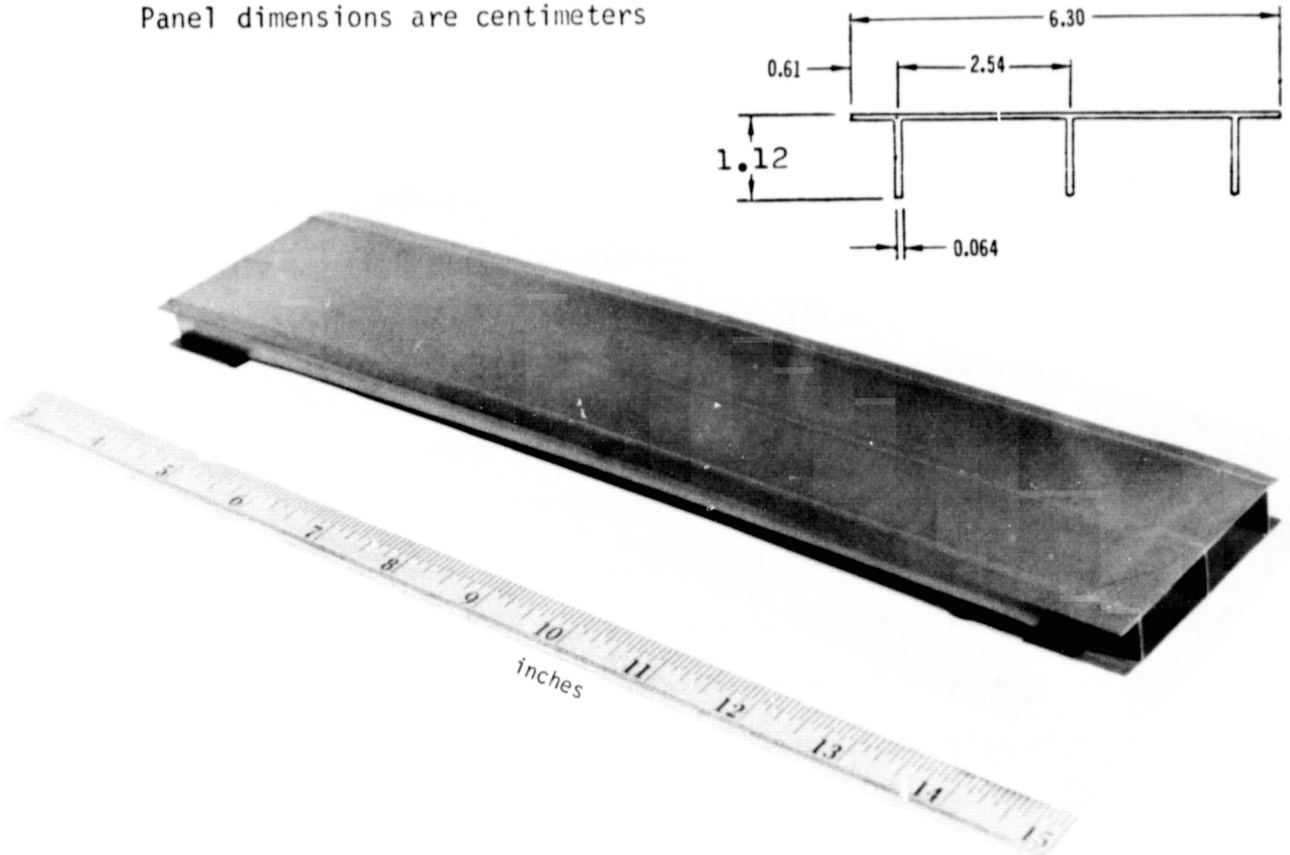

FIGURE B-6 SUBSIZE PANEL L7 CROSS SECTION AND PHOTOGRAPH AFTER TEST

MEASUREMENT LOCATION (REF. FIGURE 5-9)	CYCLES				
	1	5	15	25	50
X=5.08 CM. (2.00 IN.)	.0373 (.0147)	.0615 (.0242)	.0947 (.0373)	.1181 (.0465)	.1499 (.0590)
X=9.19 CM. (3.62 IN.)	.0602 (.0237)	.1041 (.0410)	.1562 (.0615)	.1943 (.0765)	.2497 (.0983)
X=11.6 CM. (4.56 IN.)	.0681 (.0268)	.1176 (.0463)	.1783 (.0702)	.2184 (.0860)	.2824 (.1112)
X=14.0 CM. (5.50 IN.)	.0706 (.0278)	.1227 (.0483)	.1816 (.0715)	.2281 (.0898)	.2951 (.1162)
X=16.4 CM. (6.44 IN.)	.0724 (.0285)	.1224 (.0482)	.1821 (.0717)	.2243 (.0883)	.2883 (.1135)
X=18.7 CM. (7.38 IN.)	.0605 (.0238)	.1049 (.0413)	.1582 (.0623)	.1935 (.0762)	.2510 (.0988)
X=22.9 CM. (9.00 IN.)	.0330 (.0130)	.0655 (.0258)	.0940 (.0370)	.1199 (.0472)	.1557 (.0613)

TABLE B-9 DEFLECTION DATA FOR SUBSIZE PANEL TEST L605-26

CYCLE TIME (Seconds)	TYPICAL MEASURED TEMPERATURE		AVERAGE MEASURED BEAM LOAD (P)	
	°F	K	LBS	Kg
100	597.	587.	-	-
200	765.	680.	-	-
300	1040.	833.	-	-
400	1524.	1102.	7.55	3.42
500	1600.	1144.	13.78	6.25
600	1650.	1172.	18.04	8.18
700	1696.	1198.	20.73	9.40
800	1697.	1198.	22.18	10.06
900	1680.	1189.	22.73	10.31
1000	1655.	1175.	23.36	10.60
1100	1635.	1164.	25.03	11.35
1200	1613.	1151.	26.93	12.22
1300	1599.	1144.	29.76	13.50
1400	1574.	1130.	33.10	15.01
1500	1538.	1110.	37.60	17.06
1600	1494.	1085.	43.84	19.89
1700	1410.	1041.	46.26	20.98
1800	1335.	997.	50.11	22.73
1900	1267.	959.	52.94	24.01
2000	1210.	928.	52.93	24.01
2100	1150.	894.	49.39	22.40
2200	1095.	864.	43.75	19.85
2300	1045.	836.	36.77	16.68
2400	995.	808.	25.18	11.42
2500	937.	776.	12.41	5.63
2600	905.	758.	5.73	2.60
2700	860.	733.	-	-
2800	829.	716.	-	-
2900	790.	694.	-	-
3000	760.	678.	-	-
3100	727.	659.	-	-
3200	700.	644.	-	-
3300	672.	629.	-	-
3400	658.	621.	-	-
3500	628.	604.	-	-
3600	610.	594.	-	-
3700	597.	587.	-	-

TABLE B–10 TRAJECTORY DATA FOR SUBSIZE PANEL TEST L605–26

Subsize Panel Test Rene' - 21

Corrugation stiffened Panel R1 was tested to 100 mission load, temperature (1169 K peak), and atmospheric pressure profiles as presented in this section. A 100 cycle midspan creep deflection of .3172 cm (.1249 inches) was attained. The panel cross section and photograph after testing are shown in Figure B-7. A uniform dark gray, almost black, oxide coating was evident on this panel after testing. Very slight waviness of the panel skin was noted. Deflection and trajectory data are presented in Tables B-11 and B-12, respectively.

Panel dimensions are centimeters

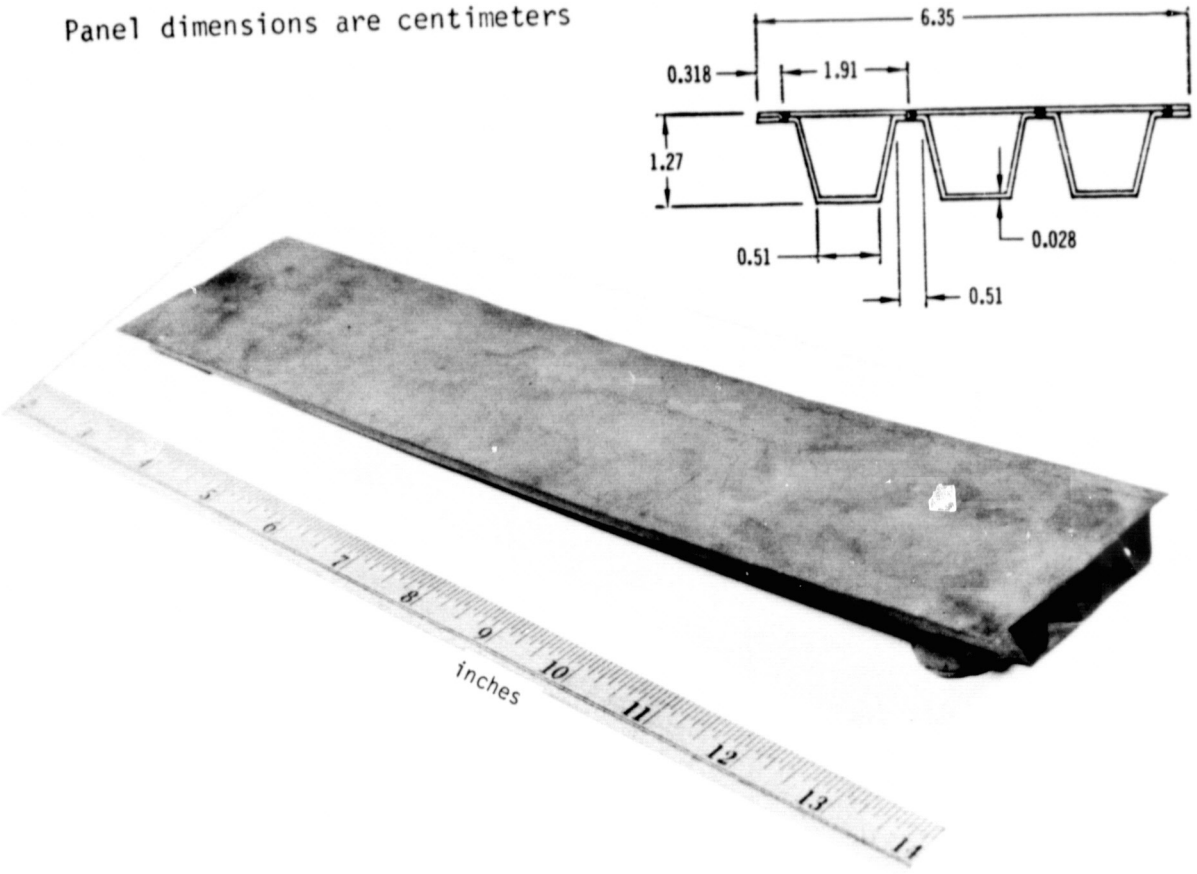

FIGURE B-7 SUBSIZE PANEL R1 CROSS SECTION AND PHOTOGRAPH AFTER TEST

MEASUREMENT LOCATION (REF. FIGURE 5-9)	CYCLES						
	1	5	15	25	50	75	100
X=5.08 CM. (2.00 IN.)	.0063 (.0025)	.0211 (.0083)	.0343 (.0135)	.0427 (.0168)	.0787 (.0310)	.1166 (.0459)	.1463 (.0576)
X=9.19 CM. (3.62 IN.)	.0140 (.0055)	.0333 (.0131)	.0612 (.0241)	.0785 (.0309)	.1392 (.0548)	.2042 (.0804)	.2603 (.1025)
X=11.6 CM. (4.56 IN.)	.0147 (.0058)	.0358 (.0141)	.0668 (.0263)	.0876 (.0345)	.1565 (.0616)	.2286 (.0900)	.2941 (.1158)
X=14.0 CM. (5.50 IN.)	.0165 (.0065)	.0371 (.0146)	.0726 (.0286)	.0940 (.0370)	.1697 (.0668)	.2502 (.0985)	.3172 (.1249)
X=16.4 CM. (6.44 IN.)	.0147 (.0058)	.0320 (.0126)	.0671 (.0264)	.0879 (.0346)	.1613 (.0635)	.2370 (.0933)	.3076 (.1211)
X=18.7 CM. (7.38 IN.)	.0135 (.0053)	.0328 (.0129)	.0643 (.0253)	.0848 (.0334)	.1544 (.0608)	.2248 (.0885)	.2908 (.1145)
X=22.9 CM. (9.00 IN.)	.0056 (.0022)	.0175 (.0069)	.0376 (.0148)	.0483 (.0190)	.0902 (.0355)	.1328 (.0523)	.1722 (.0678)

TABLE B-11 DEFLECTION DATA FOR SUBSIZE PANEL TEST RENE' - 21

CYCLE TIME (Seconds)	TYPICAL MEASURED TEMPERATURE		AVERAGE MEASURED BEAM LOAD (P)	
	°F	K	LBS	Kg
100	561.	567.	-	-
200	720.	655.	-	-
300	990.	805.	-	-
400	1427.	1048.	12.16	5.52
500	1526.	1103.	21.93	9.95
600	1590.	1139.	28.02	12.71
700	1642.	1168.	32.14	14.58
800	1645.	1169.	34.42	15.61
900	1640.	1166.	35.32	16.02
1000	1625.	1158.	36.33	16.48
1100	1595.	1141.	39.14	17.75
1200	1572.	1129.	42.15	19.12
1300	1550.	1116.	46.80	21.23
1400	1525.	1103.	52.10	23.63
1500	1495.	1086.	59.71	27.08
1600	1457.	1065.	68.90	31.25
1700	1385.	1025.	72.68	32.97
1800	1310.	983.	78.89	35.78
1900	1232.	940.	82.51	37.43
2000	1175.	908.	82.46	37.40
2100	1115.	875.	75.74	34.36
2200	1061.	845.	66.70	30.26
2300	1005.	814.	55.00	24.95
2400	960.	789.	36.02	16.34
2500	915.	764.	16.05	7.28
2600	870.	739.	-	-
2700	830.	716.	-	-
2800	796.	698.	-	-
2900	755.	675.	-	-
3000	722.	656.	-	-
3100	691.	639.	-	-
3200	655.	619.	-	-
3300	640.	611.	-	-
3400	621.	600.	-	-
3500	600.	589.	-	-
3600	580.	578.	-	-
3700	561.	567.	-	-

TABLE B-12 TRAJECTORY DATA FOR SUBSIZE PANEL TEST RENE'-21

Subsize Panel Test Rene' - 22

Corrugation stiffened Panel R2 was tested to 50 constant load (45.2 Kg) temperature (1111 K) profiles per Table 6-3 and Figure 5-1(a). Cycle time at load and peak temperature was 20 minutes and atmospheric pressure was maintained constant at approximately 1.3 Pa. A 50 cycle midspan creep deflection of .1750 cm (.0689 inches) was attained. A uniform yellow-green oxide coating was noted on the specimen after testing. This oxide was not as adherent to the panel surface as that obtained for test Rene' - 21. A somewhat greater degree of skin waviness was obtained in this panel. The panel photograph after testing and creep deflection data are shown in Figure B-8 and Table B-13, respectively.

Panel dimensions are centimeters

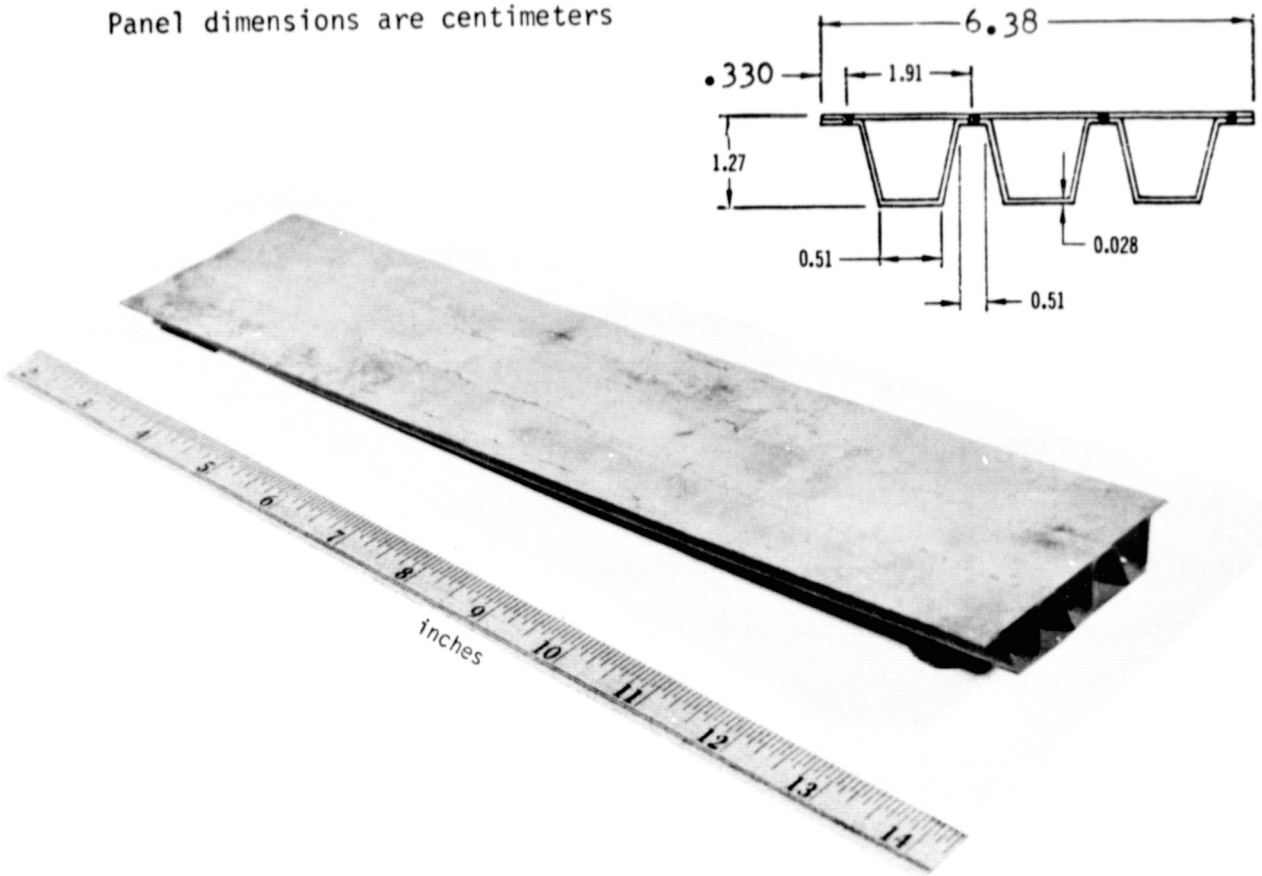

FIGURE B–8 SUBSIZE PANEL R2 CROSS SECTION AND PHOTOGRAPH AFTER TEST

MEASUREMENT LOCATION (REF. FIGURE 5-9)	CYCLES				
	1	5	15	25	50
X=5.08 CM. (2.00 IN.)	.0130 (.0051)	.0152 (.0060)	.0330 (.0130)	.0429 (.0169)	.0744 (.0293)
X=9.19 CM. (3.62 IN.)	.0274 (.0108)	.0371 (.0146)	.0612 (.0241)	.0838 (.0330)	.1425 (.0561)
X=11.6 CM. (4.56 IN.)	.0279 (.0110)	.0384 (.0151)	.0693 (.0273)	.0930 (.0366)	.1585 (.0624)
X=14.0 CM. (5.50 IN.)	.0300 (.0118)	.0422 (.0166)	.0759 (.0299)	.1026 (.0404)	.1750 (.0689)
X=16.4 CM. (6.44 IN.)	.0292 (.0115)	.0394 (.0155)	.0765 (.0301)	.1003 (.0395)	.1753 (.0690)
X=18.7 CM. (7.38 IN.)	.0180 (.0071)	.0320 (.0126)	.0643 (.0253)	.0902 (.0355)	.1595 (.0628)
X=22.9 CM. (9.00 IN.)	.0163 (.0064)	.0213 (.0084)	.0396 (.0156)	.0549 (.0216)	.0935 (.0368)

TABLE B–13 DEFLECTION DATA FOR SUBSIZE PANEL TEST RENE' – 22

Subsize Panel Test Rene' - 23

Corrugation stiffened Panel R3 was tested to 50 constant load (56.6 Kg) and temperature (1111 K) profiles as presented in Table 6-3 and Figure 5-1(a). Cycle time at load and peak temperature was 20 minutes and atmospheric pressure was maintained constant at approximately 1.3 Pa. A 50 cycle midspan creep deflection of .4392 cm (.1729 inches) was attained. A slightly lighter uniform yellow-green oxide was obtained on this panel than obtained in test Rene' - 22. A somewhat greater degree of panel skin waviness was obtained on this panel than either of the other two Rene panels tested. The panel photograph after testing and creep deflection data are presented in Figure B-9 and Table B-14, respectively.

Panel dimensions are centimeters

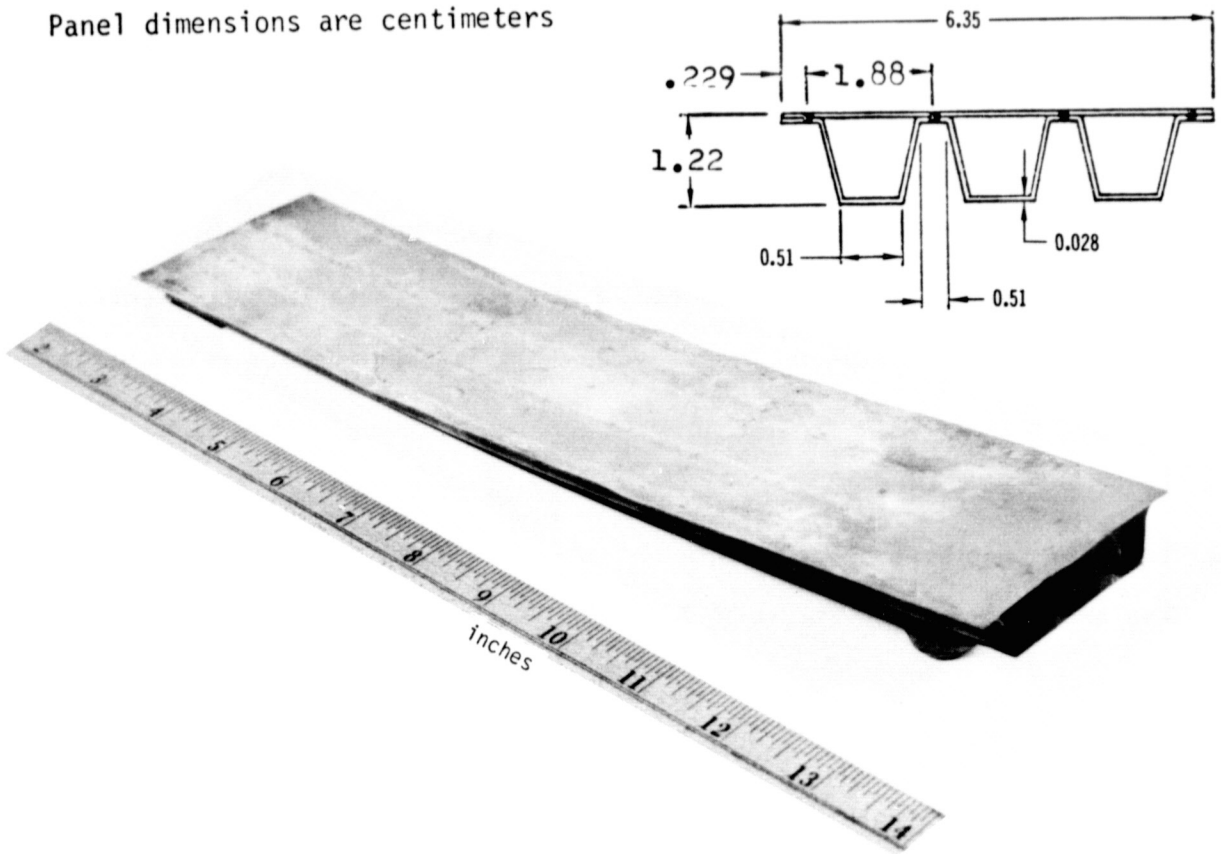

FIGURE B–9 SUBSIZE PANEL R3 CROSS SECTION AND PHOTOGRAPH AFTER TEST

MEASUREMENT LOCATION (REF. FIGURE 5-9)	CYCLES				
	1	5	15	25	50
X=5.08 CM. (2.00 IN.)	.0203 (.0080)	.0444 (.0175)	.0782 (.0308)	.1067 (.0420)	.1946 (.0766)
X=9.19 CM. (3.62 IN.)	.0442 (.0174)	.0841 (.0331)	.1476 (.0581)	.1963 (.0773)	.3604 (.1419)
X=11.6 CM. (4.56 IN.)	.0505 (.0199)	.0947 (.0373)	.1661 (.0654)	.2212 (.0871)	.4089 (.1610)
X=14.0 CM. (5.50 IN.)	.0511 (.0201)	.0975 (.0384)	.1748 (.0688)	.2349 (.0925)	.4392 (.1729)
X=16.4 CM. (6.44 IN.)	.0503 (.0198)	.0960 (.0378)	.1715 (.0675)	.2322 (.0914)	.4354 (.1714)
X=18.7 CM. (7.38 IN.)	.0505 (.0199)	.0940 (.0370)	.1666 (.0656)	.2256 (.0888)	.4249 (.1673)
X=22.9 CM. (9.00 IN.)	.0277 (.0109)	.0541 (.0213)	.0922 (.0363)	.1280 (.0504)	.2372 (.0934)

TABLE B–14 DEFLECTION DATA FOR SUBSIZE PANEL TEST RENE' – 23

Subsize Panel Test Titanium-21

Corrugation stiffened Panel T1 was tested to 50 constant load (43.0 Kg) and temperature (783 K) profiles as presented in Table 6-4, and Figure 5-1(a). Cycle time at load and peak temperature was 20 minutes and atmospheric pressure was maintained constant at approximately 1.3 Pa. A 50 cycle midspan deflection of .5799 cm (.2283 inches) was attained. The oxide coating evident on this panel was a uniform deep purple-gold. The panel photograph after testing and creep deflection data are presented in Figure B-10 and Table B-15, respectively. Severe buckling of the panel skin was evident after testing.

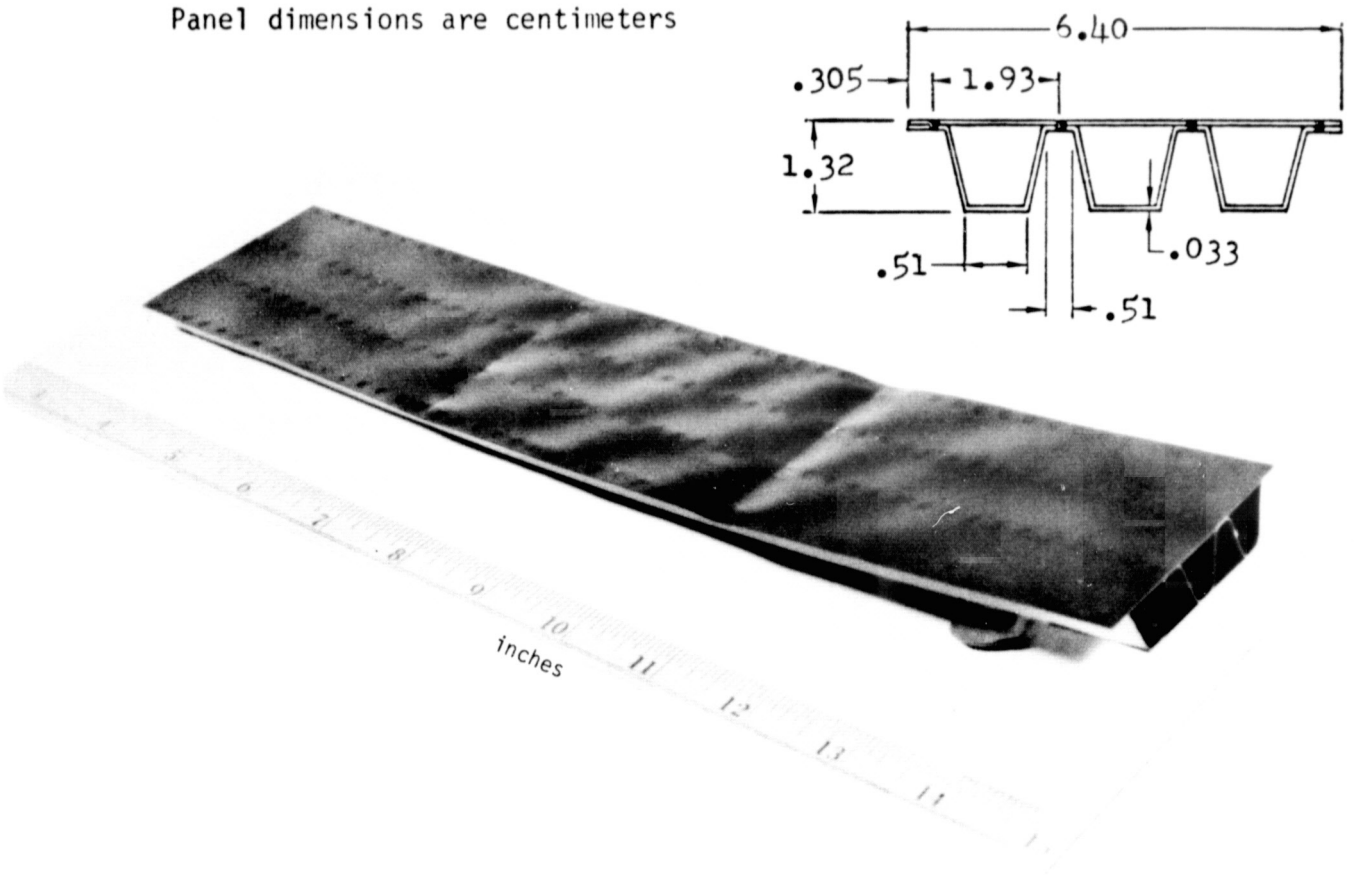

FIGURE B–10 SUBSIZE PANEL T1 CROSS SECTION AND PHOTOGRAPH AFTER TEST

MEASUREMENT LOCATION (REF. FIGURE 5-9)	CYCLES				
	1	5	15	25	50
X=5.08 CM. (2.00 IN.)	.0574 (.0226)	.1067 (.0420)	.1577 (.0621)	.2388 (.0940)	.2784 (.1096)
X=9.19 CM. (3.62 IN.)	.1019 (.0401)	.1867 (.0735)	.2814 (.1108)	.3541 (.1394)	.5090 (.2004)
X=11.6 CM. (4.56 IN.)	.1090 (.0429)	.2007 (.0790)	.3033 (.1194)	.3825 (.1506)	.5461 (.2150)
X=14.0 CM. (5.50 IN.)	.1125 (.0443)	.2093 (.0824)	.3175 (.1250)	.4026 (.1585)	.5799 (.2283)
X=16.4 CM. (6.44 IN.)	.1115 (.0439)	.2083 (.0820)	.3185 (.1254)	.4026 (.1585)	.5829 (.2295)
X=18.7 CM. (7.38 IN.)	.1067 (.0420)	.2004 (.0789)	.3111 (.1225)	.3952 (.1556)	.5855 (.2305)
X=22.9 CM. (9.00 IN.)	.0622 (.0245)	.1140 (.0449)	.1740 (.0685)	.2233 (.0879)	.3200 (.1260)

TABLE B–15 DEFLECTION DATA FOR SUBSIZE PANEL TEST TITANIUM – 21

Subsize Panel Test Titanium-22

Corrugation stiffened Panel T2 was tested to 100 constant load (31.1 Kg) and temperature (783 K) profiles as presented in Table 6-4, and Figure 5-1(a). Cycle time at load and peak temperature was 20 minutes and atmospheric pressure was maintained constant at approximately 1.3 Pa. A 100 cycle midspan deflection of .4714 cm (.1856 inches) was attained. This test was a repeat of test titanium-21 except that the load was lowered in an attempt to reduce skin buckling. A slight amount of buckling was evident, however, after the 100 cycle test. A spotty light silvery blue oxide was obtained on this panel, possibly indicating that this panel was subjected to higher temperatures. At one end (approximately <5.0 cm), the panel was a purple-gold color similar to that obtained in panel test titanium-21. The panel photograph, after testing and creep deflection data, are presented in Figure B-11 and Table B-16, respectively.

Panel dimensions are centimeters

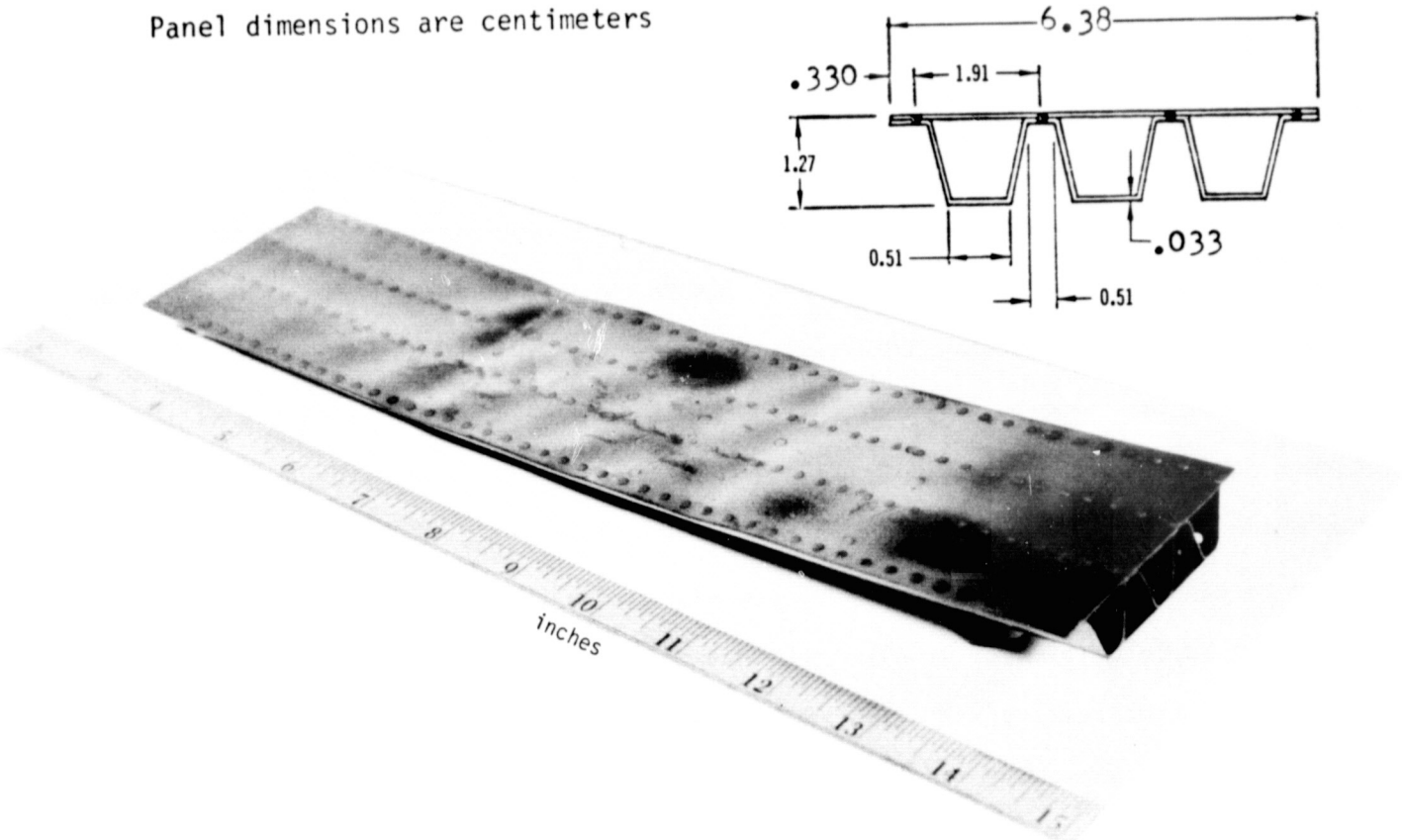

FIGURE B–11 SUBSIZE PANEL T2 CROSS SECTION AND PHOTOGRAPH AFTER TEST

MEASUREMENT LOCATION (REF. FIGURE 5-9)	CYCLES						
	1	5	15	25	50	75	100
X=5.08 CM. (2.00 IN.)	.0401 (.0158)	.0698 (.0275)	.1087 (.0428)	.1245 (.0490)	.1638 (.0645)	.1984 (.0781)	.2266 (.0892)
X=9.19 CM. (3.62 IN.)	.0698 (.0275)	.1222 (.0481)	.1859 (.0732)	.2197 (.0865)	.2916 (.1148)	.3485 (.1372)	.4044 (.1592)
X=11.6 CM. (4.56 IN.)	.0775 (.0305)	.1346 (.0530)	.2047 (.0806)	.2416 (.0951)	.3198 (.1259)	.3833 (.1509)	.4448 (.1751)
X=14.0 CM. (5.50 IN.)	.0810 (.0319)	.1412 (.0556)	.2146 (.0845)	.2543 (.1001)	.3363 (.1324)	.4051 (.1595)	.4714 (.1856)
X=16.4 CM. (6.44 IN.)	.0790 (.0311)	.1377 (.0542)	.2106 (.0829)	.2499 (.0984)	.3327 (.1310)	.3990 (.1571)	.4661 (.1835)
X=18.7 CM. (7.38 IN.)	.0732 (.0288)	.1295 (.0510)	.1996 (.0786)	.2367 (.0932)	.3185 (.1254)	.3848 (.1515)	.4524 (.1781)
X=22.9 CM. (9.00 IN.)	.0442 (.0174)	.0767 (.0302)	.1163 (.0458)	.1367 (.0538)	.1854 (.0730)	.2184 (.0860)	.2550 (.1004)

TABLE B–16 DEFLECTION DATA FOR SUBSIZE PANEL TEST TITANIUM – 22

Subsize Panel Test Titanium-23 and -24

Corrugation stiffened Panel T3 and T4 were tested to mission load, temperature (783 K peak), and atmospheric pressure profiles as outlined in Table 6-4. A 100 cycle midspan deflection of .2951 cm (.1162 inches) was attained in test Titanium-23 and a 50 cycle midspan deflection of .2342 cm (.0922 inches) was attained in test Titanium-24. These two tests were intended to be replicates although a minor variation occurred in peak applied load as noted in Table 6-4. Only very slight waviness of the panel skins was evident after testing. A purple-gold oxide was present on both panels T3 and T4, similar to that obtained in test Titanium-21.

Panel photographs after testing and deflection data are presented in Figures B-12 and B-13 and in Tables B-17 and B-18. Because the trajectories were essentially the same for the two tests, the data for test Titanium-23 is presented in Table B-19 as typical for both tests.

Panel dimensions are centimeters

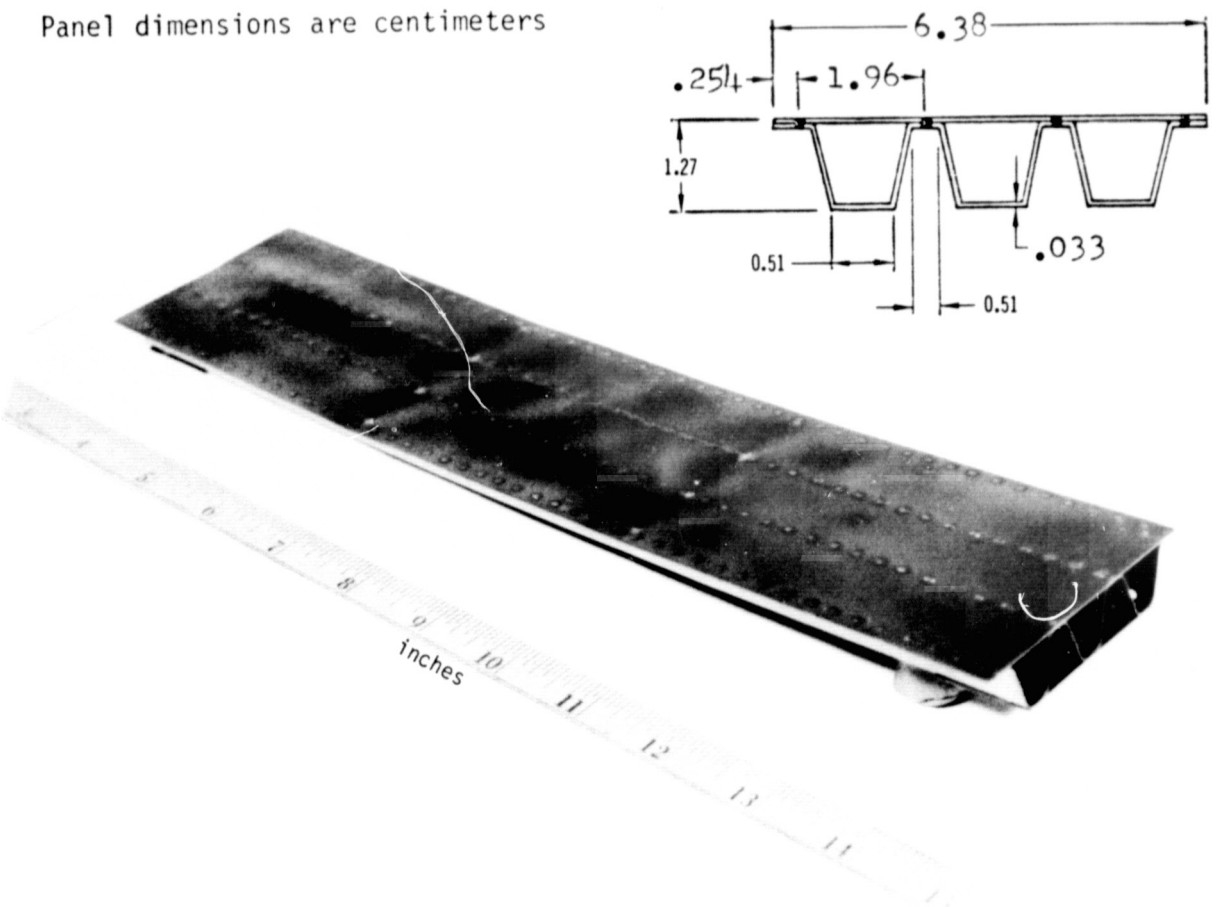

FIGURE B–12 SUBSIZE PANEL T3 CROSS SECTION AND PHOTOGRAPH AFTER TEST

MEASUREMENT LOCATION (REF. FIGURE 5-9)	CYCLES						
	1	5	15	25	50	75	100
X=5.08 CM. (2.00 IN.)	.0310 (.0122)	.0508 (.0200)	.0803 (.0316)	.0859 (.0338)	.1090 (.0429)	.1323 (.0521)	.1471 (.0579)
X=9.19 CM. (3.62 IN.)	.0610 (.0240)	.0955 (.0376)	.1402 (.0552)	.1580 (.0622)	.2009 (.0791)	.2400 (.0945)	.2631 (.1036)
X=11.6 CM. (4.56 IN.)	.0655 (.0258)	.0965 (.0380)	.1501 (.0591)	.1722 (.0678)	.2179 (.0858)	.2568 (.1011)	.2832 (.1115)
X=14.0 CM. (5.50 IN.)	.0688 (.0271)	.1092 (.0430)	.1570 (.0618)	.1803 (.0710)	.2291 (.0902)	.2667 (.1050)	.2951 (.1162)
X=16.4 CM. (6.44 IN.)	.0696 (.0274)	.1082 (.0426)	.1562 (.0615)	.1793 (.0706)	.2281 (.0898)	.2647 (.1042)	.2934 (.1155)
X=18.7 CM. (7.38 IN.)	.0658 (.0259)	.1026 (.0404)	.1488 (.0586)	.1730 (.0681)	.2210 (.0870)	.2540 (.1000)	.2814 (.1108)
X=22.9 CM. (9.00 IN.)	.0335 (.0132)	.0536 (.0211)	.0843 (.0332)	.0955 (.0376)	.1207 (.0475)	.1397 (.0550)	.1547 (.0609)

TABLE B–17 DEFLECTION DATA FOR SUBSIZE PANEL TEST TITANIUM – 23

Panel dimensions are centimeters

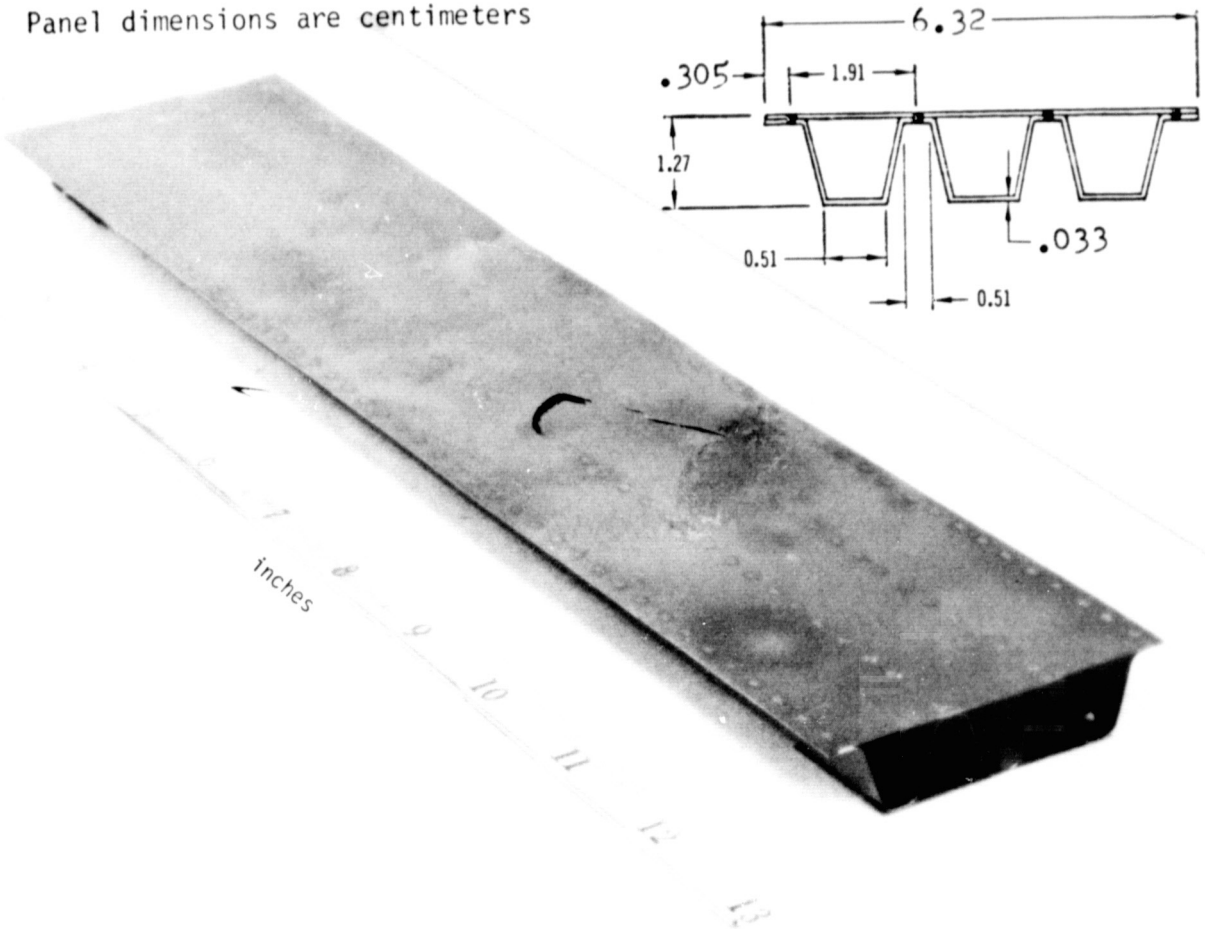

FIGURE B-13 SUBSIZE PANEL T4 CROSS SECTION AND PHOTOGRAPH AFTER TEST

MEASUREMENT LOCATION (REF. FIGURE 5-9)	CYCLES				
	1	5	15	25	50
X=5.08 CM. (2.00 IN.)	.0394 (.0155)	.0671 (.0264)	.0810 (.0319)	.0963 (.0379)	.1140 (.0449)
X=9.19 CM. (3.62 IN.)	.0726 (.0286)	.1168 (.0460)	.1486 (.0585)	.1740 (.0685)	.2098 (.0826)
X=11.6 CM. (4.56 IN.)	.0772 (.0304)	.1219 (.0480)	.1565 (.0616)	.1831 (.0721)	.2233 (.0879)
X=14.0 CM. (5.50 IN.)	.0798 (.0314)	.1245 (.0490)	.1628 (.0641)	.1908 (.0751)	.2342 (.0922)
X=16.4 CM. (6.44 IN.)	.0790 (.0311)	.1191 (.0469)	.1590 (.0626)	.1864 (.0734)	.2301 (.0906)
X=18.7 CM. (7.38 IN.)	.0757 (.0298)	.1113 (.0438)	.1519 (.0598)	.1775 (.0699)	.2210 (.0870)
X=22.9 CM. (9.00 IN.)	.0444 (.0175)	.0645 (.0254)	.0866 (.0341)	.1013 (.0399)	.1267 (.0499)

TABLE B-18 DEFLECTION DATA FOR SUBSIZE PANEL TEST TITANIUM - 24

CYCLE TIME (Seconds)	TYPICAL MEASURED TEMPERATURE		AVERAGE MEASURED BEAM LOAD (P)	
	°F	K	LBS	Kg
100	380.	466.	-	-
200	425.	491.	-	-
300	550.	561.	-	-
400	738.	665.	18.40	8.35
500	896.	753.	32.40	14.70
600	935.	775.	42.31	19.19
700	947.	781.	48.60	22.04
800	950.	783.	52.34	23.74
900	936.	775.	53.81	24.41
1000	923.	768.	55.34	25.10
1100	911.	761.	59.40	26.94
1200	902.	756.	63.51	28.81
1300	892.	751.	70.85	32.14
1400	880.	744.	78.78	35.73
1500	865.	736.	89.25	40.48
1600	846.	725.	104.66	47.47
1700	818.	710.	110.80	50.26
1800	787.	693.	119.62	54.26
1900	750.	672.	127.01	57.61
2000	717.	654.	127.16	57.68
2100	686.	636.	119.53	54.22
2200	657.	619.	106.34	48.24
2300	626.	603.	90.20	40.91
2400	598.	588.	64.55	29.28
2500	570.	572.	32.68	14.82
2600	542.	556.	13.90	6.31
2700	519.	544.	-	-
2800	495.	530.	-	-
2900	471.	517.	-	-
3000	451.	506.	-	-
3100	434.	496.	-	-
3200	418.	488.	-	-
3300	403.	479.	-	-
3400	392.	473.	-	-
3500	385.	469.	-	-
3600	382.	468.	-	-
3700	380.	466.	-	-

TABLE B-19 TRAJECTORY DATA FOR SUBSIZE PANEL TEST TITANIUM-23 AND -24

Subsize Panel Test Titanium-25

Rib-stiffened Panel T7 was tested to 50 mission load, temperature (783 K peak), and atmospheric pressure profiles as outlined in Table 6-4. A 50 cycle midspan deflection of .2040 cm (.0803 inches) was attained. A uniform slivery blue oxide, comparable to that obtained for test Titanium-22, was evident on the panel after testing. The panel photograph after testing and deflection data are presented in Figure B-14 and Table B-20, respectively. Trajectory data for this test are presented in Table B-21.

Panel dimensions are centimeters

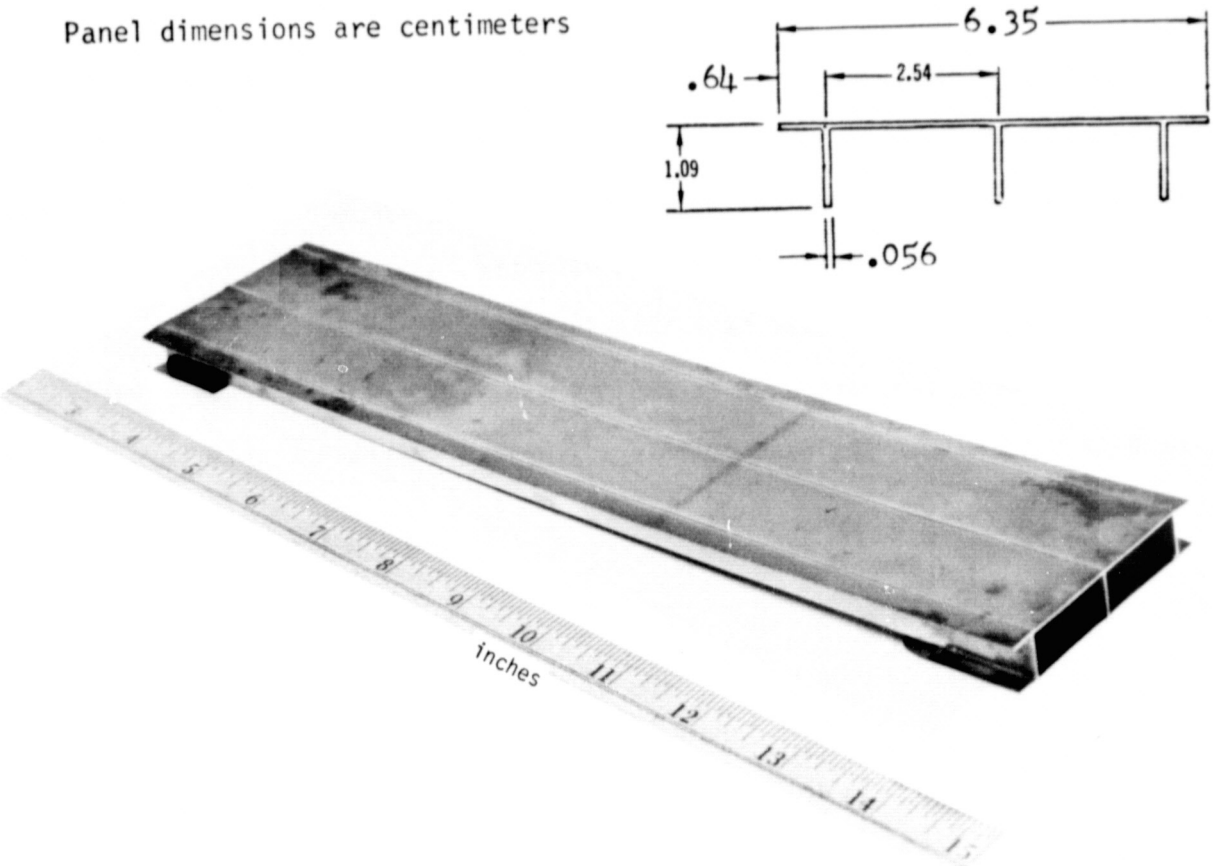

FIGURE B–14 SUBSIZE PANEL T7 CROSS SECTION AND PHOTOGRAPH AFTER TEST

MEASUREMENT LOCATION (REF. FIGURE 5-9)	CYCLES				
	1	5	15	25	50
X=5.08 CM. (2.00 IN.)	.0272 (.0107)	.0450 (.0177)	.0622 (.0245)	.0762 (.0300)	.0965 (.0380)
X=9.19 CM. (3.62 IN.)	.0457 (.0180)	.0818 (.0322)	.1034 (.0407)	.1278 (.0503)	.1633 (.0643)
X=11.6 CM. (4.56 IN.)	.0551 (.0217)	.0884 (.0348)	.1207 (.0475)	.1491 (.0587)	.1910 (.0752)
X=14.0 CM. (5.50 IN.)	.0597 (.0235)	.0927 (.0365)	.1290 (.0508)	.1588 (.0625)	.2040 (.0803)
X=16.4 CM. (6.44 IN.)	.0577 (.0227)	.0894 (.0352)	.1237 (.0487)	.1549 (.0610)	.1976 (.0778)
X=18.7 CM. (7.38 IN.)	.0526 (.0207)	.0818 (.0322)	.1113 (.0438)	.1384 (.0545)	.1778 (.0700)
X=22.9 CM. (9.00 IN.)	.0310 (.0122)	.0495 (.0195)	.0678 (.0267)	.0843 (.0332)	.1074 (.0423)

TABLE B–20 DEFLECTION DATA FOR SUBSIZE PANEL TEST TITANIUM – 25

CYCLE TIME (Seconds)	TYPICAL MEASURED TEMPERATURE		AVERAGE MEASURED BEAM LOAD (P)	
	°F	K	LBS	Kg
100	380.	466.	-	-
200	425.	491.	-	-
300	550.	561.	-	-
400	738.	665.	8.55	3.88
500	896.	753.	16.39	7.43
600	935.	775.	21.71	9.85
700	947.	781.	25.17	11.42
800	950.	783.	27.09	12.29
900	936.	775.	27.96	12.68
1000	923.	768.	28.70	13.02
1100	911.	761.	30.85	13.99
1200	902.	756.	33.21	15.06
1300	892.	751.	36.84	16.71
1400	880.	744.	41.00	18.60
1500	865.	736.	46.42	21.06
1600	846.	725.	54.65	24.79
1700	818.	710.	58.00	26.31
1800	787.	693.	62.64	28.41
1900	750.	672.	66.74	30.27
2000	717.	654.	66.78	30.29
2100	686.	636.	62.77	28.47
2200	657.	619.	55.77	25.30
2300	626.	603.	47.29	21.45
2400	598.	588.	33.84	15.35
2500	570.	572.	16.92	7.67
2600	542.	556.	6.78	3.08
2700	519.	544.	-	-
2800	495.	530.	-	-
2900	471.	517.	-	-
3000	451.	506.	-	-
3100	434.	496.	-	-
3200	418.	488.	-	-
3300	403.	479.	-	-
3400	392.	473.	-	-
3500	385.	469.	-	-
3600	382.	468.	-	-
3700	380.	466.	-	-

TABLE B-21 TRAJECTORY DATA FOR SUBSIZE PANEL TEST TITANIUM -25

Subsize Panel Test Titanium-26

Rib-stiffened Panel L8 was tested to 50 constant load (51.8 Kg) and temperature (714 K) profiles as presented in Table 6-4, and Figure 5-1(a). Cycle time at load and peak temperature was 20 minutes and atmospheric pressure was maintained constant at approximately 1.3 Pa. A 50 cycle midspan deflection of .2553 cm (.1005 inches) was attained. A blotched slivery blue oxide was evident on the panel, after testing, over approximately two thirds of its length. The remainder of the panel was gold in color. This nonuniformity in color was attributed to poor cleaning of the specimen. The panel photograph after testing and creep deflection data are presented in Figure B-15 and Table B-22, respectively.

Panel dimensions are centimeters

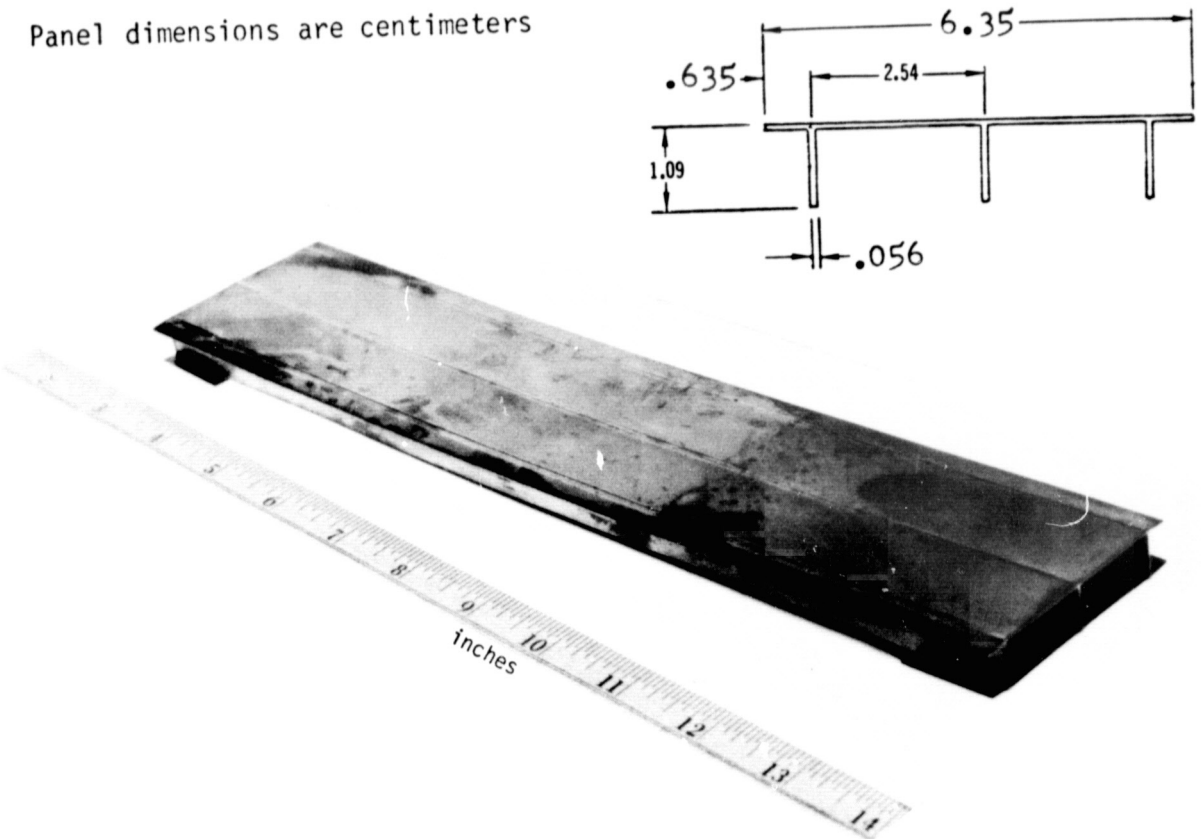

FIGURE B-15 SUBSIZE PANEL T8 CROSS SECTION AND PHOTOGRAPH AFTER TEST

MEASUREMENT LOCATION (REF. FIGURE 5-9)	CYCLES				
	1	5	15	25	50
X=5.08 CM. (2.00 IN.)	.0373 (.0147)	.0610 (.0240)	.0859 (.0338)	.0953 (.0375)	.1199 (.0472)
X=9.19 CM. (3.62 IN.)	.0716 (.0282)	.1092 (.0430)	.1529 (.0602)	.1651 (.0650)	.2103 (.0828)
X=11.6 CM. (4.56 IN.)	.0808 (.0318)	.1232 (.0485)	.1735 (.0683)	.1935 (.0762)	.2400 (.0945)
X=14.0 CM. (5.50 IN.)	.0846 (.0333)	.1303 (.0513)	.1847 (.0727)	.2070 (.0815)	.2553 (.1005)
X=16.4 CM. (6.44 IN.)	.0825 (.0325)	.1262 (.0497)	.1816 (.0715)	.2027 (.0798)	.2489 (.0980)
X=18.7 CM. (7.38 IN.)	.0732 (.0288)	.1113 (.0438)	.1621 (.0638)	.1803 (.0710)	.2235 (.0880)
X=22.9 CM. (9.00 IN.)	.0450 (.0177)	.0681 (.0268)	.1003 (.0395)	.1123 (.0442)	.1377 (.0542)

TABLE B-22 DEFLECTION DATA FOR SUBSIZE PANEL TEST TITANIUM - 26

Subsize Panel Test TDNiCr-21

Corrugation stiffened Panel TD1 was tested to 50 constant load (10.3 Kg) and temperature 1478 K (2200°F) profiles as presented in Table 6-5, and Figure 5-1(a). Cycle time at load and peak temperature was 20 minutes and atmospheric pressure was maintained constant at approximately 1.3 Pa. A 50 cycle midspan deflection of .0391 cm (.0154 inches) was attained and a uniform bright green low pressure oxide was evident on the panel after testing. The panel photograph after testing and creep deflection data are presented in Figure B-16 and Table B-23, respectively.

Panel dimensions are centimeters

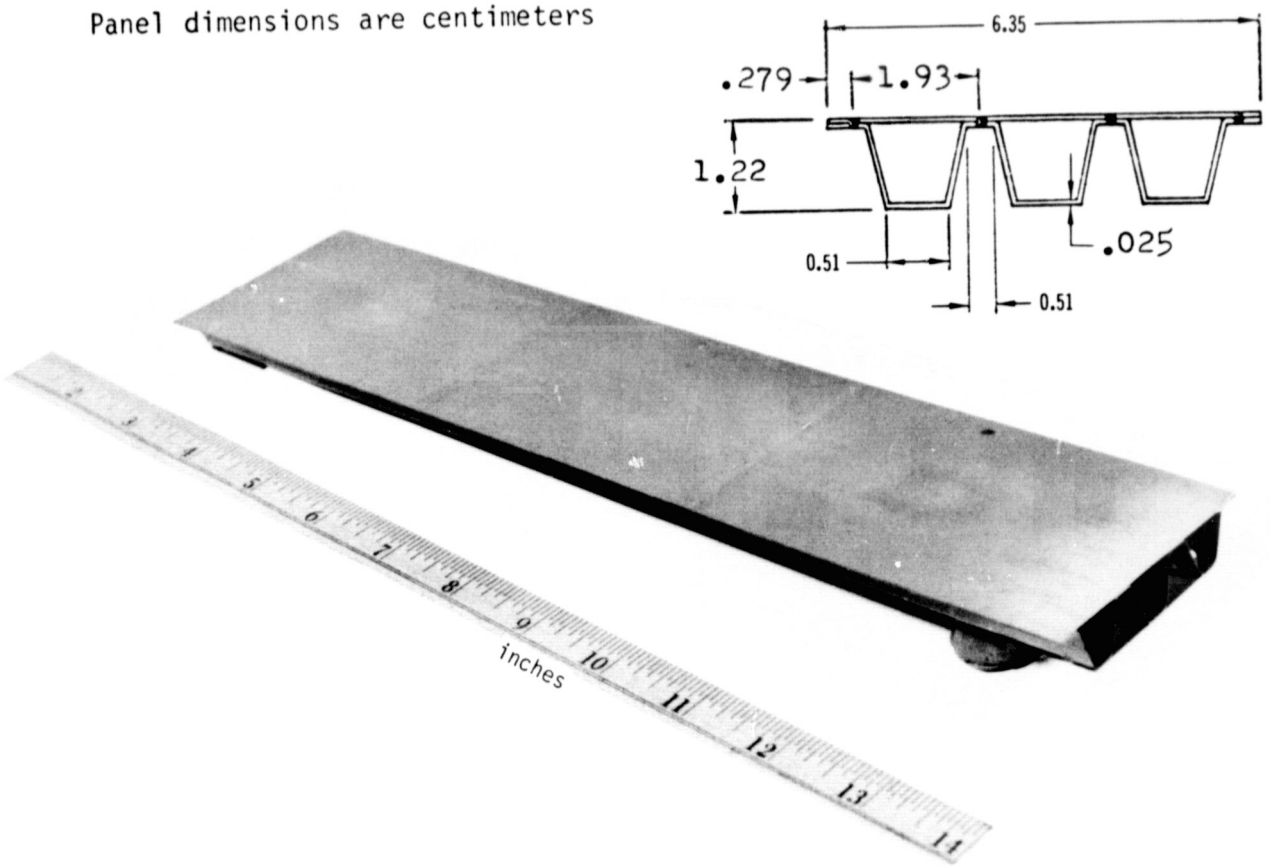

FIGURE B–16 SUBSIZE PANEL TD1 CROSS SECTION AND PHOTOGRAPH AFTER TEST

MEASUREMENT LOCATION (REF. FIGURE 5-9)	CYCLES				
	1	5	15	25	50
X=5.08 CM. (2.00 IN.)	.0038 (.0015)	.0063 (.0025)	.0114 (.0045)	.0135 (.0053)	.0211 (.0083)
X=9.19 CM. (3.62 IN.)	.0061 (.0024)	.0112 (.0044)	.0206 (.0081)	.0241 (.0095)	.0381 (.0150)
X=11.6 CM. (4.56 IN.)	.0076 (.0030)	.0124 (.0049)	.0226 (.0089)	.0257 (.0101)	.0378 (.0149)
X=14.0 CM. (5.50 IN.)	.0076 (.0030)	.0124 (.0049)	.0229 (.0090)	.0269 (.0106)	.0391 (.0154)
X=16.4 CM. (6.44 IN.)	.0071 (.0028)	.0117 (.0046)	.0216 (.0085)	.0251 (.0099)	.0376 (.0148)
X=18.7 CM. (7.38 IN.)	.0102 (.0040)	.0163 (.0064)	.0262 (.0103)	.0320 (.0126)	.0427 (.0168)
X=22.9 CM. (9.00 IN.)	.0033 (.0013)	.0046 (.0018)	.0117 (.0046)	.0150 (.0059)	.0193 (.0076)

TABLE B–23 DEFLECTION DATA FOR SUBSIZE PANEL TEST TDNiCR–21

Subsize Panel Test TDNiCr-22

Corrugation stiffened Panel TD2 was tested to 100 mission load, temperature (1478 K peak), and atmospheric pressure profiles as outlined in Table 6-5. A 100 cycle midspan deflection of .0572 cm (.0225 inches) was attained. The oxide formed was a uniform gray green color. The panel photograph after testing and deflection data are presented in Figure B-17 and Table B-24, respectively. Trajectory data for this test are presented in Table B-25.

Panel dimensions are centimeters

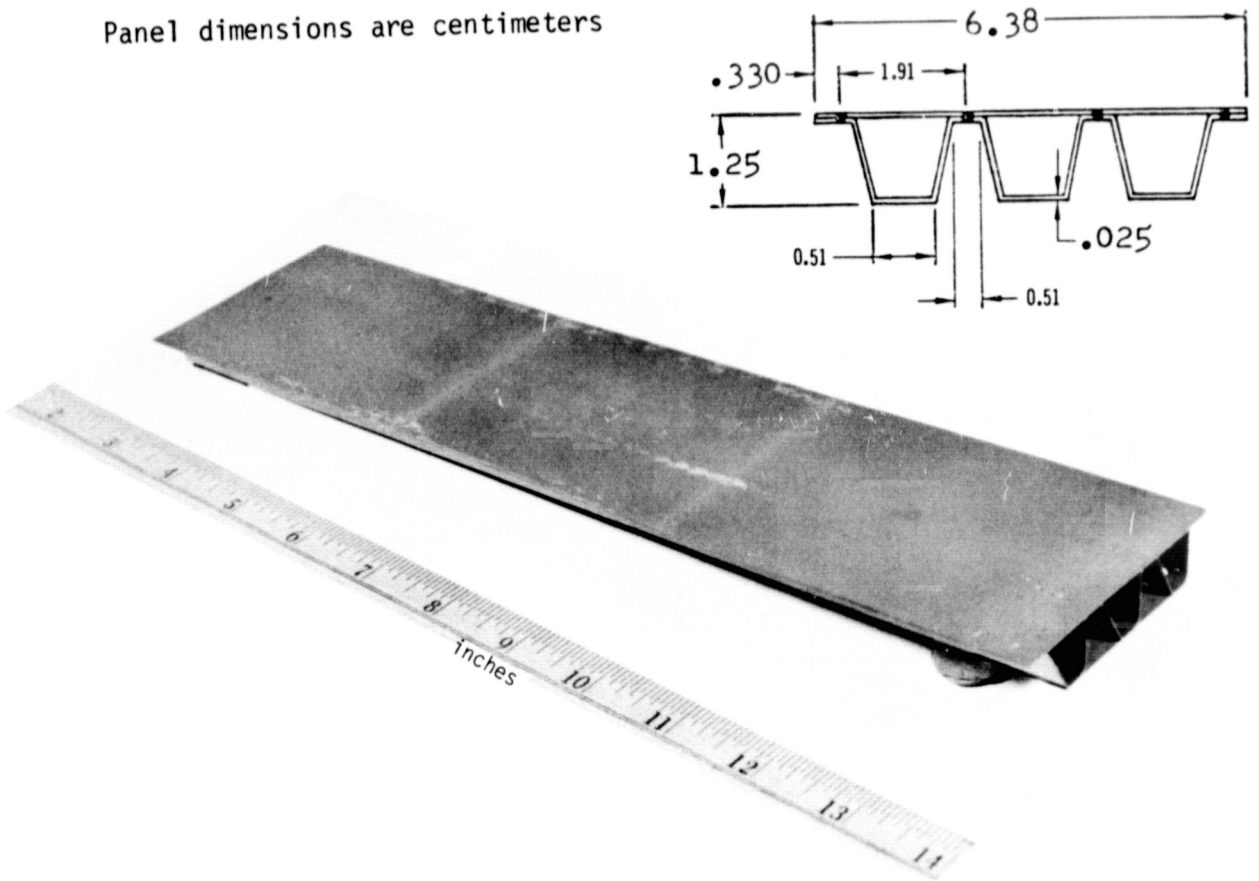

FIGURE B–17 SUBSIZE PANEL TD2 CROSS SECTION AND PHOTOGRAPH AFTER TEST

MEASUREMENT LOCATION (REF. FIGURE 5-9)	CYCLES						
	1	5	15	25	50	75	100
X=5.08 CM. (2.00 IN.)	.0041 (.0016)	.0079 (.0031)	.0079 (.0031)	.0122 (.0048)	.0249 (.0098)	.0236 (.0093)	.0287 (.0113)
X=9.19 CM. (3.62 IN.)	.0124 (.0049)	.0178 (.0070)	.0168 (.0066)	.0241 (.0095)	.0465 (.0183)	.0460 (.0181)	.0521 (.0205)
X=11.6 CM. (4.56 IN.)	.0124 (.0049)	.0201 (.0079)	.0168 (.0066)	.0264 (.0104)	.0478 (.0188)	.0495 (.0195)	.0556 (.0219)
X=14.0 CM. (5.50 IN.)	.0124 (.0049)	.0216 (.0085)	.0165 (.0065)	.0269 (.0106)	.0483 (.0190)	.0505 (.0199)	.0572 (.0225)
X=16.4 CM. (6.44 IN.)	.0109 (.0043)	.0191 (.0075)	.0150 (.0059)	.0267 (.0105)	.0455 (.0179)	.0470 (.0185)	.0536 (.0211)
X=18.7 CM. (7.38 IN.)	.0091 (.0036)	.0165 (.0065)	.0137 (.0054)	.0229 (.0090)	.0401 (.0158)	.0417 (.0164)	.0480 (.0189)
X=22.9 CM. (9.00 IN.)	.0058 (.0023)	.0109 (.0043)	.0086 (.0034)	.0127 (.0050)	.0236 (.0093)	.0226 (.0089)	.0277 (.0109)

TABLE B– 24 DEFLECTION DATA FOR SUBSIZE PANEL TEST TDNiCR–22

CYCLE TIME (Seconds)	TYPICAL MEASURED TEMPERATURE		AVERAGE MEASURED BEAM LOAD (P)	
	°F	K	LBS	Kg
100	850.	728.	-	-
200	1120.	878.	-	-
300	1430.	1050.	-	-
400	1880.	1300.	4.65	2.11
500	2050.	1394.	7.73	3.51
600	2130.	1439.	9.66	4.38
700	2180.	1466.	10.86	4.93
800	2200.	1478.	11.51	5.22
900	2165.	1458.	11.77	5.34
1000	2150.	1450.	12.12	5.50
1100	2120.	1433.	13.03	5.91
1200	2090.	1416.	14.00	6.35
1300	2065.	1403.	15.51	7.04
1400	2040.	1389.	17.19	7.80
1500	1980.	1355.	19.65	8.91
1600	1940.	1333.	22.10	10.02
1700	1850.	1283.	23.28	10.56
1800	1745.	1225.	25.26	11.46
1900	1660.	1178.	26.28	11.92
2000	1575.	1130.	26.28	11.92
2100	1510.	1094.	24.03	10.90
2200	1440.	1055.	21.11	9.58
2300	1365.	1014.	17.38	7.88
2400	1320.	989.	11.24	5.10
2500	1260.	955.	4.92	2.23
2600	1215.	930.	2.78	1.26
2700	1170.	905.	-	-
2800	1125.	880.	-	-
2900	1080.	855.	-	-
3000	1045.	836.	-	-
3100	1010.	816.	-	-
3200	970.	794.	-	-
3300	945.	780.	-	-
3400	915.	764.	-	-
3500	880.	744.	-	-
3600	860.	733.	-	-
3700	850.	728.	-	-

TABLE B-25 TRAJECTORY DATA FOR SUBSIZE PANEL TEST TDNiCR-22